



Pacific
Northwest
NATIONAL LABORATORY

PNNL-29370

High-Resolution Regional Wave Hindcast for Hawaii

November 2019

G García-Medina
Z Yang
N Li
K F Cheung
T Wang
WC Wu



Prepared for the U.S. Department of Energy
under Contract DE-AC05-76RL01830

DISCLAIMER

This report was prepared as an account of work sponsored by an agency of the United States Government. Neither the United States Government nor any agency thereof, nor Battelle Memorial Institute, nor any of their employees, makes **any warranty, express or implied, or assumes any legal liability or responsibility for the accuracy, completeness, or usefulness of any information, apparatus, product, or process disclosed, or represents that its use would not infringe privately owned rights.** Reference herein to any specific commercial product, process, or service by trade name, trademark, manufacturer, or otherwise does not necessarily constitute or imply its endorsement, recommendation, or favoring by the United States Government or any agency thereof, or Battelle Memorial Institute. The views and opinions of authors expressed herein do not necessarily state or reflect those of the United States Government or any agency thereof.

PACIFIC NORTHWEST NATIONAL LABORATORY
operated by
BATTELLE
for the
UNITED STATES DEPARTMENT OF ENERGY
under Contract DE-AC05-76RL01830

Printed in the United States of America

Available to DOE and DOE contractors from the
Office of Scientific and Technical Information,
P.O. Box 62, Oak Ridge, TN 37831-0062;
ph: (865) 576-8401
fax: (865) 576-5728
email: reports@adonis.osti.gov

Available to the public from the National Technical Information Service
5301 Shawnee Rd., Alexandria, VA 22312
ph: (800) 553-NTIS (6847)
email: [<https://www.ntis.gov/about>](mailto:orders@ntis.gov)
Online ordering: <http://www.ntis.gov>

High-Resolution Regional Wave Hindcast for Hawaii

November 2019

G García-Medina
Z Yang
N Li
K F Cheung
T Wang
WC Wu

Prepared for
the U.S. Department of Energy
under Contract DE-AC05-76RL01830

Pacific Northwest National Laboratory
Richland, Washington 99354

Summary

This report summarizes modeling efforts for hindcasting of wave climate within the exclusive economic zone (EEZ) around the state of Hawaii. Specifically, the report provides detailed description of model mesh development, sensitivity analysis of the configuration of model parameters, data used for model forcing and validation, model skill assessment, and model outputs for resource characterization.

The unstructured, nested-grid modeling approach incorporates a regional high-resolution SWAN (Simulating WAves Nearshore) model within the global-regional WAVEWATCH III® (WW3) wave model. The models were configured to comply with the International Electrotechnical Commission (IEC) Technical Standards for wave energy resource characterization. The SWAN model domain covers the entire EEZ with a spatial resolution of approximately 300 m in the nearshore region. Two levels of WW3 nested grids, from 0.5 arc-degree at global to 7.5 arc-minute at regional scale, were used to provide boundary conditions that drive the high-resolution nearshore SWAN model. The WW3 and SWAN models were forced by 0.5 arc-degree Climate Forecast System Reanalysis wind and 5 km regional Weather Research and Forecasting wind, respectively.

Wave resource and bulk wave parameters were simulated for a 32-year period from 1979 to 2010, and were subsequently validated using wave buoy data within the model domain. Model performance was evaluated using a set of error statistics. Overall, the model shows good skills in reproducing the wave climate in the Hawaii EEZ in both spatial and temporal domains. Comparisons of time series and scatter plots for the six IEC resource parameters and the associated error statistics tables, and horizontal two-dimensional plots of annually averaged and monthly averaged IEC parameters are provided.

Acknowledgments

This study was funded by the U.S. Department of Energy, Office of Energy Efficiency & Renewable Energy, Water Power Technologies Office under Contract DE-AC05-76RL01830 to Pacific Northwest National Laboratory.

A steering committee, chaired by Dr. Bryson Robertson of Oregon State University, provided external oversight for, input to, and review of this modeling study. Steering committee members include Dr. Henrique Alves of the National Oceanic and Atmospheric Administration; Dr. Brian Polagye of Pacific Marine Energy Center at University of Washington; Dr. James Behrens of the Coastal Data Information Program at the University of California San Diego; Dr. Pukha Lenee-Bluhm of Columbia Power; Bill Staby of Resolute Marine Energy, and Mr. Sean Anderton of Ocean Renewable Power Company.

The model computations were performed using resources available through Research Computing at Pacific Northwest National Laboratory (PNNL). PNNL is operated by Battelle for the U.S. Department of Energy under Contract DE-AC05-76RL01830.

Acronyms and Abbreviations

CDIP	Coastal Data Information Program
CFL	Courant–Friedrichs–Lewy
CFSR	Climate Forecast System Reanalysis
EEZ	exclusive economic zone
EPRI	Electric Power Research Institute, Inc.
GSE	Garden Sprinkler Effect
Hz	hertz
IEC	International Electrotechnical Commission
km	kilometer(s)
kW/m	kilowatt(s) per meter
m	meter(s)
MHK	marine and hydrokinetic
NDBC	National Data Buoy Center
NCEP	National Centers for Environmental Prediction
NOAA	National Oceanic and Atmospheric Administration
NREL	National Renewable Energy Laboratory
<i>PE</i>	percentage error
<i>R</i>	correlation coefficient
<i>RMSE</i>	root-mean-square-error
s	second(s)
<i>SI</i>	scatter index
ST	source term
SWAN	Simulating WAves Nearshore
TB	terabyte(s)
TS	Technical Specification
UnSWAN	Unstructured-grid Simulating Waves Nearshore
WRF	Weather Research and Forecasting
WW3	WAVEWATCH III
yr	year(s)

Contents

Summary	iii
Acknowledgments.....	iv
Acronyms and Abbreviations.....	v
Contents	ii
1.0 Introduction	5
2.0 Study Area and Data	8
2.1 Hawaii.....	8
2.2 Measured Data for Model Validation	8
2.3 Atmospheric Forcing	10
3.0 Methods	13
3.1 WW3 Model Configuration	13
3.2 Unstructured-grid SWAN Model Configuration	14
3.2.1 Model Convergence	16
3.2.2 Source Terms.....	20
3.2.3 Practical Aspects	21
4.0 Model Hindcast and Validation	23
4.1 IEC Resource Parameters	23
4.2 Model Validation	28
4.3 Data Output	32
5.0 Conclusion	37
6.0 References.....	38
Appendix A – Monthly Distributions of IEC Wave Resource Parameters from 1979–2010 around Hawaii	A.1
Appendix B – Comparisons of the Model-Simulated Six IEC Parameters with Observed Data at CDIP and NDBC Buoys.....	B.1
Appendix C – Performance Metrics for Simulated IEC Resource Parameters	C.1

Figures

Figure 1.1. Annual wave power density distribution in U.S. coastal regions, based on NOAA's 4 arc-minute resolution WW3 hindcasts.	6
Figure 2.1. Wave buoy stations for model validation. PMNM stands for the Papahānaumokuākea Marine National Monument (PMNM), EEZ for exclusive economic zone. SWAN boundary points are shown as black dots.....	10
Figure 2.2. (a) The global distribution of CFSR wind field on 6:00 14 January 2010. The SWAN domain is outlined in black. A snapshot of the high-resolution Weather Research and Forecasting wind field over the complete domain (b)	

and a close-up to show the details resolved by the model (c). Panels (b) and (c) are on the same color scale.....	11
Figure 2.3. WRF and CFSR zonal (top) and meridional (bottom) instantaneous wind blending.....	12
Figure 3.1. Model domains for the Hawaii wave hindcast.	14
Figure 3.2. (a) Resolution of the mesh based on the element area. (b-c) Mesh details showing density, coastline, and element transition.....	15
Figure 3.3. Model-data comparisons for significant wave height (a) and peak wave period (b) for different integration time steps close to the SWAN boundary.....	16
Figure 3.4. Same as Figure 3.3 but for CDIP 106, which is approximately 900 km from the northwestern model boundary.....	17
Figure 3.5. Convergence time series for a simulation with maximum number of iterations set at 5.	18
Figure 3.6. Significant wave height comparison at Buoy (a,b) 51101 and (c,d) Buoy 106 for a six-month simulation with one and two iterations of the implicit model solution.....	19
Figure 3.7. Significant wave height for different iterations of the model development.....	20
Figure 3.8. Model sensitivity to source term package for significant wave height (a-b) and peak wave period (c-d) at selected buoys.	21
Figure 3.9. Absolute percent error between a cold-started simulation and a simulation that has been continuously running for 6 months.	22
Figure 3.10. Spatial distribution of errors in significant wave height due to model spin-up. Model errors after an initial stationary solution (a), after 1 day of non-stationary simulation (b), and after 6 days (c) are shown with respect to a simulation that is not affected by spin-up effects.	22
Figure 4.1. Simulated 32-year annual distribution of six IEC wave resource characterization parameters: (a) omnidirectional wave power, (b) significant wave height, (c) energy period, (d) spectral width, (e) direction of maximum directionally resolved wave power, and (f) directionality coefficient.	26
Figure 4.2. Simulated monthly distribution of six IEC wave resource parameters in January: (a) omnidirectional wave power, (b) significant wave height, (c) energy period, (d) spectral width, (e) direction of maximum directionally resolved wave power, and (f) directionality coefficient.....	27
Figure 4.3. Simulated monthly distribution of six IEC wave resource parameters in July: (a) omnidirectional wave power, (b) significant wave height, (c) energy period, (d) spectral width, (e) direction of maximum directionally resolved wave power, and (f) directionality coefficient.....	28
Figure 4.4. Time series (top) and scatter plots (bottom) of the six modeled and observed IEC wave resource parameters from October 2017 to March 2018 at Buoy 46263 in California.	31
Figure 4.5. Spectral output locations near Ni'ihau and Kaua'i.	33
Figure 4.6. Spectral output locations near Oahu.	34
Figure 4.7. Spectral output locations near Moloka'i, Lana'i, Maui, and Kaho'olawe.	35
Figure 4.8. Spectral output locations near Hawaii.	36

Tables

Table 2.1.	Summary of available data derived from the wave buoys during the hindcast period.*	9
Table 3.1.	Summary of nested WW3 model grids.....	13
Table 3.2.	Time steps for WW3.	14
Table 3.3.	Model-data comparisons for different integration time steps during January 2010.	17
Table 3.4.	IEC-TS homologation table for a Class 2 (Feasibility) study for the model setup.....	22
Table 4.2.	Summary of temporal averages of the root-mean-square-error and linear correlation coefficient for the six IEC wave resource parameters at buoys with spectral data.....	32
Table 4.3.	Output inventory.	32

1.0 Introduction

Ocean waves have the highest amount of energy among the U.S. marine and hydrokinetic (MHK) energy resources, which also include tidal and ocean currents, ocean thermal gradients, and river streams. The first U.S. nationwide wave resource assessment was conducted based on a 51-month wave hindcast using 4 arc-minute-resolution nested grids within the global WAVEWATCHIII® (WW3) wave model generated by the National Oceanic and Atmospheric Administration (NOAA) (EPRI 2011, Tolman and WAVEWATCH III Development Group 2014). The Electric Power Research Institute, Inc.'s (EPRI's) study estimated the available wave energy resources at 130 TWh/yr for Hawaii. In terms of energy density, Hawaii lags the U.S. West Coast and Alaska but is ahead of the Gulf, Atlantic, and Caribbean Coasts (Figure 1.1). Because Hawaii is more than 3600 km from the continental United States or any other major continent, having a diverse energy portfolio is of interest to the state for energy resilience purposes. Estimates from the U.S. Energy Information Administration (www.eia.gov) put the 2016 energy consumption for commercial, residential, and industrial purposes in Hawaii at 40 TWh.¹ Wave energy harvesting can help offset imported fossil fuels (i.e., coal and petroleum), which accounted for 82.4% of the state's energy production in 2018.²

The nationwide wave resource assessment provides a valuable first-order estimate of wave resources at a regional scale, which helps identify and prioritize regions for near-term market development. These assessments are conducted using coarse-grid models over large areas, resulting in adequate predictions for deep water regions, yet high uncertainty in the nearshore region (National Research Council 2013). However, most wave energy converters are designed for deployment in nearshore areas for low installation and maintenance costs. It is important to conduct a long-term, high-resolution wave hindcast in nearshore and shallow-water areas to improve the accuracy of these assessments and aid developers and regulators in the wave energy planning, design, and permitting process.

The present work was commissioned by the U.S. Department of Energy's Water Power Technologies Office to address the limitations of the existing wave energy characterization studies. To address these issues a 32-year wave hindcast for the exclusive economic zone surrounding Hawaii at a high spatial and temporal resolution was conducted using numerical modeling by the Pacific Northwest National Laboratory. The results will be disseminated and made available to interested stakeholders through the National Renewable Energy Laboratory.

¹ <https://www.eia.gov/state/?sid=HI> Accessed 30 April 2019

² <http://energy.hawaii.gov/resources/dashboard-statistics> Accessed 30 April 2019

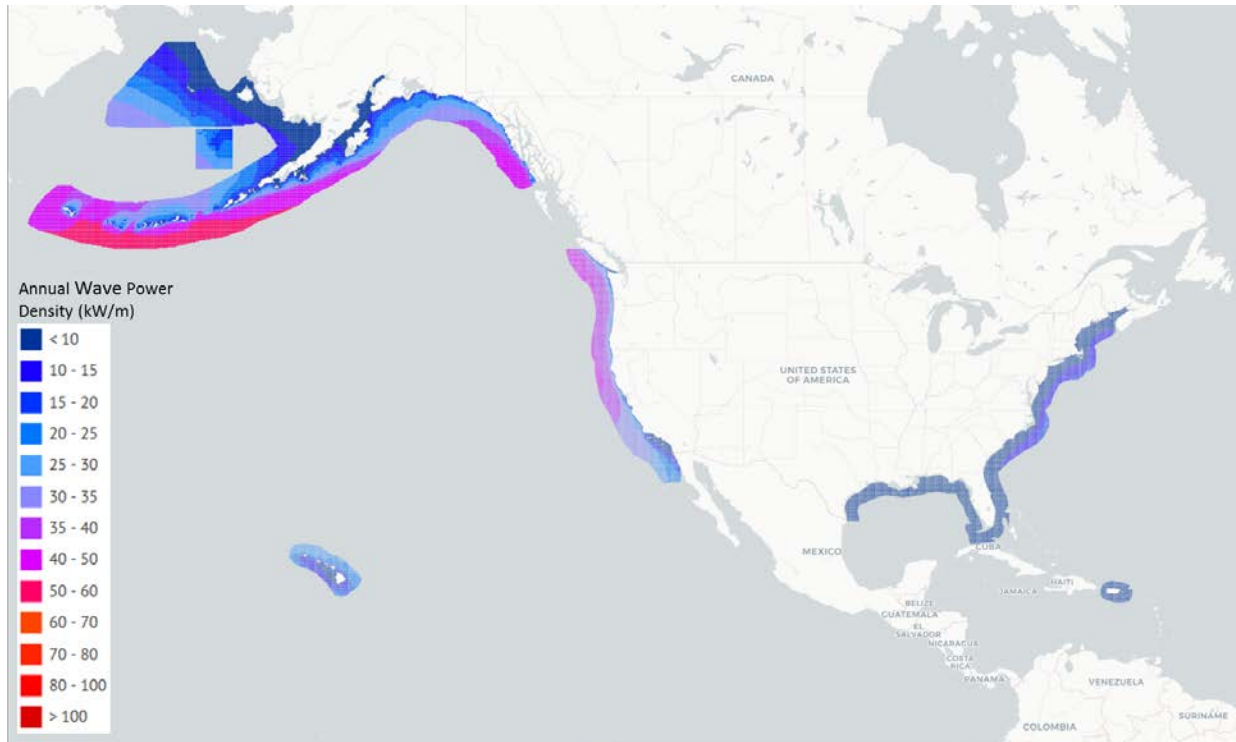


Figure 1.1. Annual wave power density distribution in U.S. coastal regions, based on NOAA's 4 arc-minute resolution WW3 hindcasts.³

High-resolution hindcasting using structured grids requires extensive computational resources even at a regional scale. The unstructured-grid modeling approach allows for accurate fitting of the mesh boundary to the shoreline at high resolution as well as computation efficiency for a large domain by increasing element size in deep water. In recent years, there have been significant developments in unstructured-grid third-generation wave models. For example, the unstructured-grid formulation of Simulating WAve Nearshore (SWAN; SWAN (2015)) has been widely used to model wave climates in many regions around the world (Cobell et al. 2013, Wu, Yang, and Wang 2018, Gallagher, Tiron, and Dias 2014, Mao et al. 2016, Mediavilla and Sepulveda 2016, Roland and Arduin 2014, Zijlema 2010, Yuk et al. 2016, Yang et al. 2019, Li et al. 2016). On the other hand, Hawaii is affected by swells generated from all corners of the Pacific Ocean (Li et al. 2016, Stopa, Cheung, and Chen 2011) that require ocean-scale models for adequate representation of the sea states. In this study, we combine WW3 and SWAN in tandem to capture wave processes from remote and local sources to characterize the wave resources for Hawaii. This combination has been implemented successfully in many different applications in the past (Yang et al. 2019, Li et al. 2016, Wu, Yang, and Wang 2018, García-Medina, Özkan-Haller, and Ruggiero 2014), in particular for the U.S. West Coast as part of a U.S. regional wave resource characterization effort (Yang et al. 2018).

In the present implementation, all integrated wave resource parameters recommended by the International Electrotechnical Commission Technical Specification (IEC-TS) were computed and stored at a high temporal-spatial resolution. The hindcast was validated using available wave buoy measurements from NOAA's National Data Buoy Center (NDBC) and the Coastal Data Information Program (CDIP). Wave parameters for partitioned components over the exclusive

³ This image was obtained from <https://maps.nrel.gov/mhk-atlas>.

economic zone around the major Hawaiian Islands were produced to support development of wave resource classification. Wave climate variabilities in space and time were analyzed based on the long-term model results. Particular attention was given to the nearshore wave resource around the islands.

2.0 Study Area and Data

The mid-Pacific study area, data sources and coverage periods, orographic effects on the air flow that might be important for wave growth, and the selected wind forcing are discussed in the following sections.

2.1 Hawaii

Hawaii has a unique wave climate because of its mid-Pacific location and extensive archipelago. The islands are exposed to swells approaching from the north and south as well as prevailing trade wind waves from the east (Stopa, Cheung, and Chen 2011). Orographic effects caused by the high and steep volcanic mountains produce local complex patterns that require high fidelity wind modeling (Hitzl, Chen, and Nguyen 2014). This suggests the need for a multi-scale approach to accurately model the multimodal sea state and careful data-model comparisons to identify any bias in the prediction of the wave regimes across the region.

2.2 Measured Data for Model Validation

Model validation was conducted using buoy data from NDBC and CDIP. There were 12 wave buoys around Hawaii during the model period of 1979 to 2010 (Table 2.1). The locations of the wave buoys used for model validation are shown in Figure 2.1. The distribution of these wave buoys covers deep and intermediate waters and many points around the islands. Two types of measured data—directional spectra and bulk wave parameters—are available and were used for model validation. Of the 12 buoys, 8 have at least 1 year of spectral data during the study period. These measurements are used to calculate the six IEC-TS recommended parameters for wave resource assessment. Model-data comparisons between these parameters are presented in Section 4.0.

Table 2.1. Summary of available data derived from the wave buoys during the hindcast period.*

Agency	Buoy	Longitude	Latitude	Depth (m)	Period		Years		
					Param	2D Spec	Param	1D	2D
CDIP	034	-157.587	21.315	91	1981 – 1996		11.4	11.4	0
CDIP	039	-159.833	22.007	110	1982 – 1993		3.8	3.8	0
CDIP	098	-157.678	21.415	89	2000 – 2010	2000 – 2010	9.5	9.5	9.5
CDIP	106	-158.117	21.671	200	2004 – 2010	2004 – 2010	7.9	7.9	7.9
CDIP	146	-157.010	20.788	201	2007 – 2010	2007 – 2010	2.9	2.9	2.9
CDIP	164	-158.303	21.101	3150	2009 – 2010	2009 – 2010	1.1	1.1	1.1
NDBC	51000	-153.781	23.535	4811	2009 – 2010	2009 – 2010	1.6	1.6	1.6
NDBC	51001	-162.000	24.453	4895	1981 – 2010	2006 – 2010	24.3	11.7	3.3
NDBC	51002	-157.696	17.037	4934	1984 – 2010		22.8	12.8	0
NDBC	51003	-160.569	19.289	4920	1984 – 2010		23.0	12.8	0
NDBC	51004	-152.364	17.604	4998	1984 – 2010	2009 – 2010	21.0	11.1	0.1
NDBC	51101	-162.075	24.361	4849	2008 – 2010	2008 – 2010	1.8	1.8	1.8

*Param refers to the availability of bulk wave parameters, spec refers to the availability of spectra.

Number of years available for frequency (1D) and directional (2D) spectra are listed separately. The depth reported in this table is approximate because the buoys drift.

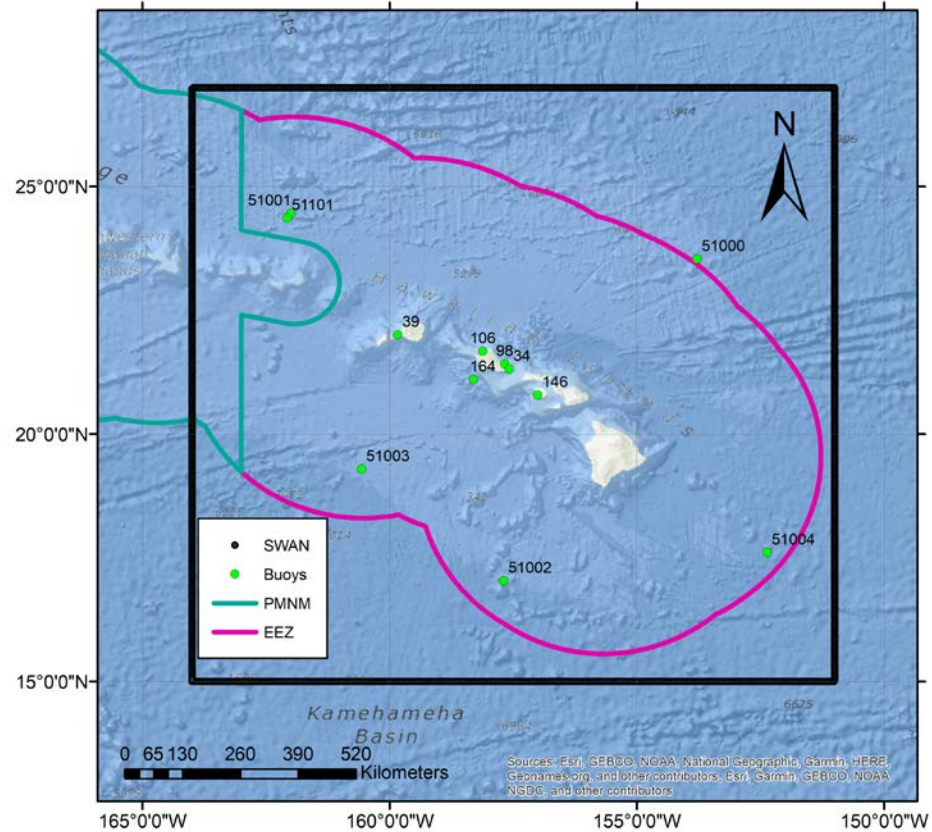


Figure 2.1. Wave buoy stations for model validation. PMNM stands for the Papahānaumokuākea Marine National Monument (PMNM), EEZ for exclusive economic zone. SWAN boundary is shown as a black box.

2.3 Atmospheric Forcing

In this study, the model hindcast covered a period of 32 years from 1979 to 2010, which corresponds to the period of the Climate Forecast System Reanalysis (CFSR), produced by the National Centers for Environmental Prediction (NCEP). The wind forcing data (wind speeds and directions) for the wave hindcast were obtained from CFSR and interpolated onto the model grid points at hourly intervals. Comparison of CFSR wind speed with observed data at a number of NDBC buoy stations shows good agreement and indicates that the reanalysis reasonably captures the diurnal and seasonal variabilities. The CFSR data meet the minimum 1-hour temporal resolution requirements for design assessments, and their 55.6 km minimum resolution is close to the feasibility class requirement of 50 km specified by the IEC-TS (IEC 2015). Figure 2.2a shows an example of global CFSR wind speed distribution with the SWAN domain outlined.

The sea ice coverage is also included in the NCEP CFSR data set in the NCEP T382 Gaussian Grid with a spatial resolution of 38 km. The sea ice data were subsequently re-projected onto the same 0.5×0.5 arc-degree regular grid as the wind forcing data and implemented as daily temporal resolution.

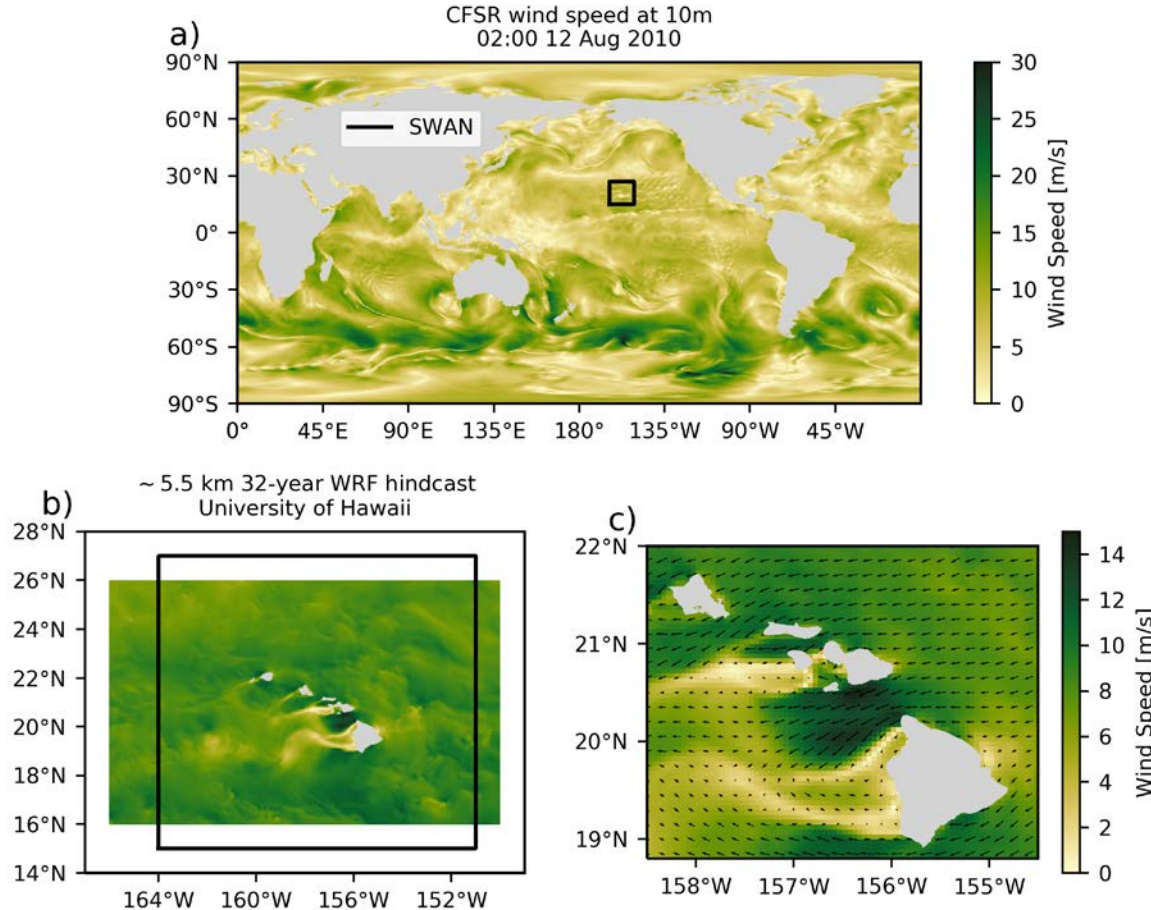


Figure 2.2. (a) The global distribution of CFSR wind field on 06:00 14 January 2010. The SWAN domain is outlined in black. A snapshot of the high-resolution Weather Research and Forecasting wind field over the complete domain (b) and a close-up to show the details resolved by the model (c). Panels (b) and (c) are on the same color scale.

The CFSR wind field and ice coverage were the primary input to the WW3 model, which provides the boundary conditions to the SWAN domain around Hawaii. A high-resolution Weather Research and Forecasting (WRF) model defines the local wind forcing. The WRF domain covers most of the SWAN model, as shown in Figure 2.2b. This model captures the local wind variability due to orographic effects (Figure 2.2c). The WRF hindcast shows good performance when compared with QuickSCAT winds; it has root-mean-squared errors of 1.5 m/s on the windward side of the islands and up to 3 m/s on the lee side (Li et al. 2016).

The SWAN model extends beyond the boundaries of the WRF model to cover the entire exclusive economic zone (EEZ). A blended wind product between CFSR and WRF was used to provide full coverage of the SWAN domain. The downscaling of the WRF model from the CFSR model for Hawaii makes both models consistent. For the wind blending a cubic spline interpolator was used between the boundaries of the WRF model and the nearest latitude of the CFSR model. Figure 2.3 shows an example wind field showing the interpolated wind fields between two parallels (26°N and 26.5°N). Both models are on a regular spherical grid, so these two parallels are 0.5° apart. The instantaneous zonal and meridional wind components from the

WRF and CFSR models were interpolated to fill the data gap. Thus, the final wind field has a 0.05° resolution over the SWAN model domain. The downscaled and interpolated wind data with a 5 km spatial resolution and 1-hour temporal resolution exceed the 50 km and 3-hour resolution requirements in the IEC-TS Class 2 assessment.

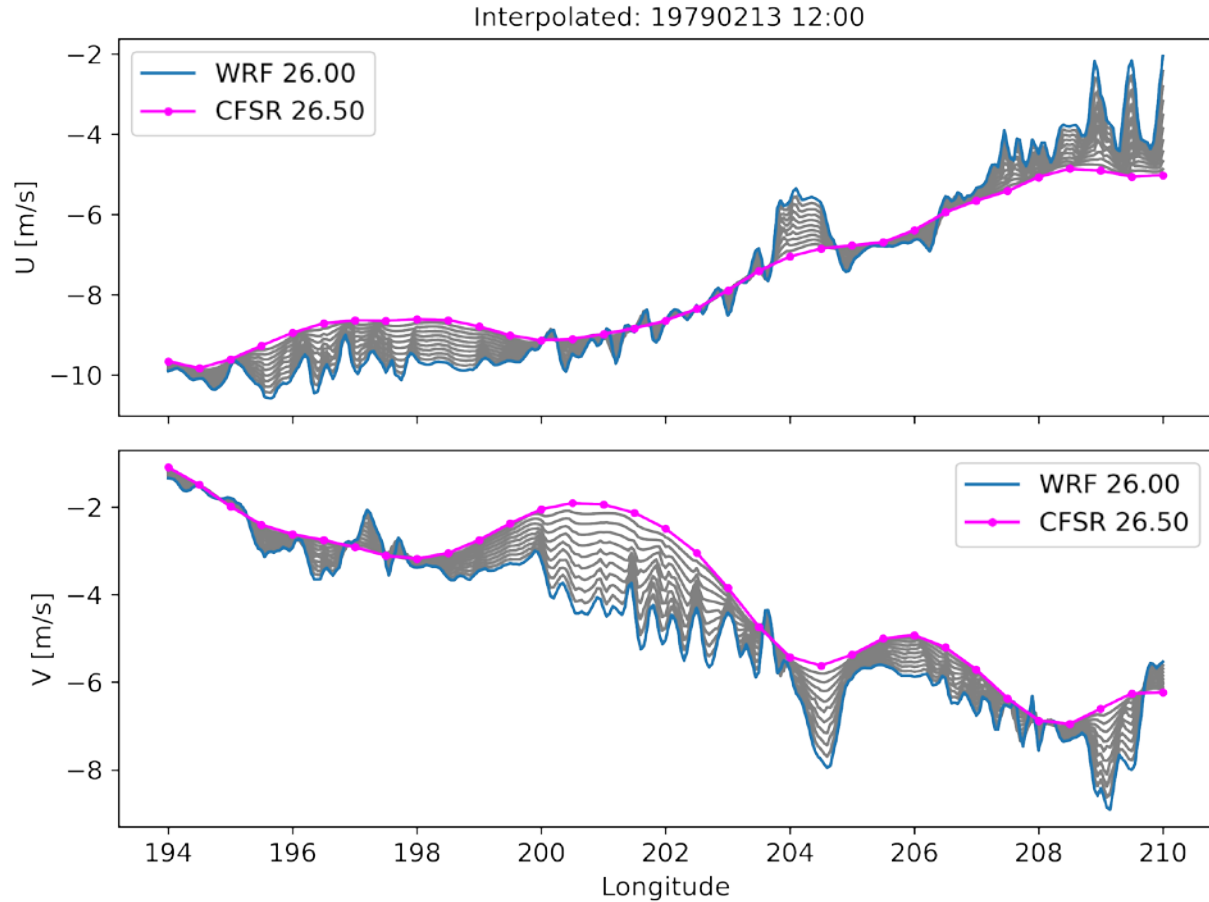


Figure 2.3. WRF, CFSR, and interpolated zonal (top) and meridional (bottom) instantaneous wind profiles.

3.0 Methods

A telescopic nested-grid modeling approach with structured WW3 (v5.16) and unstructured-grid SWAN (v41.10) models was used in this study. Two levels of WW3 nested grids were set up to describe wave climates from global to regional scales and provide boundary conditions to the high-resolution nearshore SWAN model for Hawaii. The configurations of the WW3 model grids are listed in Table 2.1. The global model on the Level 1 (L1) grid has a resolution of 0.5 arc-degree, about 52.2 km in the zonal direction at 20°N and 55.6 km in the meridional direction. The L2 model covers the entire EEZ of Hawaii, including the Papahānaumokuākea Marine National Monument (PMNM), as shown in Figure 2.1 at a 4 times higher resolution of 13 km. Boundary conditions for the high-resolution SWAN model are taken from the L2 model. Based on a wave model test bed study (Yang et al. 2017) and the regional wave hindcast for the West Coast (Yang et al. 2018), the ST4 source term package (Ardhuin et al. 2010) in WW3 improves model prediction of wave power density. Therefore, the ST4 physics package was used in all WW3 model runs conducted in this study.

3.1 WW3 Model Configuration

Two levels of structured-grid WW3 models were used, similar to previous studies conducted in the Pacific Northwest (Yang et al. 2017, Wu, Yang, and Wang 2018, García-Medina, Özkan-Haller, and Ruggiero 2014, García-Medina et al. 2013, Yang et al. 2018) and Hawaii (Stopa, Cheung, and Chen 2011, Li et al. 2016). The L1 model is based on the global WW3 model of the NOAA NCEP that has a 0.5-degree grid resolution. The L2 regional grid that has a resolution of 7.5 arc-minutes was nested into the global model; the bathymetry comes from theETOPO1 global relief model (Amante and Eakins 2009), which has a spatial resolution of 1 arc-minute. The effect of islands with areas smaller than or similar to the grid size was included in the model by means of a sub-grid module (Tolman 2003). The model domain coverage, spatial resolution, and grid size, and the number of active grid points for the WW3 models are summarized in Table 3.1.

Table 3.1. Summary of nested WW3 model grids.

Grid Name	Coverage	Resolution (long x lat)	Resolution [km] (zonal x meridional) at 20°N	Active Grid Points	Agency
Global Grid L1	77.5°S – 77.5°N 0 – 360°W	0.5° × 0.5° (30' × 30')	52.2 × 55.6	191,352	NOAA
Nested Grid L2	12.0° – 34.0°N 175°E – 145.0°W	0.125° × 0.125° (7.5' × 7.5')	13.1 × 13.9	56,723	PNNL

The time steps used in the WW3 model are summarized in Table 3.2. For WW3, each model grid requires four time steps: (1) the global time step Δt_g , (2) the spatial propagation time step Δt_{xy} , (3) the intra-spectral propagation time step Δt_k , and (4) the source term time step Δt_s (WW3DG 2016). The spatial propagation time step Δt_{xy} must conform with the Courant–Friedrichs–Lowy (CFL) limit to ensure model stability.

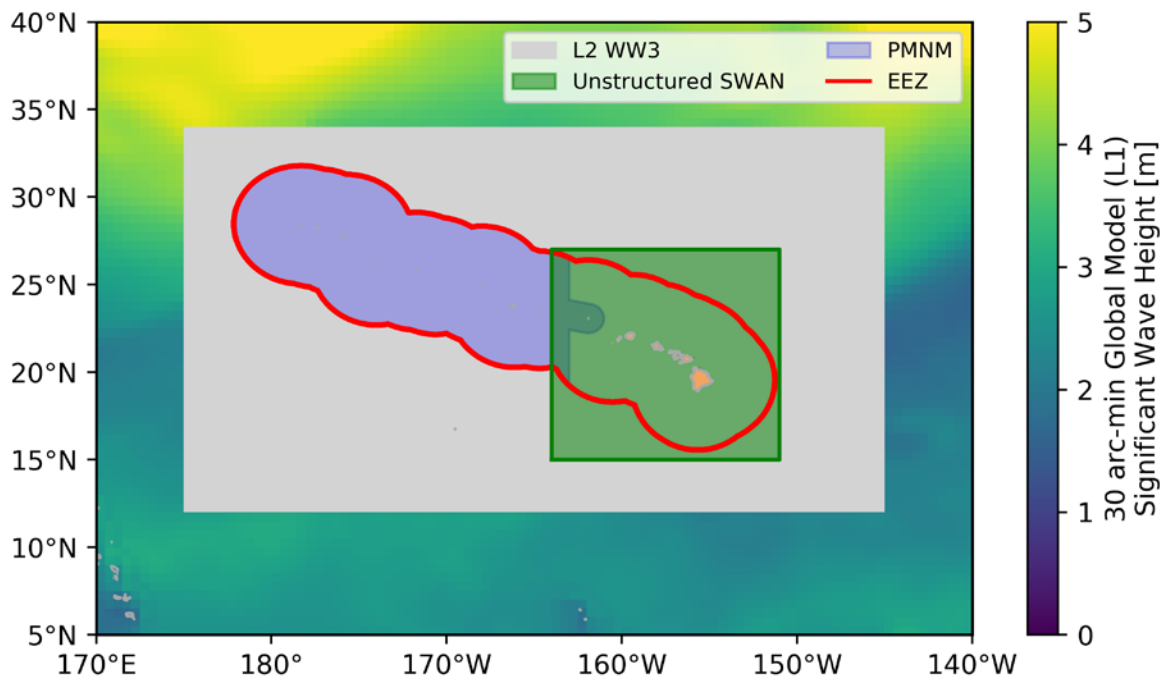
Table 3.2. Time steps for WW3.

Nested Grid	Δt_g (s)	Δt_{xy} (s)	Δt_k (s)	Δt_s (s)
L1	1,800	600	900	30
L2	450	150	225	15

All WW3 simulations used 24 direction bins from 0 to 360 degrees and 29 frequency bins with a logarithmic increment factor of 1.1 from 0.035 Hz to 0.505 Hz. This spectral resolution meets the minimum requirements specified in the IEC-TSSs(IEC 2015), i.e., a minimum of 25 frequency components and 24 to 48 directional components and a frequency range covering at least 0.04 to 0.5 Hz.

3.2 Unstructured-grid SWAN Model Configuration

An unstructured-grid SWAN model is used in high-resolution nearshore simulations to account for wave transformation processes in shallow water. The model was developed to cover the EEZ around the major Hawaiian Islands, as shown in Figure 3.1. The model mesh was created starting from the coastlines and expanding to fill the entire domain. The coastline from the major Hawaiian Islands was obtained from the state of Hawaii, Office of Planning,⁴ and the Global Self-consistent, Hierarchical, High-resolution Geography v2.3.7 database was used for the Northwestern Hawaiian Islands (Wessel and Smith 1996). The coastline polygons were subsampled with a maximum resolution of 300 m to ensure good nearshore coverage consistent with a Class 2 IEC-TS assessment. Selected images of the mesh are shown in Figure 3.2.

**Figure 3.1. Model domains for the Hawaii wave hindcast.**

⁴ <http://planning.hawaii.gov/gis/download-gis-data/> Accessed 23 January 2019.

The mesh size is specified to have a resolution finer than 500 m within 30 km from the coastline and coarser than 300 m for water depths less than 500 m. This ensures the model has enough resolution to capture the effect of underwater volcanoes and small islands in wave propagation, as seen in the northwestern end of the domain in Figure 3.2a. This effect has been shown to be important in other regions (e.g. Sosa, Cavalieri, and Portilla-Yandun 2017, García-Medina et al. 2013). Smooth transitions were specified during mesh development by restricting the area change between neighboring elements to a maximum of 10% (see Figure 3.2b-d). At the ocean boundaries the mesh has a resolution of 5 km, resulting in a ratio with the boundary forcing (WW3-L2) of less than 3. The resulting model has 700,414 nodes and 1,393,661 elements.

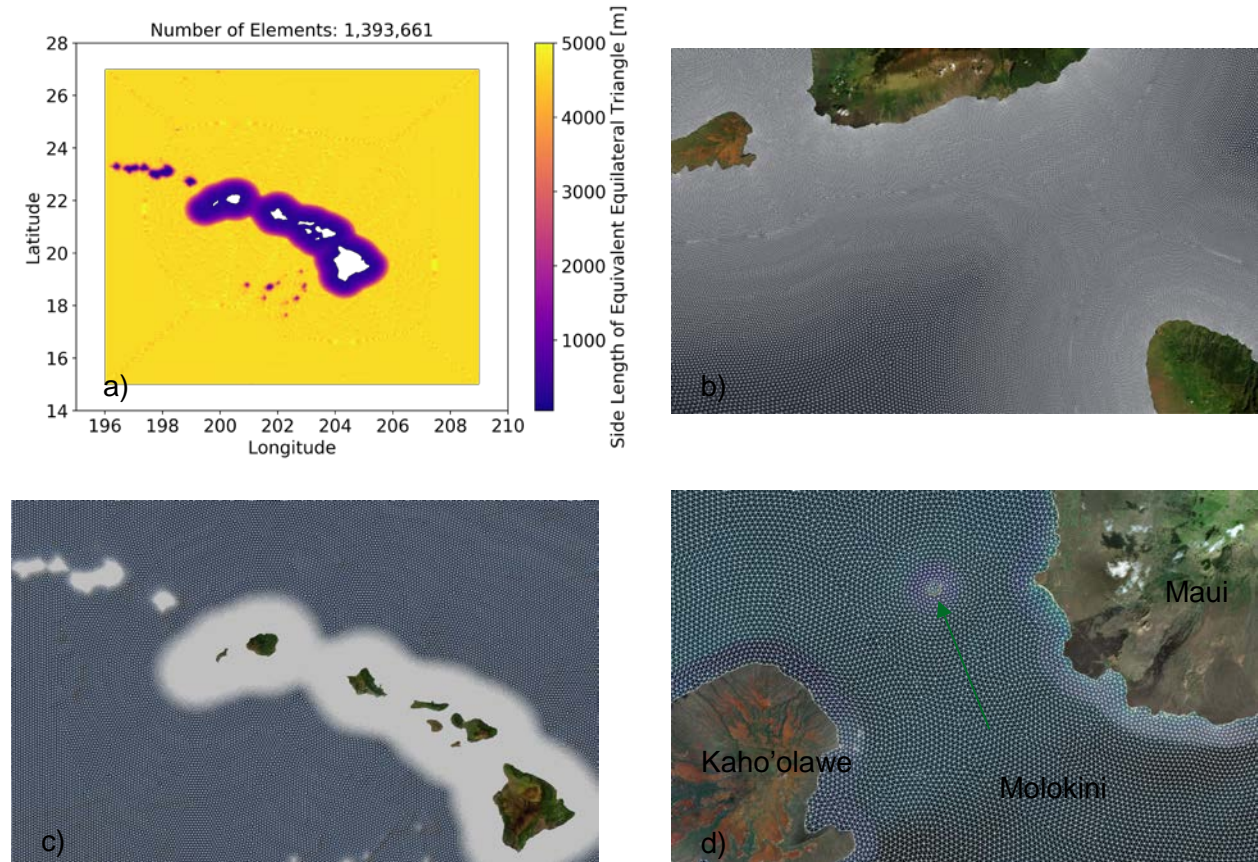


Figure 3.2. (a) Resolution of the mesh based on the element area. (b-c) Mesh details showing density, coastline, and element transition.

The model bathymetry was interpolated from multiple sources in the following order of priority:

1. Hawaii digital elevation model with 50 m spatial resolution from the University of Hawaii⁵
2. Digital elevation model of Ka'ula with 1 km spatial resolution⁵
3. Multibeam survey of Nihoa with 20 m spatial resolution⁶
4. ETOPO1 for global coverage (Amante and Eakins 2009).

The model is configured with the World Geodetic System 84 spheroid and the mean sea level as the vertical datum.

⁵ <http://www.soest.hawaii.edu/HMRG/multibeam/bathymetry.php> Accessed December 2018.

⁶ <http://www.soest.hawaii.edu/pibhmc> Accessed 9 February 2019.

3.2.1 Model Convergence

Model convergence tests were performed to find an optimal balance between model accuracy and runtime.

3.2.1.1 Numerical Solution

In its unstructured mesh version, the SWAN model implements a first-order implicit Euler scheme that is not restrained by the CFL condition (Zijlema 2010). This results in an unconditionally stable model whose the accuracy is not affected by the time step. Therefore, the optimal time step is chosen based on model-data comparisons. Three 1-month simulations were performed to determine an adequate time step for satisfactory results. Similar to the regional hindcast effort for the West Coast (Yang et al. 2018), a 10-minute time step (Δt) is sufficient to resolve the offshore wave conditions. Close to the offshore boundary at NDBC Buoy 51101, the model produces qualitatively good results particularly when predicting the arrival time of swell such as the 23 s period on 16 January 2010 (Figure 3.3). This is not unexpected given the relatively short distance of that station from the boundaries (Figure 2.1). However, far from the model boundaries, close to the main islands, the arrival time of storms are strongly affected by the integration time step. Figure 3.4 shows model-data comparisons at the Waimea Buoy. The arrival time of the swell lags 24 hours when using an integration time step of 10 min. Significantly better model agreement is found as the time step is reduced.

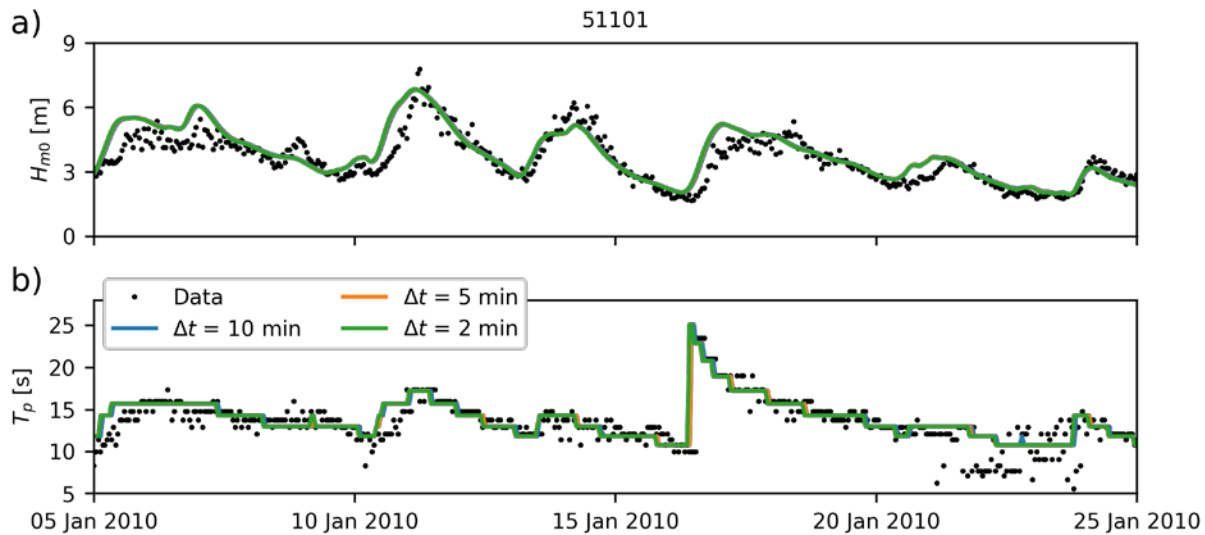


Figure 3.3. Model-data comparisons for significant wave height (a) and peak wave period (b) for different integration time steps close to the SWAN boundary.

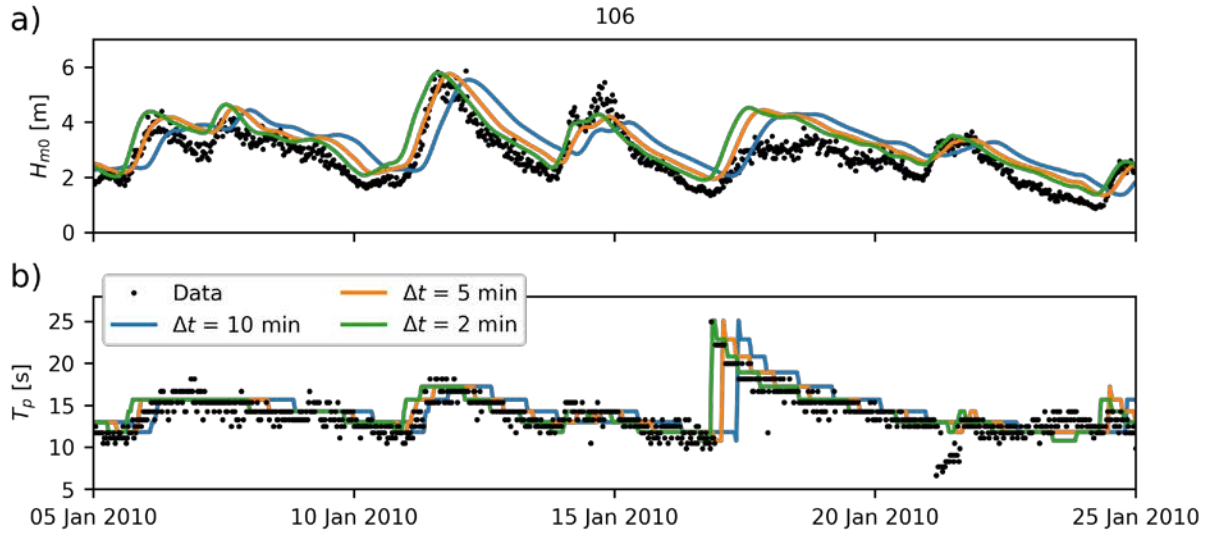


Figure 3.4. Same as Figure 3.3 but for CDIP 106, which is approximately 900 km from the northwestern model boundary.

A quantitative comparison is shown in Table 3.3 by computing error statistics for bulk wave parameters. Significant improvement of the model performance in the nearshore is seen for both significant wave height and peak wave period with the smaller integration time step. Based on this sensitivity analysis, an integration time step of 2 minutes was chosen for all model simulations.

Table 3.3. Model-data comparisons for different integration time steps during January 2010.

Buoy	Simulation	Significant Wave Height			Peak Wave Period		
		RMSE [m]	PE [%]	R	RMSE [s]	PE [%]	R
51101	Δt = 2 min	0.60	9.3	0.88	2.08	7.2	0.68
	Δt = 5 min	0.59	9.4	0.88	1.99	7.2	0.71
	Δt = 10 min	0.57	9.5	0.89	1.98	7.3	0.72
	Δt = 2 min	0.58	19.2	0.91	1.54	3.3	0.77
106	Δt = 5 min	0.60	20.0	0.89	1.76	3.9	0.69
	Δt = 10 min	0.84	23.3	0.83	2.32	5.2	0.46

To solve the interactions between directional quadrants, SWAN employs a Gauss-Seidel technique that operates independently on the quadrants of the spectral computational grid. Multiple iterations might be needed to reach a converging solution. Because the number of iterations is directly proportional to the runtime, it is desirable to evaluate the model's sensitivity to this parameter. Figure 3.5 shows the number of iterations required to achieve convergence for a model configuration for which the maximum number of iterations was set at 5. The model was found to converge very fast, as expected from the node ordering scheme employed in the solution algorithm (Zijlema 2010). Only for very few instances does the model need more than two iterations to achieve convergence.

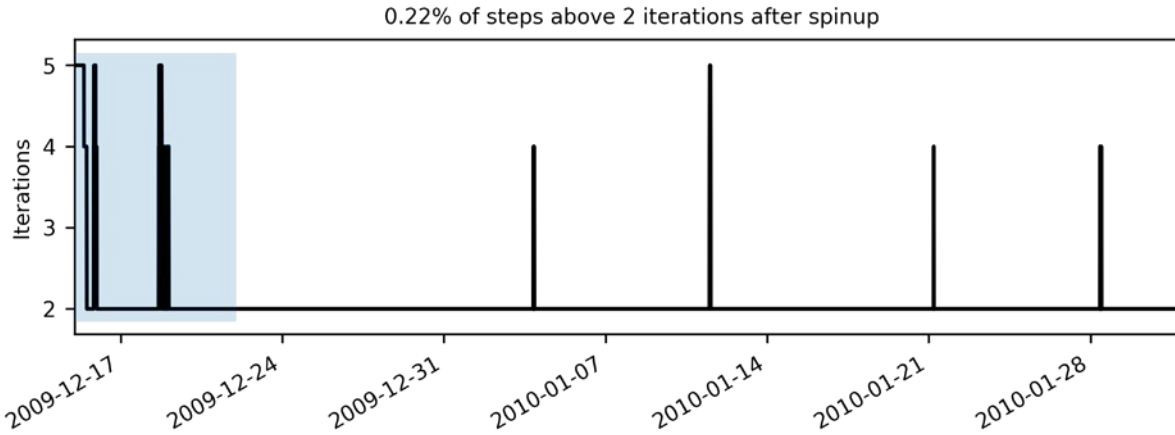


Figure 3.5. Convergence time series for a simulation with maximum number of iterations set at 5.

Given that more than 99.5% of the time the model converged with two iterations, we evaluated the results with one iteration. However, the convergence time series with one iteration cannot be plotted, so we compared the significant wave heights at all buoys and show two representative sets of results in Figure 3.6. The significant wave height from simulations with one iteration is very similar to that with two iterations. These results are in agreement with the findings of Allandadi et al. (2019) using a similar model on the U.S. East Coast. Thus, we used one iteration in computing the interactions in the directional quadrants and a time step of 2 minutes based on the sensitivity analysis.

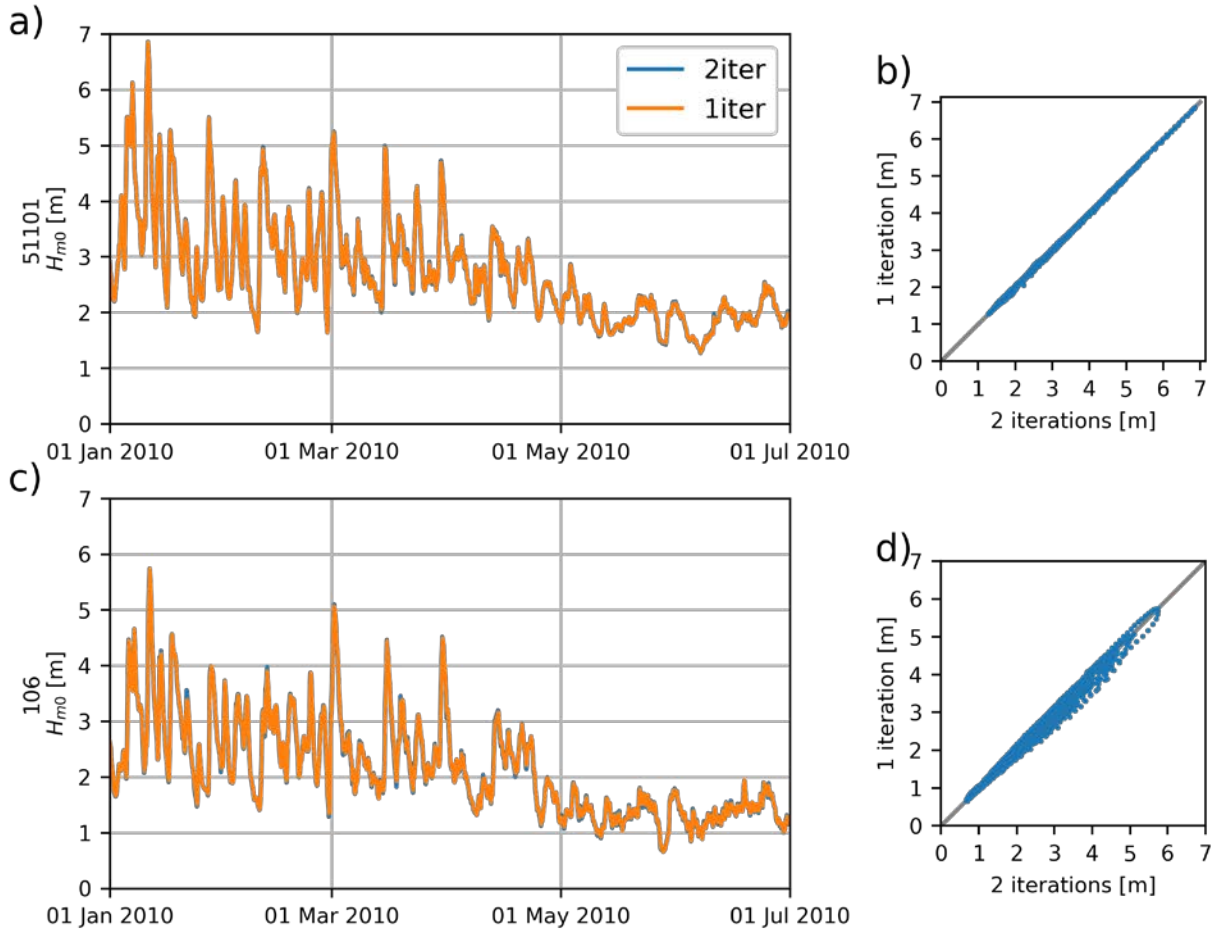


Figure 3.6. Significant wave height comparison at Buoy (a,b) 51101 and (c,d) Buoy 106 for a six-month simulation with one and two iterations of the implicit model solution.

3.2.1.2 Spectral Resolution

Spectral resolution is important when describing wave refraction and mitigating the Garden Sprinkler Effect (GSE; (Booij and Holthuijsen 1987)). The IEC-TS recommends a directional resolution of 10° for a Class 2 assessment using numerical models. When an earlier version of the model mesh was tested with that resolution, GSE was evident around the islands (as shown in Figure 3.7a). The GSE was mitigated by increasing the directional resolution to 7.5° in combination with the reduced time step of 2 minutes (Figure 3.7d). Figure 3.7 shows snapshots of significant wave height at the same time stamp with different model configurations to illustrate the sensitivity analysis made to ensure this effect was mitigated. The GSE was assessed qualitatively and was found to be greatly reduced by the combination of parameters selected.

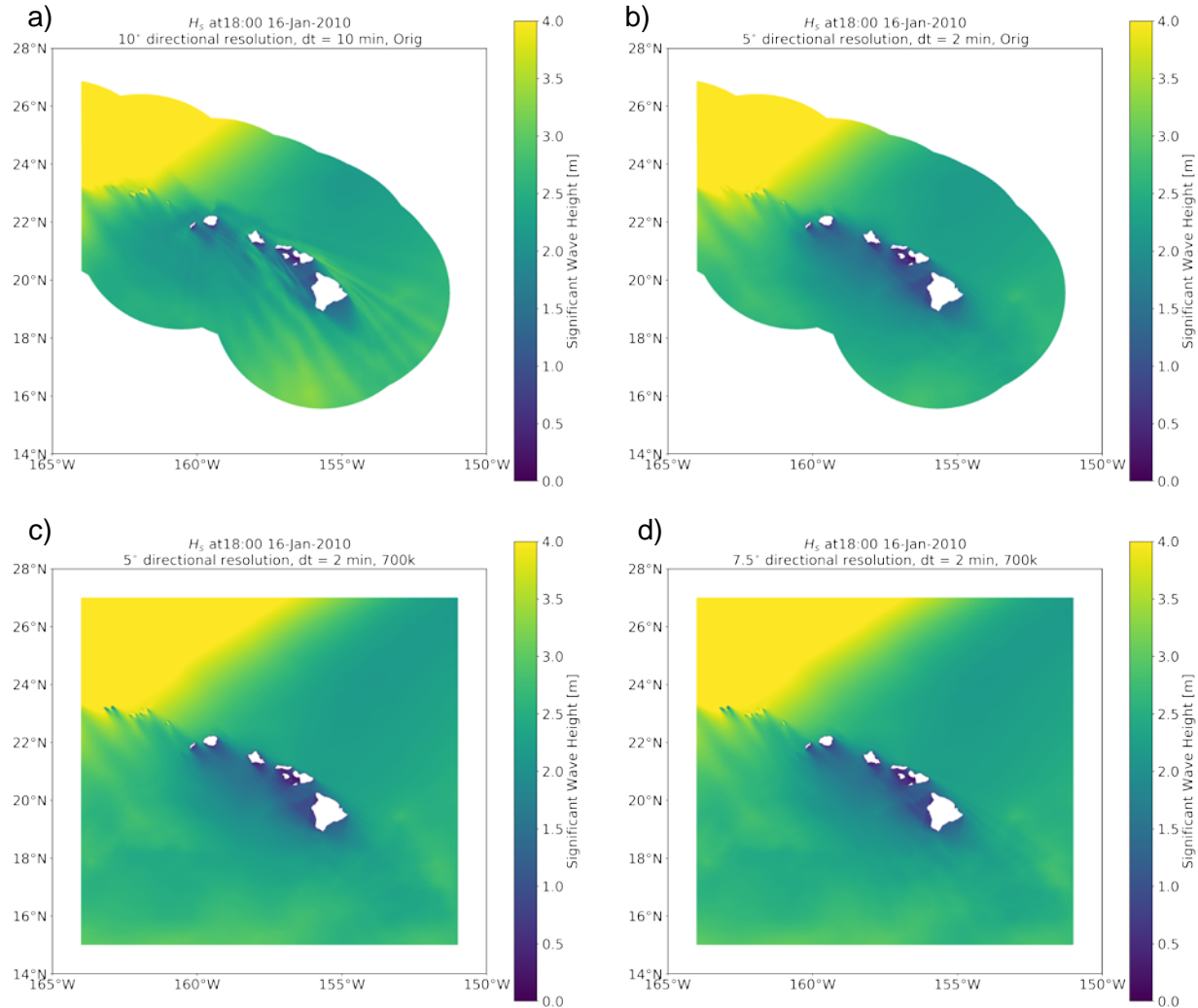


Figure 3.7. Significant wave height for different iterations of the model development.

3.2.2 Source Terms

In our previous studies of the U.S. West Coast and Alaska the default SWAN source term package of (Janssen 1989, 1991) was implemented with successful results. However, Li et al. (2016) implemented the source term package of van der Westhuysen, Zijlema, and Battjes (2007) for a hindcast study for Hawaii. Therefore, the differences between both source terms were investigated within the context of the current numerical model. Figure 3.8 shows the computed significant wave height and peak period time series at selected buoys using the two source term packages for January 2010. We found that both source term packages produce nearly identical results, indicating equally good performance. Thus, for consistency with our previous studies and to simplify comparisons between regions, the default SWAN source term package was selected for wind growth and whitecapping.

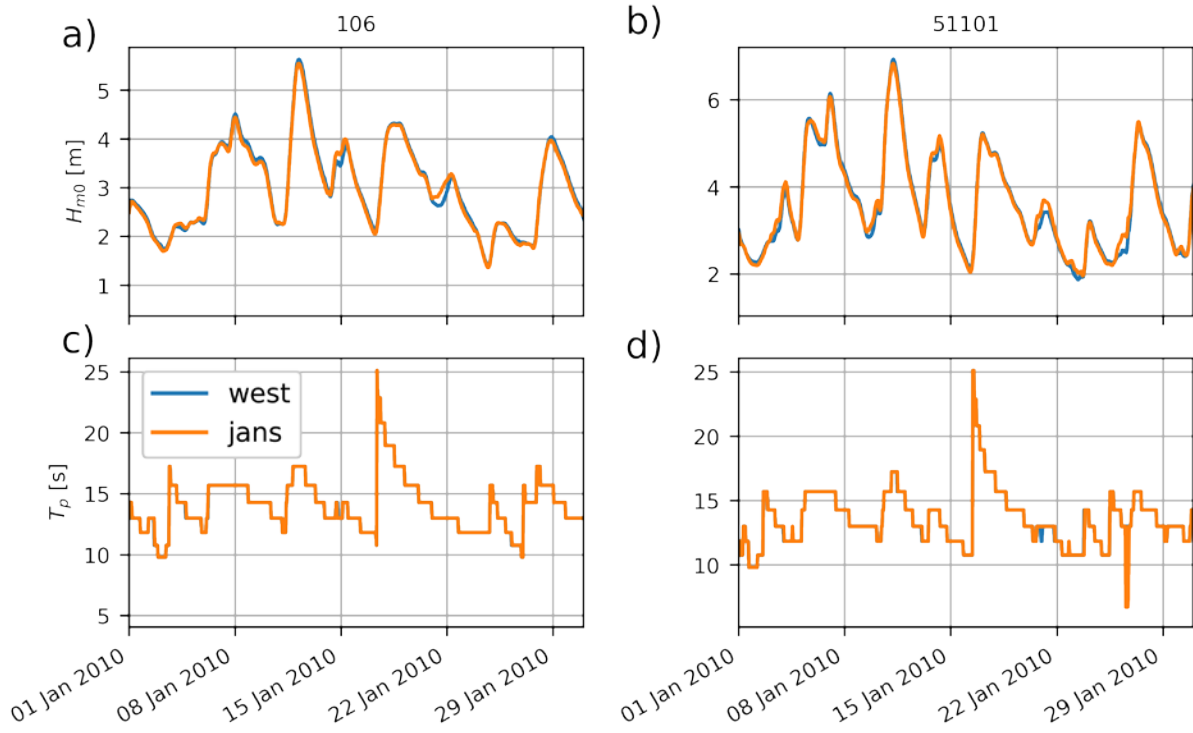


Figure 3.8. Model sensitivity to source term package for significant wave height (a-b) and peak wave period (c-d) at selected buoys.

In addition to the wind related source terms, the source terms for bottom friction, depth-induced breaking, and triad interactions were activated for the model simulations. No sensitivity analysis for these source terms was performed and thus the model was configured with the default values.

3.2.3 Practical Aspects

The SWAN model was executed using 240 CPUs available through Research Computing at Pacific Northwest National Laboratory. One year of elapsed time took 10 days of wall clock time. A total of 35 TB of data were produced based on the output plan. For practical reasons the 32-year hindcast was partitioned into 64 segments. The model run for each segment was started 7 days in advance to ensure adequate time for propagation of trans-Pacific swells to reach the interior of the model domain. An initial condition was estimated using the stationary mode for the time-dependent computation. The 7-day lead time along with the estimated initial condition was determined based on a sensitivity analysis. The results are cross-compared with a cold-started computation that has been continuously running for 6 months free of initial condition errors. Figure 3.9 shows the absolute error in significant wave height as a function of the spin-up time, averaged over the entire domain. The model errors reduce to less than 1% within 2 days of spin-up. Additionally, we looked at the spatial distribution of errors. Using December 2007 as an example, Figure 3.10 shows how the error is significant far from the boundaries and is gradually reduced with time. Based on this analysis, we determined that a 7 day ramp-up period is sufficient to ensure results free of initial condition errors.

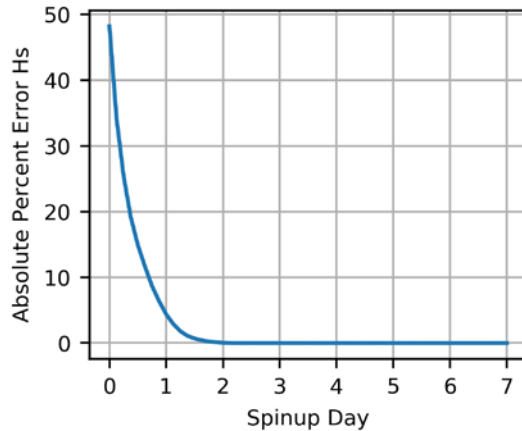


Figure 3.9. Absolute percent error between a cold-started simulation and a simulation that has been continuously running for 6 months.

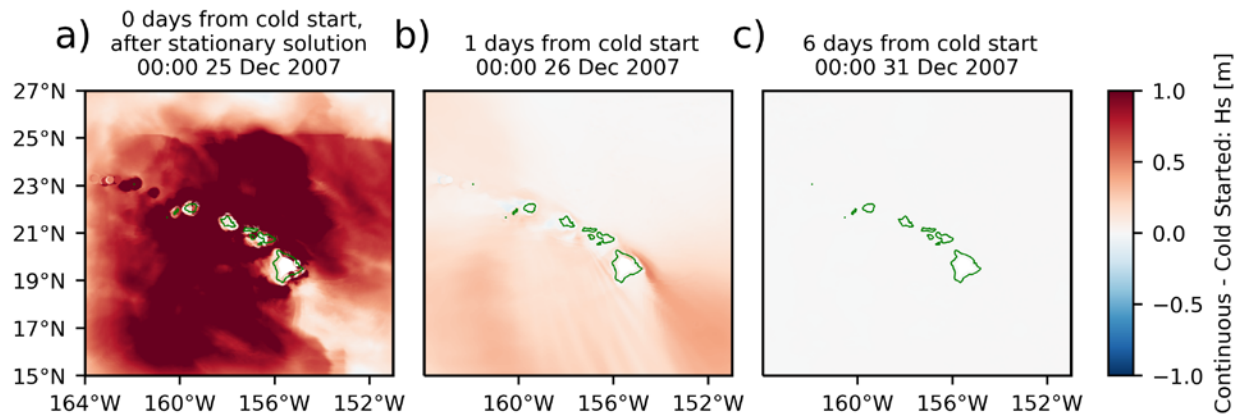


Figure 3.10. Spatial distribution of errors in significant wave height due to model spin-up. Model errors after an initial stationary solution (a), after 1 day of non-stationary simulation (b), and after 6 days (c) are shown with respect to a simulation that is not affected by spin-up effects.

The final model configuration is provided in Table 3.4, which meets a Class 2 wave resource assessment based on the IEC-TS.

Table 3.4. IEC-TS homologation table for a Class 2 (Feasibility) study for the model setup

Criterion	IEC Requirement	PNNL Hawaii Study
Coarsest spatial resolution	500 m	Maximum of 300 m within 30 km from shore
Minimum output intervals	3 h	3 h
Minimum number of wave frequency bins	25	31
Minimum number of directional bins	36	48

4.0 Model Hindcast and Validation

The regional wave hindcast for Hawaii was conducted using the unstructured-grid SWAN model for the period of 1979–2010. In this section we present relevant results for wave resource characterization and model validation, and an inventory of the model output. Model hindcast and validation for the six IEC-recommended wave resource parameters are discussed.

4.1 IEC Resource Parameters

The six wave resource parameters recommended by IEC-TS (2015) were calculated from the model results at every grid point and compared with available measurements. The six IEC parameters include omnidirectional wave power, significant wave height, energy period, spectral width, direction of maximum directionally resolved wave power, and directionality coefficient — all of which are defined below.

The omnidirectional wave power, J , is the sum of the contributions to energy flux from each of the components of the wave spectrum,

$$J = \rho g \sum_{i,j} c_{g,i} S_{ij} \Delta f_i \Delta \theta_j \quad (1)$$

where ρ = the density of sea water,
 g = the acceleration due to gravity,
 $c_{g,i}$ = the group velocity,
 Δf_i = the frequency bin width at each discrete frequency index i , and
 $\Delta \theta_i$ = the direction bin width at each discrete direction index j .

Directionally integrated parameters are calculated from one-dimensional (unresolved) frequency variance density using the equation

$$S_i = \sum_j S_{ij} \Delta \theta_j. \quad (2)$$

For the present study, the significant wave height is defined as the zeroth spectral moment

$$H_s \sim H_{m0} = 4\sqrt{m_0}, \quad (3)$$

where the moments of a variance spectrum are generally defined as

$$m_n = \sum_i f_i^n S_i \Delta f_i. \quad (4)$$

H_s is typically paired with the energy period, T_e , calculated as

$$T_e = \frac{m_{-1}}{m_0}, \quad (5)$$

to define a sea state. The energy period is the variance-weighted mean period of the directionally unresolved variance density spectrum. It is preferred over the peak period, because it is not sensitive to the spectral shape.

The spectral width, ϵ_0

$$\epsilon_0 = \sqrt{\frac{m_0 m_{-2}}{(m_{-1})^2} - 1}, \quad (6)$$

is a measure of the spreading of energy in the wave spectrum. The directionally resolved wave power is the sum of the wave power at each direction, θ :

$$J_\theta = \rho g \sum_{i,j} c_{g,i} S_{ij} \Delta f_i \Delta \theta_j \cos(\theta - \theta_j) \delta$$

$$\begin{cases} \delta = 1, & \cos(\theta - \theta_j) \geq 0 \\ \delta = 0, & \cos(\theta - \theta_j) < 0 \end{cases} \quad (7)$$

where J_θ is the directionally resolved wave power in direction θ . The maximum time-averaged wave power propagating in a single direction, J_{θ_J} , is the maximum value of J_θ . The corresponding direction, $\theta_{J_{max}}$, is the direction of maximum directionally resolved wave power and describes the characteristic direction of the sea state.

The directionality coefficient, d , is the ratio of the maximum directionally resolved wave power to the omnidirectional wave power,

$$d_\theta = \frac{J_{\theta_{J_{max}}}}{J}, \quad (8)$$

which is a characteristic measure of directional spreading of wave power.

Of the six IEC parameters, only two—significant wave height (H_{m0}) and energy period (T_e)—are calculated in SWAN as default bulk parameters. Therefore, the SWAN source codes were modified to calculate the other four IEC parameters (J , ϵ_0 , θ_J , d_θ) internally and add them in the output options (Yang et al. 2018).

Figure 4.1 shows the spatial distributions of the six IEC parameters averaged over 32 years. In general, higher wave power density occurs on the north and northeastern shores of the islands (Figure 4.1a). Those shores are exposed to the north swells, which have wave power above ~30 kW/m. The wave power is focused on the southeastern side of the seamounts and small islands northwest of Ni'ihiwai due to refraction. The average H_{m0} follows the same pattern as the wave power. In general, the energy period is on the order of 10 s, except for the western shore of Hawaii, where the south swell is dominant because of the sheltering of the winter north swells and the year-round east wind waves. The spectral width is smaller in open waters than in the sheltered areas of the wind waves. The maximum directionally resolved wave power arrives from the north-northeast on average (Figure 4.1e) for the northern and northeastern shores of the major islands. South of the archipelago the waves travel from the northeast. Finally, alongshore variations in the directionality coefficient are present around all islands.

The directionality coefficient is high on the lee side of Ni'ihi and Kaua'i because of being exposed to the northwestern swell, which is quite regular over the course of the year.

Spatial distributions of the six parameters averaged for each month from January to December are provided in Appendix A. The monthly averages in January (highest average J) and July (lowest average J) are shown in Figure 4.2 and Figure 4.3, respectively, to demonstrate the strong seasonal variations. J , H_s , T_e , and d_θ are much greater in the winter because of the north swell. Weak seasonal variations are also observed in ϵ_0 and θ_J , which feature slightly higher values in the summer because of the trade wind waves.

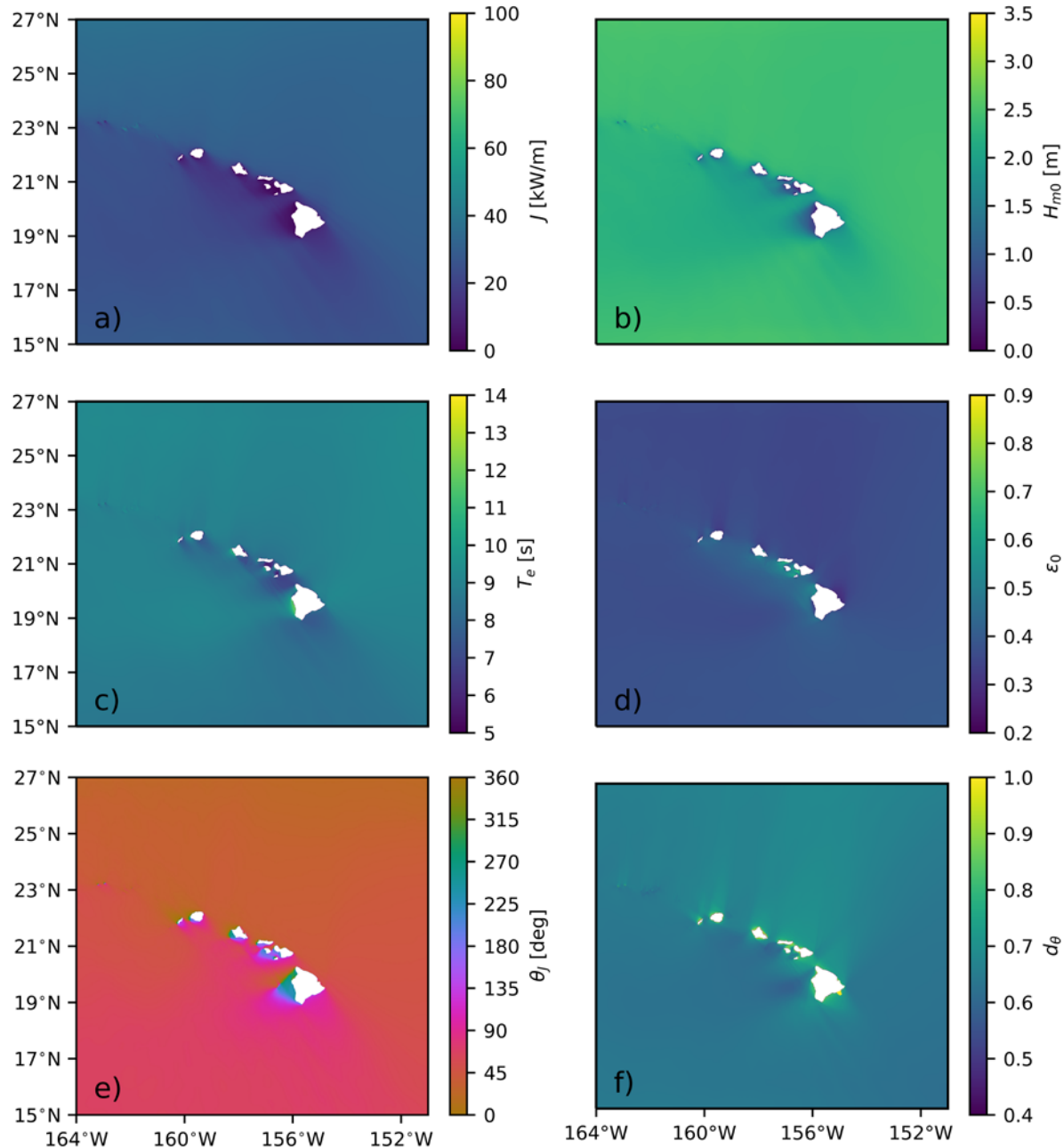


Figure 4.1. Simulated 32-year annual distribution of six IEC wave resource characterization parameters: (a) omnidirectional wave power, (b) significant wave height, (c) energy period, (d) spectral width, (e) direction of maximum directionally resolved wave power, and (f) directionality coefficient.

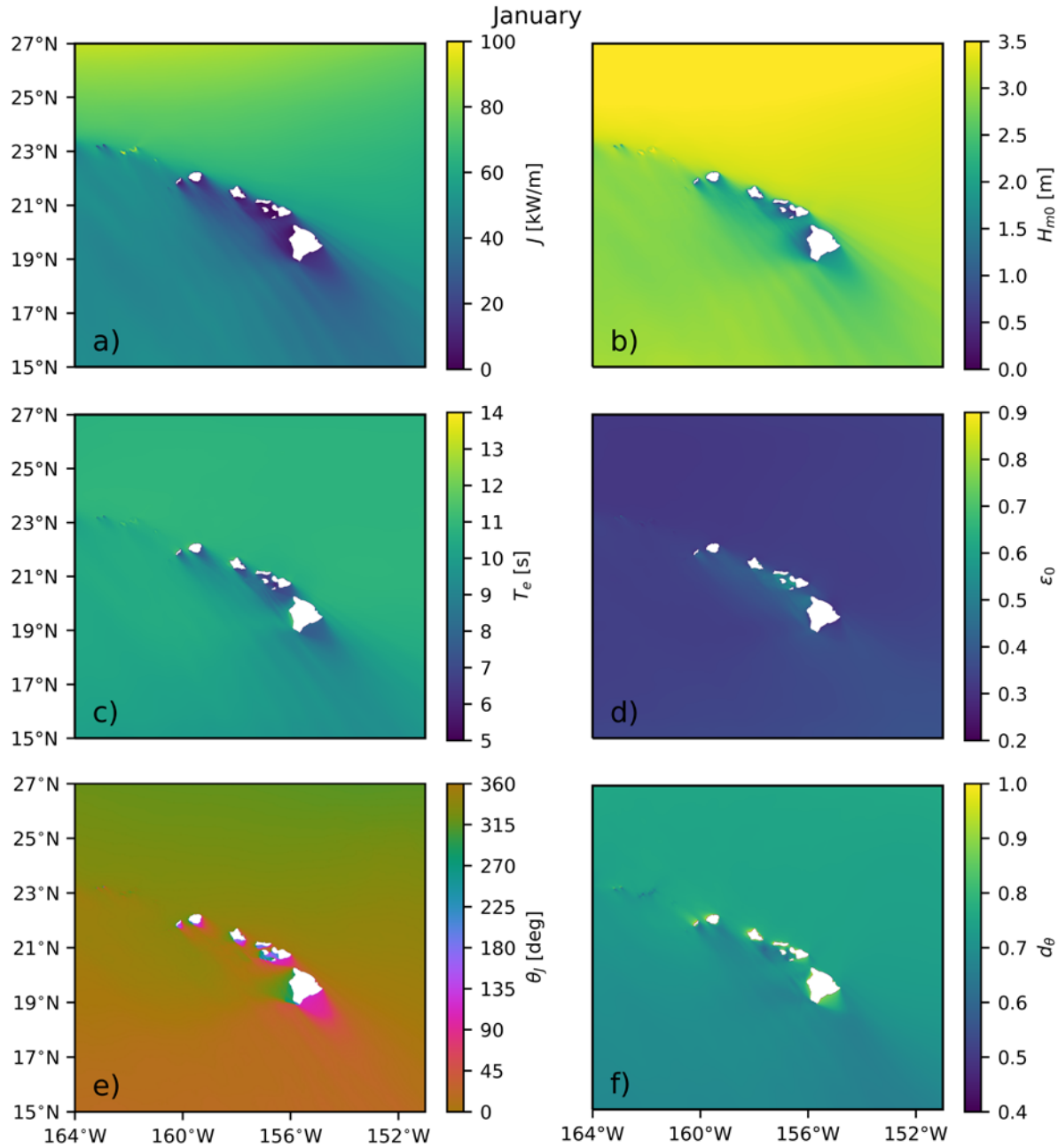


Figure 4.2. Simulated monthly distribution of six IEC wave resource parameters in January:
 (a) omnidirectional wave power, (b) significant wave height, (c) energy period, (d)
 spectral width, (e) direction of maximum directionally resolved wave power, and (f)
 directionality coefficient.

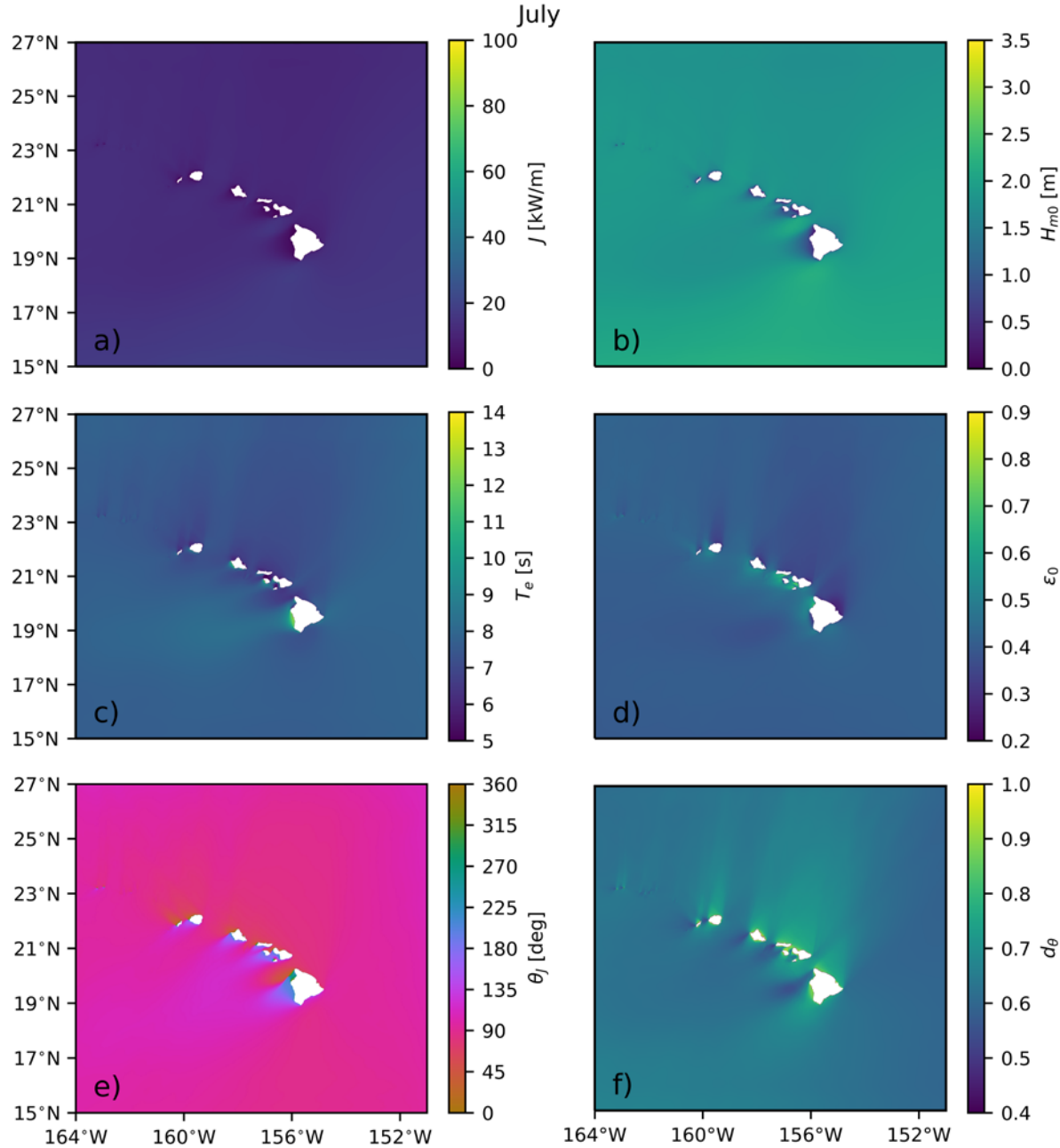


Figure 4.3. Simulated monthly distribution of six IEC wave resource parameters in July:
 (a) omnidirectional wave power, (b) significant wave height, (c) energy period,
 (d) spectral width, (e) direction of maximum directionally resolved wave power, and
 (f) directionality coefficient.

4.2 Model Validation

In this study, model validation was conducted by comparing the six simulated and measured IEC parameters at buoy stations. Specifically, the time history and scatter plots from the two data sets were generated and model performance metrics were calculated to evaluate the model skills in terms of the six IEC parameters. The following performance metrics used in

previous studies (Yang et al. 2017, García-Medina et al. 2013, García-Medina, Özkan-Haller, and Ruggiero 2014, Wu, Yang, and Wang 2018) were adopted here for model validation.

The root-mean-square-error (*RMSE*), sometimes referred as the root-mean-square-deviation, is defined as

$$RMSE = \sqrt{\frac{\sum_{i=1}^N (P_i - M_i)^2}{N}} \quad (9)$$

where N is the number of observations, M_i is the measured value, and P_i is the predicted value. *RMSE* represents the sample standard deviation of the differences between predicted and measured values.

The percentage error (*PE*) is defined as

$$PE(\%) = \frac{100}{N} \sum_{i=1}^N \left(\frac{P_i - M_i}{M_i} \right) \quad (10)$$

which is the average over the period of comparison.

The scatter index (*SI*) is the *RMSE* normalized by the average of all measured values over the period of comparison, where

$$SI = \frac{RMSE}{\bar{M}}, \quad (11)$$

where the overbar indicates the mean of the measured values.

Model bias, which represents the average difference between the predicted and measured value, is defined as

$$Bias = \frac{1}{N} \sum_{i=1}^N (P_i - M_i). \quad (12)$$

Percentage bias is defined as

$$Bias(\%) = \frac{\sum_{i=1}^N P_i - \sum_{i=1}^N M_i}{\sum_{i=1}^N M_i} \cdot 100 \quad (13)$$

which is literally the normalized bias.

The linear correlation coefficient, R , is defined as

$$R = \frac{\sum_{i=1}^N (M_i - \bar{M})(P_i - \bar{P})}{\sqrt{(\sum_{i=1}^N (M_i - \bar{M})^2)(\sum_{i=1}^N (P_i - \bar{P})^2)}} \quad (14)$$

and is a measure of the strength of the linear relationship between the predicted and measured values. In computing error statistics for directional variables, the smaller of the clockwise and counter-clockwise differences is selected. Figure 4.4 shows, as an example, the time series and

scatter plots of the IEC parameters at Buoy 164 for 2010. The time series shows the seasonality of the resource and model performance, while the scatter plots illustrate quantitatively the model performance. Similar plots at other stations and years are presented in Appendix B.

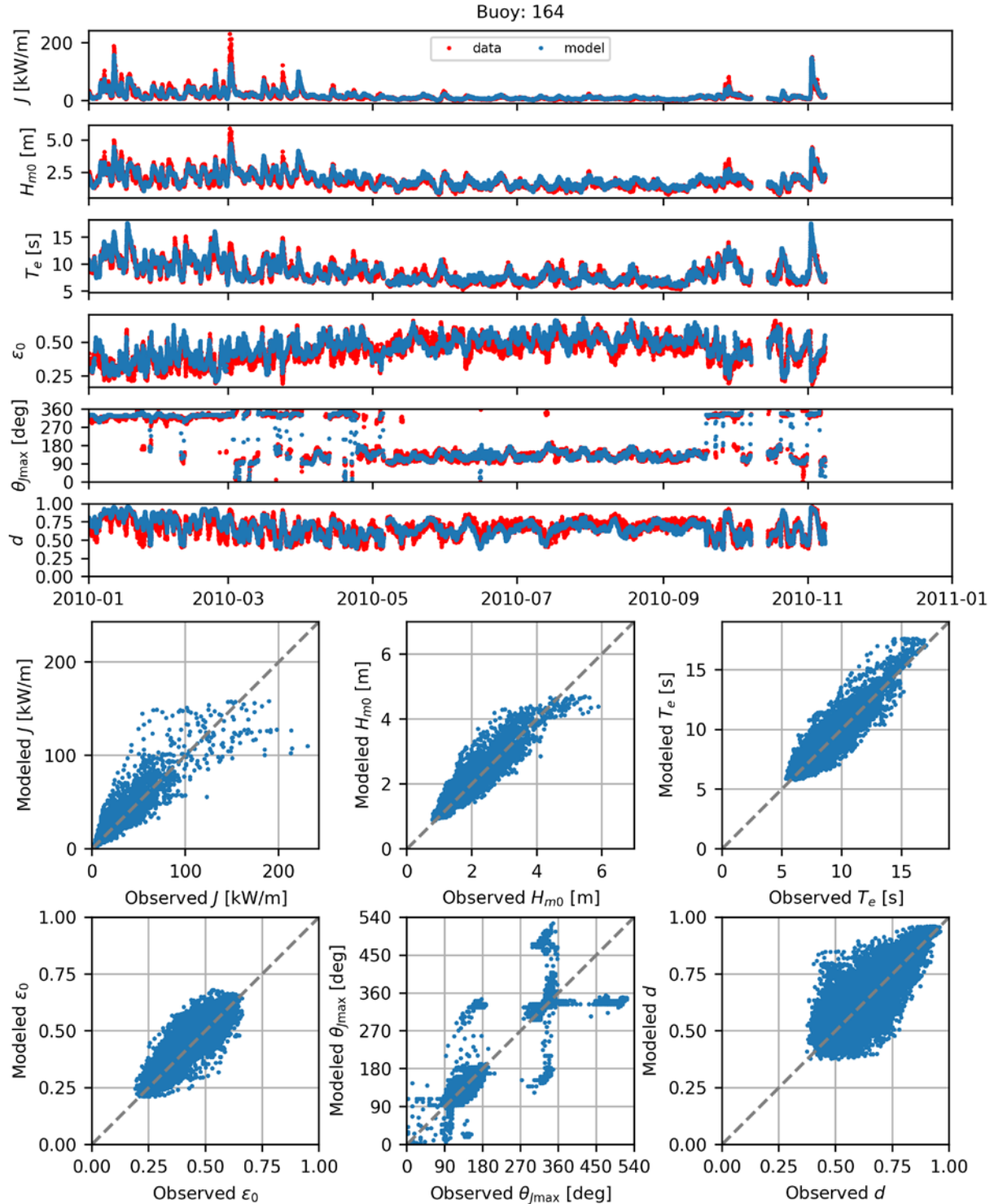


Figure 4.4. Time series (top) and scatter plots (bottom) of the six modeled and observed IEC wave resource parameters from October 2017 to March 2018 at Buoy 46263 in California.

The annual performance metrics (error statistics) for the six IEC resource parameters were calculated at every spectral buoy station and are provided in Appendix C. The error statistics

over the 32 years at every buoy station were calculated and are provided in 6.0Appendix C. As an example, the *RMSE* and linear correlation coefficient (*R*), as listed in Table 4.1, are the most commonly used model performance metrics. Overall, error statistics between model results and observed data show good model performance in terms of the six IEC parameters. For example, the R values are above 0.8 for J , H_s , and T_e at most stations. The values for ϵ_0 , θ_J , and d_θ are lower, but are considered well correlated because of the challenge in simulating wave direction and spectral spreading with 7.5° bins as well as high uncertainties in the direction measurements.

Table 4.1. Summary of temporal averages of the root-mean-square-error and linear correlation coefficient for the six IEC wave resource parameters at buoys with spectral data.

Buoy #	J (kW/m)		H_{mo} (m)		T_e (s)		ϵ_0 (-)		θ_{Jmax} (deg)		d (-)	
	RMSE	R	RMSE	R	RMSE	R	RMSE	R	RMSE	R	RMSE	R
034	9	0.81	0.37	0.83	0.8	0.84	0.08	0.71	-	-	-	-
039	17	0.84	0.53	0.84	1.5	0.81	0.10	0.66	-	-	-	-
098	6	0.89	0.25	0.90	0.5	0.92	0.04	0.76	18	0.98	0.06	0.76
106	12	0.90	0.34	0.92	0.9	0.94	0.06	0.76	18	0.99	0.07	0.65
146	2	0.81	0.20	0.78	2.0	0.64	0.10	0.50	31	0.69	0.10	0.71
164	8	0.91	0.28	0.91	0.8	0.92	0.06	0.83	43	0.92	0.09	0.75
51000	17	0.89	0.40	0.89	0.9	0.92	0.06	0.62	38	0.95	0.09	0.72
51001	21	0.85	0.44	0.88	1.0	0.88	0.06	0.59	43	0.95	0.11	0.61
51002	10	0.85	0.32	0.86	0.9	0.87	0.06	0.61	-	-	-	-
51003	11	0.84	0.33	0.86	1.0	0.84	0.06	0.54	-	-	-	-
51004	10	0.85	0.29	0.88	0.92	0.86	0.05	0.65	42	0.94	0.09	0.52
51101	17	0.88	0.40	0.90	0.8	0.91	0.05	0.72	40	0.95	0.11	0.64

4.3 Data Output

Bulk wave parameters and spectral partitions were output at 3-hour intervals for all the computational grid over the 32-year hindcast. The bulk and spectral parameters are stored in separate files for each month in the CF (climate and forecast) conventions. In addition, frequency-direction spectra are output at locations based on distance from coast and depth criteria. The number of output points are listed in Table 4.2. The location maps of the spectral output are shown in Figure 4.5 through Figure 4.8.

Table 4.2. Output inventory.

Type	Grid	Number of Points	Temporal Resolution
Bulk wave parameters	Computational	700,414	3 h
Spectral partitions	Computational	700,414	3 h
Wave Spectra	100 m isobath	874	1h
Wave Spectra	2 km from shore	744	1h
Wave Spectra	5 km from shore	165	1h

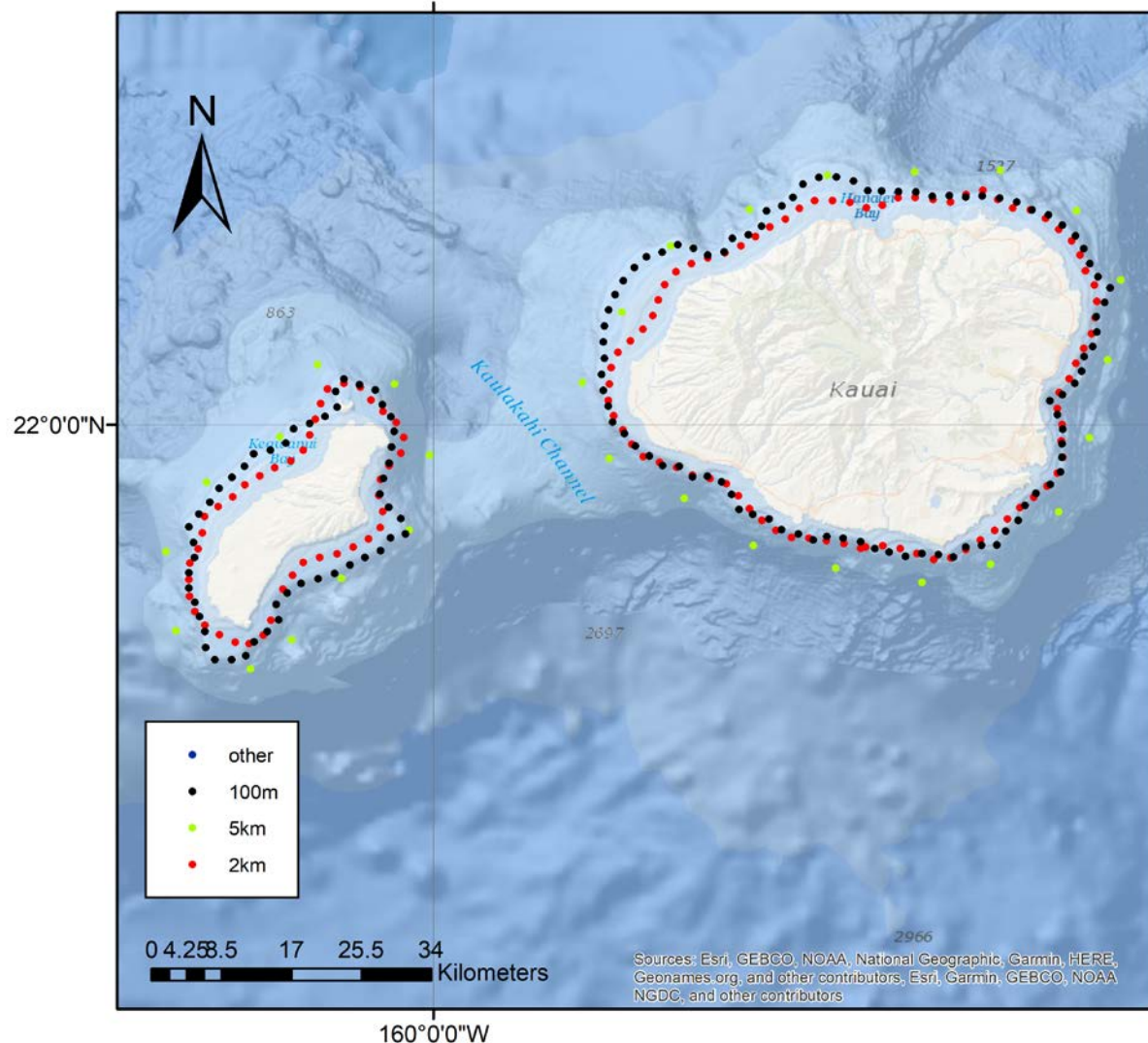


Figure 4.5. Spectral output locations near Ni'ihiwai and Kauai.

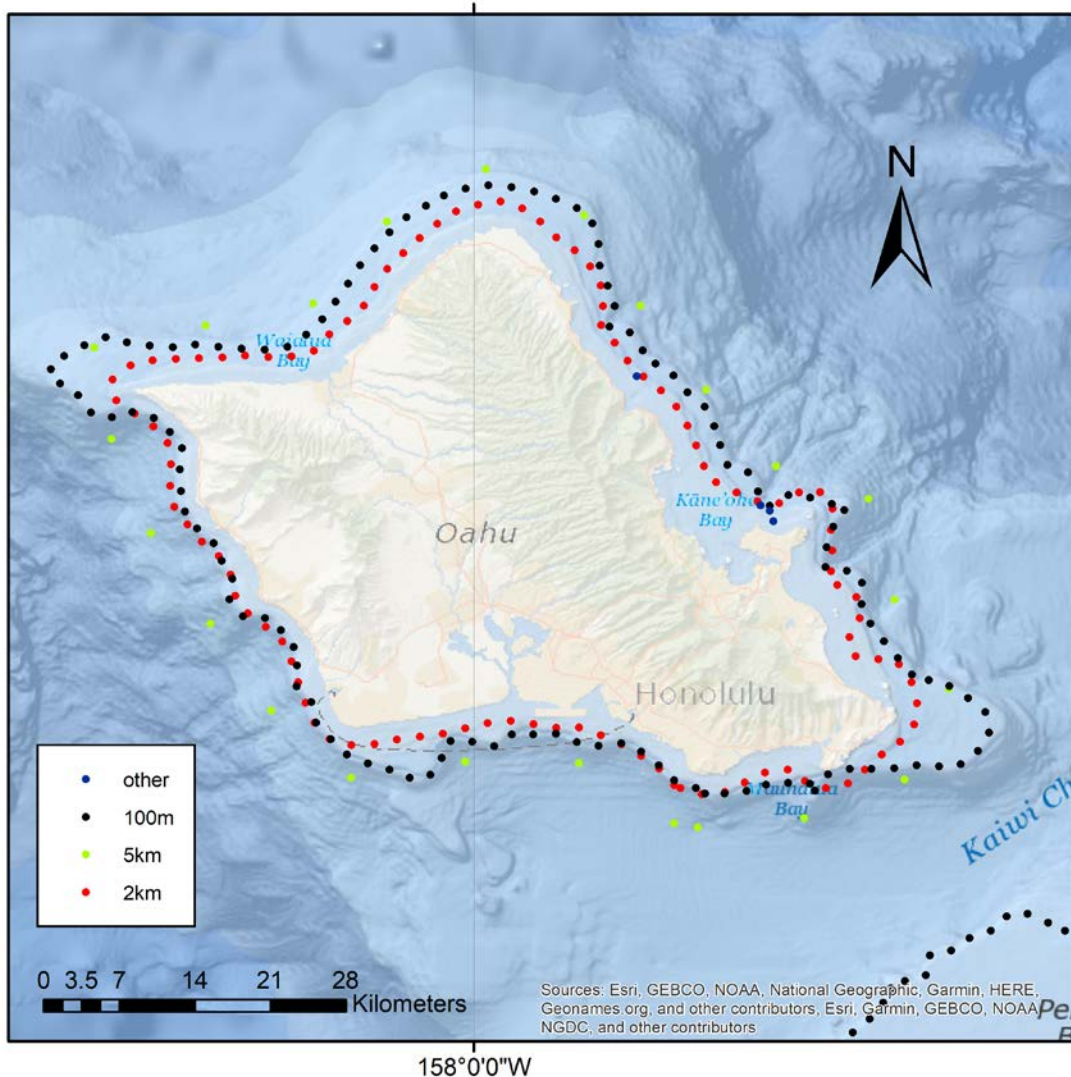


Figure 4.6. Spectral output locations near Oahu.

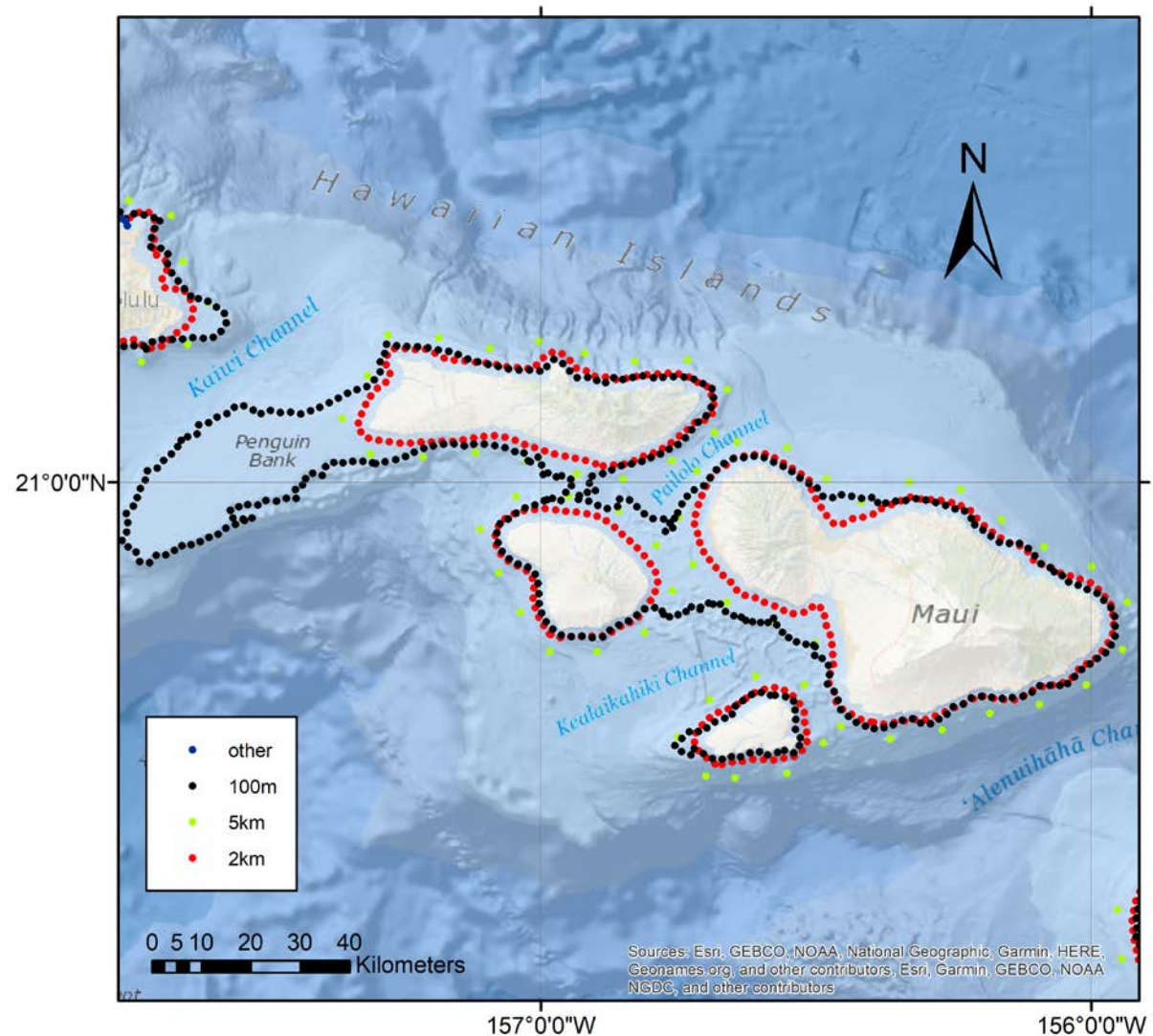


Figure 4.7. Spectral output locations near Moloka'i, Lanai, Maui, and Kaho'olawe.

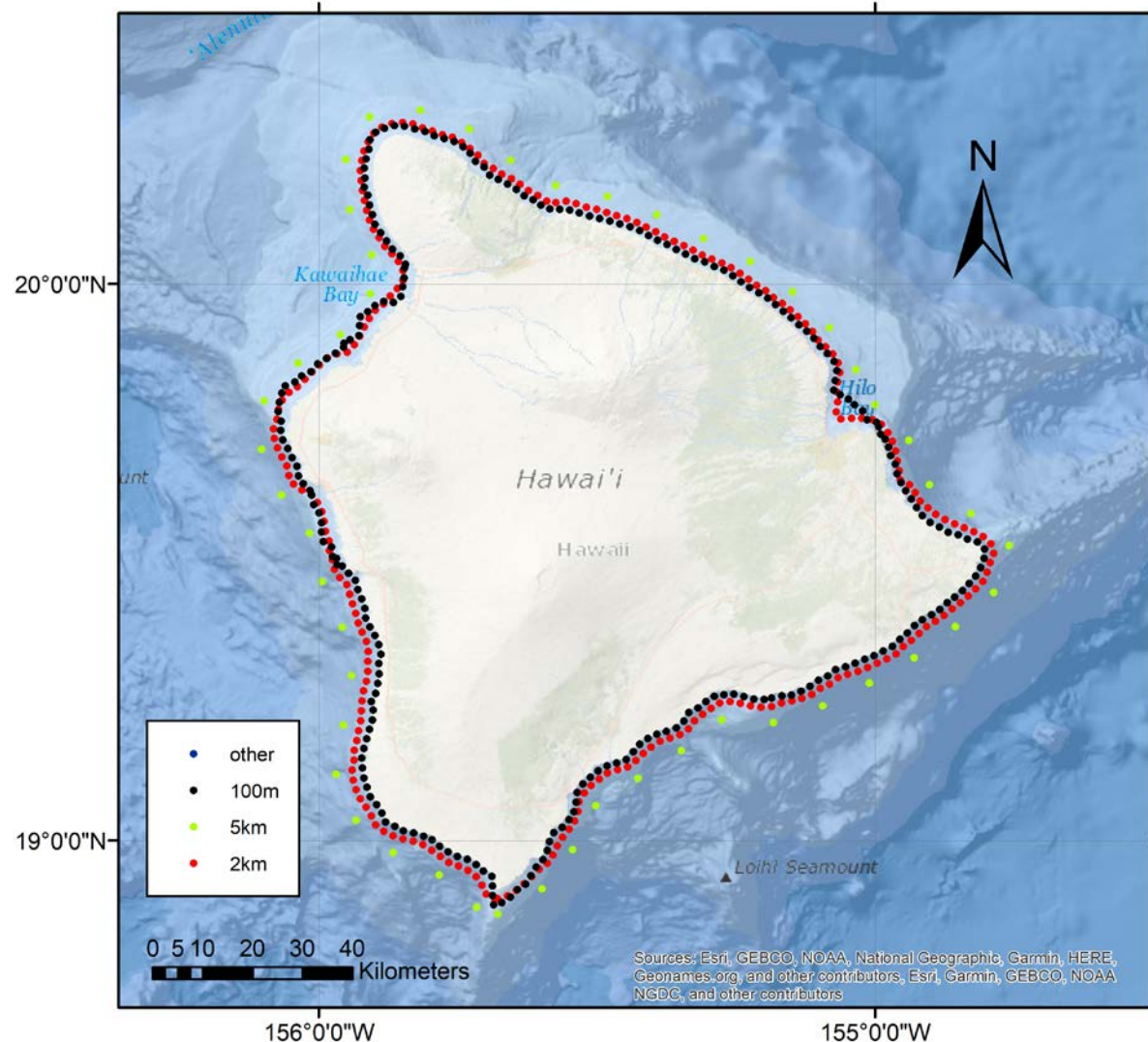


Figure 4.8. Spectral output locations near Hawaii.

5.0 Conclusion

A high-resolution, 32-year hindcast that covers the EEZ around the major Hawaiian Islands has been developed. The hindcast includes the six IEC-TS parameters recommended for wave energy characterization. The hindcast parameters have been compared with available buoy measurements for development of model performance metrics. The hindcast shows good performance in reproducing the wave climate and improving the resource characterization in the nearshore. The long-term high-resolution hindcast generated from this study provides important information not only for the design and siting of wave energy converters in nearshore regions, but also for prioritizing hotspots for near-term market opportunities and development. Wave climate parameters generated from this modeling effort will be used to update wave resource assessment data for the U.S. Department of Energy Marine and Hydrokinetic Energy Atlas.⁷

⁷ <https://maps.nrel.gov/mhk-atlas>

6.0 References

- Allandadi, M. N., B. Gunawan, J. Lai, R. Y. He, and V. S. Neary. 2019. "Development and validation of a regional-scale high-resolution unstructured model for wave energy resource characterization along the US East Coast." *Renewable Energy* 136:500-511. doi: 10.1016/j.renene.2019.01.020.
- Amante, Christopher, and Barry W Eakins. 2009. "ETOPO1 arc-minute global relief model: procedures, data sources and analysis."
- Ardhuin, Fabrice, Erick Rogers, Alexander V. Babanin, Jean-François Filipot, Rudy Magne, Aaron Roland, Andre van der Westhuysen, Pierre Queffeulou, Jean-Michel Lefevre, Lotfi Aouf, and Fabrice Collard. 2010. "Semiempirical Dissipation Source Functions for Ocean Waves. Part I: Definition, Calibration, and Validation." *Journal of Physical Oceanography* 40 (9):1917-1941. doi: 10.1175/2010jpo4324.1.
- Booij, N., and L. H. Holthuijsen. 1987. "Propagation of Ocean Waves in Discrete Spectral Wave Models." *Journal of Computational Physics* 68 (2):307-326. doi: 10.1016/0021-9991(87)90060-X.
- Cobell, Z., H. H. Zhao, H. J. Roberts, F. R. Clark, and S. Zou. 2013. "Surge and Wave Modeling for the Louisiana 2012 Coastal Master Plan." *Journal of Coastal Research*:88-108. doi: 10.2112/SI_67_7.
- EPRI. 2011. Mapping and Assessment of the United States Ocean Wave Energy Resource. In *EPRI 2011 Technical Report to U.S. Department of Energy*. Palo Alto, California: Electric Power Research Institute.
- Gallagher, S., R. Tiron, and F. Dias. 2014. "A long-term nearshore wave hindcast for Ireland: Atlantic and Irish Sea coasts (1979-2012)." *Ocean Dynamics* 64 (8):1163-1180. doi: 10.1007/s10236-014-0728-3.
- García-Medina, Gabriel, H. Tuba Özkan-Haller, and Peter Ruggiero. 2014. "Wave resource assessment in Oregon and southwest Washington, USA." *Renewable Energy* 64:203-214. doi: 10.1016/j.renene.2013.11.014.
- García-Medina, Gabriel, H. Tuba Özkan-Haller, Peter Ruggiero, and Jeffrey Oskamp. 2013. "An Inner-Shelf Wave Forecasting System for the U.S. Pacific Northwest." *Weather and Forecasting* 28 (3):681-703. doi: 10.1175/waf-d-12-00055.1.
- Hitzl, D. E., Y. L. Chen, and H. V. Nguyen. 2014. "Numerical Simulations and Observations of Airflow through the 'Alenuihaha Channel, Hawaii.'" *Monthly Weather Review* 142 (12):4696-4718. doi: 10.1175/Mwr-D-13-00312.1.
- IEC. 2015. Marine energy – wave, tidal and other water current converters – Part 101: Wave energy resource assessment and characterization. Geneva, Switzerland: International Electrotechnical Commission.

Janssen, P. A. E. M. 1989. "Wave-Induced Stress and the Drag of Air-Flow over Sea Waves." *Journal of Physical Oceanography* 19 (6):745-754. doi: 10.1175/1520-0485(1989)019<0745:WISATD>2.0.CO;2.

Janssen, P. A. E. M. 1991. "Quasi-Linear Theory of Wind-Wave Generation Applied to Wave Forecasting." *Journal of Physical Oceanography* 21 (11):1631-1642. doi: 10.1175/1520-0485(1991)021<1631:Qltoww>2.0.Co;2.

Li, N., K. F. Cheung, J. E. Stopa, F. Hsiao, Y. L. Chen, L. Vega, and P. Cross. 2016. "Thirty-four years of Hawaii wave hindcast from downscaling of climate forecast system reanalysis." *Ocean Modelling* 100:78-95. doi: 10.1016/j.ocemod.2016.02.001.

Mao, M., A. J. van der Westhuysen, M. Xia, D. J. Schwab, and A. Chawla. 2016. "Modeling wind waves from deep to shallow waters in Lake Michigan using unstructured SWAN." *Journal of Geophysical Research-Oceans* 121 (6):3836-3865. doi: 10.1002/2015JC011340.

Mediavilla, D. G., and H. H. Sepulveda. 2016. "Nearshore assessment of wave energy resources in central Chile (2009-2010)." *Renewable Energy* 90:136-144. doi: 10.1016/j.renene.2015.12.066.

National Research Council. 2013. An Evaluation of the U.S. Department of Energy's Marine and Hydrokinetic Resource Assessments. Washington, DC.

Roland, A., and F. Arduin. 2014. "On the developments of spectral wave models: numerics and parameterizations for the coastal ocean." *Ocean Dynamics* 64 (6):833-846. doi: 10.1007/s10236-014-0711-z.

Sosa, J., L. Cavalieri, and J. Portilla-Yandun. 2017. "On the interaction between ocean surface waves and seamounts." *Ocean Dynamics* 67 (12):1553-1565. doi: 10.1007/s10236-017-1107-7.

Stopa, J. E., K. F. Cheung, and Y. L. Chen. 2011. "Assessment of wave energy resources in Hawaii." *Renewable Energy* 36 (2):554-567. doi: 10.1016/j.renene.2010.07.014.

SWAN. 2015. SWAN: User Manual, Cycle III version 41.01A. Delft, The Netherlands: Delft University of Technology.

Tolman, H. L. 2003. "Treatment of unresolved islands and ice in wind wave models." *Ocean Modelling* 5 (3):219-231. doi: 10.1016/S1463-5003(02)00040-9.

Tolman, H.L., and WAVEWATCH III Development Group. 2014. User manual and system documentation of WAVEWATCH III® version 4.18. College Park, MD 20740: National Oceanic and Atmospheric Administration, National Weather Service, National Centers for Environmental Prediction.

van der Westhuysen, A. J., M. Zijlema, and J. A. Battjes. 2007. "Nonlinear saturation-based whitecapping dissipation in SWAN for deep and shallow water." *Coastal Engineering* 54 (2):151-170. doi: 10.1016/j.coastaleng.2006.08.006.

Wessel, P., and W. H. F. Smith. 1996. "A global, self-consistent, hierarchical, high-resolution shoreline database." *Journal of Geophysical Research-Solid Earth* 101 (B4):8741-8743. doi: 10.1029/96jb00104.

Wu, W.-C., Z. Yang, and T. Wang. 2018. "Wave Resource Characterization Using an Unstructured Grid Modeling Approach." *Energies* 11 (3):15. doi: 10.3390/en11030605.

WW3DG, (The WAVEWATCH III Development Group). 2016. User manual and system documentation of WAVEWATCH III version 5.16. College Park, MD, USA: NOAA/NWS/NCEP/MMAB.

Yang, Z., V. S. Neary, T. Wang, B. Gunawan, A. R. Dallman, and W. Wu. 2017. "A wave model test bed study for wave energy resource characterization." *Renewable Energy*. doi: 10.1016/j.renene.2016.12.057.

Yang, Z., W. C. Wu, T. Wang, and L. Castrucci. 2018. High-Resolution Regional Wave Hindcast for the U.S. West Coast. Richland, WA: PNNL.

Yang, Zhaoqing, Gabriel García-Medina, Wei-Cheng Wu, Taiping Wang, L. Ruby Leung, Luca Castrucci, and Guillaume Mauger. 2019. "Modeling analysis of the swell and wind-sea climate in the Salish Sea." *Estuarine, Coastal and Shelf Science*. doi: 10.1016/j.ecss.2019.04.043.

Yuk, J. H., K. O. Kim, K. T. Jung, and B. H. Choi. 2016. "Swell Prediction for the Korean Coast." *Journal of Coastal Research* 32 (1):131-141. doi: 10.2112/Jcoastres-D-14-00208.1.

Zijlema, M. 2010. "Computation of wind-wave spectra in coastal waters with SWAN on unstructured grids." *Coastal Engineering* 57 (3):267-277. doi: 10.1016/j.coastaleng.2009.10.011.

Appendix A – Monthly Distributions of IEC Wave Resource Parameters from 1979–2010 around Hawaii

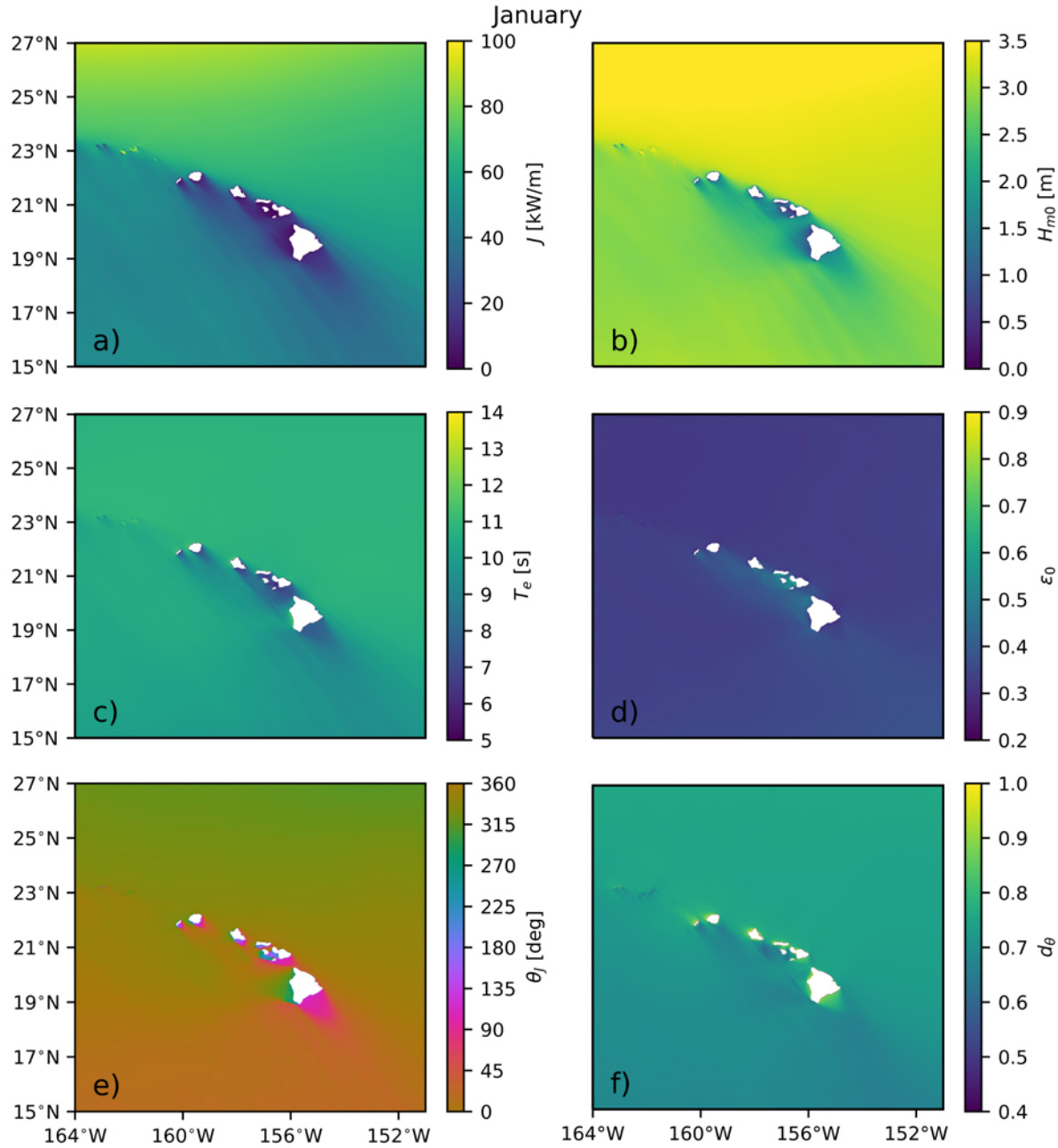


Figure A.1. Monthly distributions of six IEC parameters in January: (a) omnidirectional wave power, (b) significant wave height, (c) energy period, (d) spectral width, (e) direction of maximum directionally resolved wave power, and (f) directionality coefficient around Hawaii.

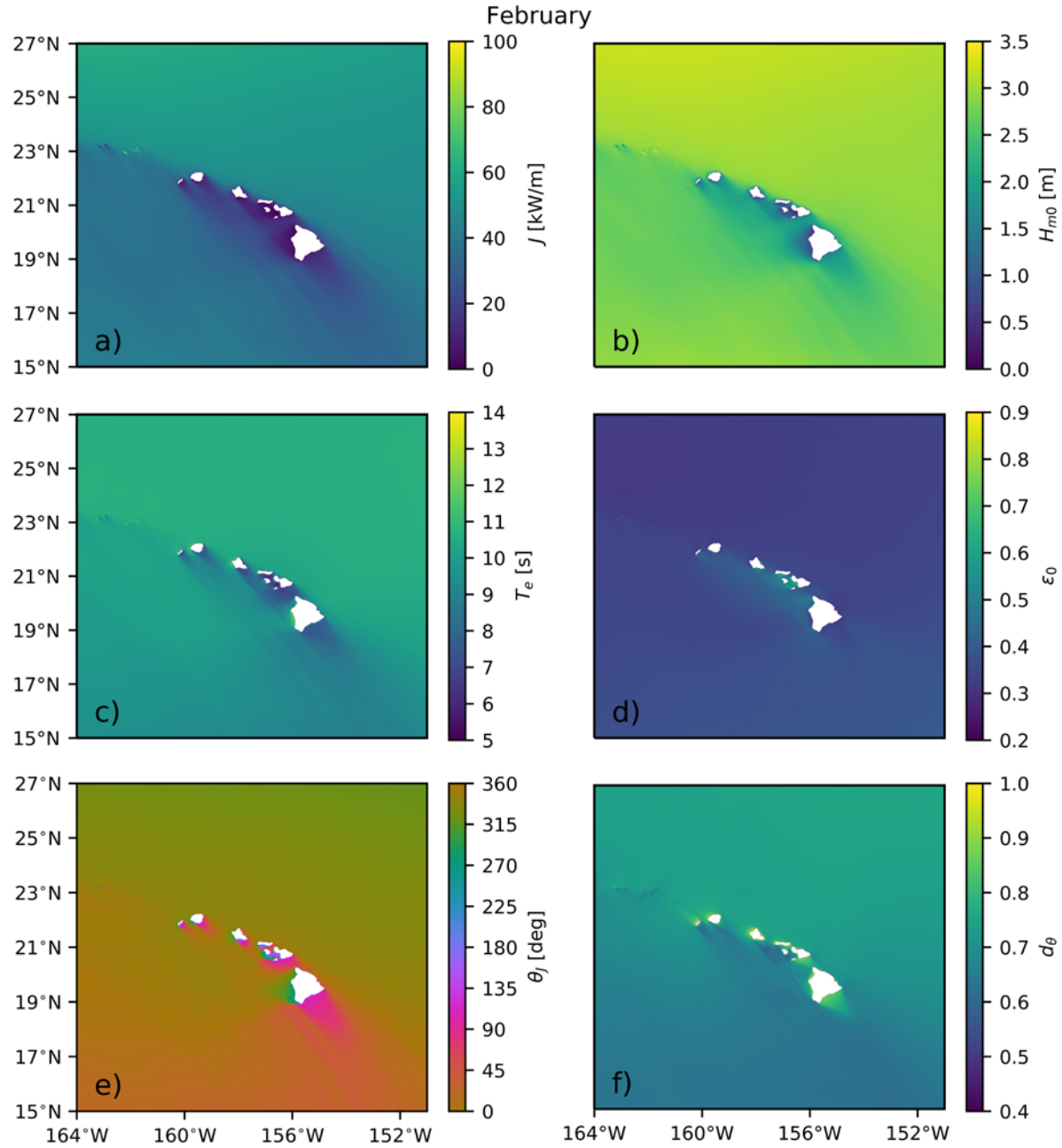


Figure A.2. Monthly distributions of six IEC parameters in February: (a) omnidirectional wave power, (b) significant wave height, (c) energy period, (d) spectral width, (e) direction of maximum directionally resolved wave power, and (f) directionality coefficient around Hawaii.

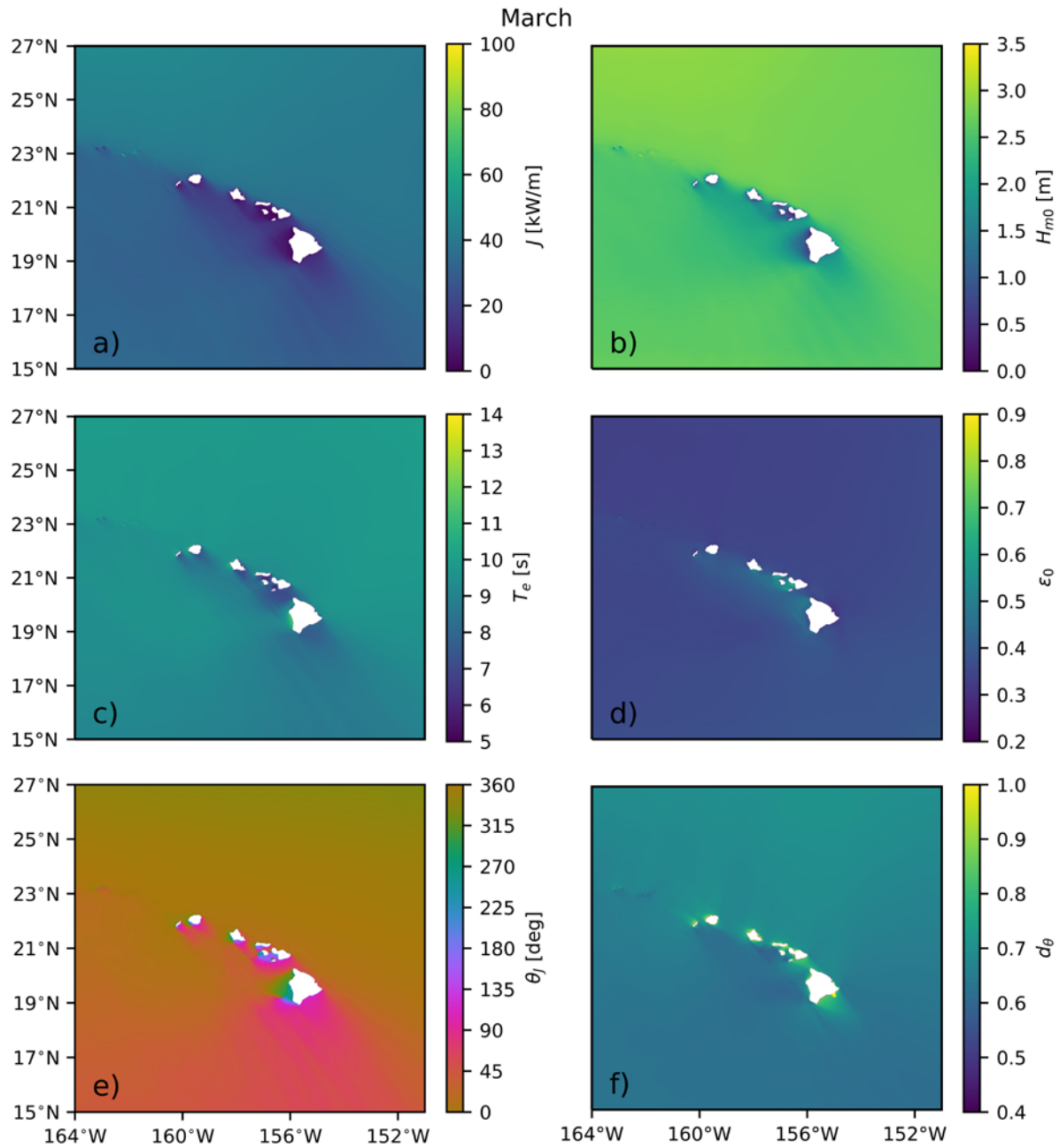


Figure A.3. Monthly distributions of six IEC parameters in March: (a) omnidirectional wave power, (b) significant wave height, (c) energy period, (d) spectral width, (e) direction of maximum directionally resolved wave power, and (f) directionality coefficient around Hawaii.

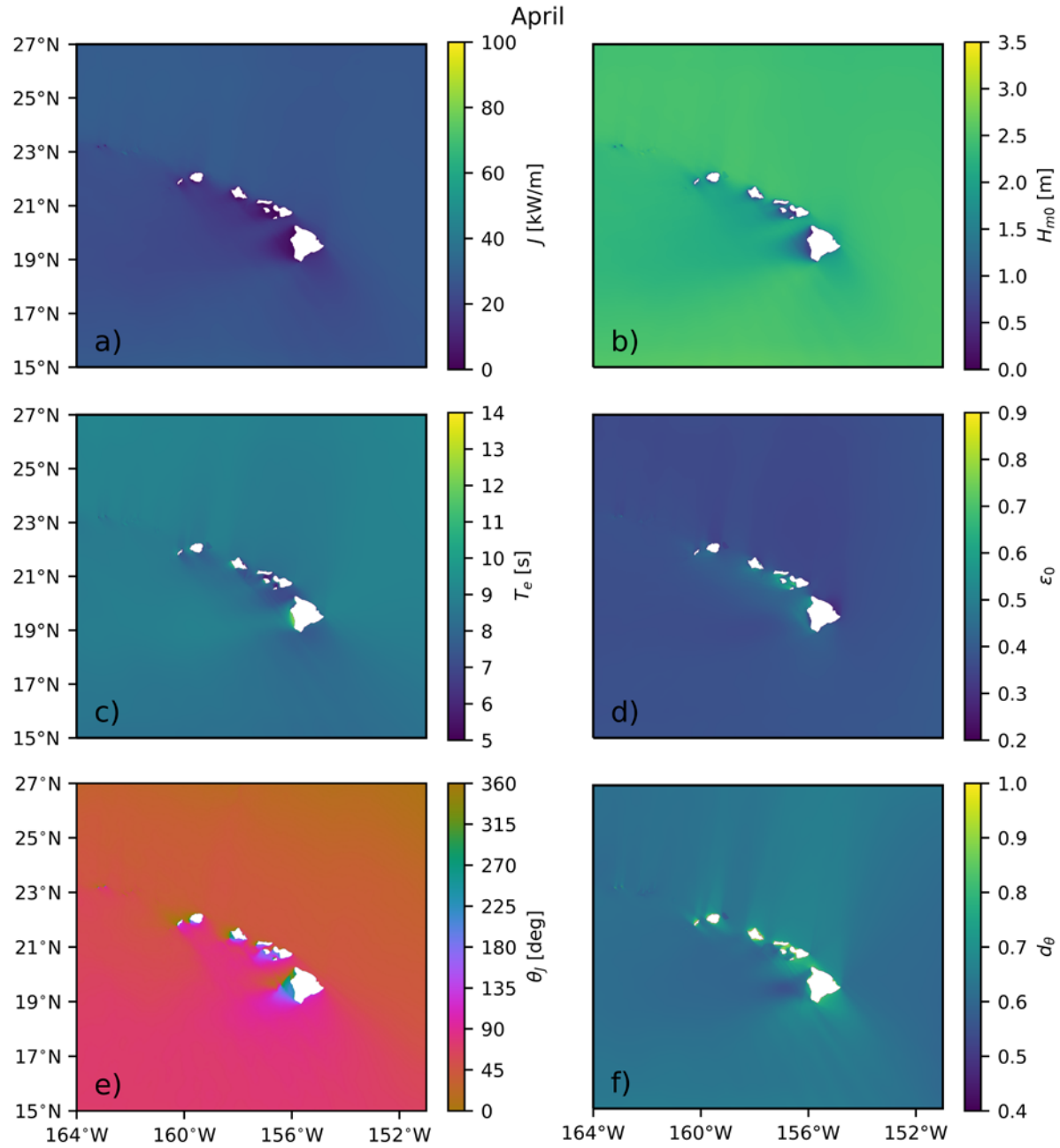


Figure A.4. Monthly distributions of six IEC parameters in April: (a) omnidirectional wave power, (b) significant wave height, (c) energy period, (d) spectral width, (e) direction of maximum directionally resolved wave power, and (f) directionality coefficient around Hawaii.

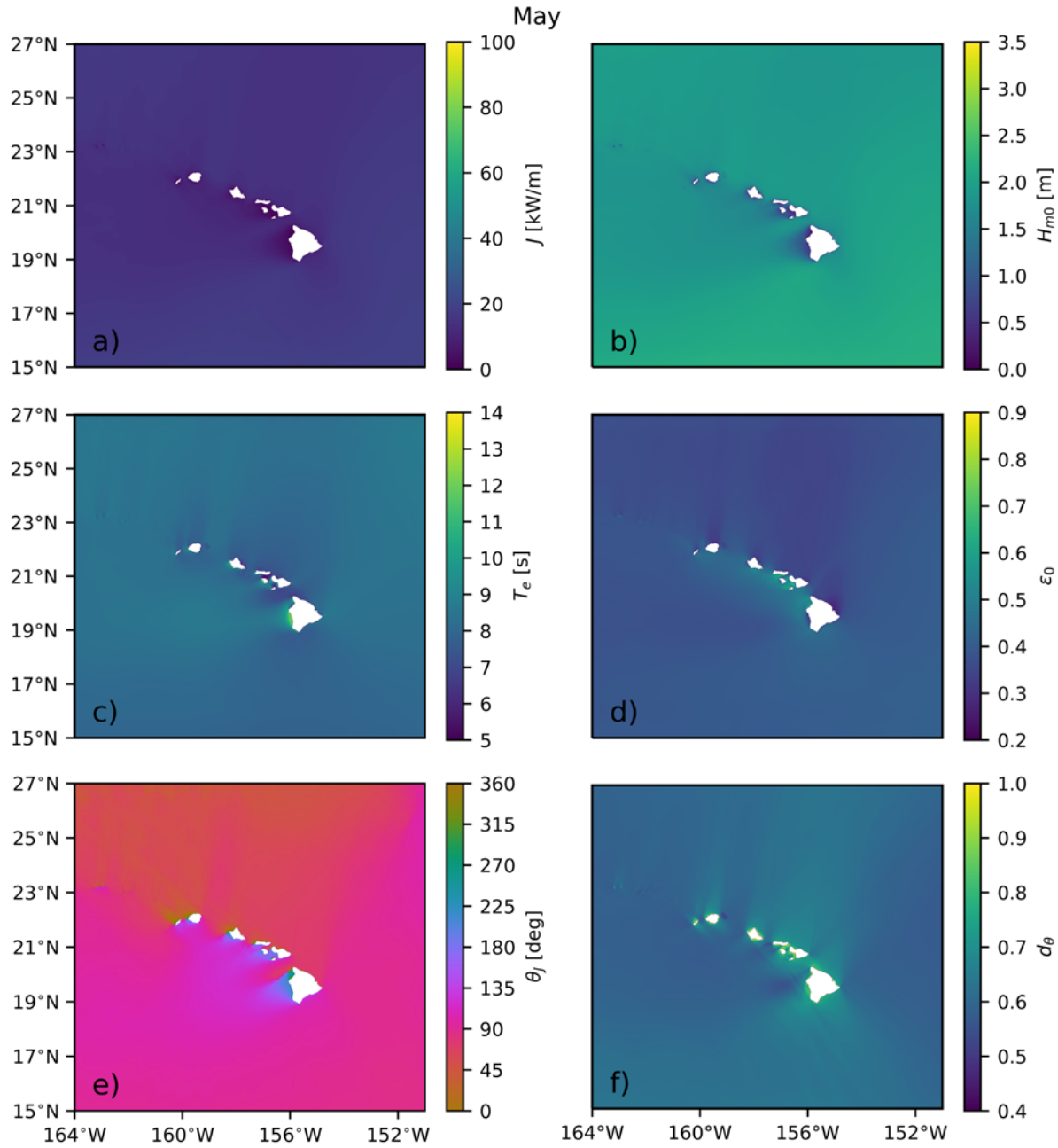


Figure A.5. Monthly distributions of six IEC parameters in May: (a) omnidirectional wave power, (b) significant wave height, (c) energy period, (d) spectral width, (e) direction of maximum directionally resolved wave power, and (f) directionality coefficient around Hawaii.

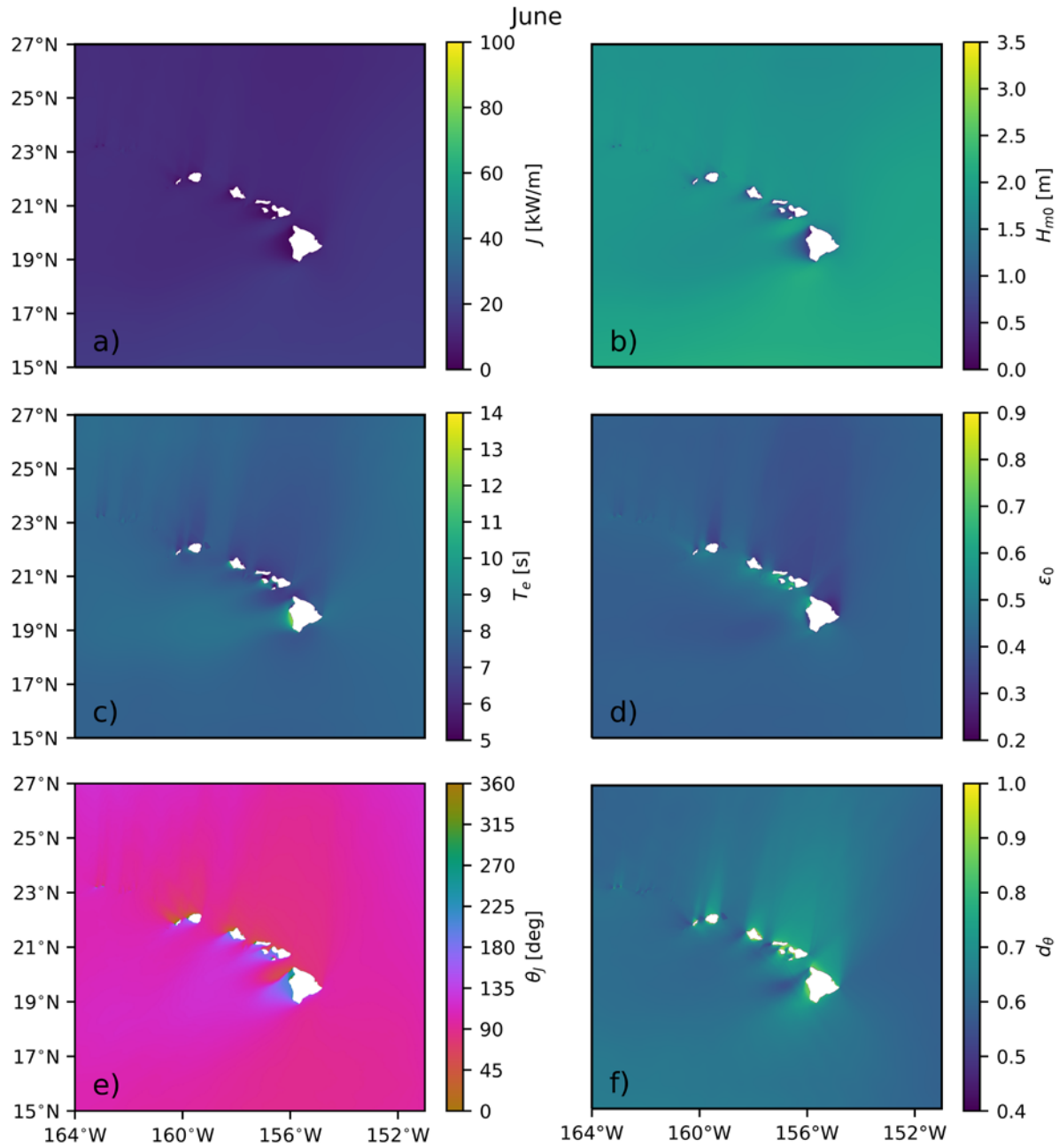


Figure A.6. Monthly distributions of six IEC parameters in June: (a) omnidirectional wave power, (b) significant wave height, (c) energy period, (d) spectral width, (e) direction of maximum directionally resolved wave power, and (f) directionality coefficient around Hawaii.

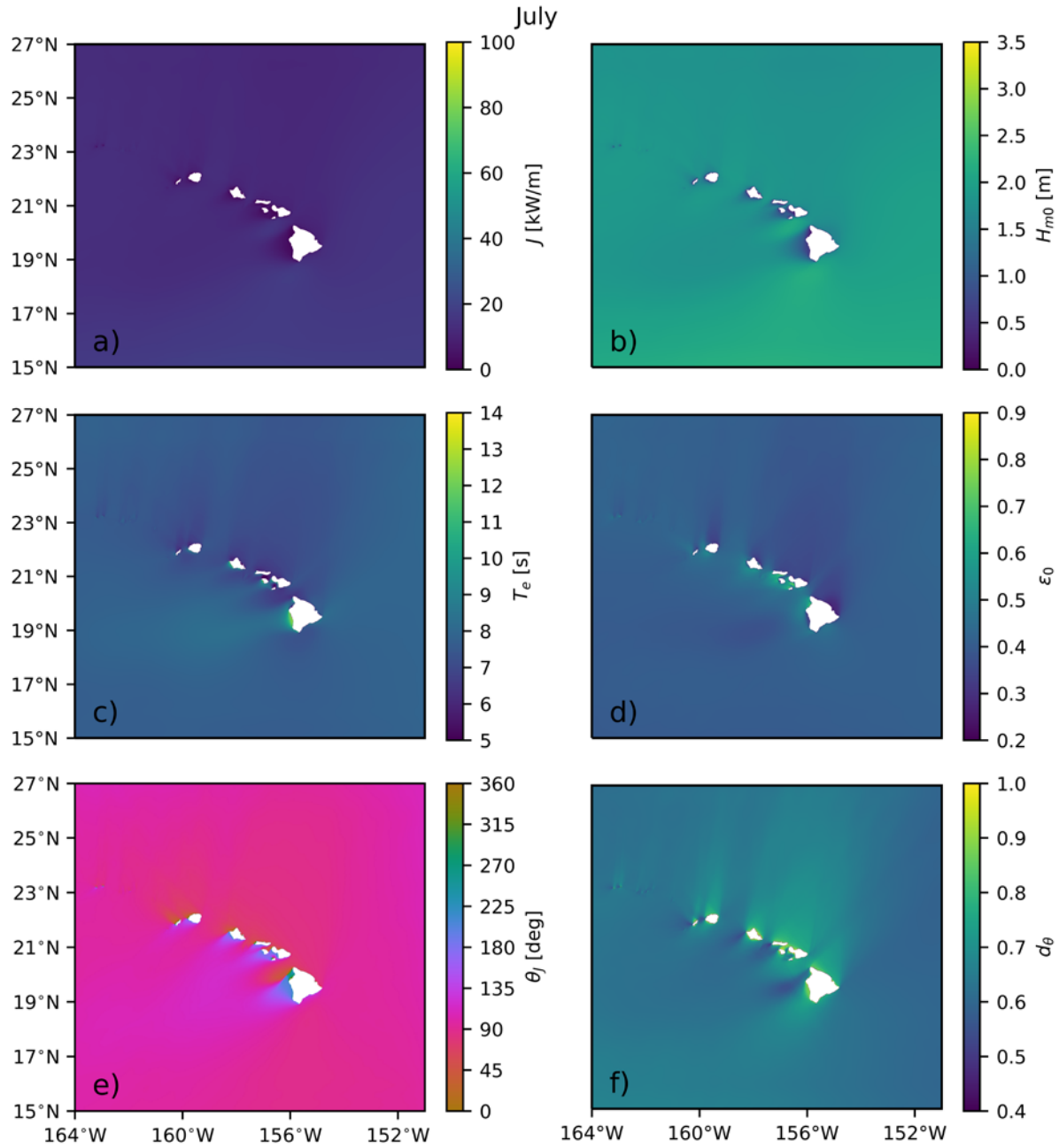


Figure A.7. Monthly distributions of six IEC parameters in July: (a) omnidirectional wave power, (b) significant wave height, (c) energy period, (d) spectral width, (e) direction of maximum directionally resolved wave power, and (f) directionality coefficient around Hawaii.

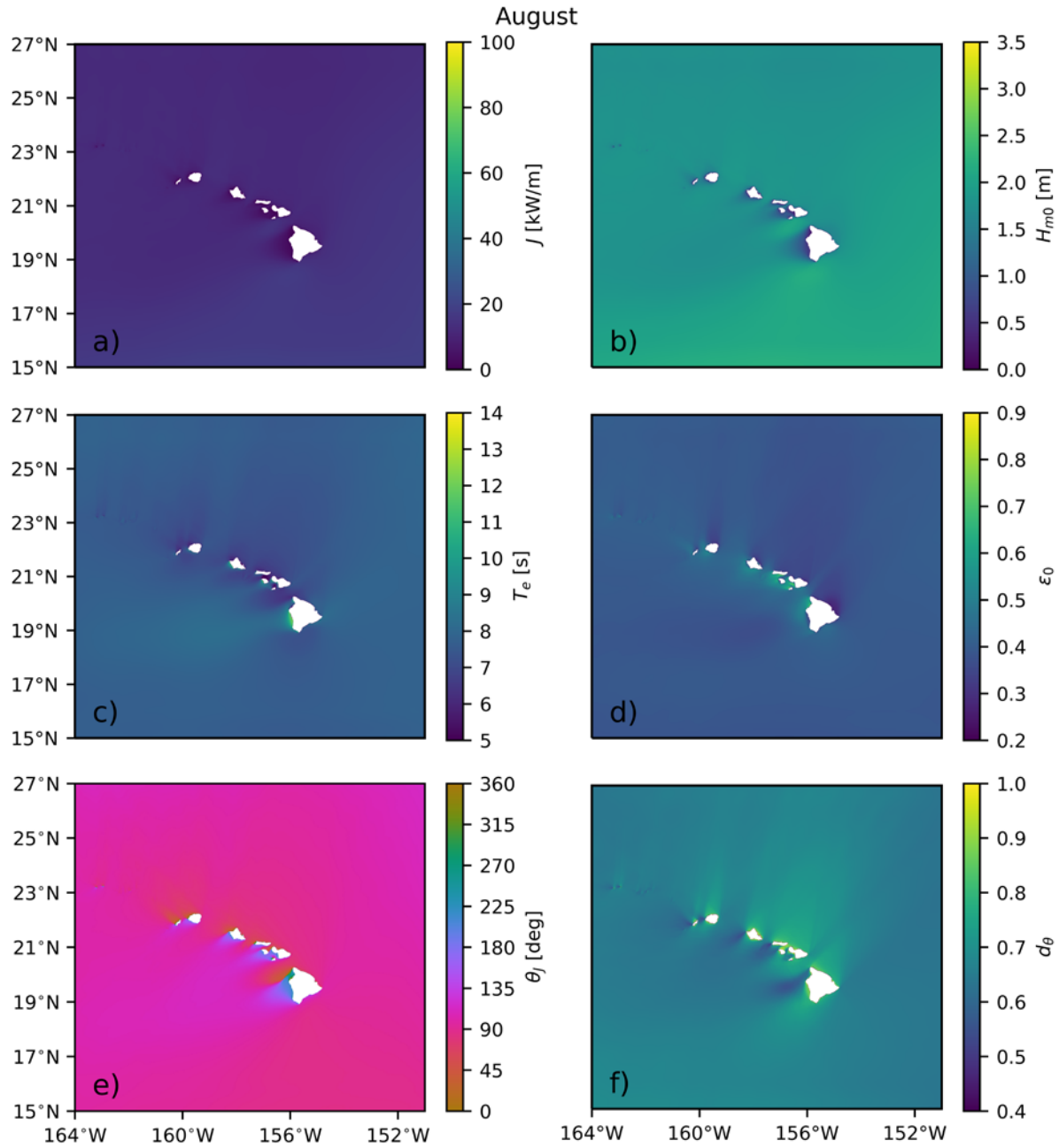


Figure A.8. Monthly distributions of six IEC parameters in August: (a) omnidirectional wave power, (b) significant wave height, (c) energy period, (d) spectral width, (e) direction of maximum directionally resolved wave power, and (f) directionality coefficient around Hawaii.

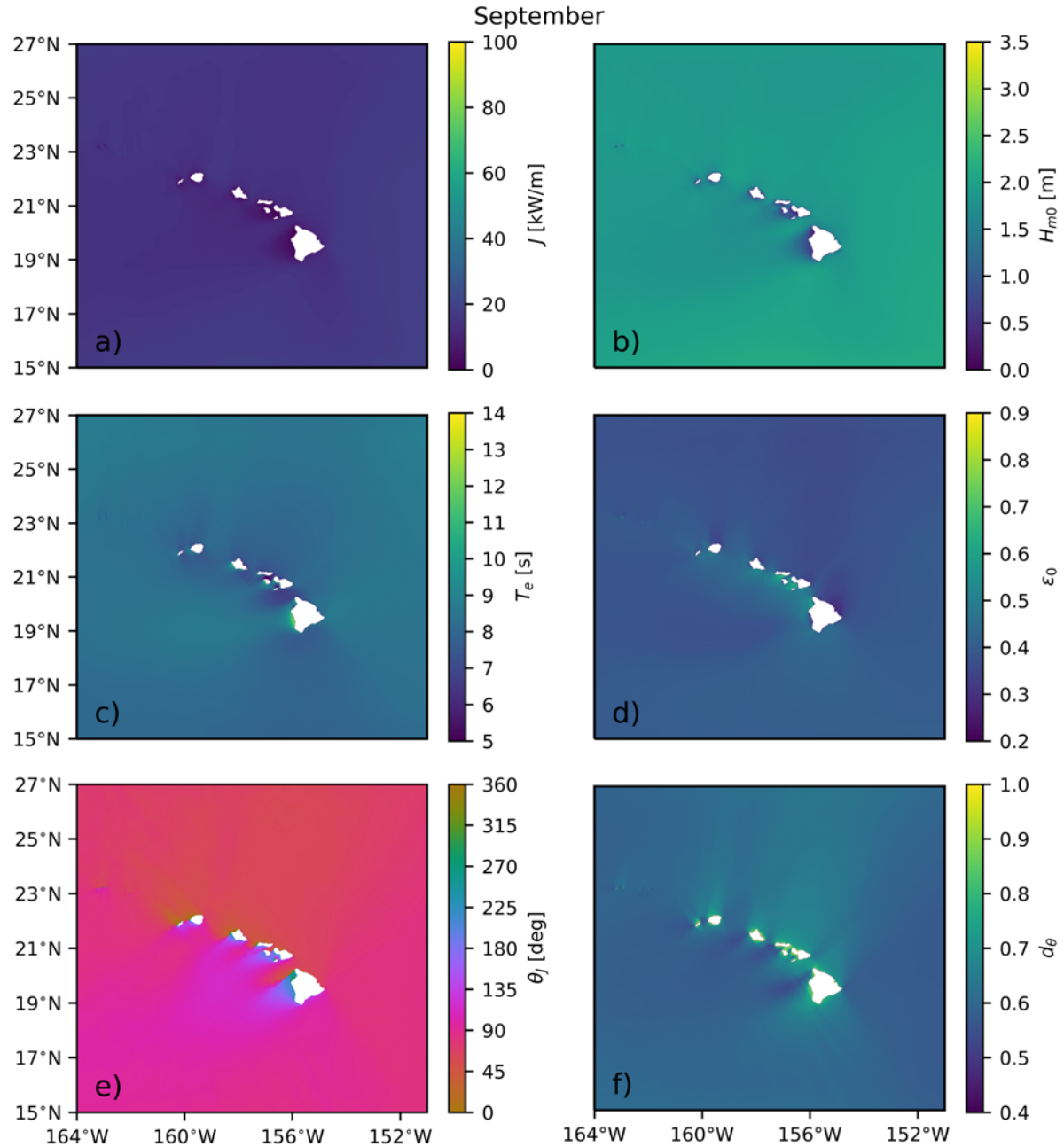


Figure A.9. Monthly distributions of six IEC parameters in September: (a) omnidirectional wave power, (b) significant wave height, (c) energy period, (d) spectral width, (e) direction of maximum directionally resolved wave power, and (f) directionality coefficient around Hawaii.

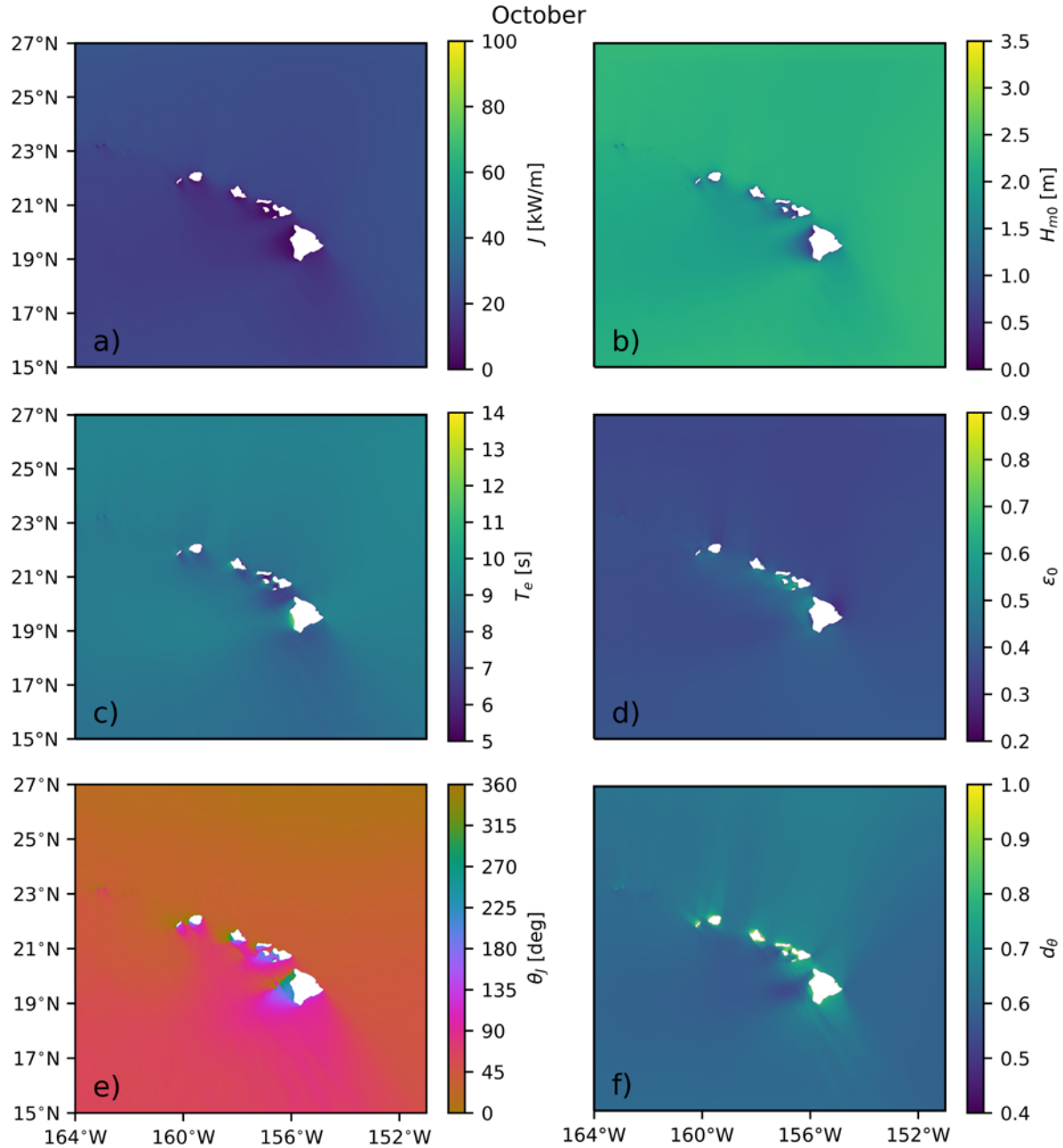


Figure A.10. Monthly distributions of six IEC parameters in October: (a) omnidirectional wave power, (b) significant wave height, (c) energy period, (d) spectral width, (e) direction of maximum directionally resolved wave power, and (f) directionality coefficient around Hawaii.

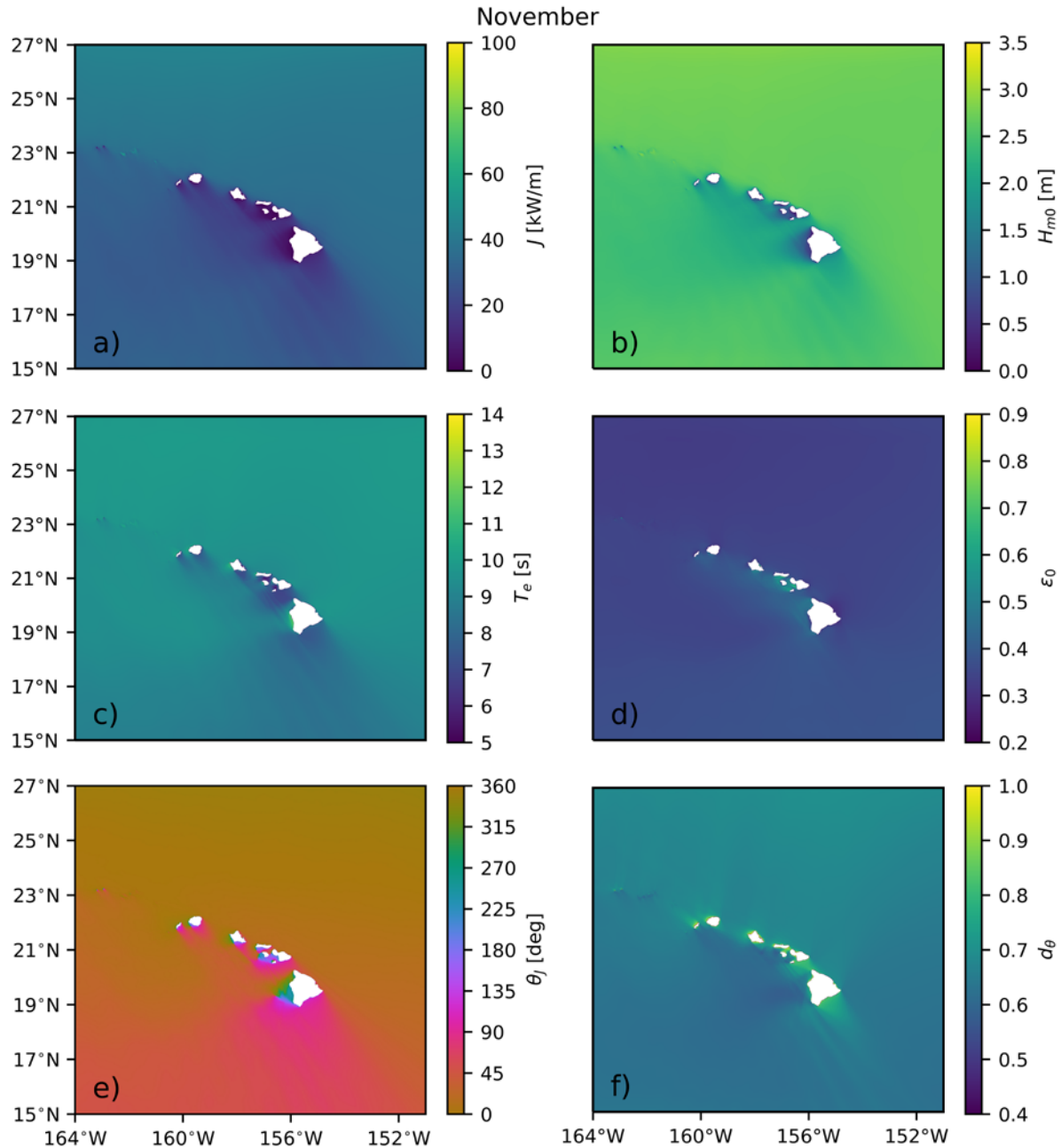


Figure A.11. Monthly distributions of six IEC parameters in November: (a) omnidirectional wave power, (b) significant wave height, (c) energy period, (d) spectral width, (e) direction of maximum directionally resolved wave power, and (f) directionality coefficient around Hawaii.

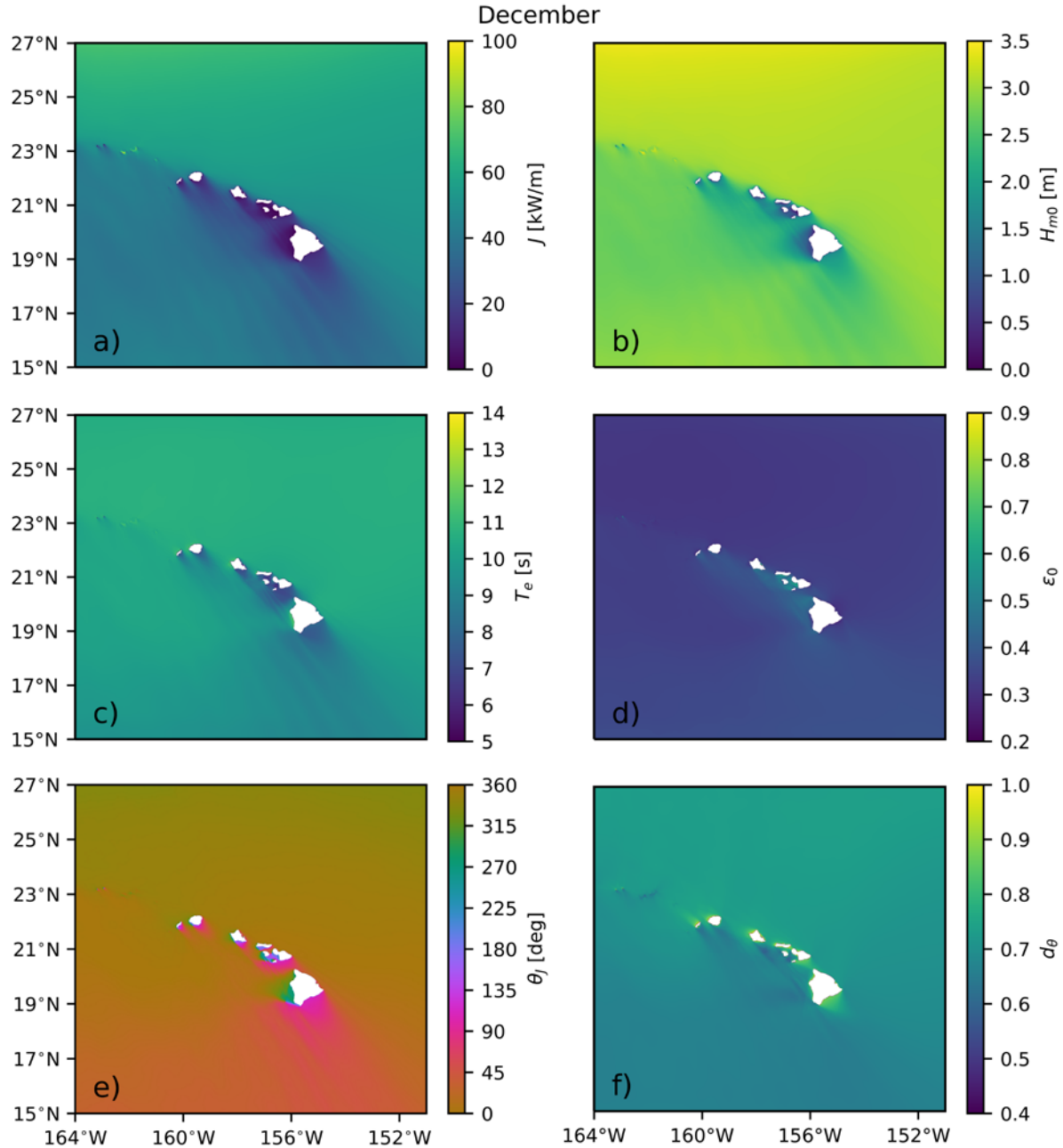


Figure A.12. Monthly distributions of six IEC parameters in December: (a) omnidirectional wave power, (b) significant wave height, (c) energy period, (d) spectral width, (e) direction of maximum directionally resolved wave power, and (f) directionality coefficient around Hawaii.

Appendix B – Comparisons of the Model-Simulated Six IEC Parameters with Observed Data at CDIP and NDBC Buoys

Figure B.1 through B.83 are Coastal Data Information Program-related plots. Figure B.54 through Figure B.116 National Data Buoy Center-related plots.

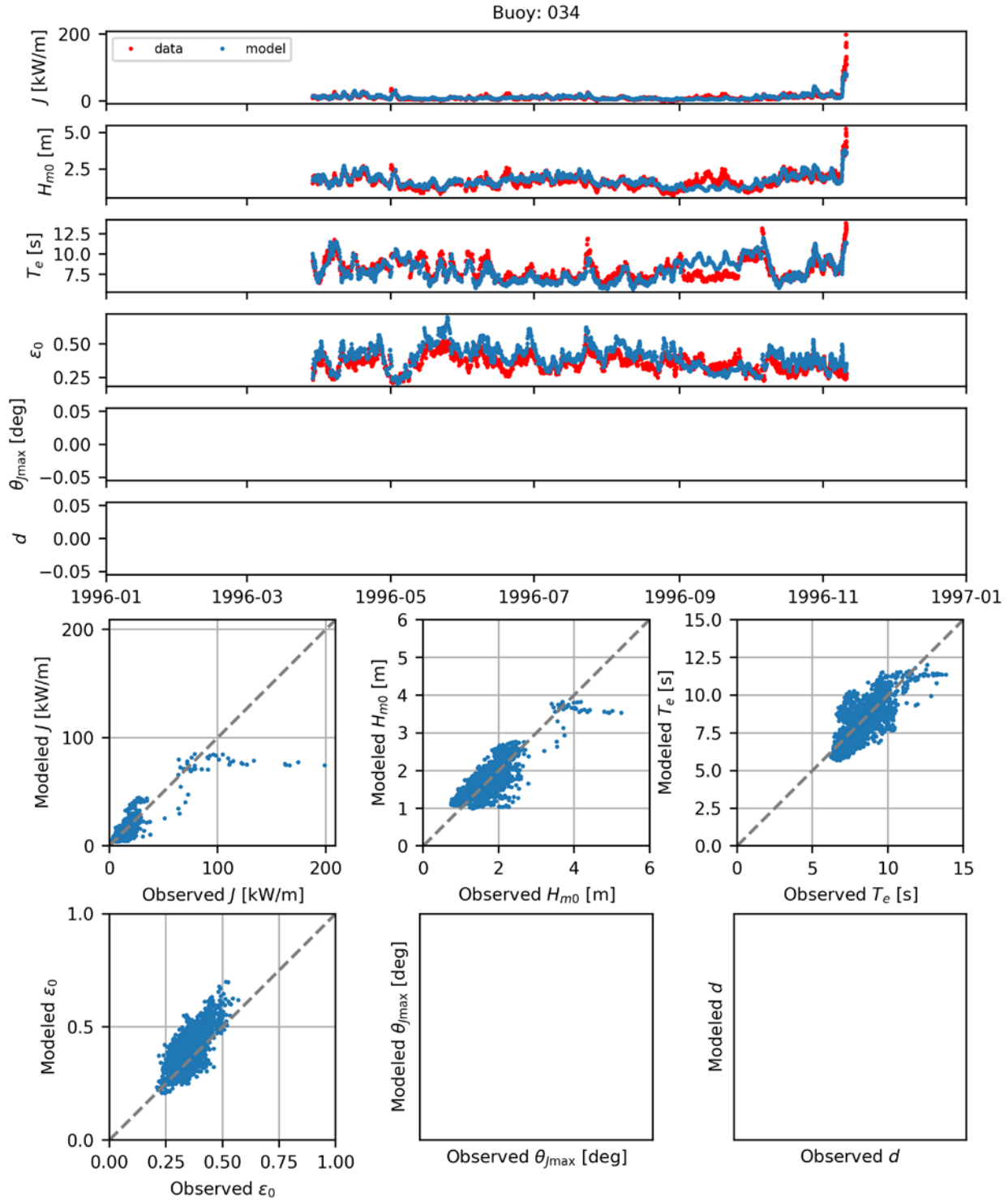


Figure B.1. Comparisons of time series (top) and scatter plots (bottom) of the six model-simulated IEC parameters with observed data at CDIP Buoy 034 for 1996.

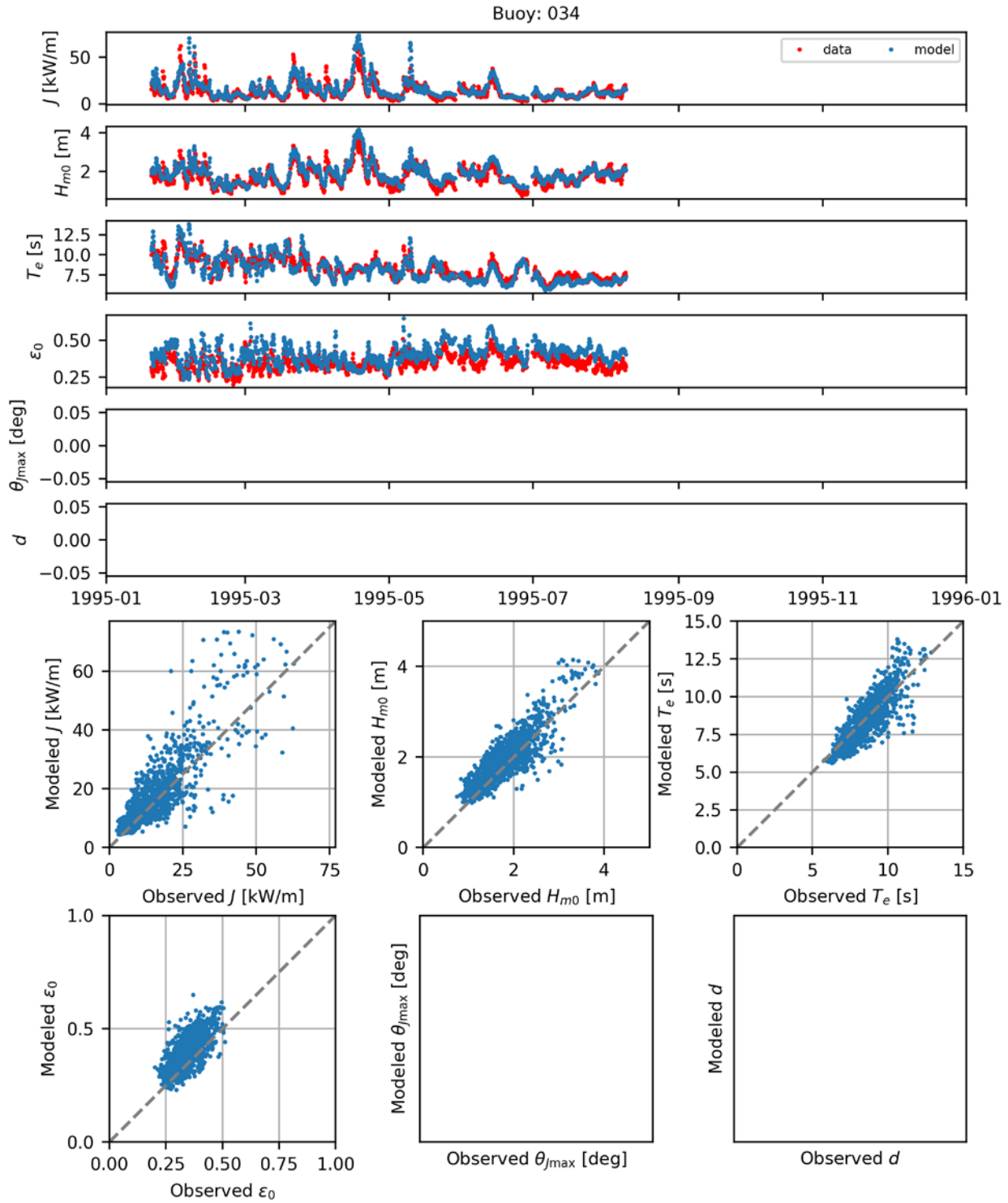


Figure B.2. Comparisons of time series (top) and scatter plots (bottom) of the six model-simulated IEC parameters with observed data at CDIP Buoy 034 for 1995.

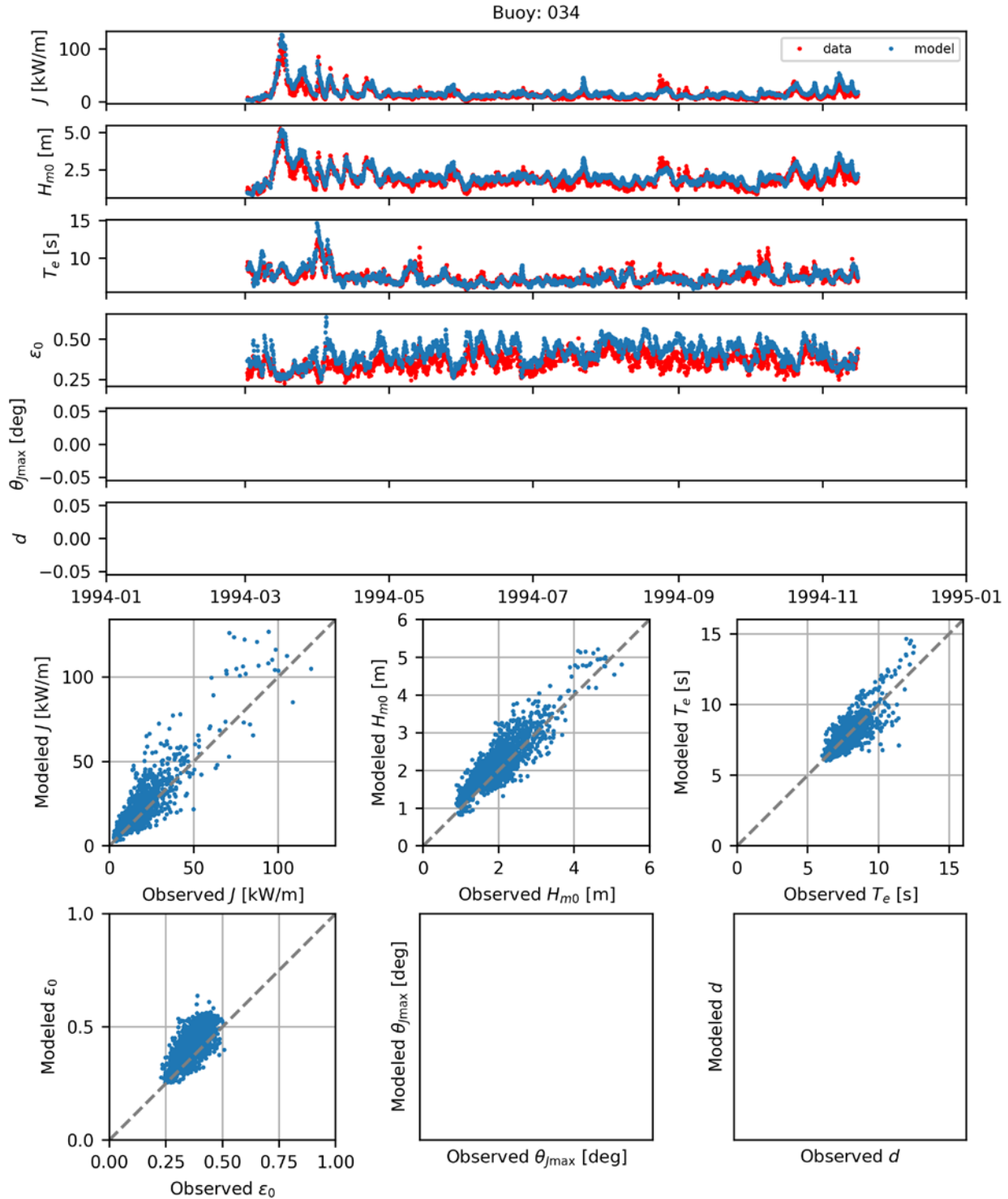


Figure B.3. Comparisons of time series (top) and scatter plots (bottom) of the six model-simulated IEC parameters with observed data at CDIP Buoy 034 for 1994.

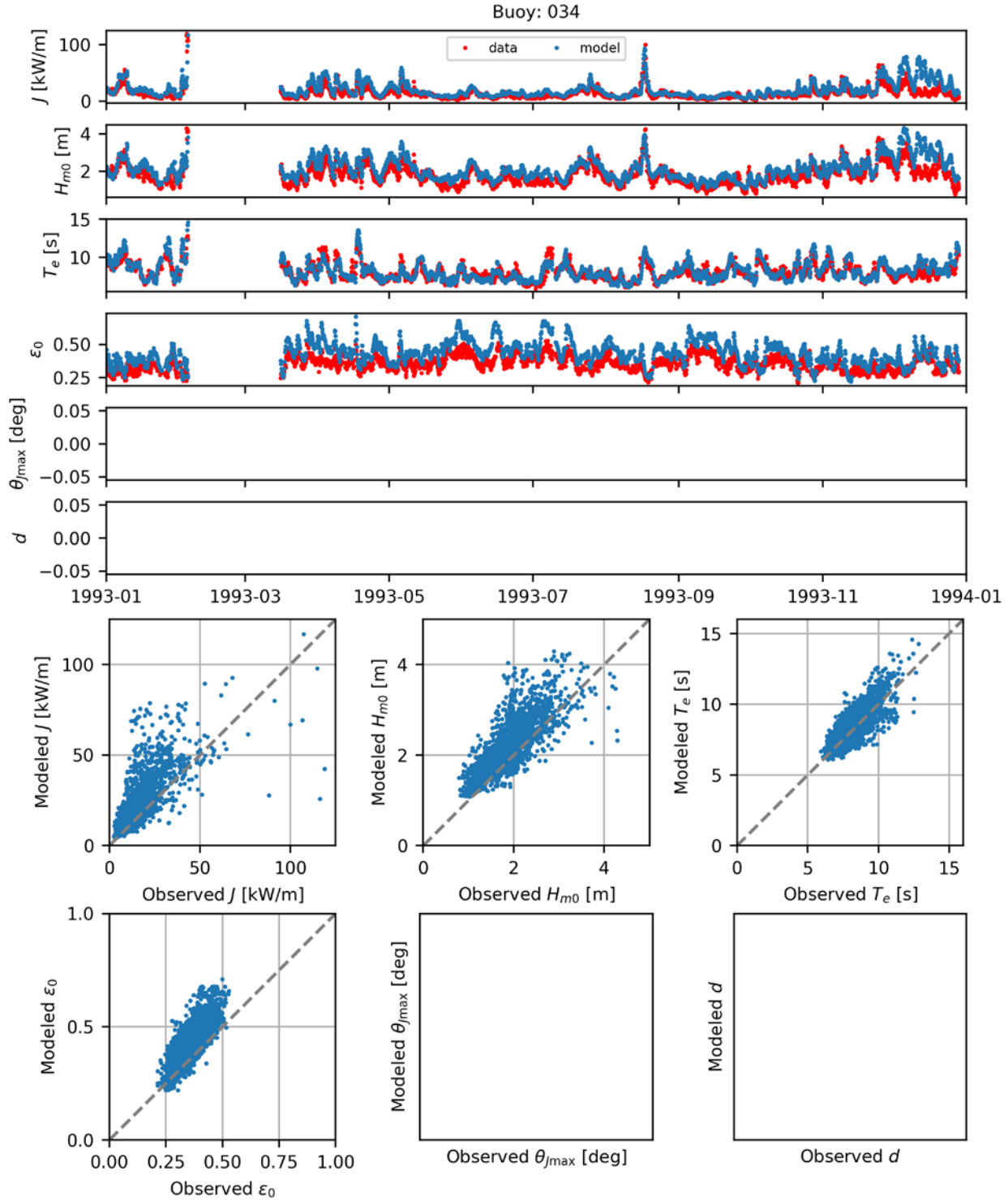


Figure B.4. Comparisons of time series (top) and scatter plots (bottom) of the six model-simulated IEC parameters with observed data at CDIP Buoy 034 for 1993.

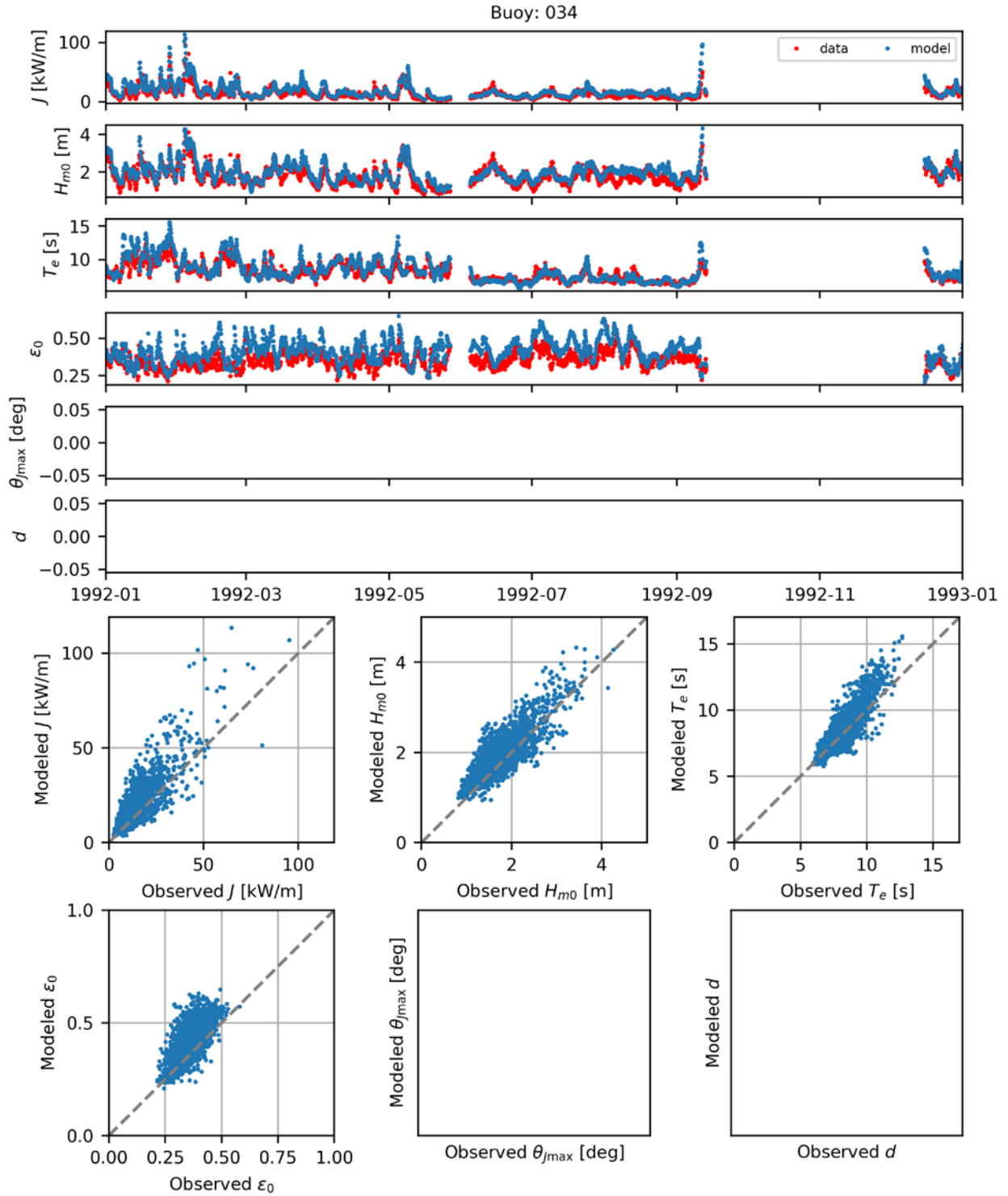


Figure B.5. Comparisons of time series (top) and scatter plots (bottom) of the six model-simulated IEC parameters with observed data at CDIP Buoy 034 for 1992.

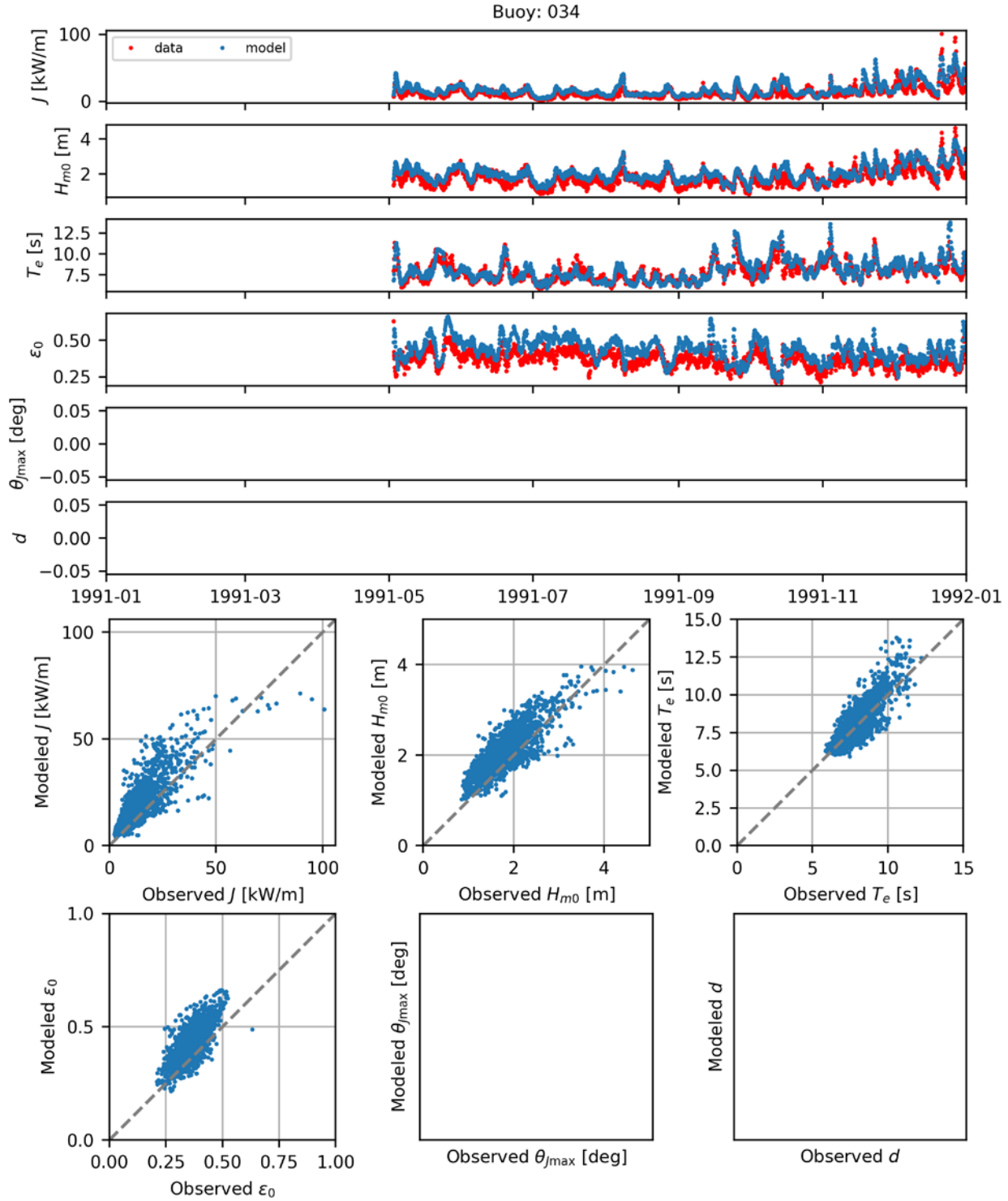


Figure B.6. Comparisons of time series (top) and scatter plots (bottom) of the six model-simulated IEC parameters with observed data at CDIP Buoy 034 for 1991.

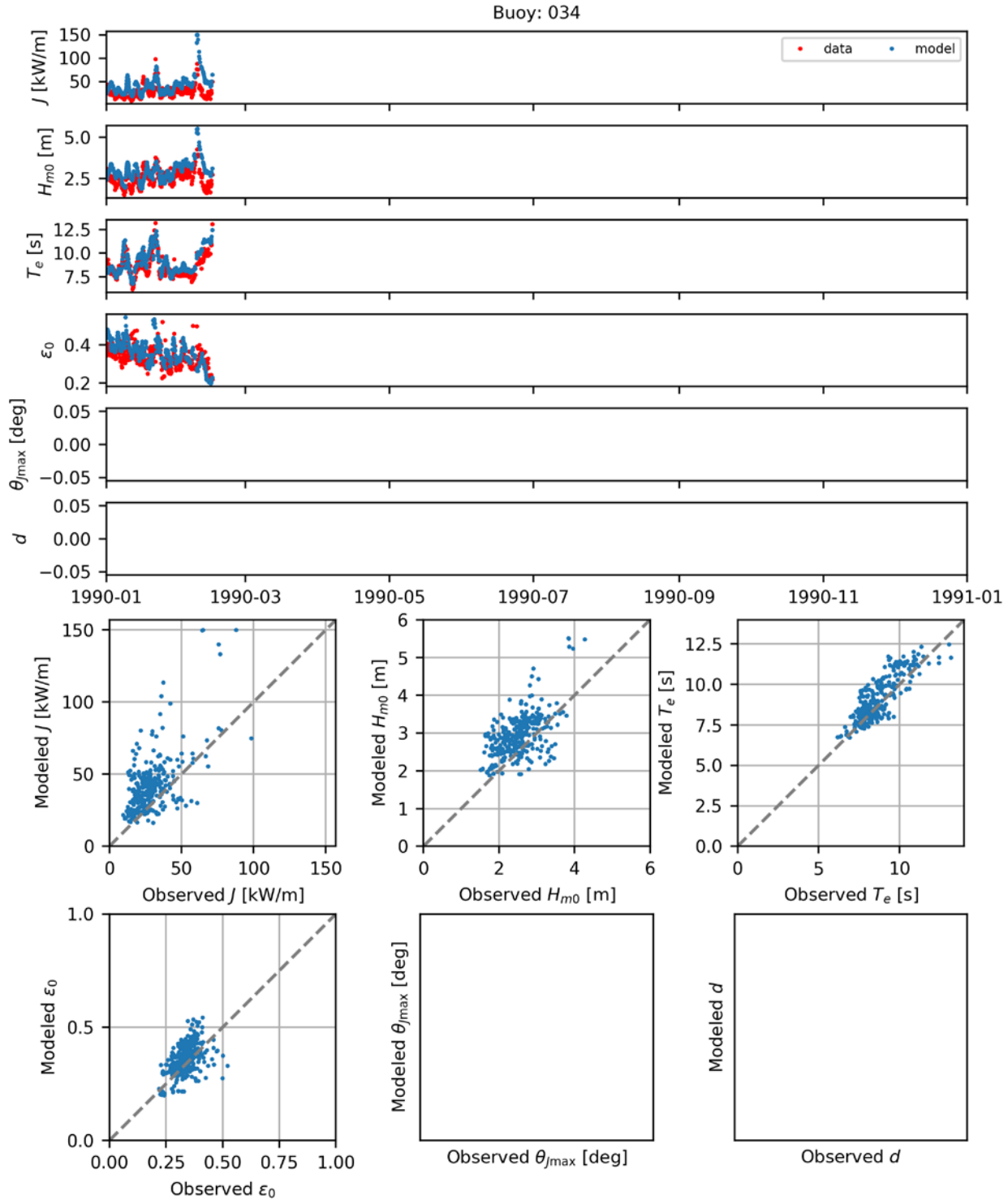


Figure B.7. Comparisons of time series (top) and scatter plots (bottom) of the six model-simulated IEC parameters with observed data at CDIP Buoy 034 for 1990.

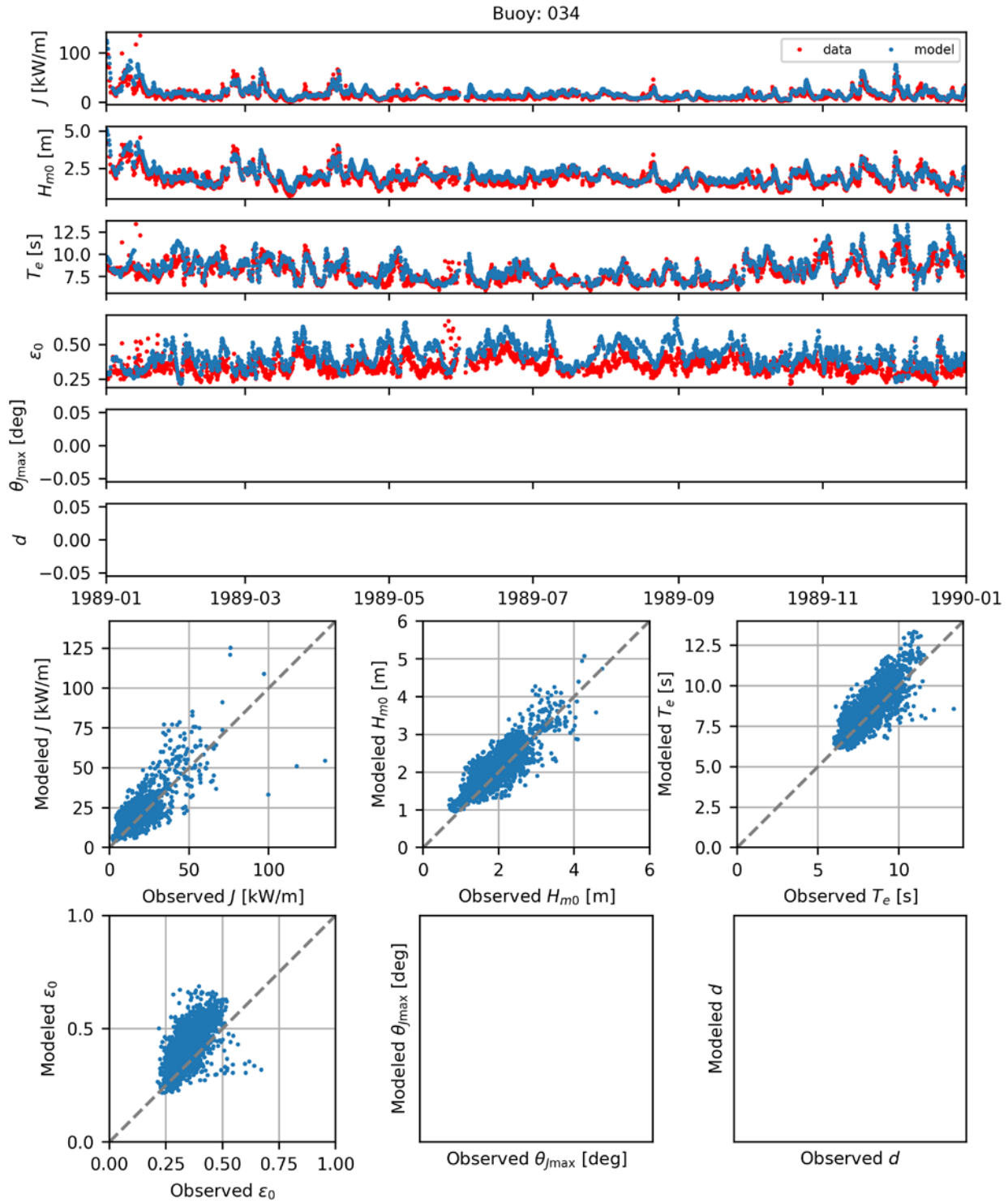


Figure B.8. Comparisons of time series (top) and scatter plots (bottom) of the six model-simulated IEC parameters with observed data at CDIP Buoy 034 for 1989.

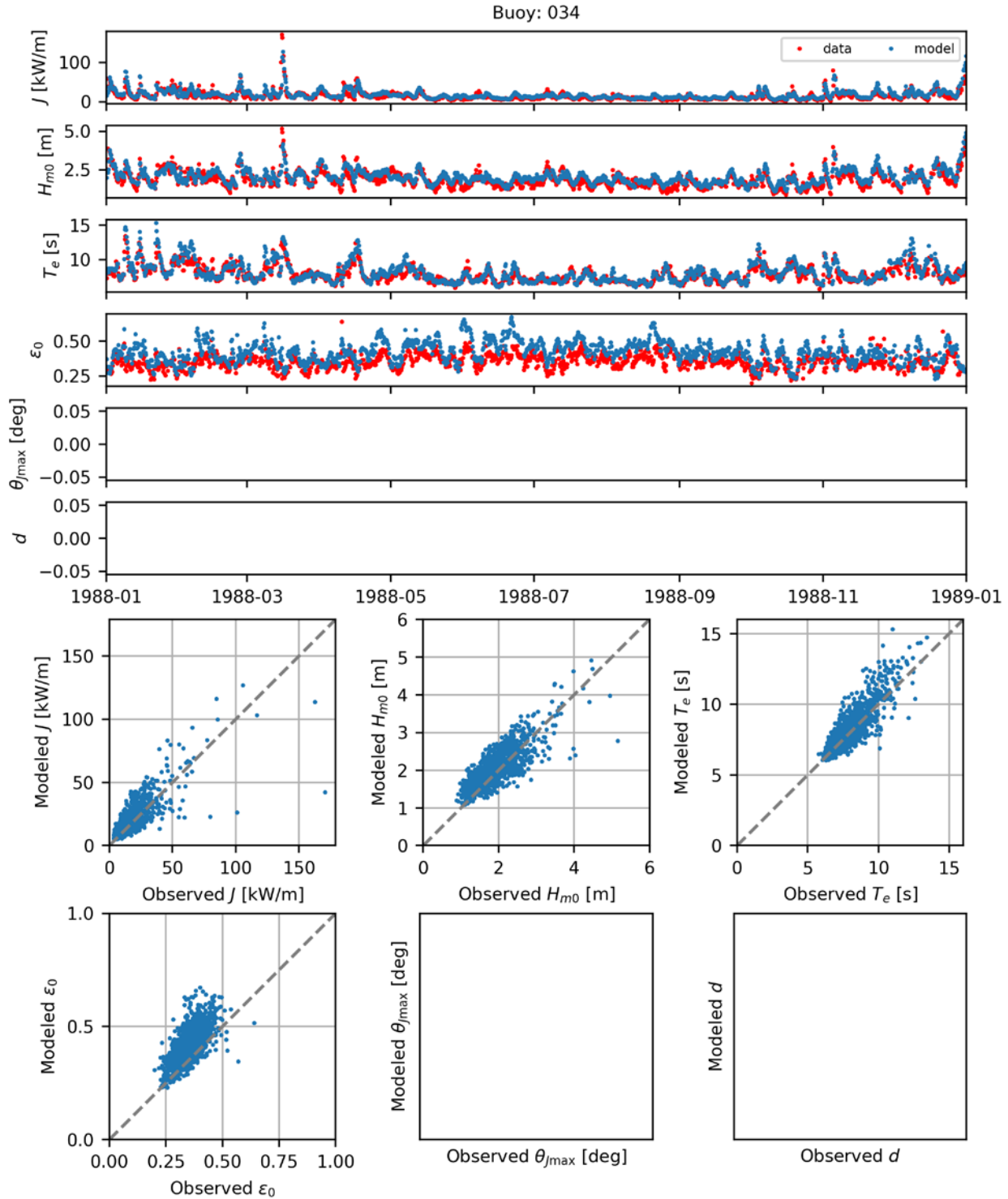


Figure B.9. Comparisons of time series (top) and scatter plots (bottom) of the six model-simulated IEC parameters with observed data at CDIP Buoy 034 for 1988.

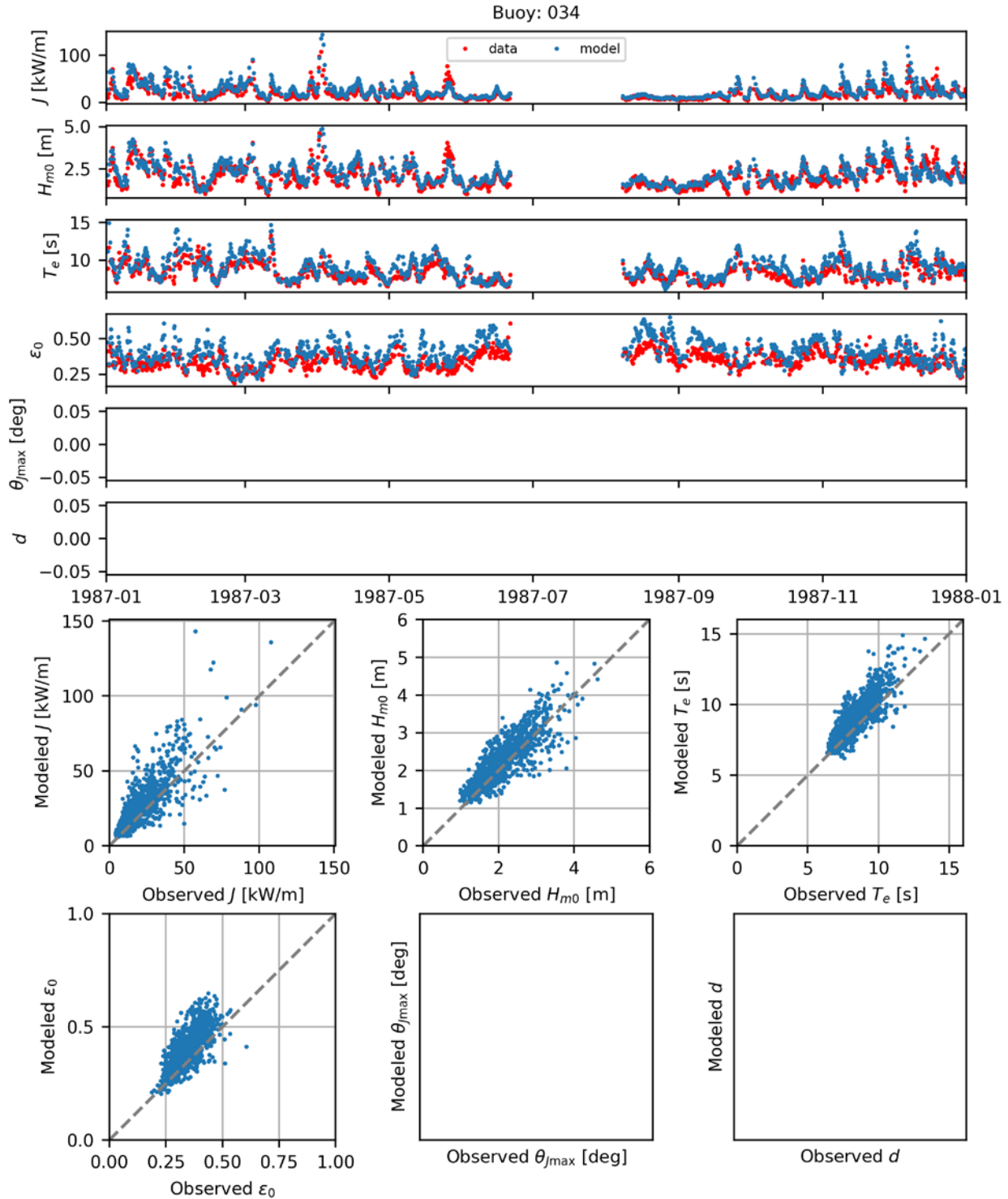


Figure B.10. Comparisons of time series (top) and scatter plots (bottom) of the six model-simulated IEC parameters with observed data at CDIP Buoy 034 for 1987.

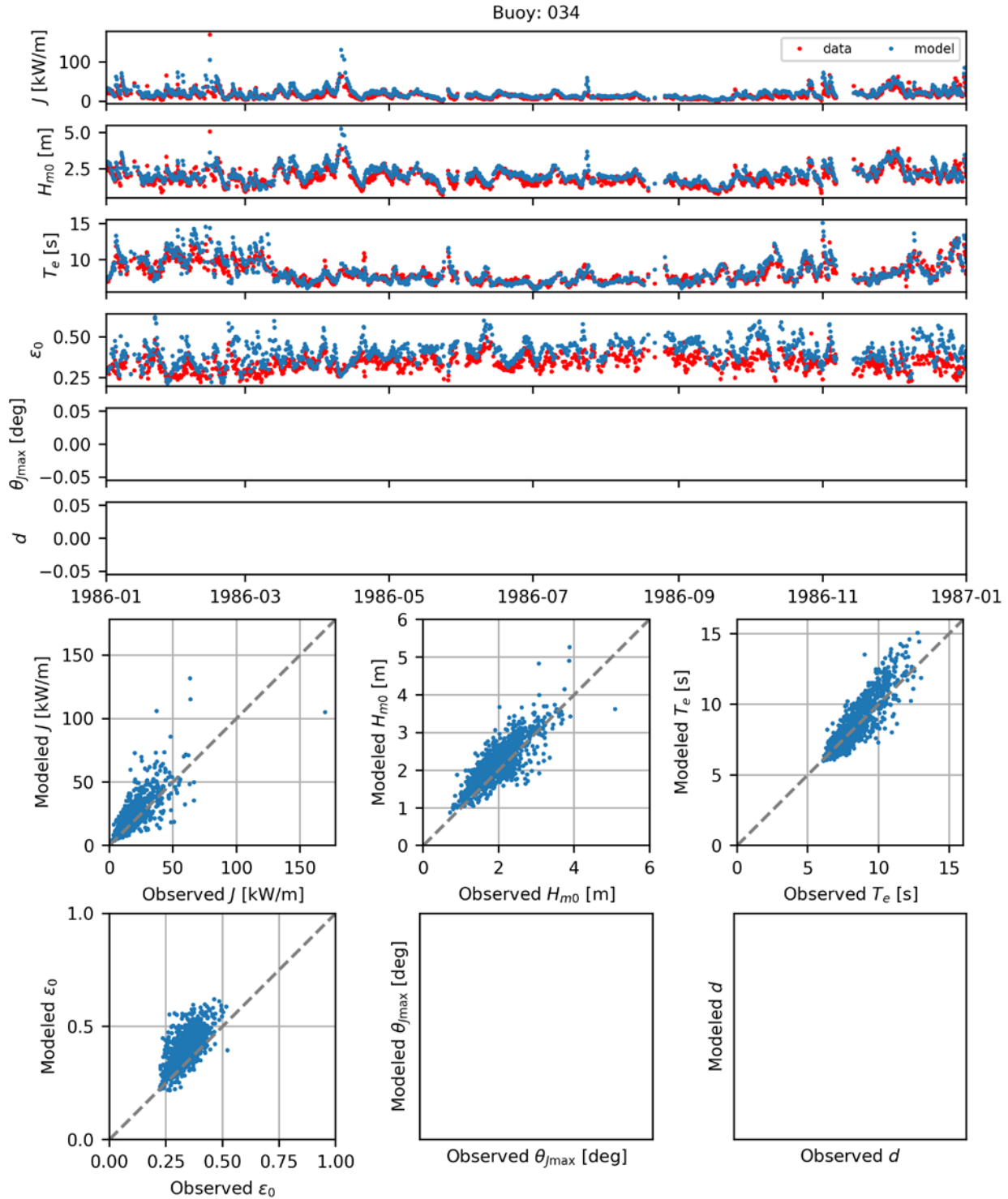


Figure B.11. Comparisons of time series (top) and scatter plots (bottom) of the six model-simulated IEC parameters with observed data at CDIP Buoy 034 for 1986.

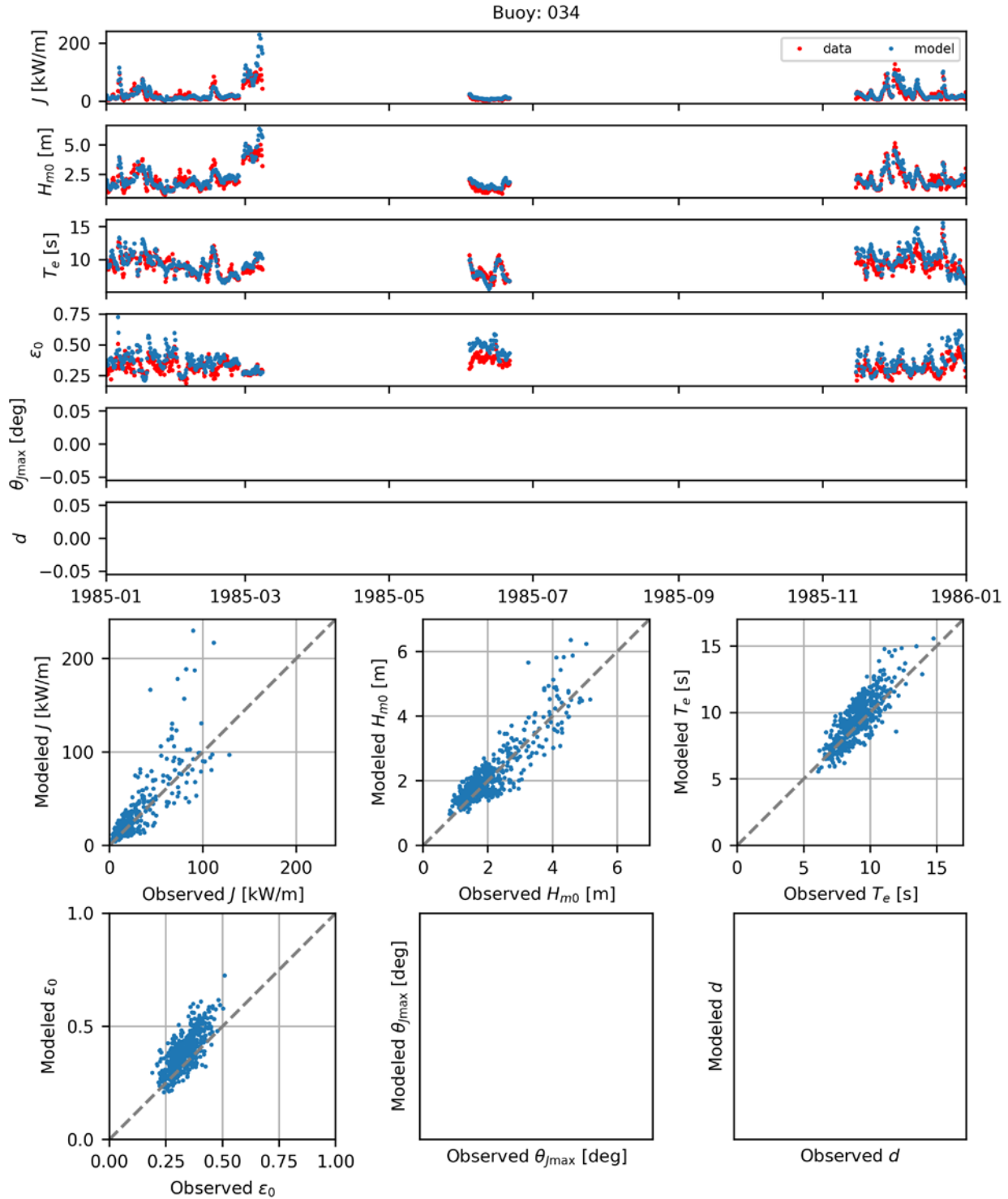


Figure B.12. Comparisons of time series (top) and scatter plots (bottom) of the six model-simulated IEC parameters with observed data at CDIP Buoy 034 for 1985.

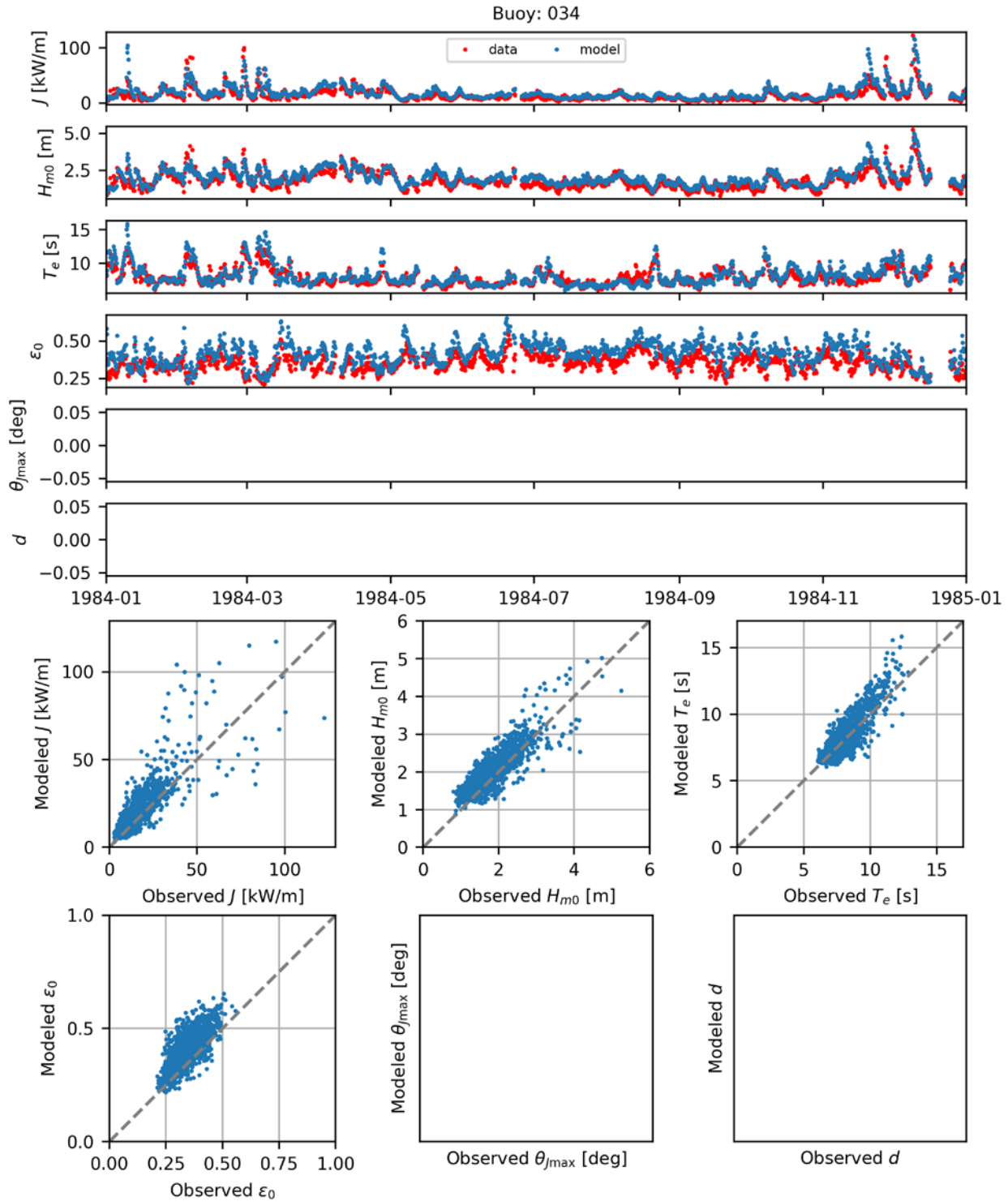


Figure B.13. Comparisons of time series (top) and scatter plots (bottom) of the six model-simulated IEC parameters with observed data at CDIP Buoy 034 for 1984.

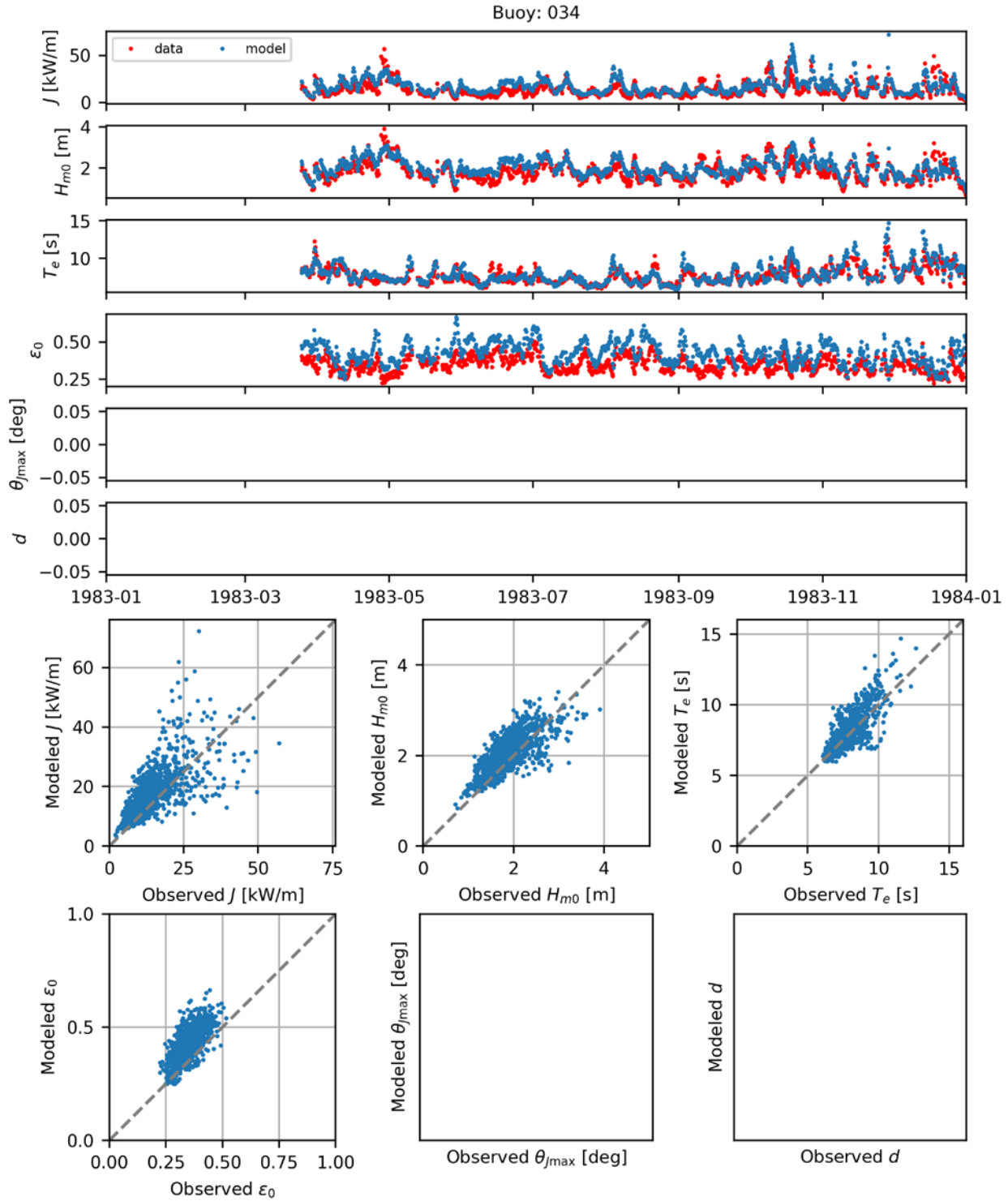


Figure B.14. Comparisons of time series (top) and scatter plots (bottom) of the six model-simulated IEC parameters with observed data at CDIP Buoy 034 for 1983.

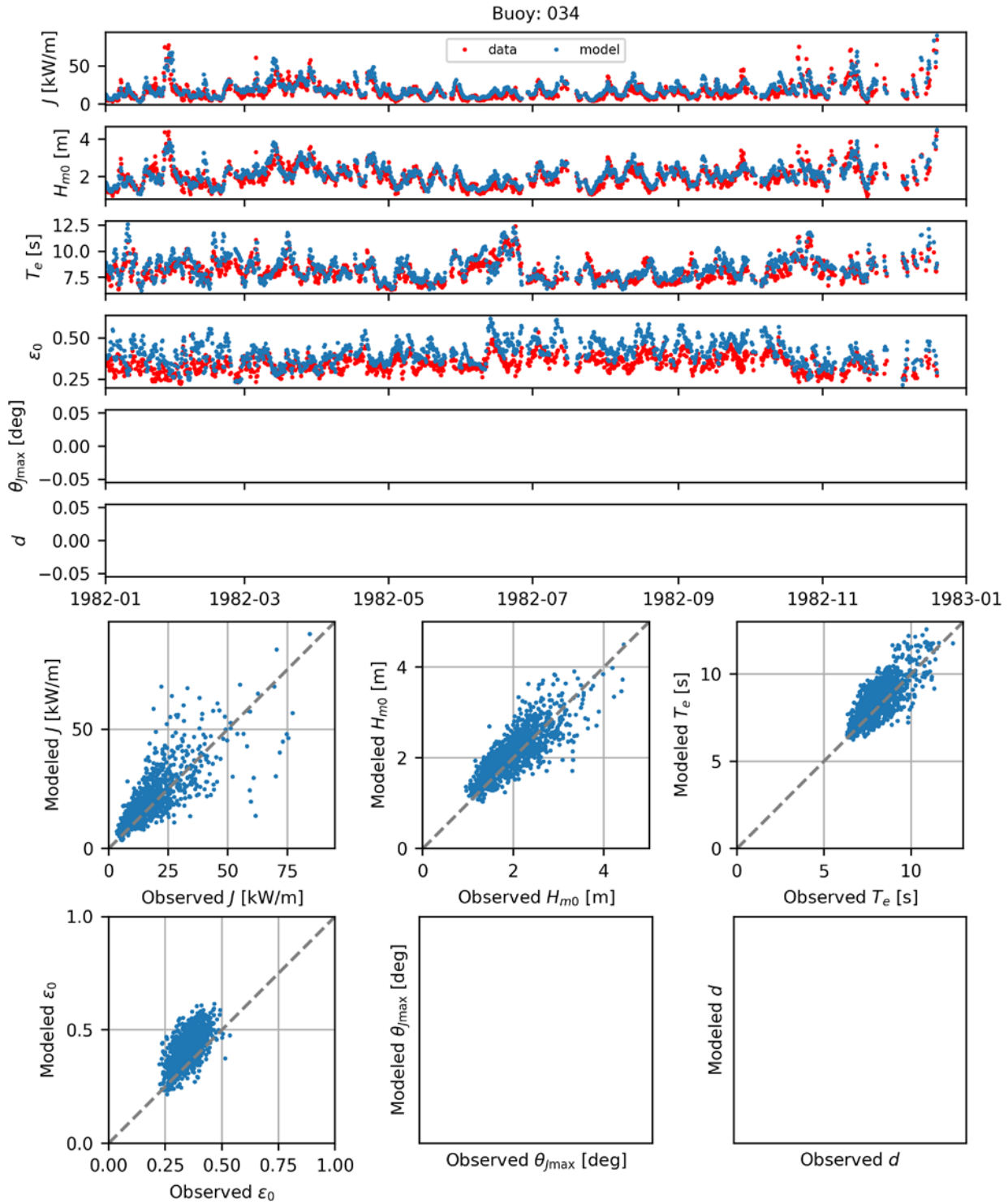


Figure B.15. Comparisons of time series (top) and scatter plots (bottom) of the six model-simulated IEC parameters with observed data at CDIP Buoy 034 for 1982.

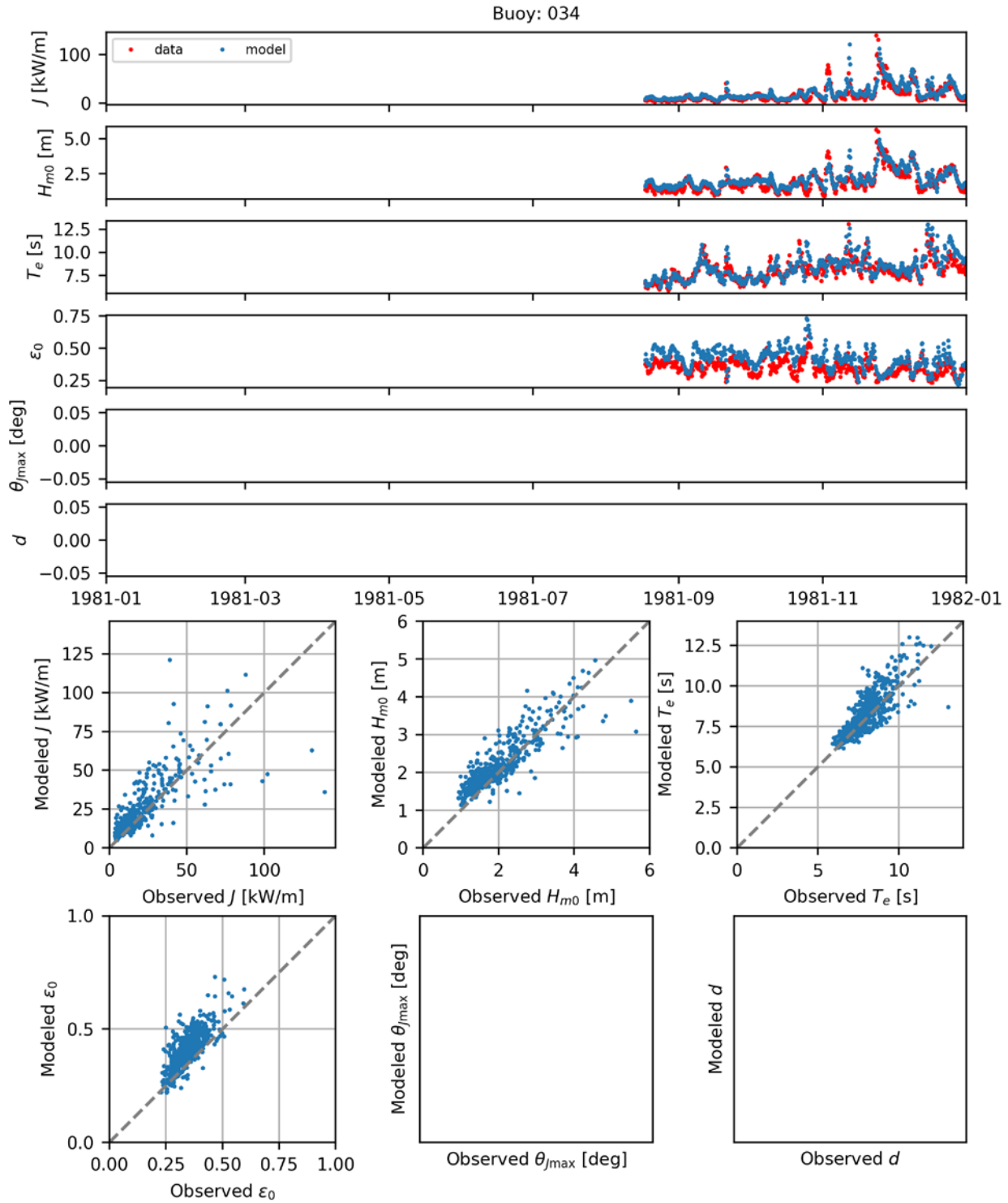


Figure B.16. Comparisons of time series (top) and scatter plots (bottom) of the six model-simulated IEC parameters with observed data at CDIP Buoy 034 for 1981.

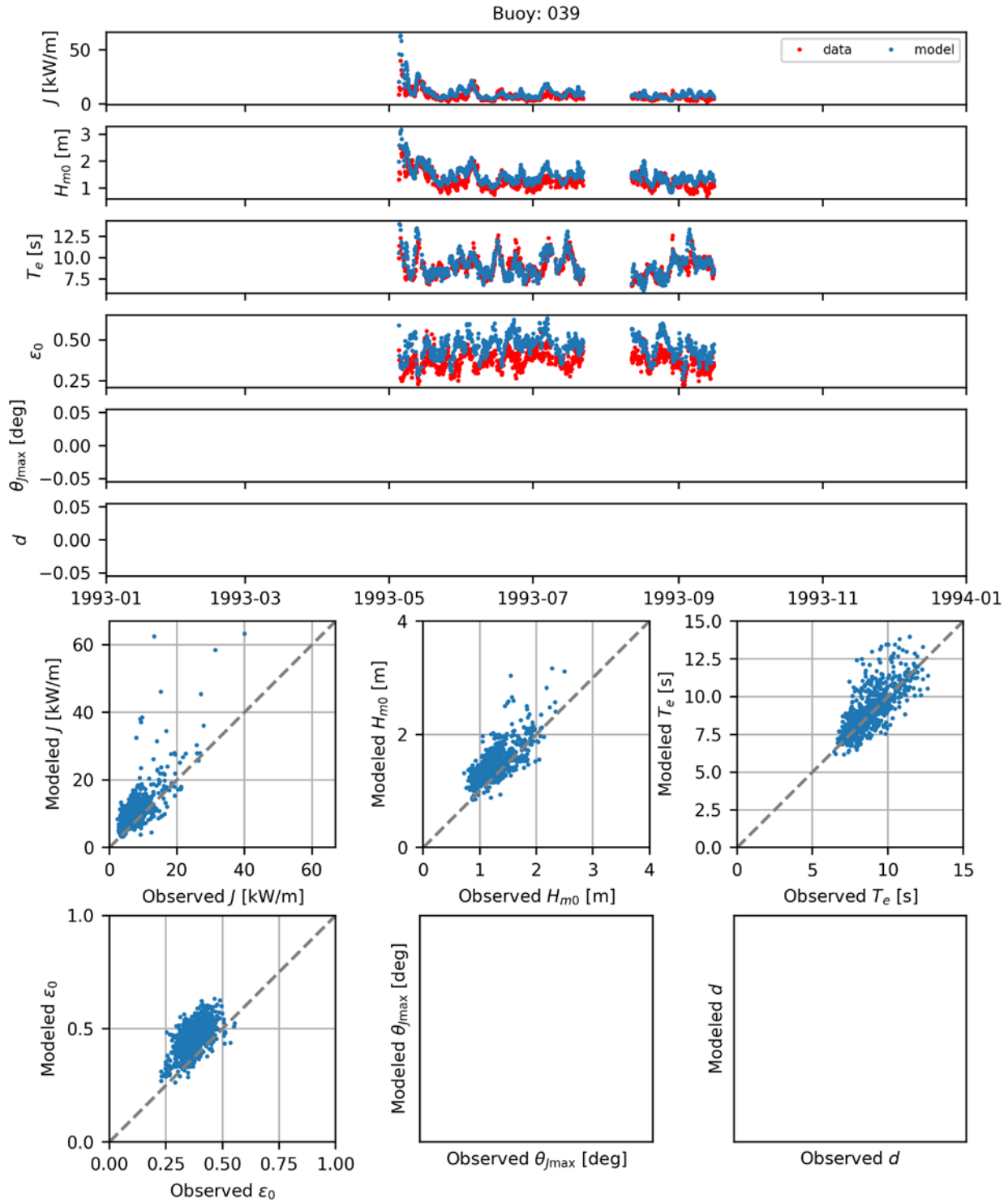


Figure B.17. Comparisons of time series (top) and scatter plots (bottom) of the six model-simulated IEC parameters with observed data at CDIP Buoy 039 for 1993.

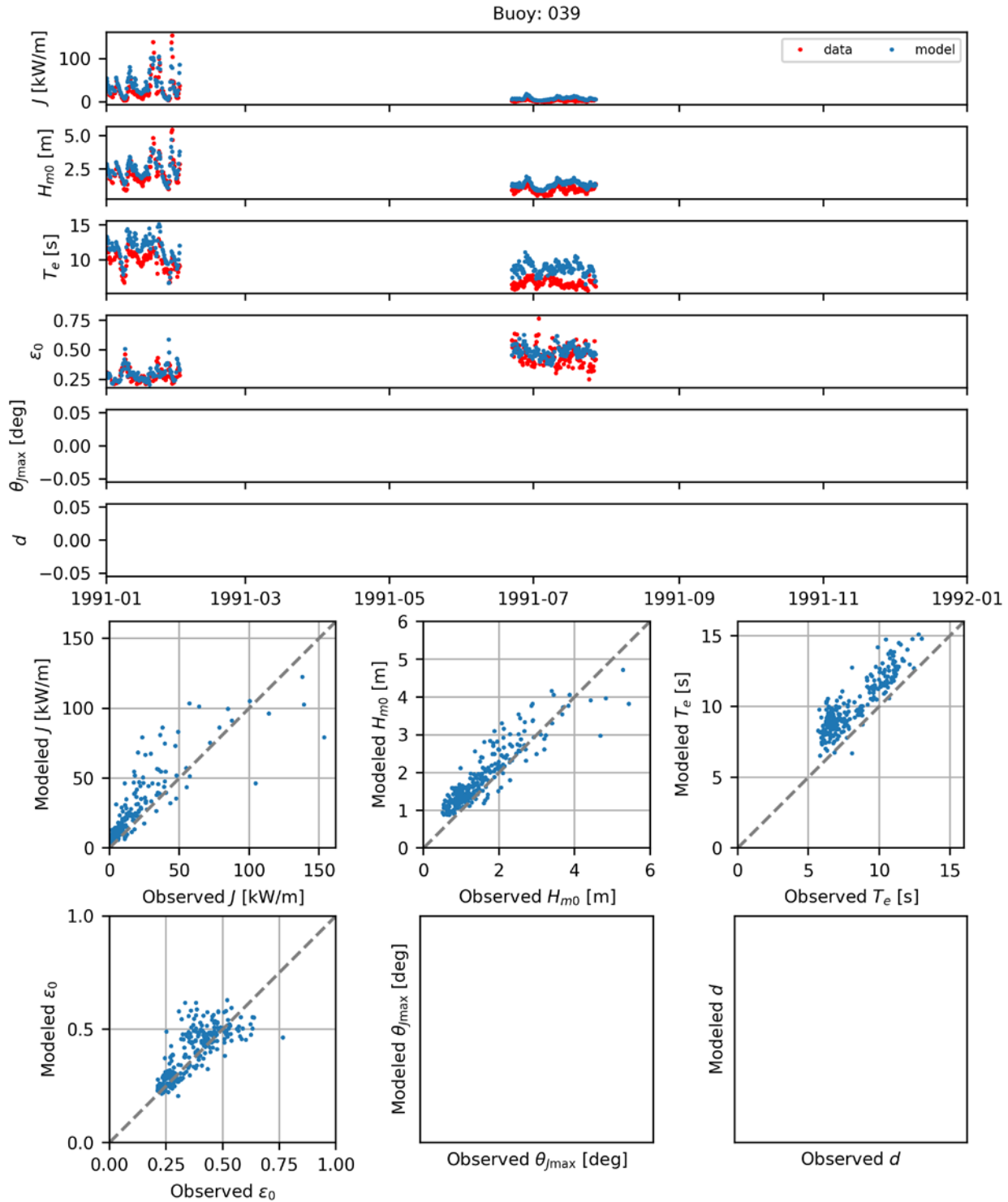


Figure B.18. Comparisons of time series (top) and scatter plots (bottom) the six model-simulated IEC parameters with observed data at CDIP Buoy 039 for 1991.

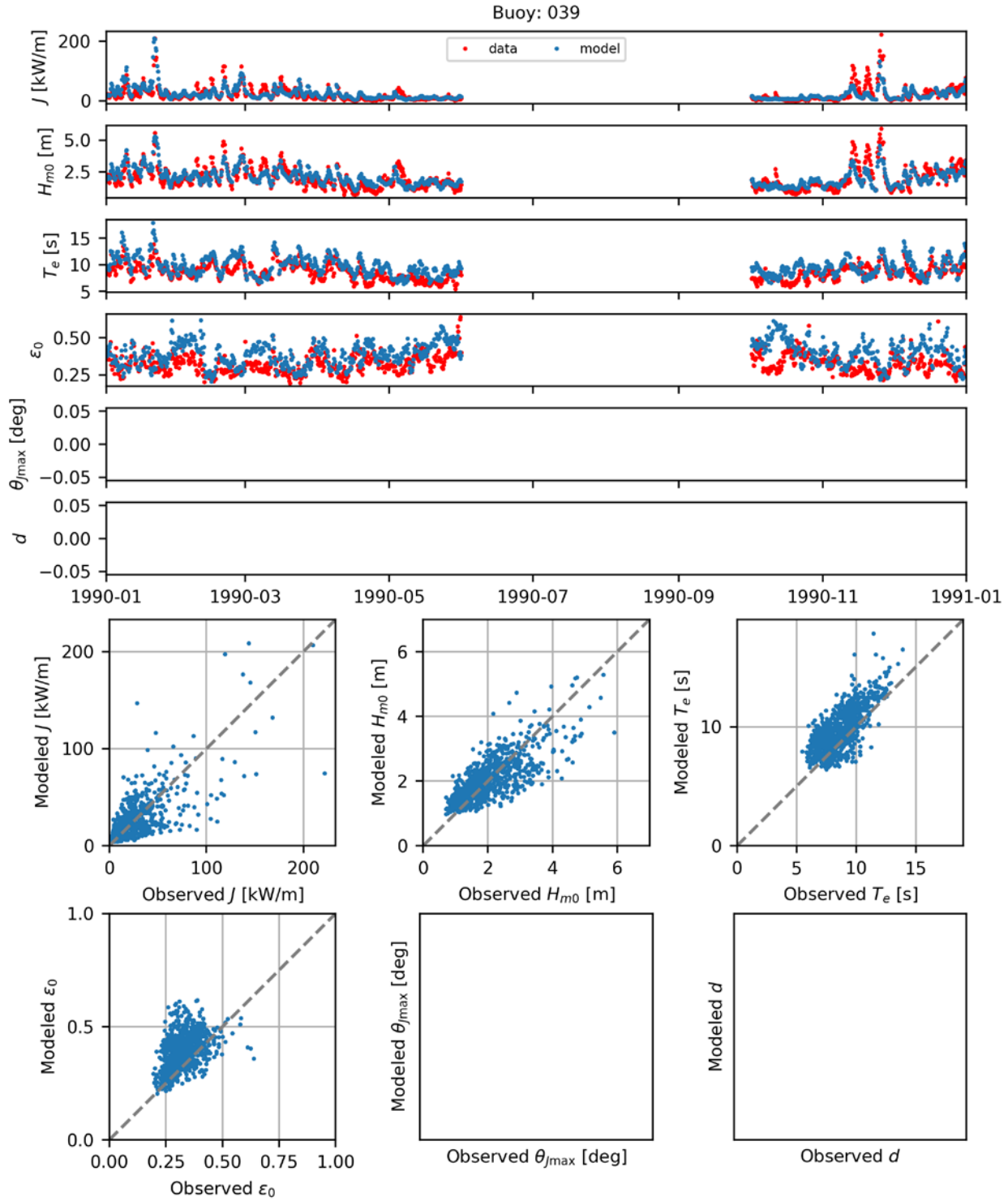


Figure B.19. Comparisons of time series (top) and scatter plots (bottom) the six model-simulated IEC parameters with observed data at CDIP Buoy 039 for 1990.

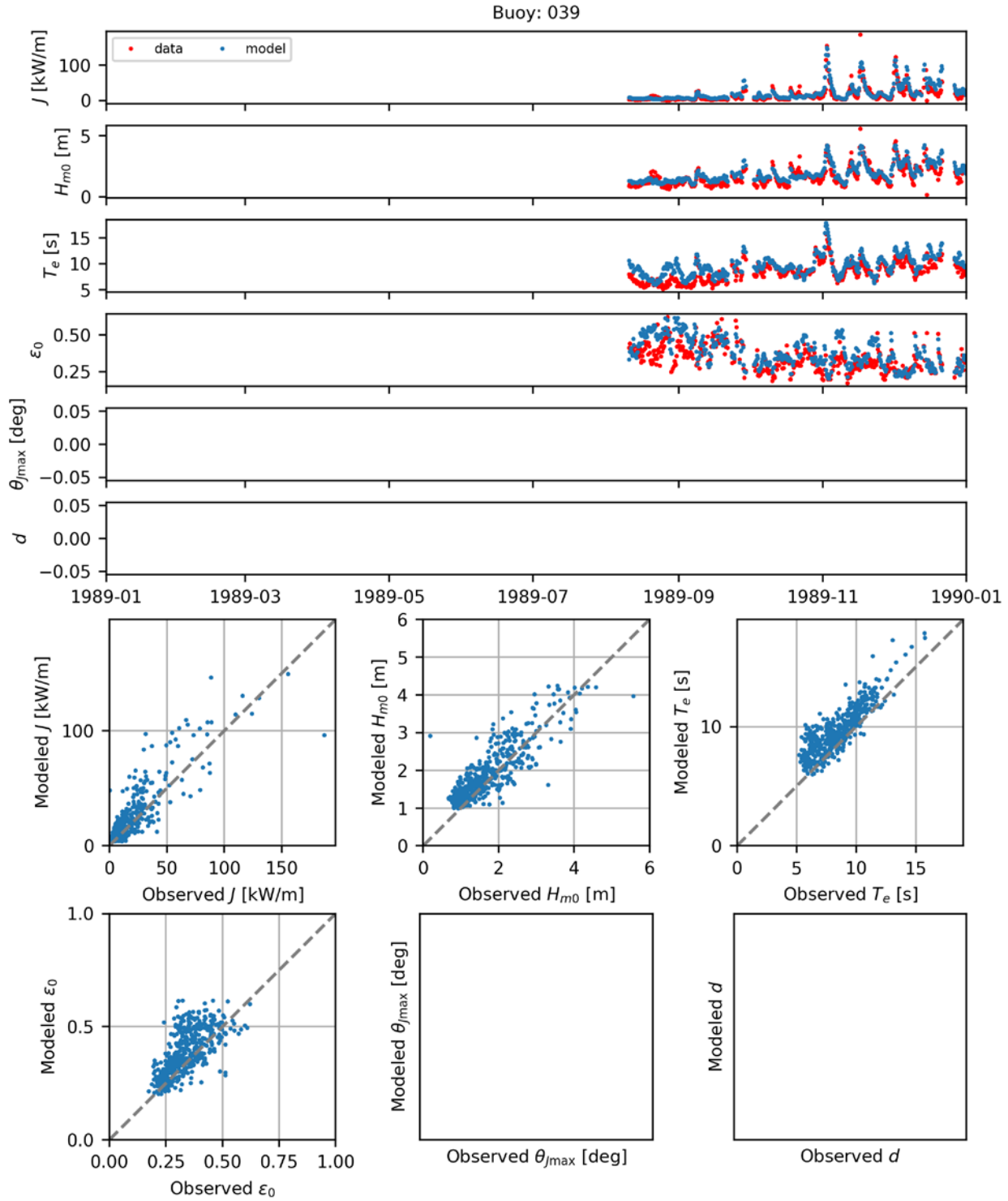


Figure B.20. Comparisons of time series (top) and scatter plots (bottom) the six model-simulated IEC parameters with observed data at CDIP Buoy 039 for 1989.

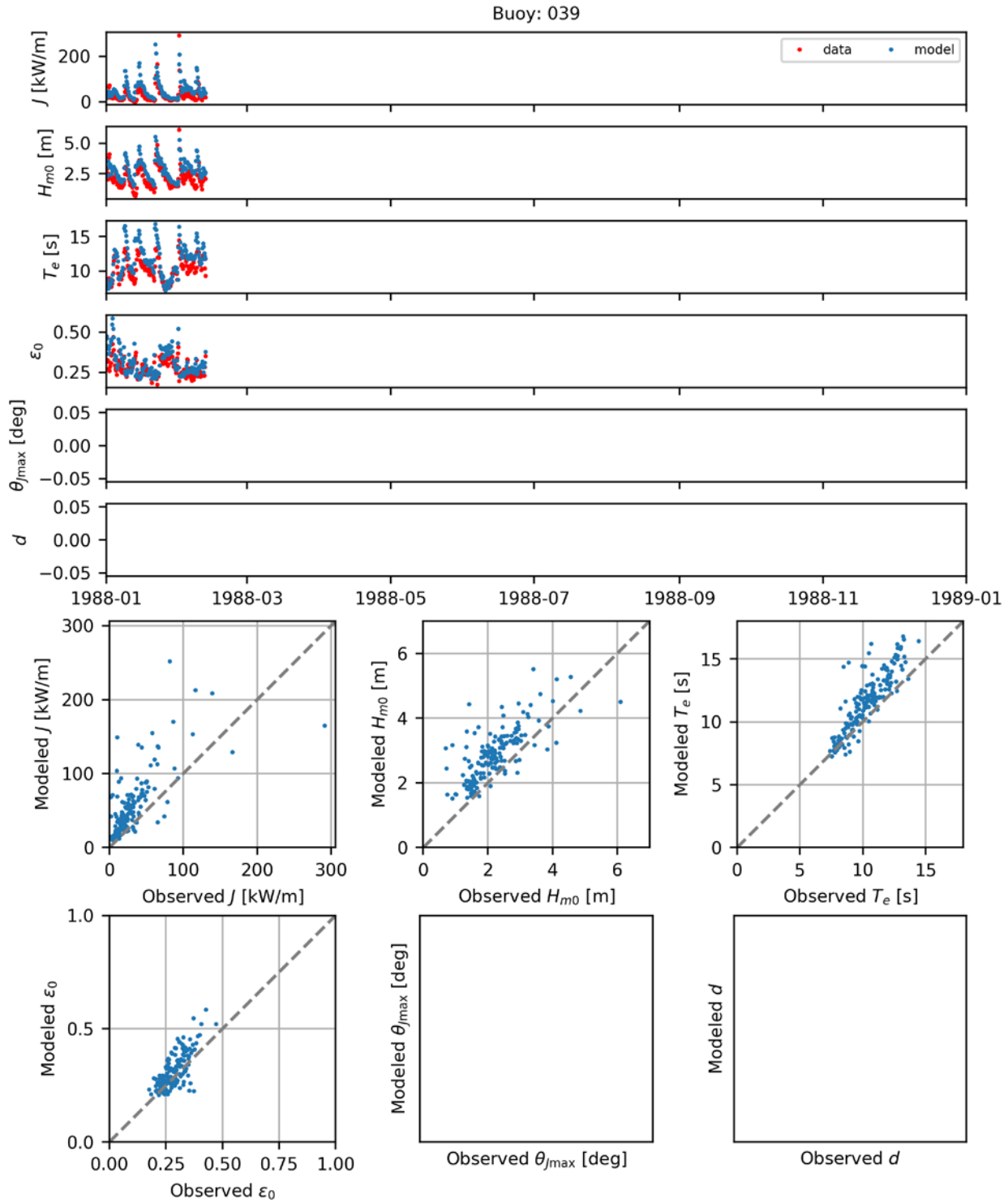


Figure B.21. Comparisons of time series (top) and scatter plots (bottom) the six model-simulated IEC parameters with observed data at CDIP Buoy 039 for 1988.

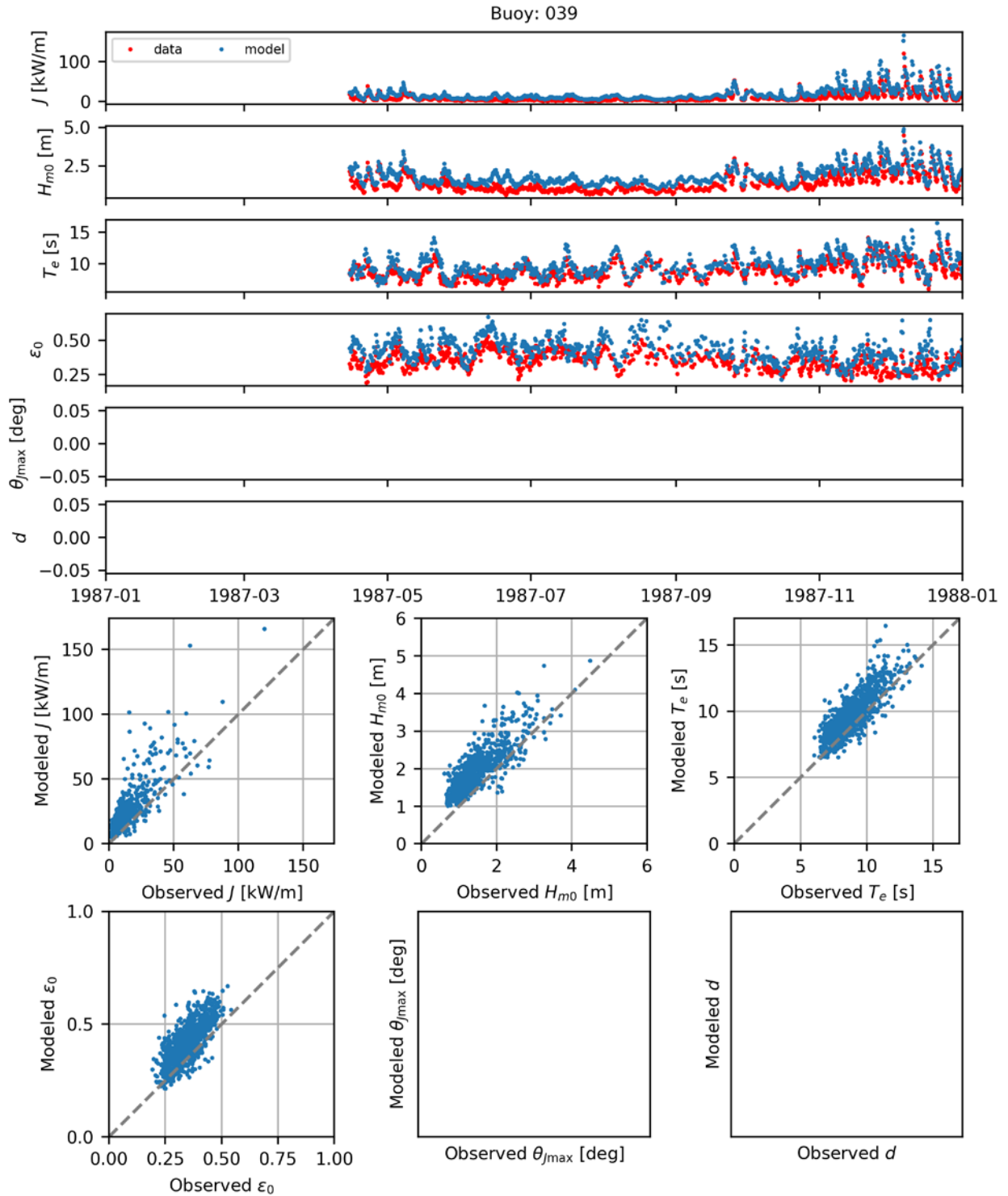


Figure B.22. Comparisons of time series (top) and scatter plots (bottom) the six model-simulated IEC parameters with observed data at CDIP Buoy 039 for 1987.

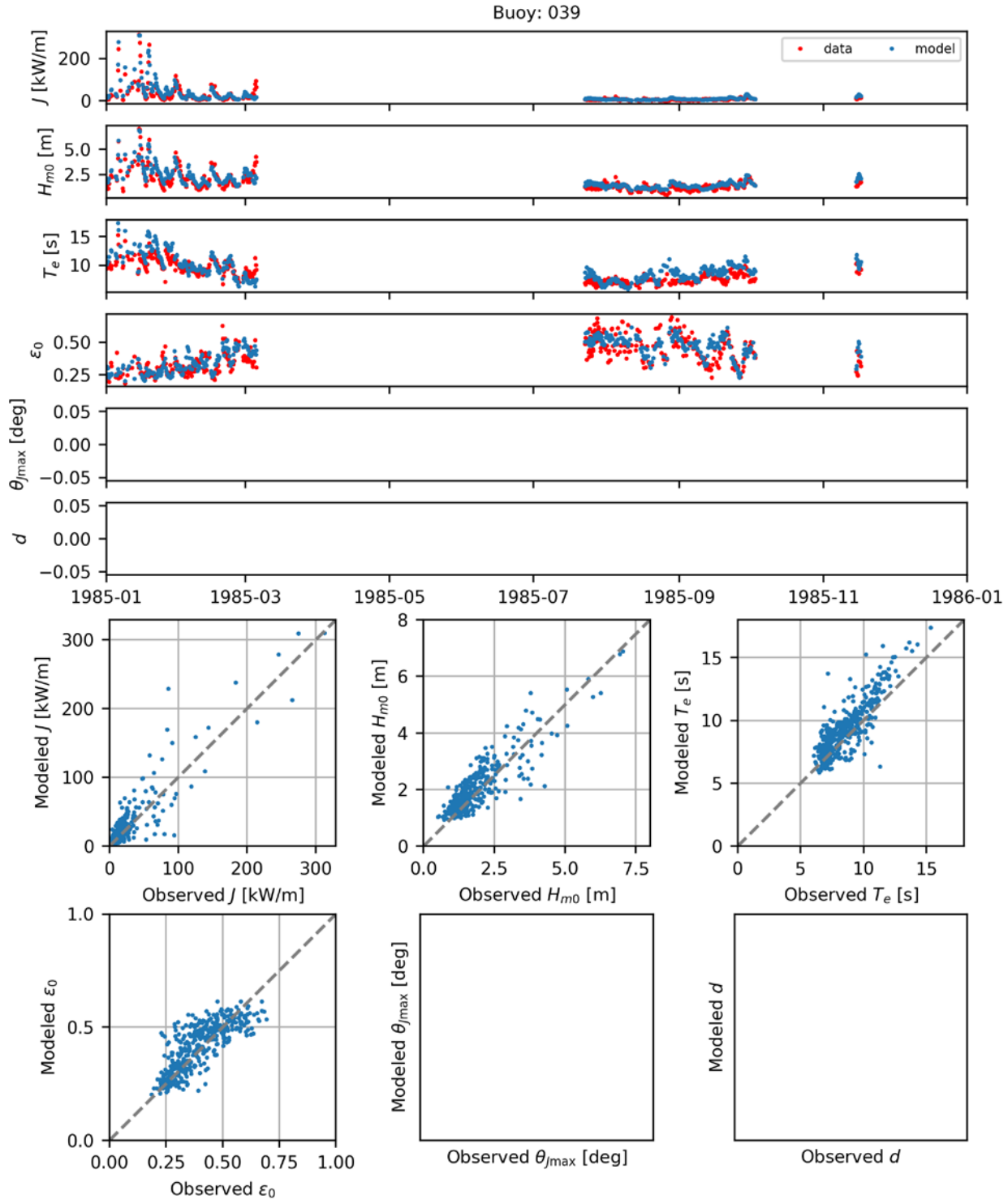


Figure B.23. Comparisons of time series (top) and scatter plots (bottom) the six model-simulated IEC parameters with observed data at CDIP Buoy 039 for 1985.

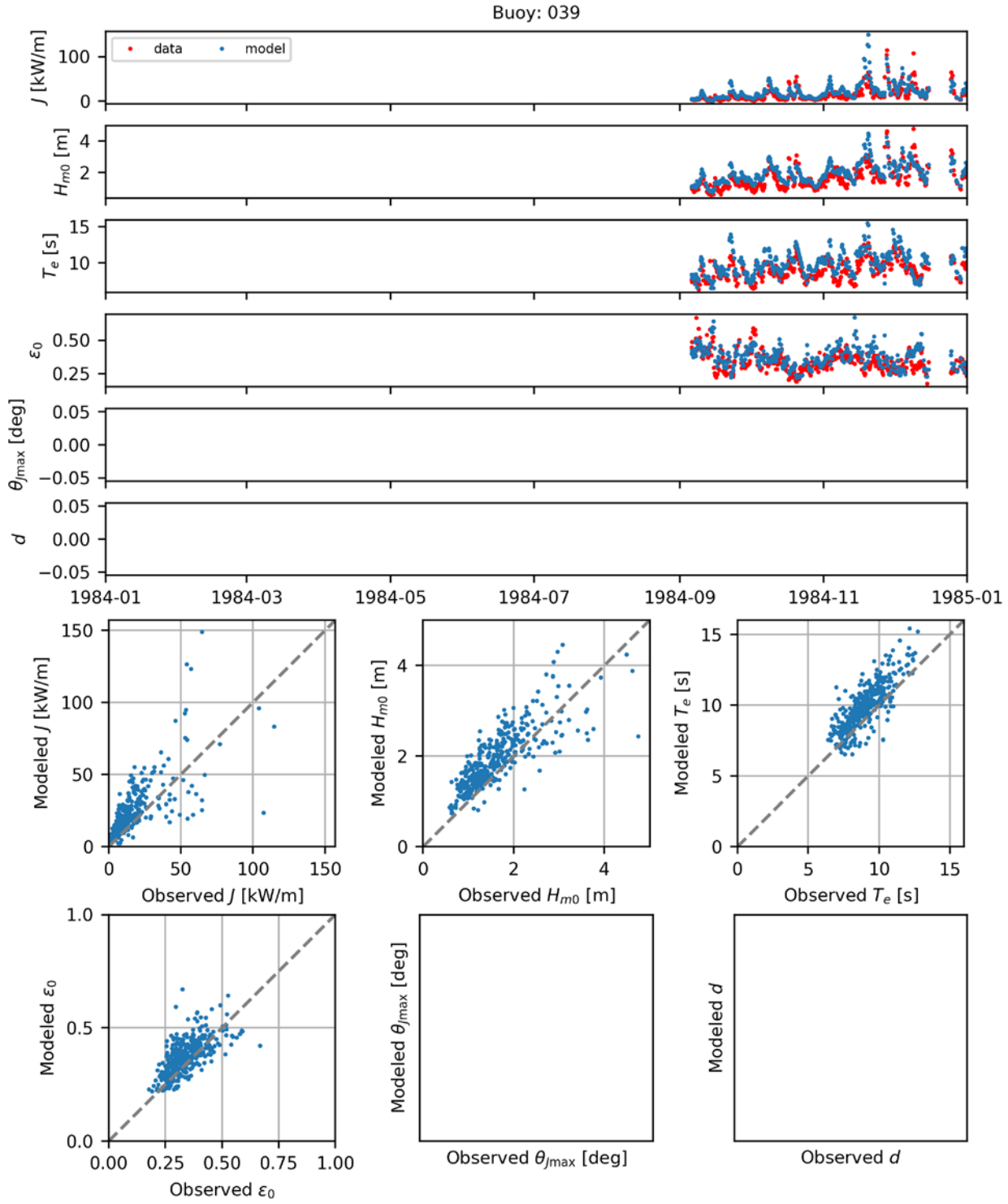


Figure B.24. Comparisons of time series (top) and scatter plots (bottom) the six model-simulated IEC parameters with observed data at CDIP Buoy 039 for 1984.

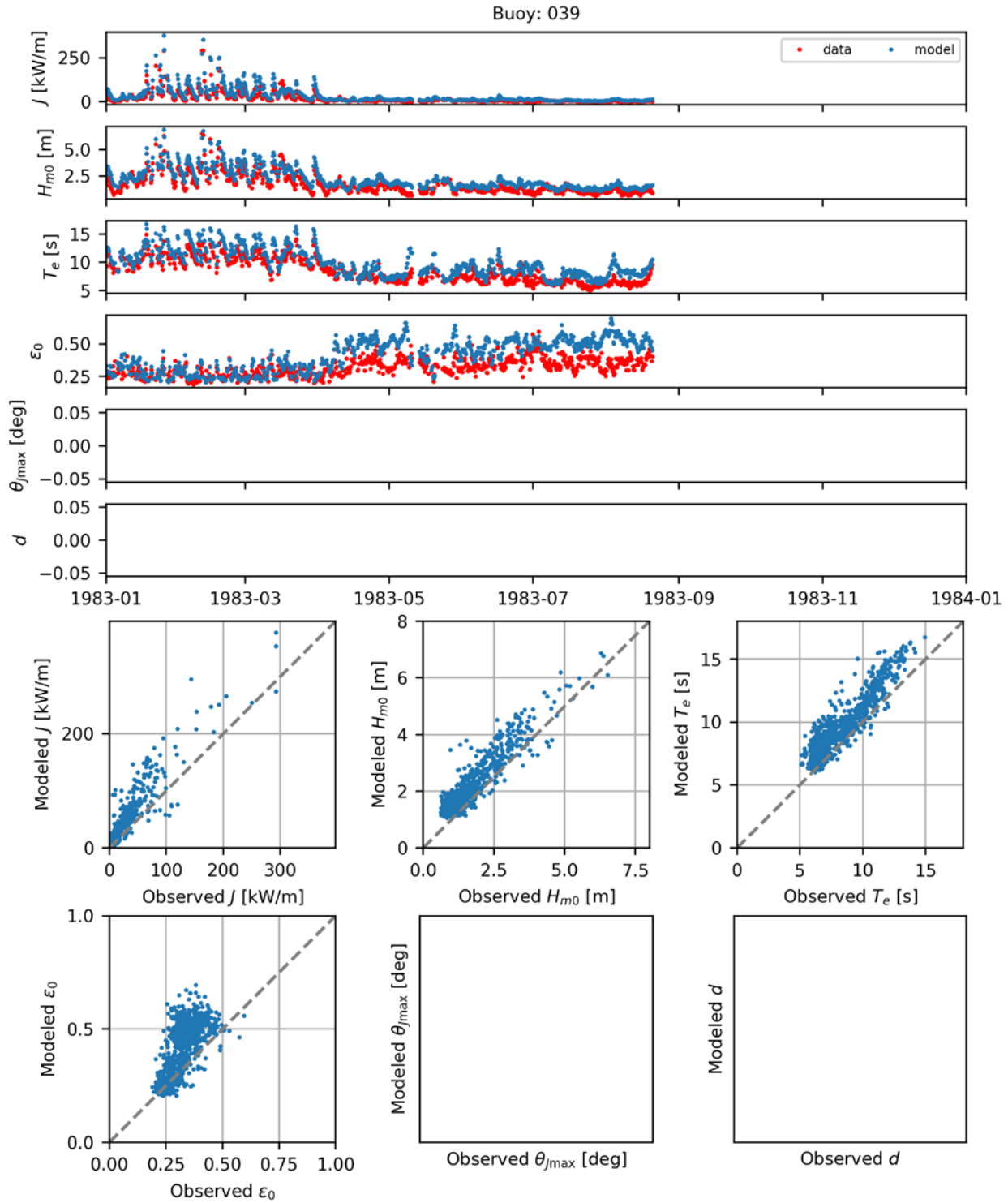


Figure B.25. Comparisons of time series (top) and scatter plots (bottom) the six model-simulated IEC parameters with observed data at CDIP Buoy 039 for 1983.

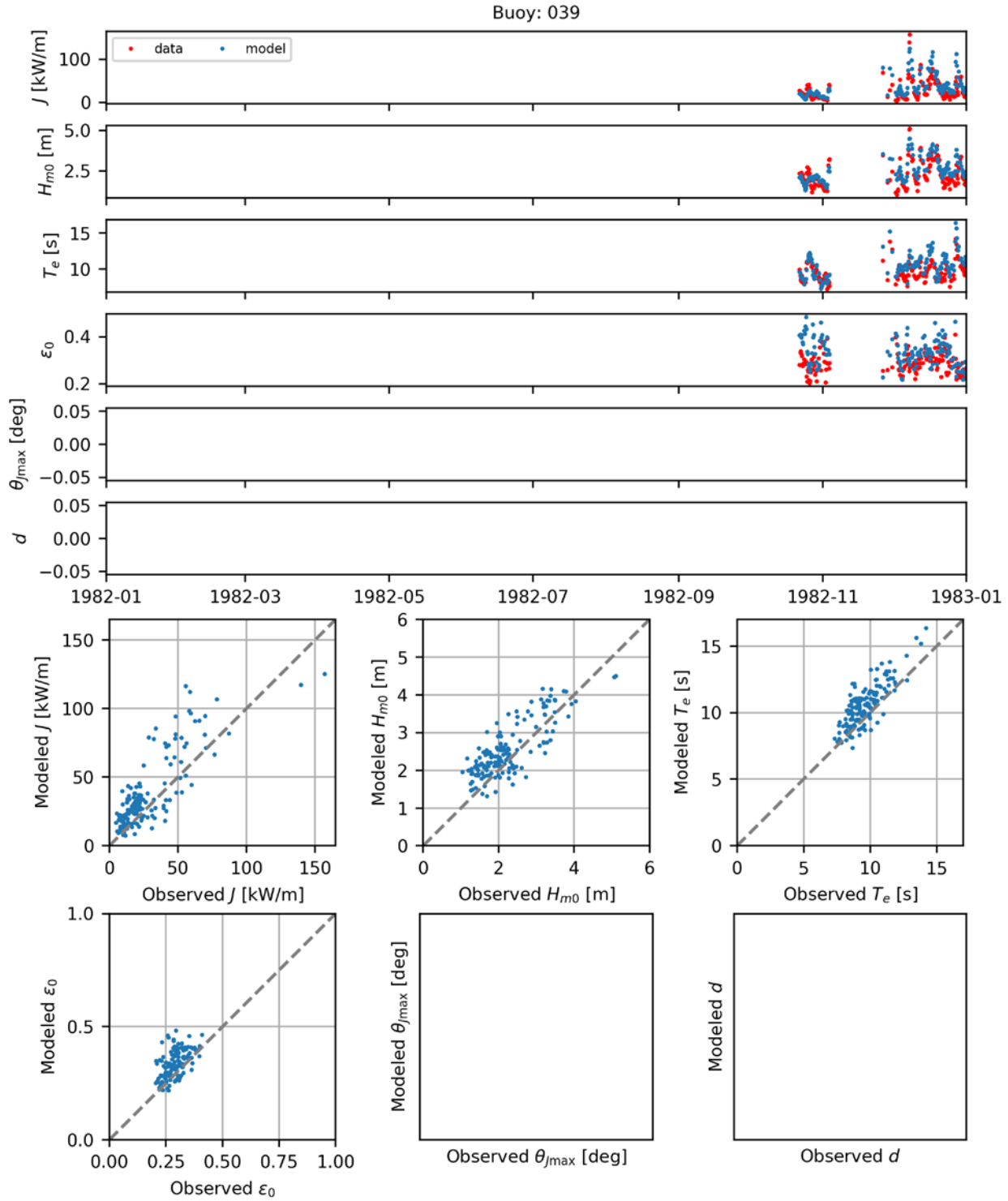


Figure B.26. Comparisons of time series (top) and scatter plots (bottom) the six model-simulated IEC parameters with observed data at CDIP Buoy 039 for 1982.

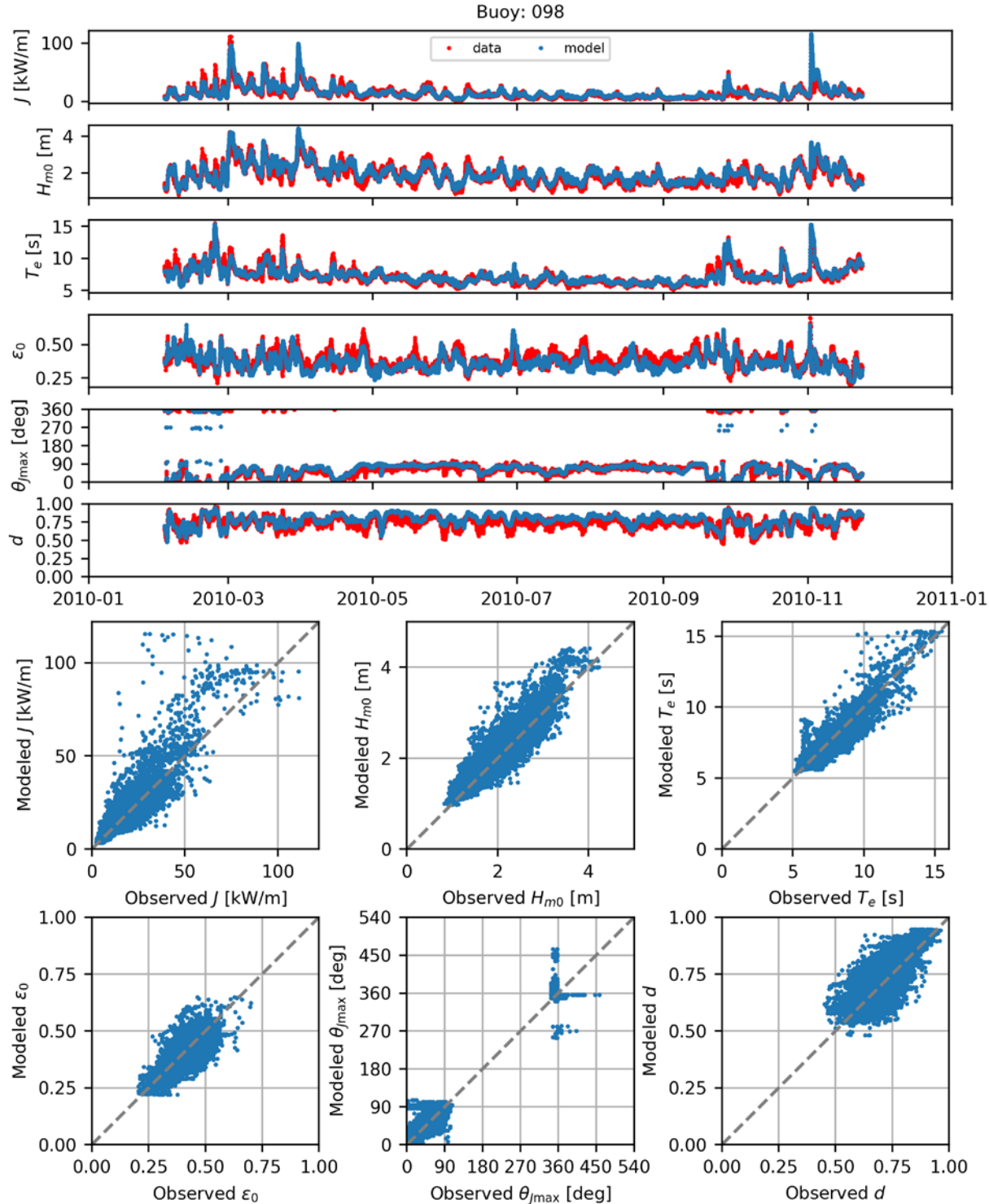


Figure B.27. Comparisons of time series (top) and scatter plots (bottom) the six model-simulated IEC parameters with observed data at CDIP Buoy 098 for 2010.

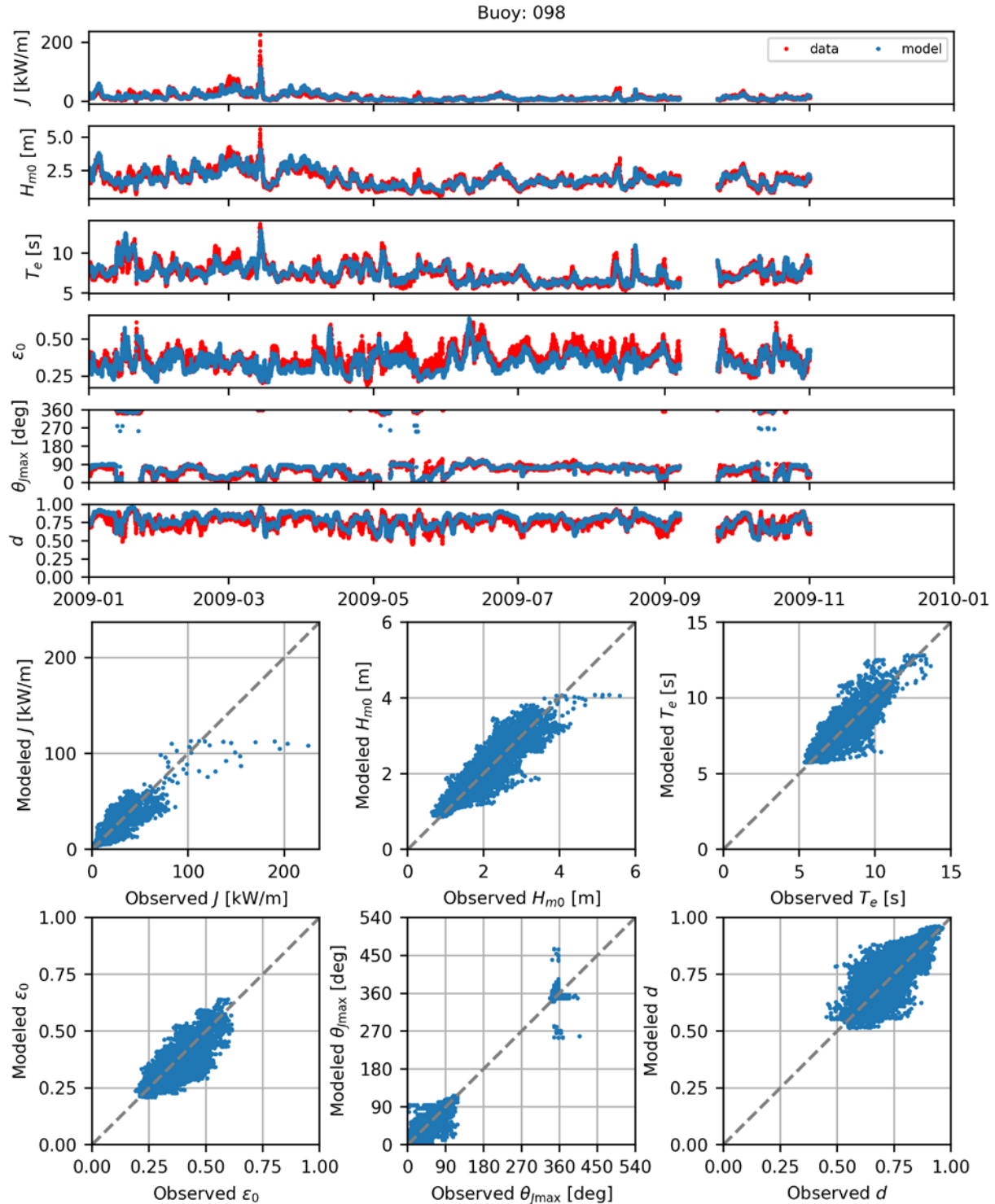


Figure B.28. Comparisons of time series (top) and scatter plots (bottom) the six model-simulated IEC parameters with observed data at CDIP Buoy 098 for 2009.

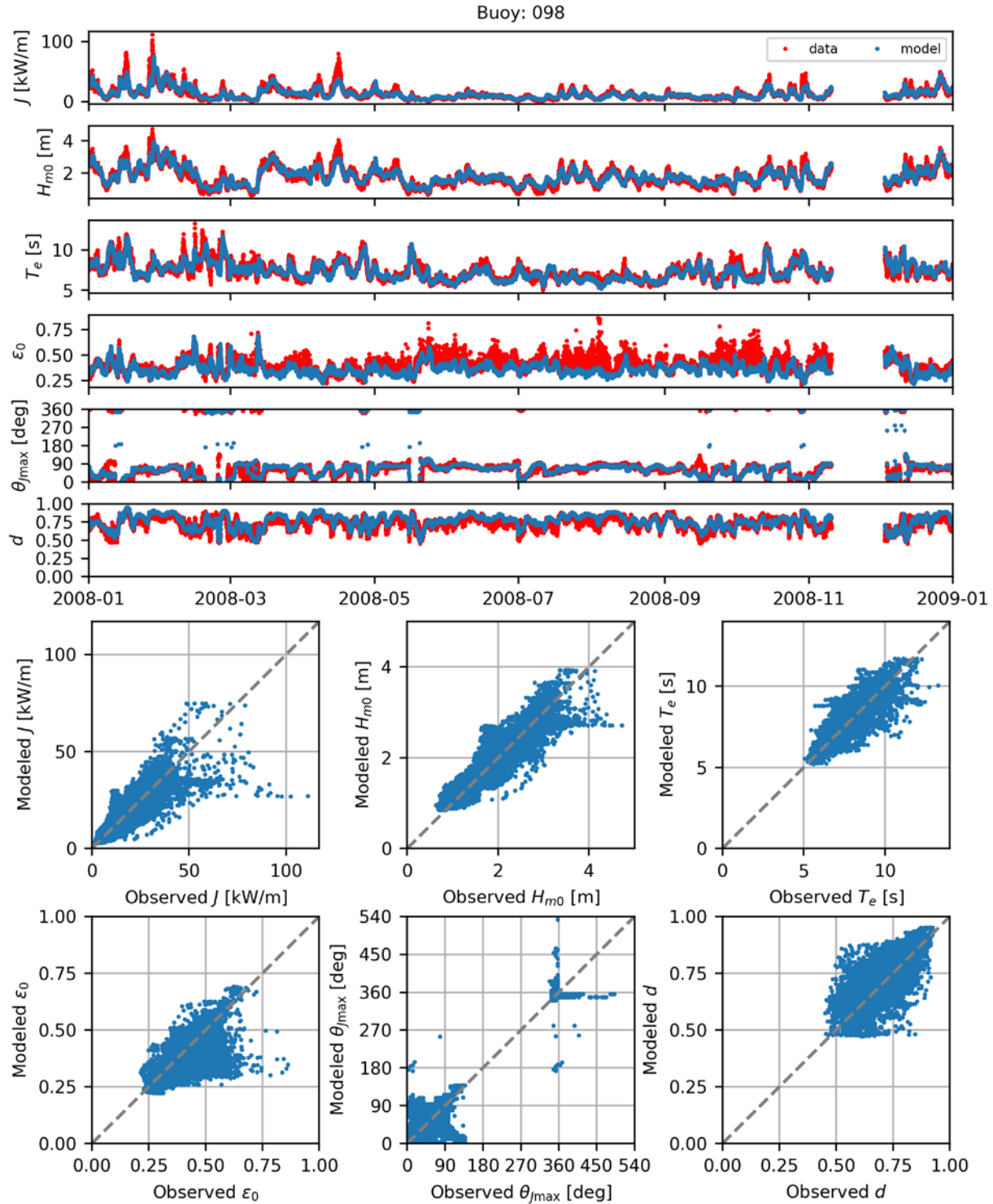


Figure B.29. Comparisons of time series (top) and scatter plots (bottom) the six model-simulated IEC parameters with observed data at CDIP Buoy 098 for 2008.

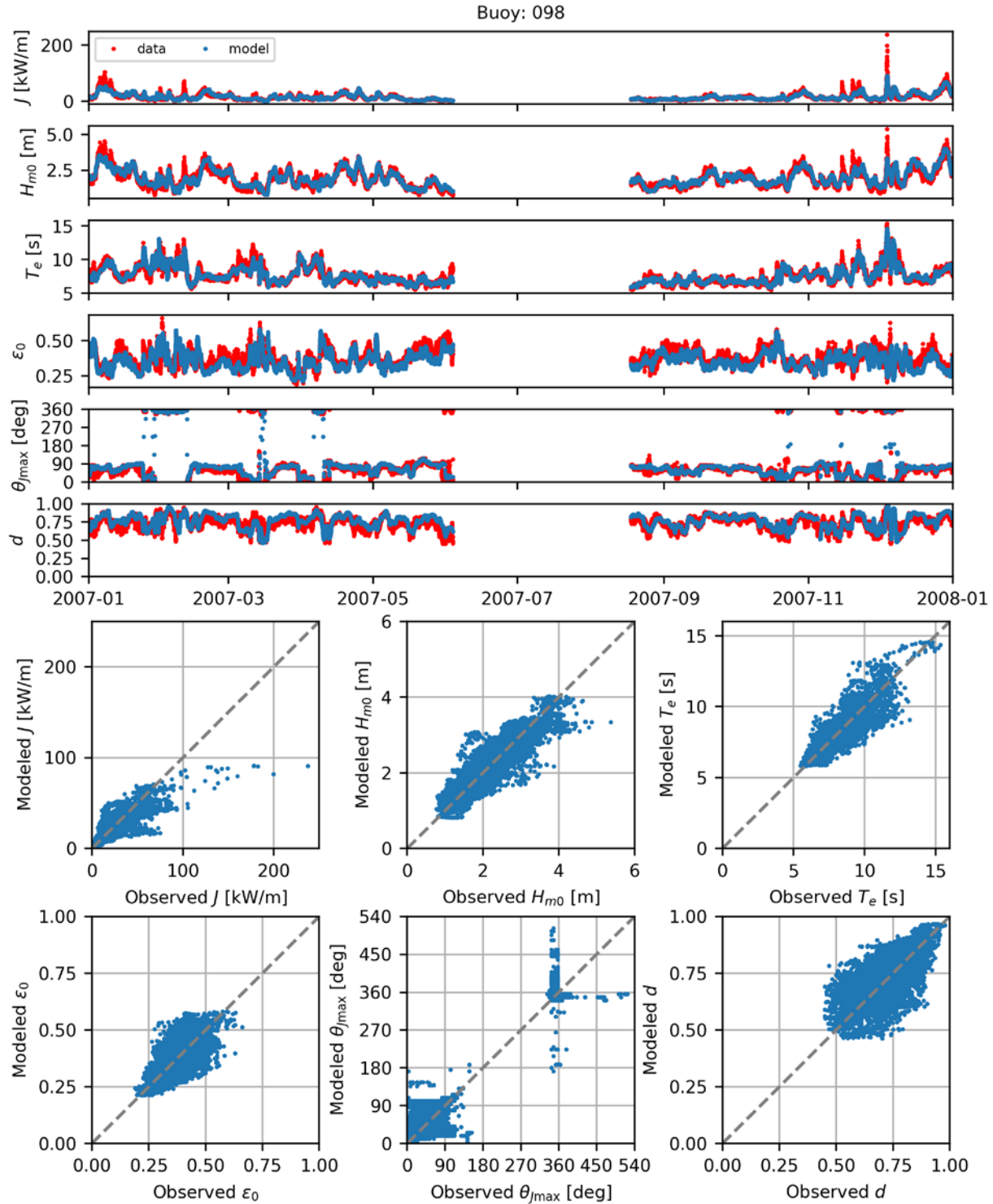


Figure B.30. Comparisons of time series (top) and scatter plots (bottom) the six model-simulated IEC parameters with observed data at CDIP Buoy 098 for 2007.

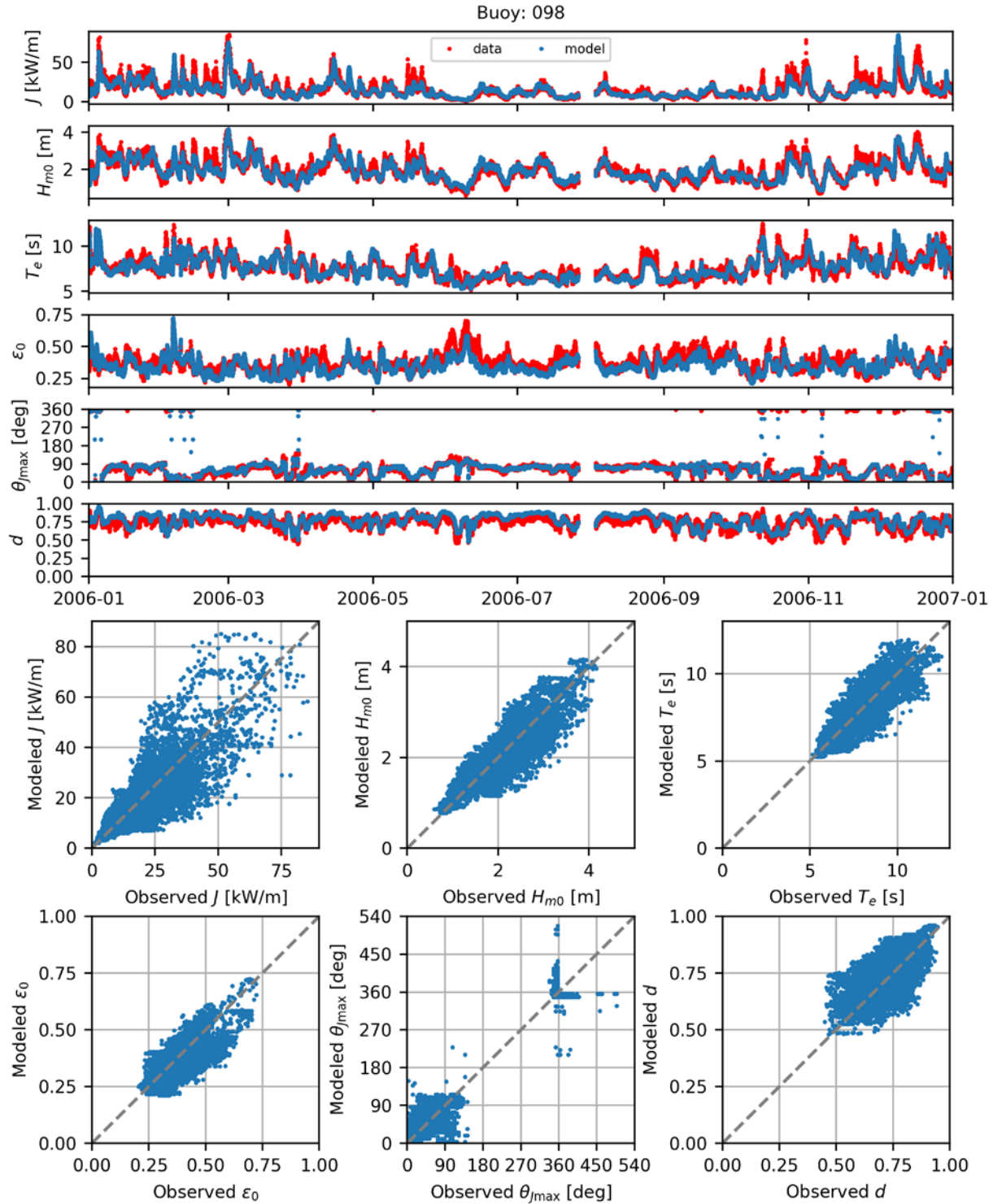


Figure B.31. Comparisons of time series (top) and scatter plots (bottom) the six model-simulated IEC parameters with observed data at CDIP Buoy 098 for 2006.

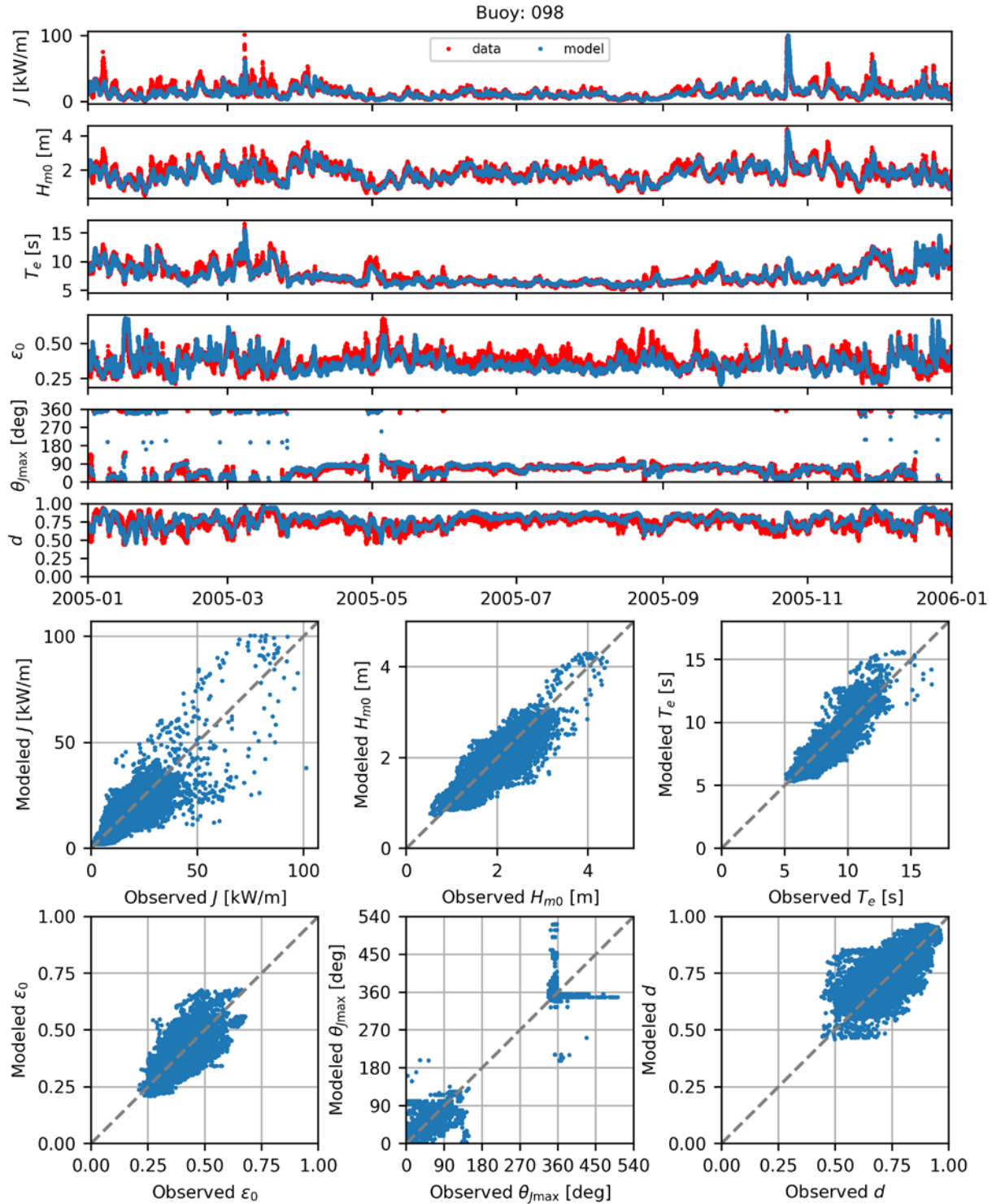


Figure B.32. Comparisons of time series (top) and scatter plots (bottom) the six model-simulated IEC parameters with observed data at CDIP Buoy 098 for 2005.

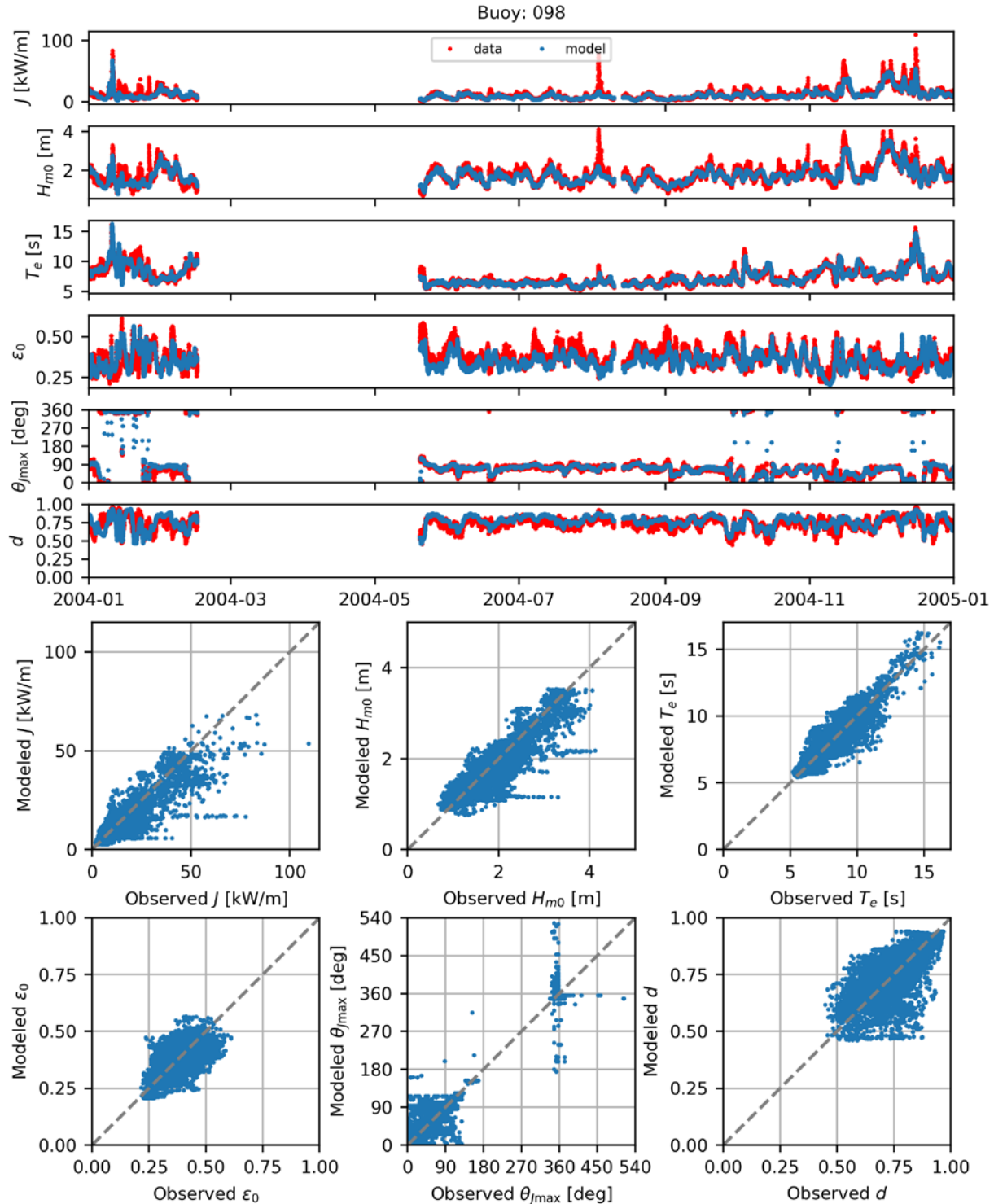


Figure B.33. Comparisons of time series (top) and scatter plots (bottom) the six model-simulated IEC parameters with observed data at CDIP Buoy 098 for 2004.

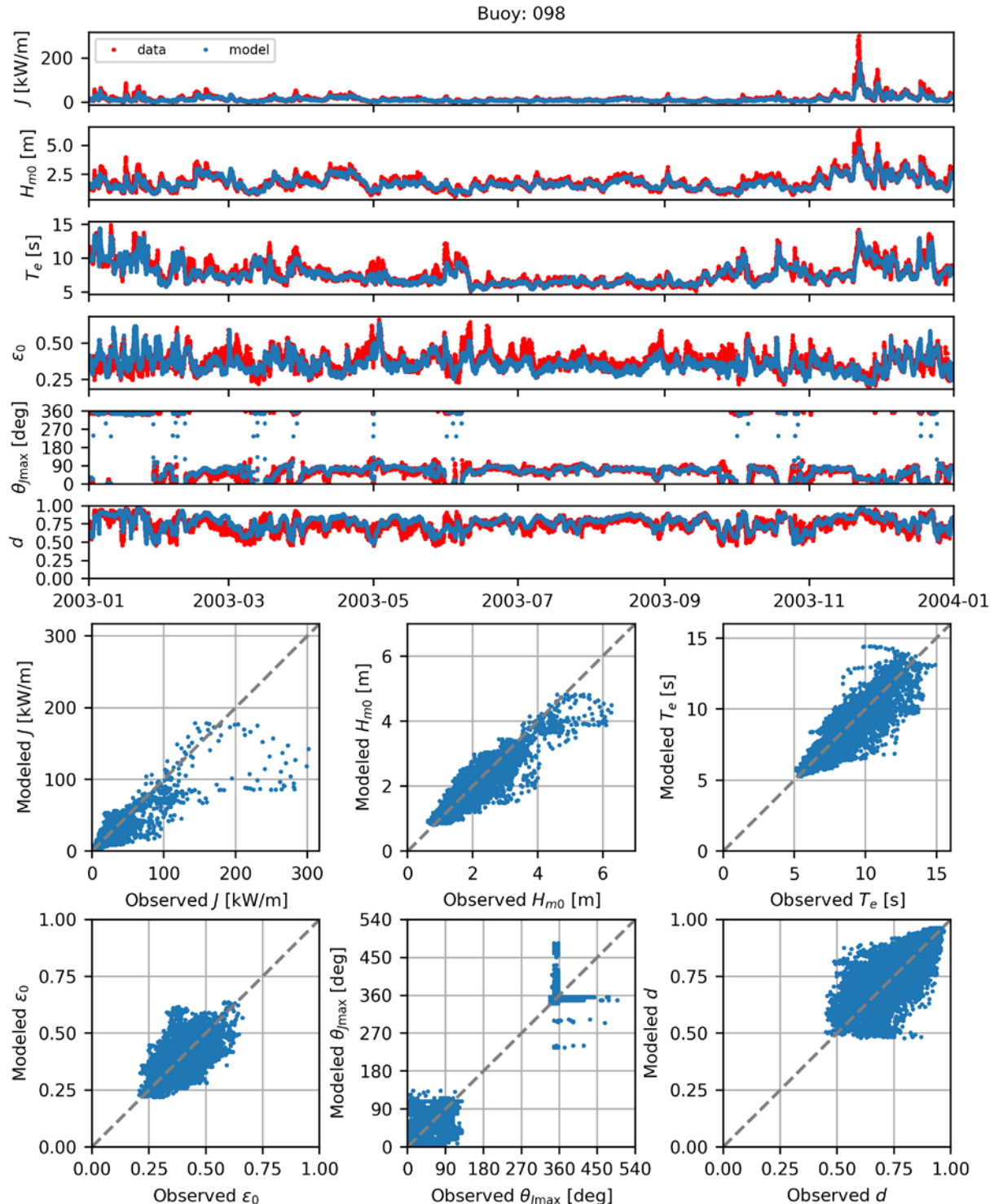


Figure B.34. Comparisons of time series (top) and scatter plots (bottom) the six model-simulated IEC parameters with observed data at CDIP Buoy 098 for 2003.

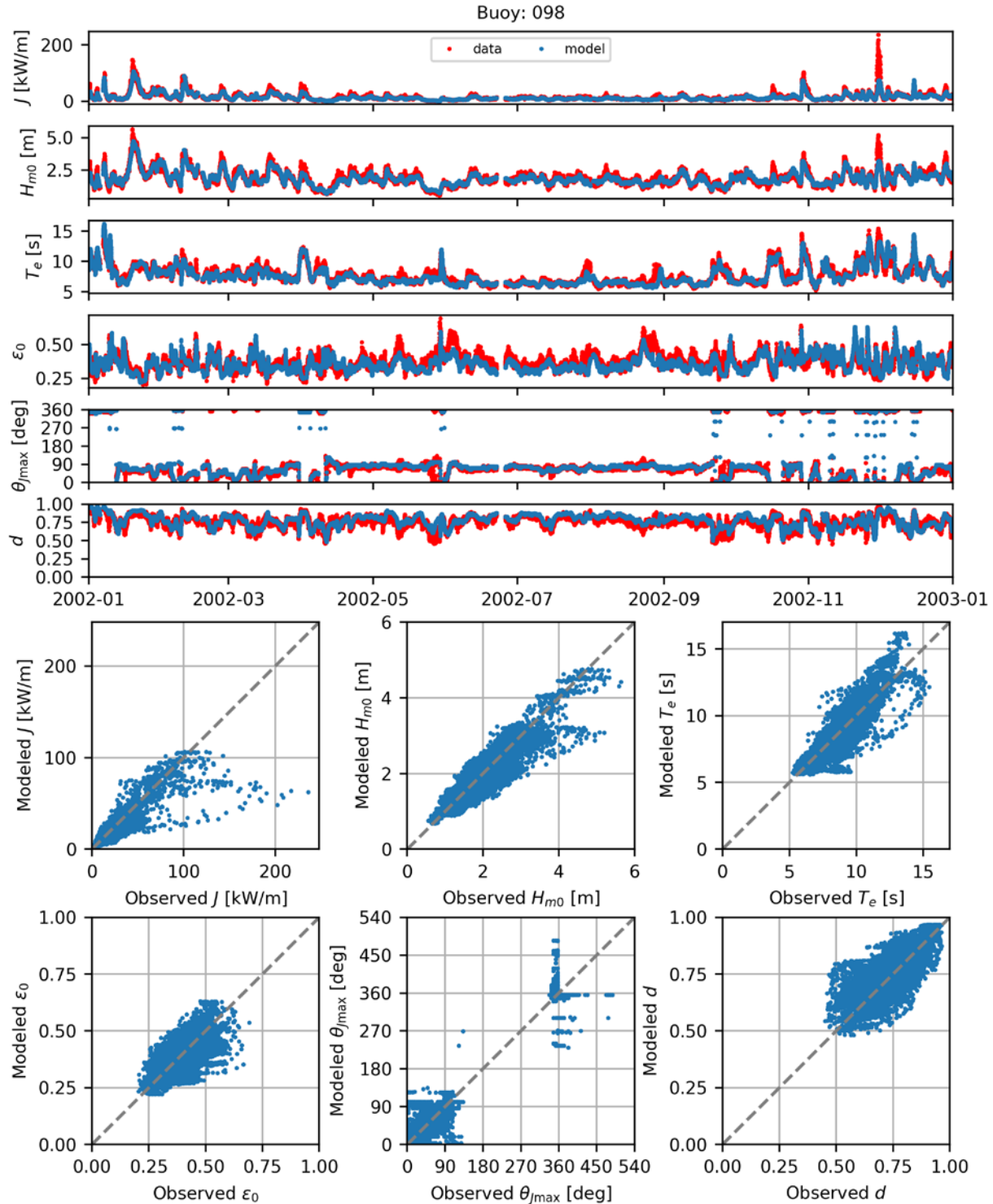


Figure B.35. Comparisons of time series (top) and scatter plots (bottom) the six model-simulated IEC parameters with observed data at CDIP Buoy 098 for 2002.

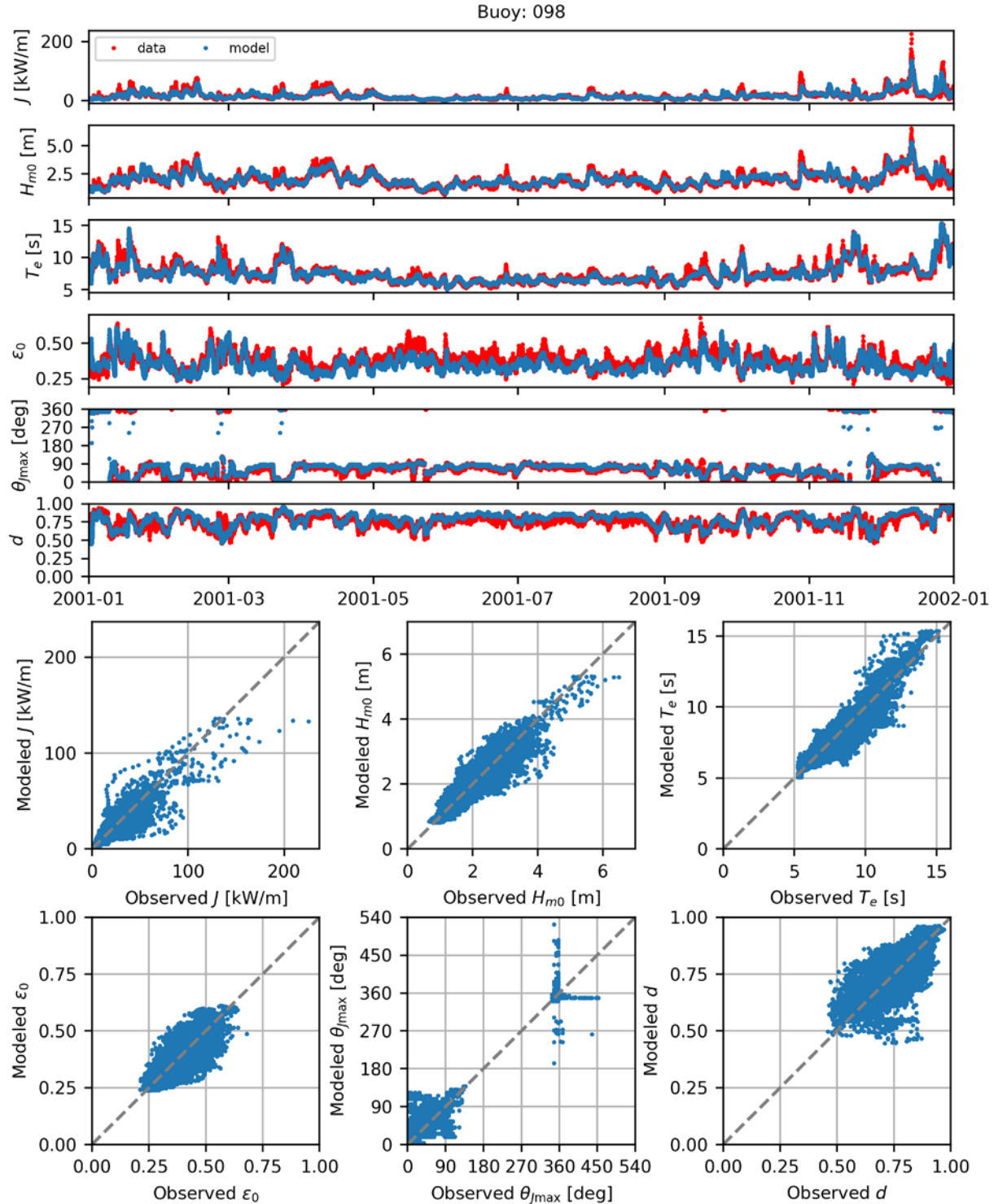


Figure B.36. Comparisons of time series (top) and scatter plots (bottom) the six model-simulated IEC parameters with observed data at CDIP Buoy 098 for 2001.

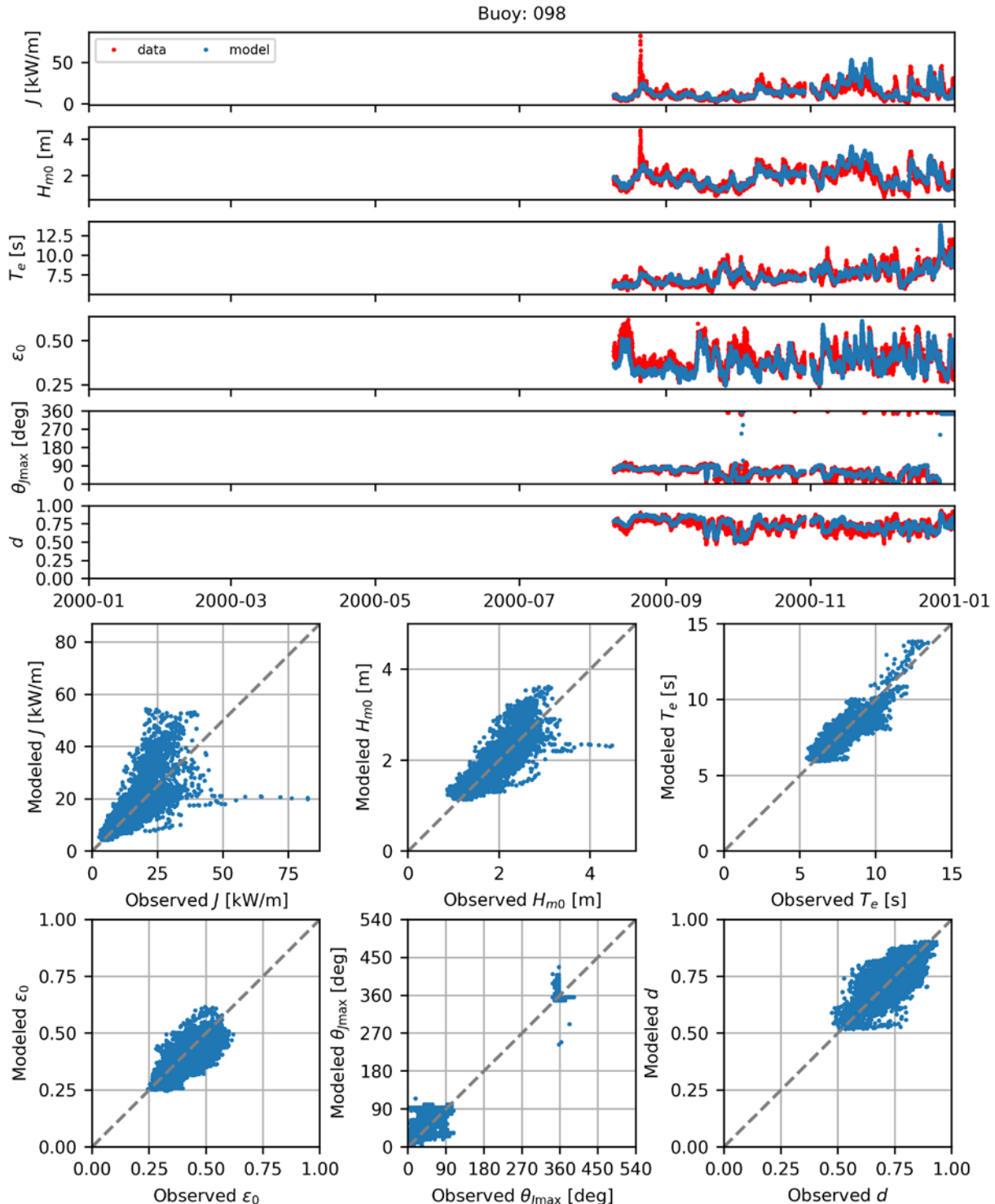


Figure B.37. Comparisons of time series (top) and scatter plots (bottom) the six model-simulated IEC parameters with observed data at CDIP Buoy 098 for 2000.

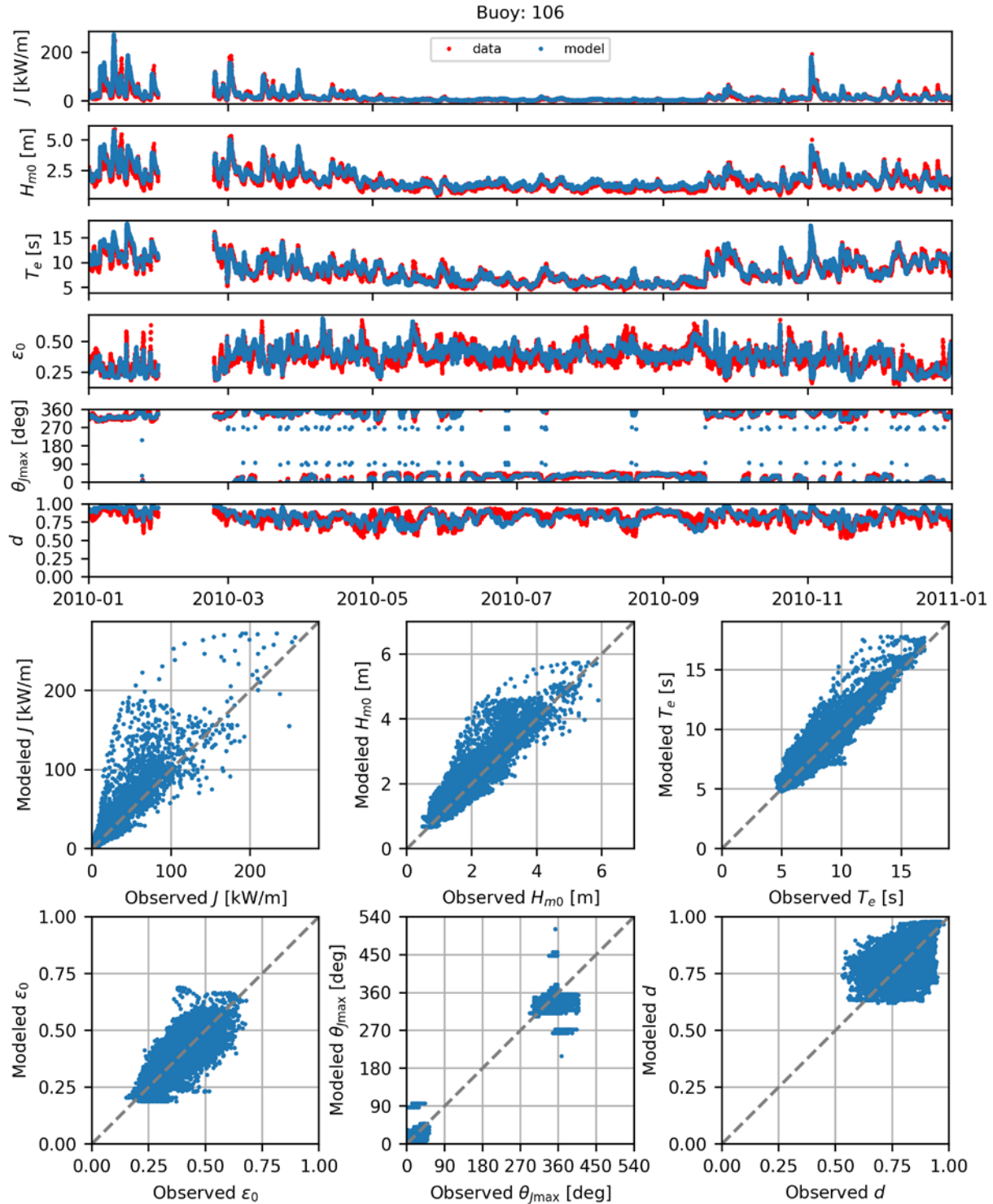


Figure B.38. Comparisons of time series (top) and scatter plots (bottom) the six model-simulated IEC parameters with observed data at CDIP Buoy 106 for 2010.

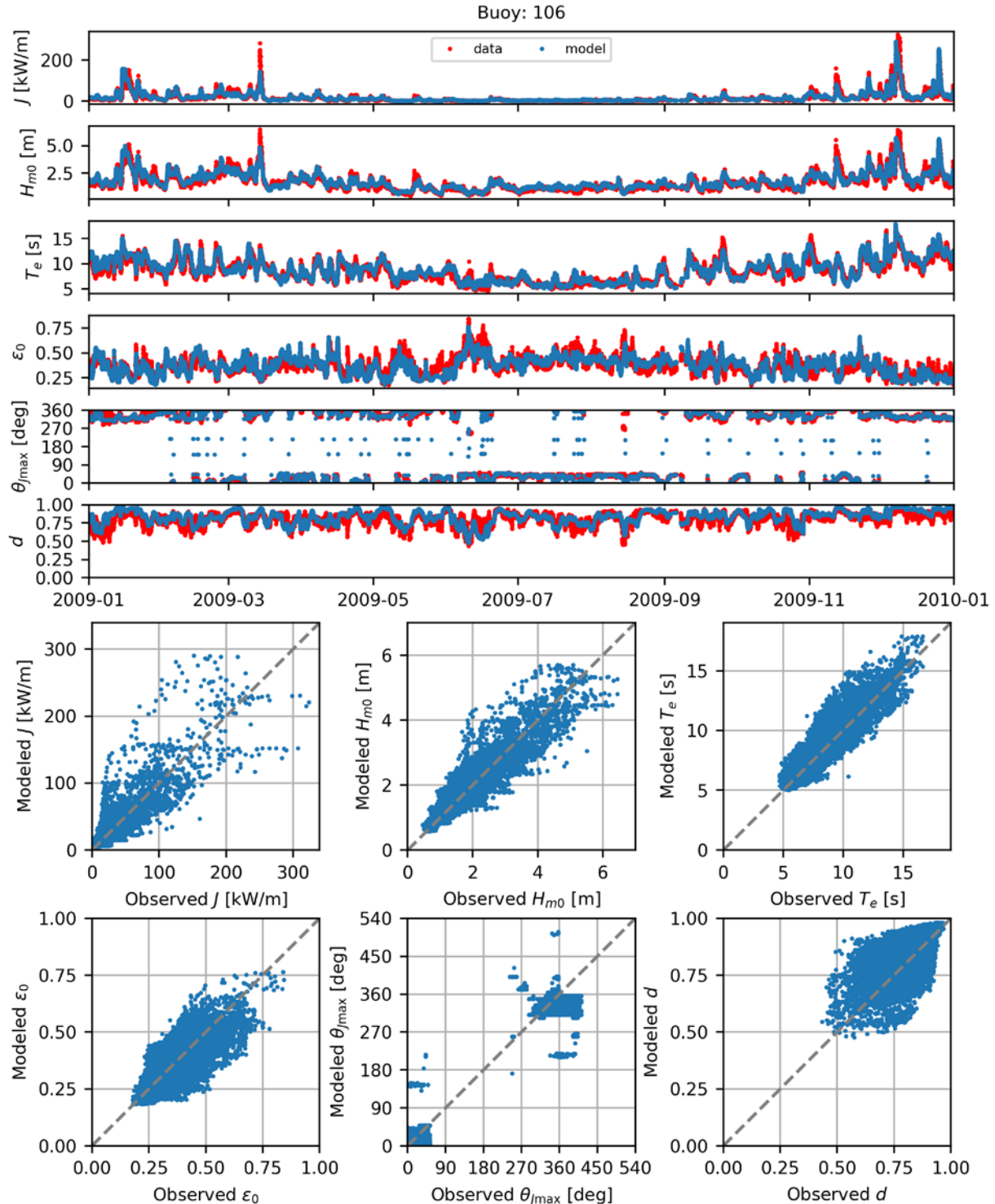


Figure B.39. Comparisons of time series (top) and scatter plots (bottom) the six model-simulated IEC parameters with observed data at CDIP Buoy 106 for 2009.

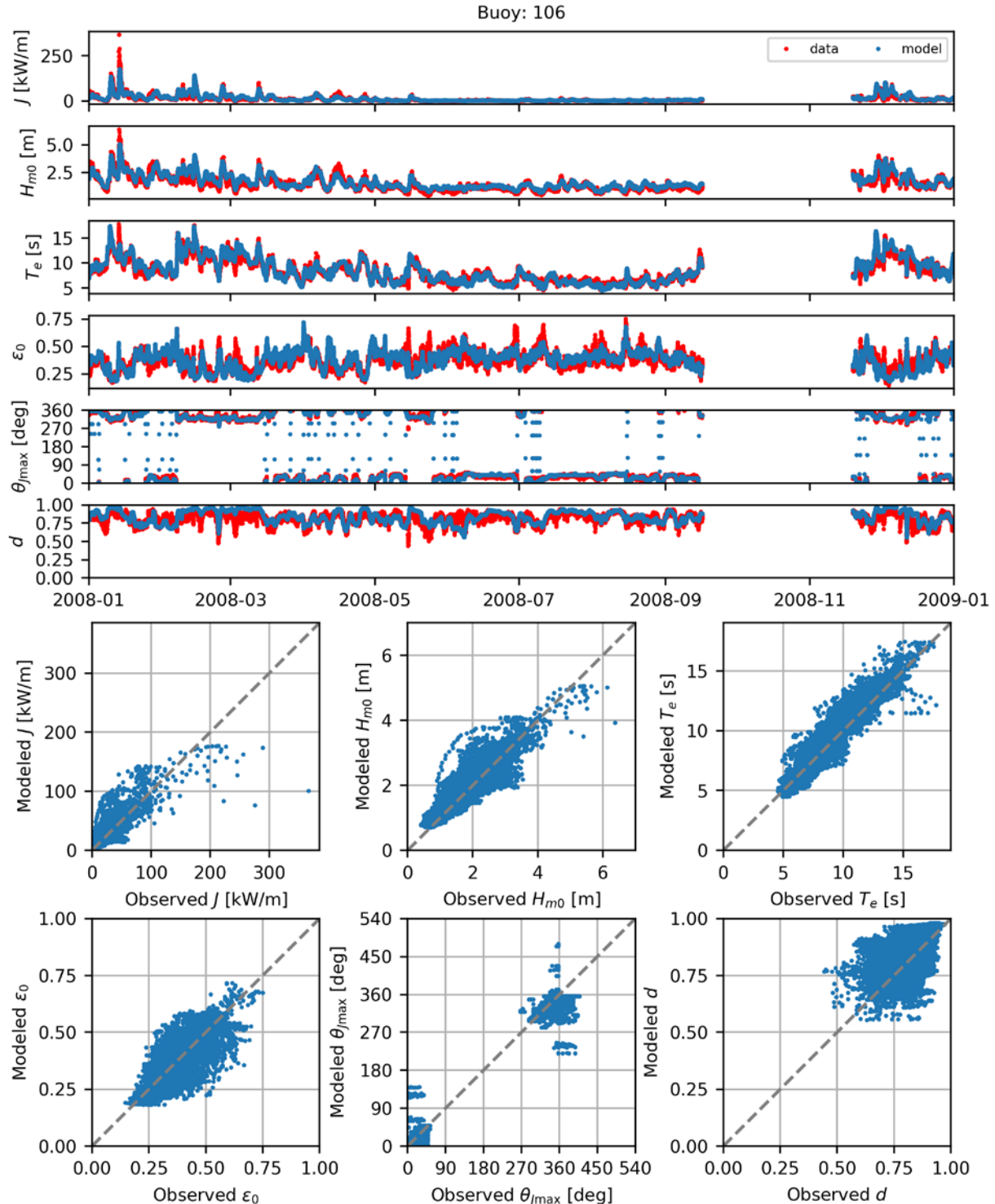


Figure B.40. Comparisons of time series (top) and scatter plots (bottom) the six model-simulated IEC parameters with observed data at CDIP Buoy 106 for 2008.

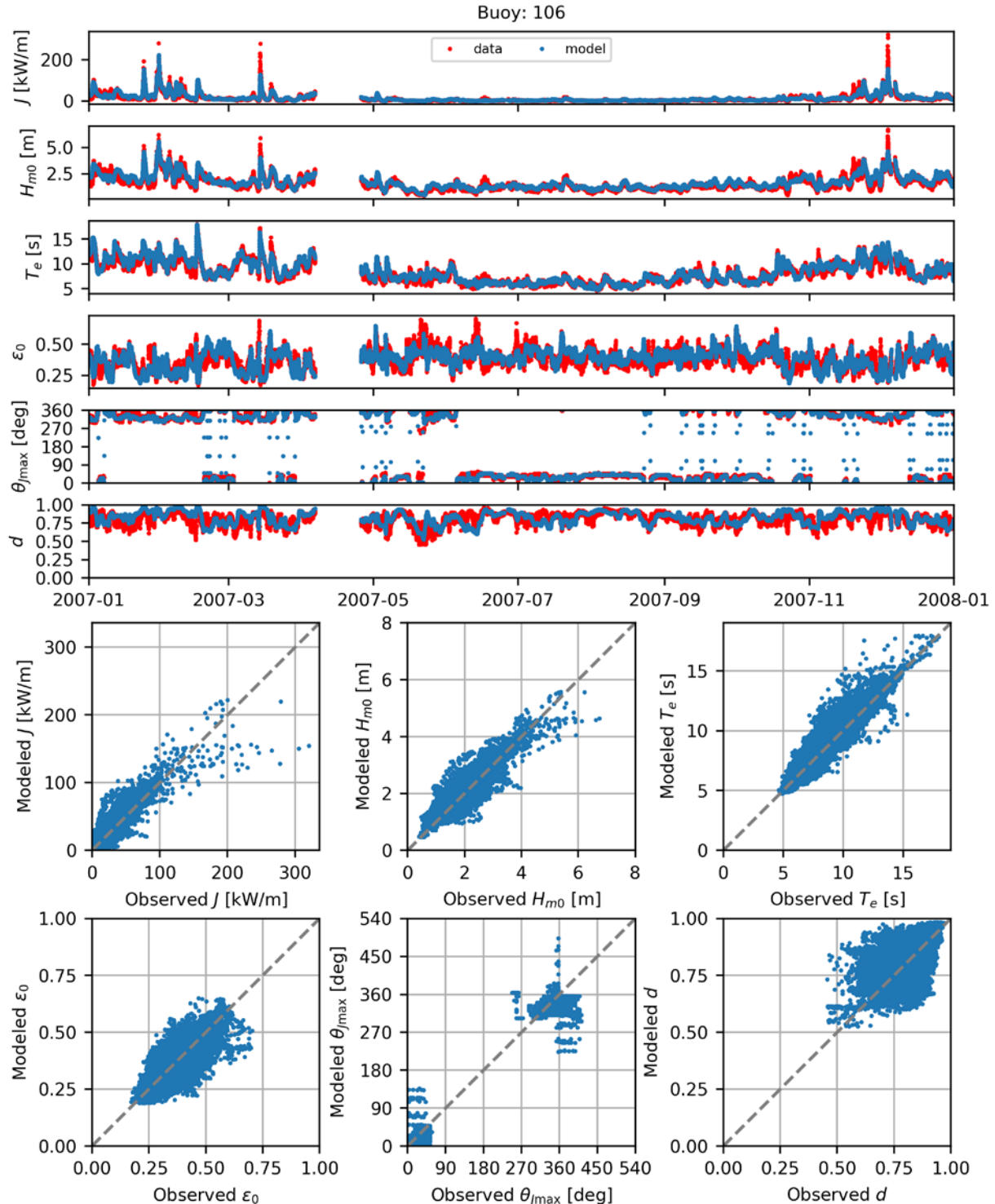


Figure B.41. Comparisons of time series (top) and scatter plots (bottom) the six model-simulated IEC parameters with observed data at CDIP Buoy 106 for 2007.

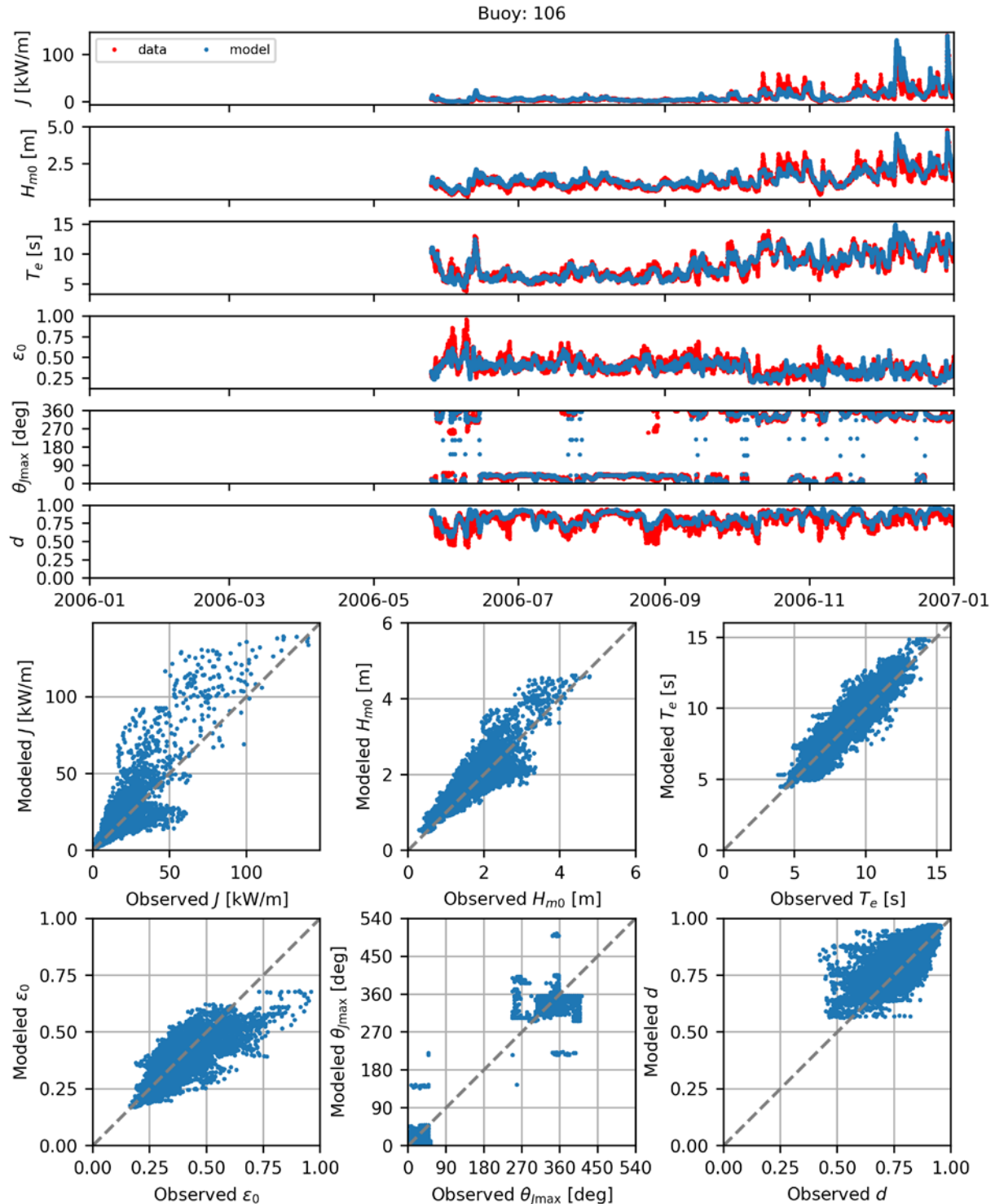


Figure B.42. Comparisons of time series (top) and scatter plots (bottom) the six model-simulated IEC parameters with observed data at CDIP Buoy 106 for 2006.

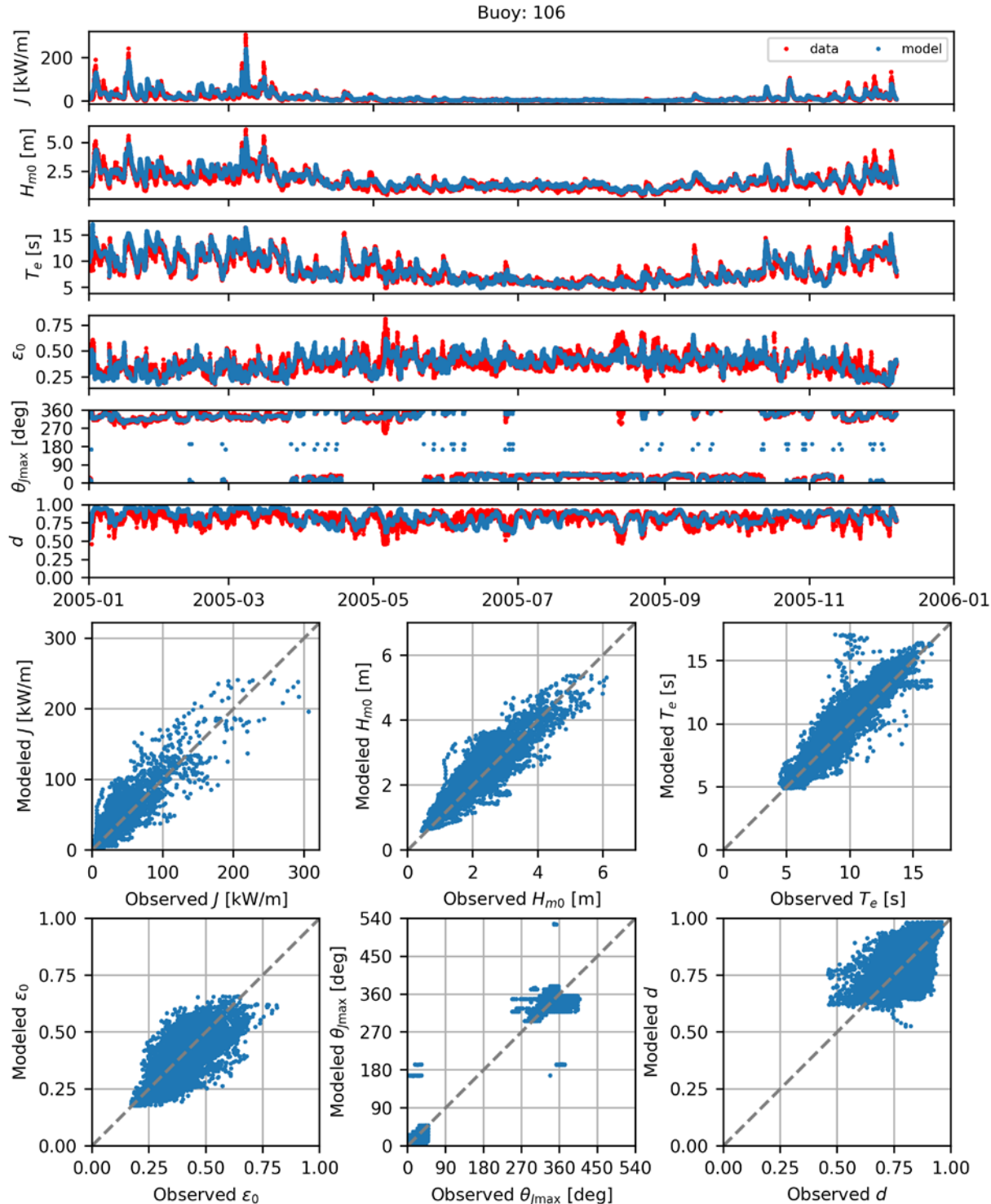


Figure B.43. Comparisons of time series (top) and scatter plots (bottom) the six model-simulated IEC parameters with observed data at CDIP Buoy 106 for 2005.

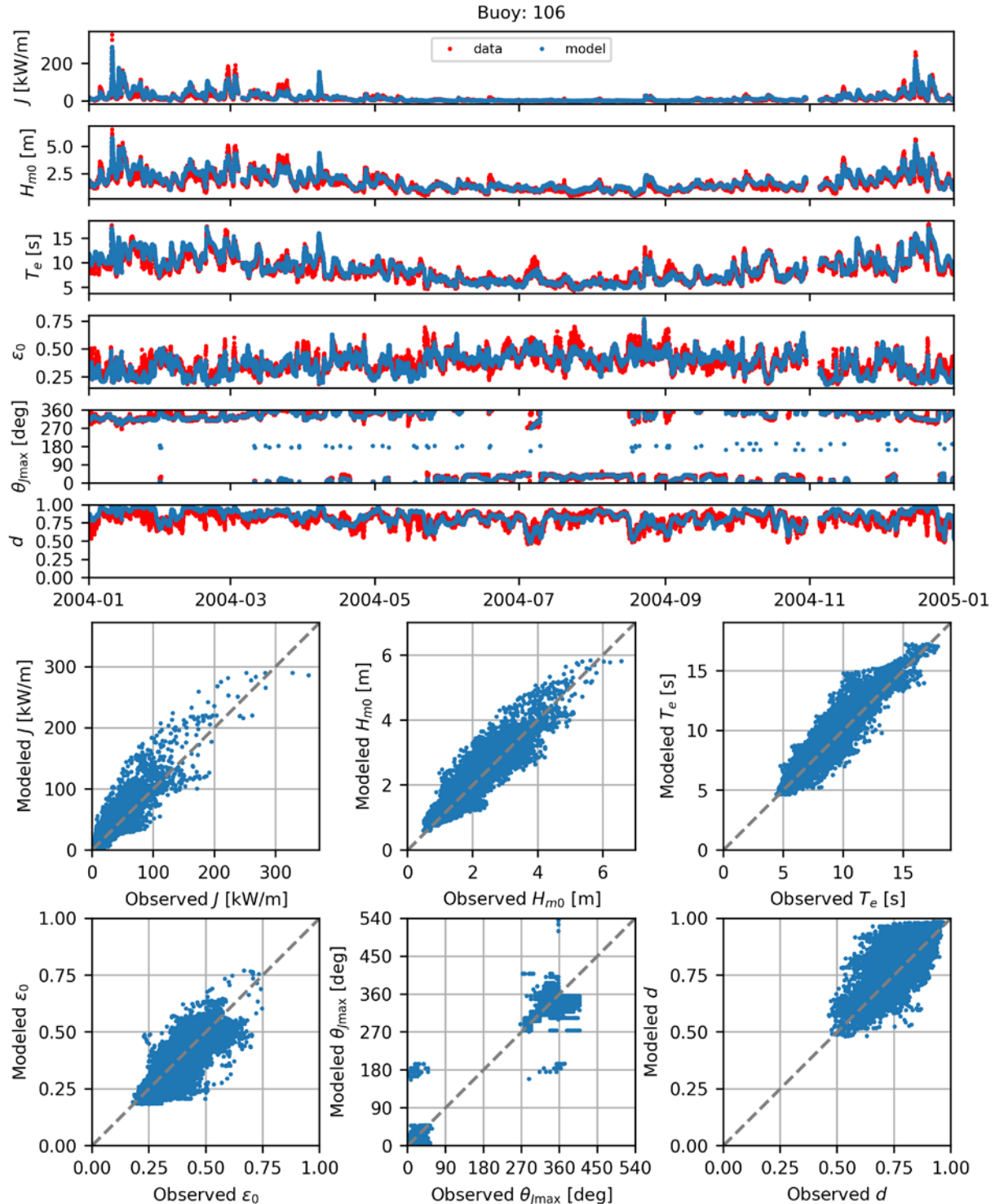


Figure B.44. Comparisons of time series (top) and scatter plots (bottom) the six model-simulated IEC parameters with observed data at CDIP Buoy 106 for 2004.

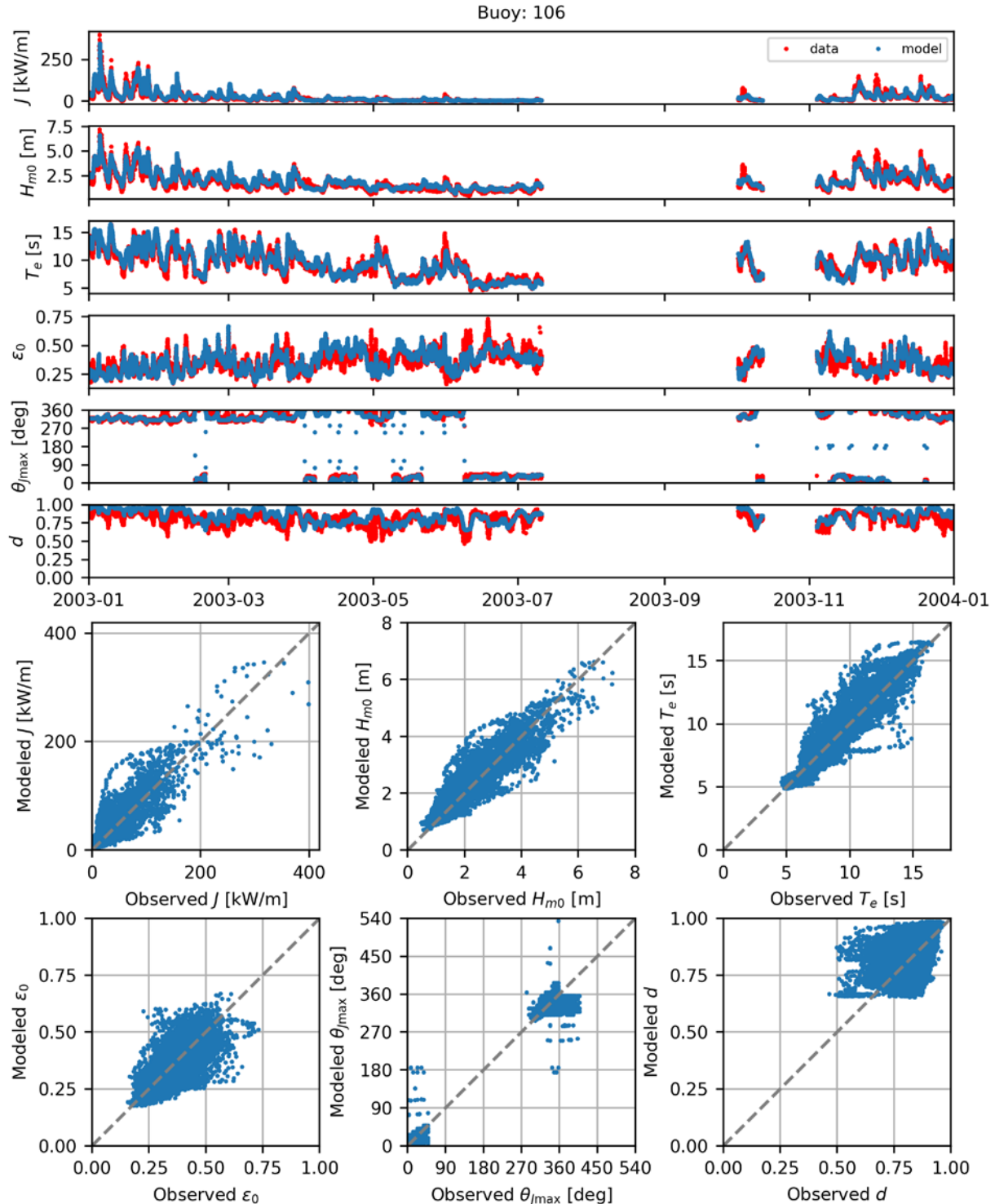


Figure B.45. Comparisons of time series (top) and scatter plots (bottom) the six model-simulated IEC parameters with observed data at CDIP Buoy 106 for 2003.

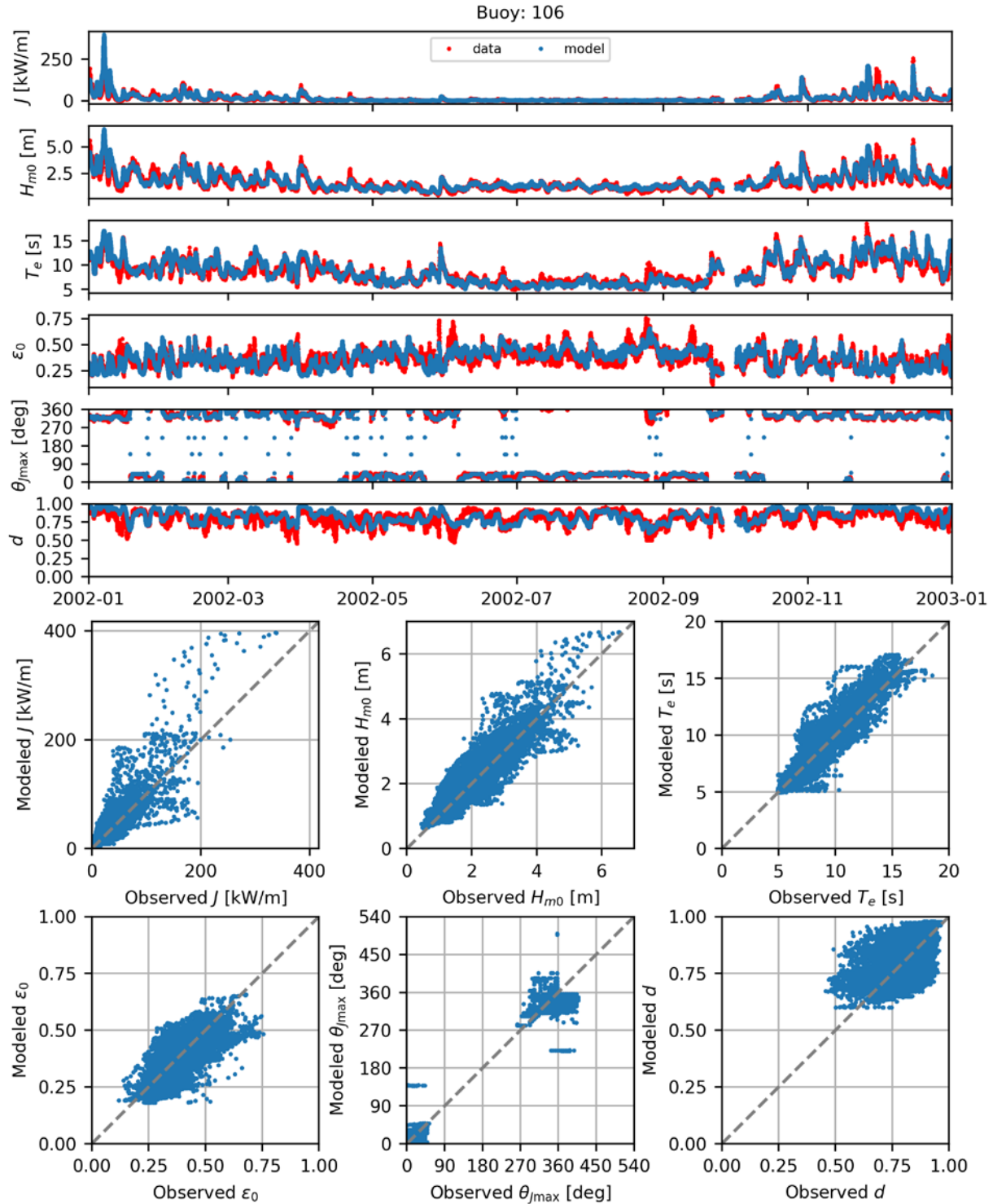


Figure B.46. Comparisons of time series (top) and scatter plots (bottom) the six model-simulated IEC parameters with observed data at CDIP Buoy 106 for 2002.

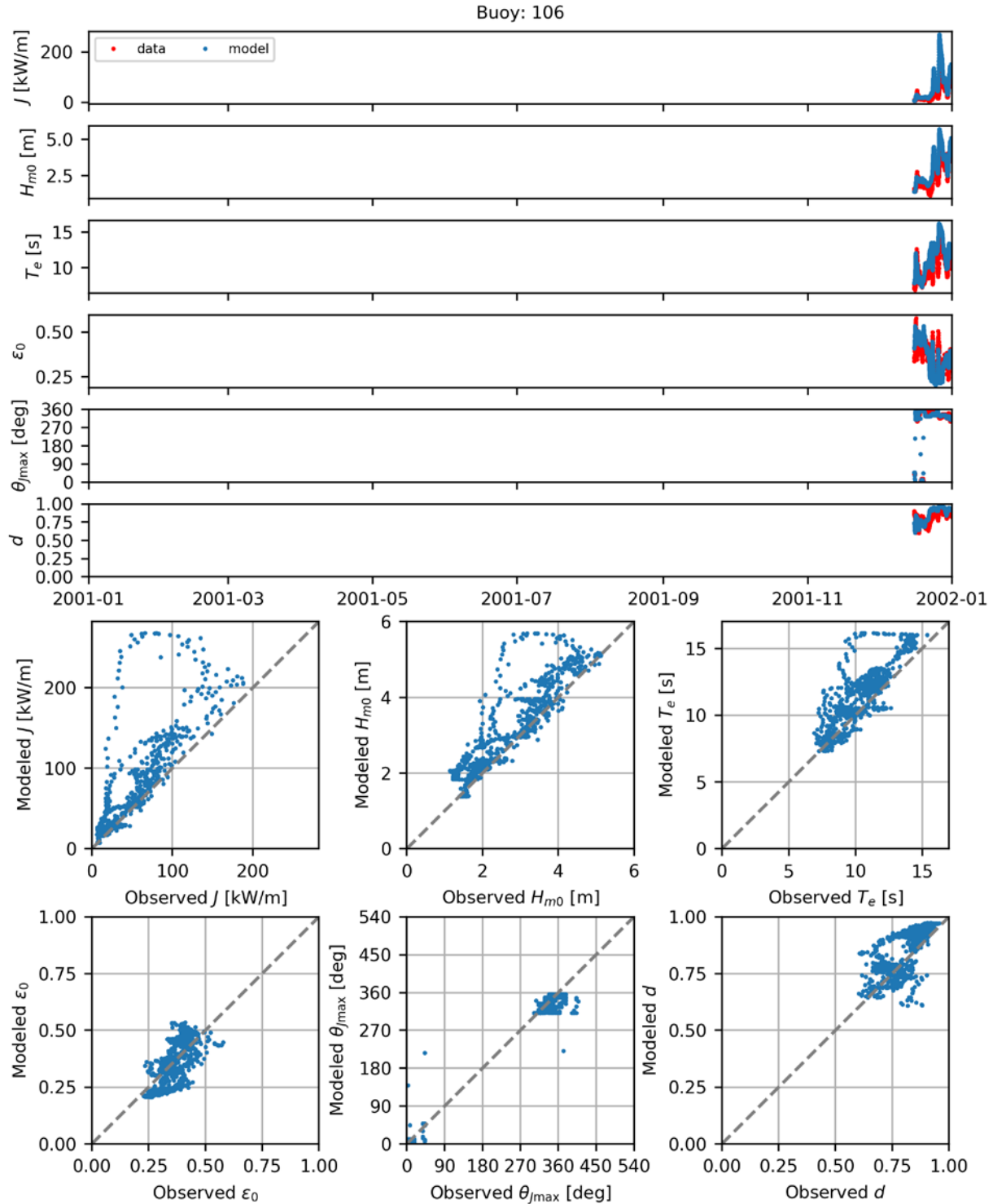


Figure B.47. Comparisons of time series (top) and scatter plots (bottom) the six model-simulated IEC parameters with observed data at CDIP Buoy 106 for 2001.

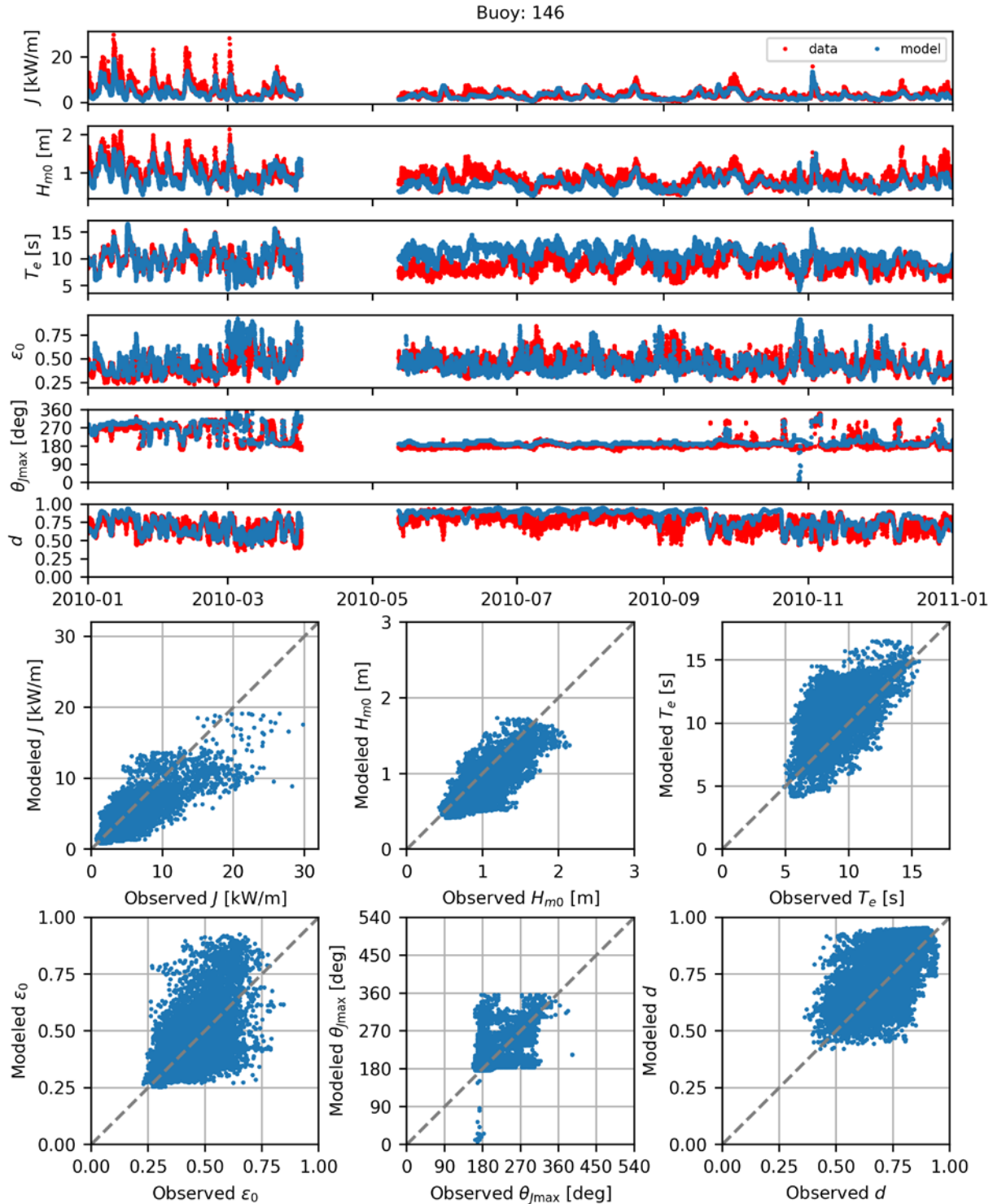


Figure B.48. Comparisons of time series (top) and scatter plots (bottom) the six model-simulated IEC parameters with observed data at CDIP Buoy 146 for 2010.

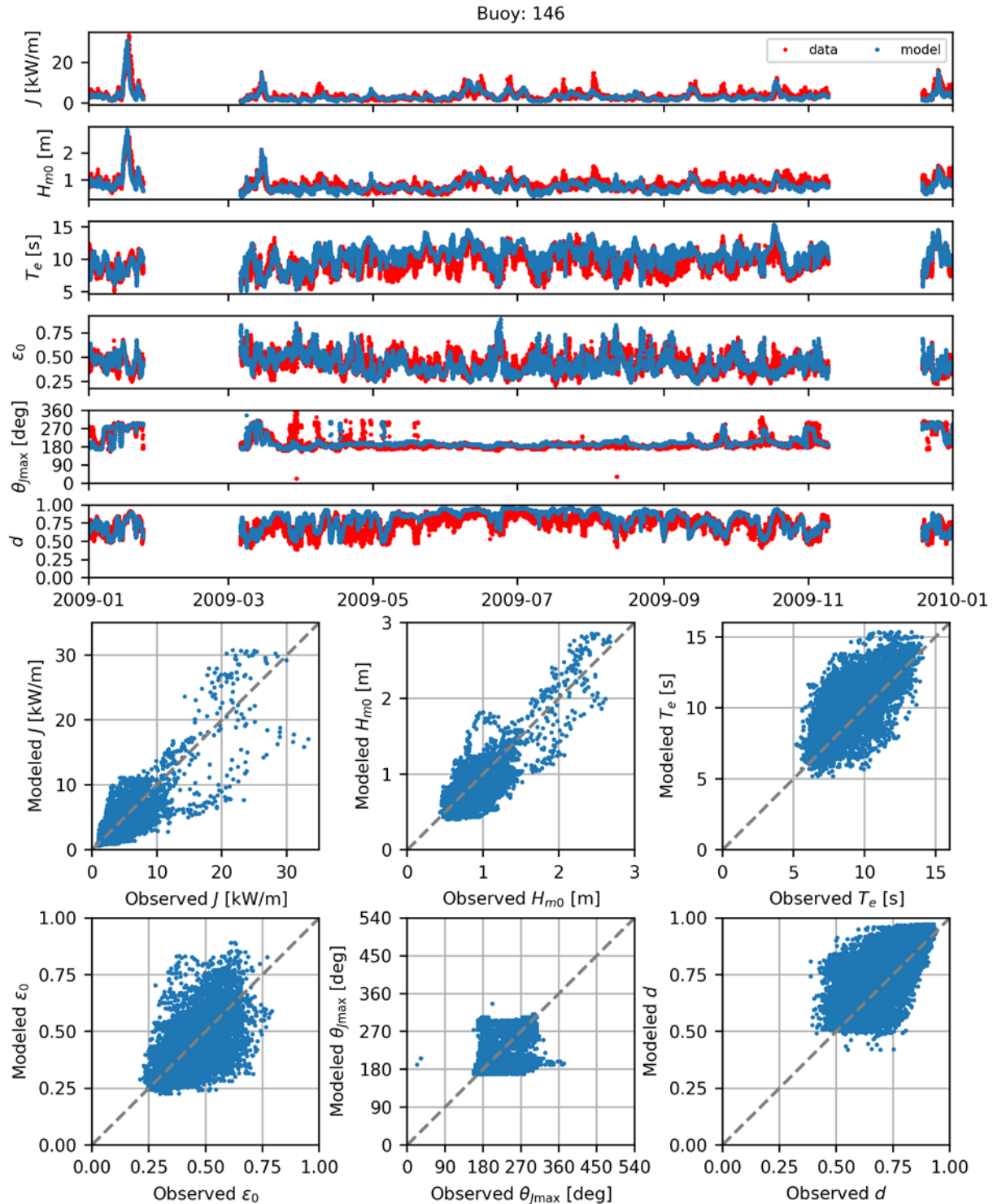


Figure B.49. Comparisons of time series (top) and scatter plots (bottom) the six model-simulated IEC parameters with observed data at CDIP Buoy 146 for 2009.

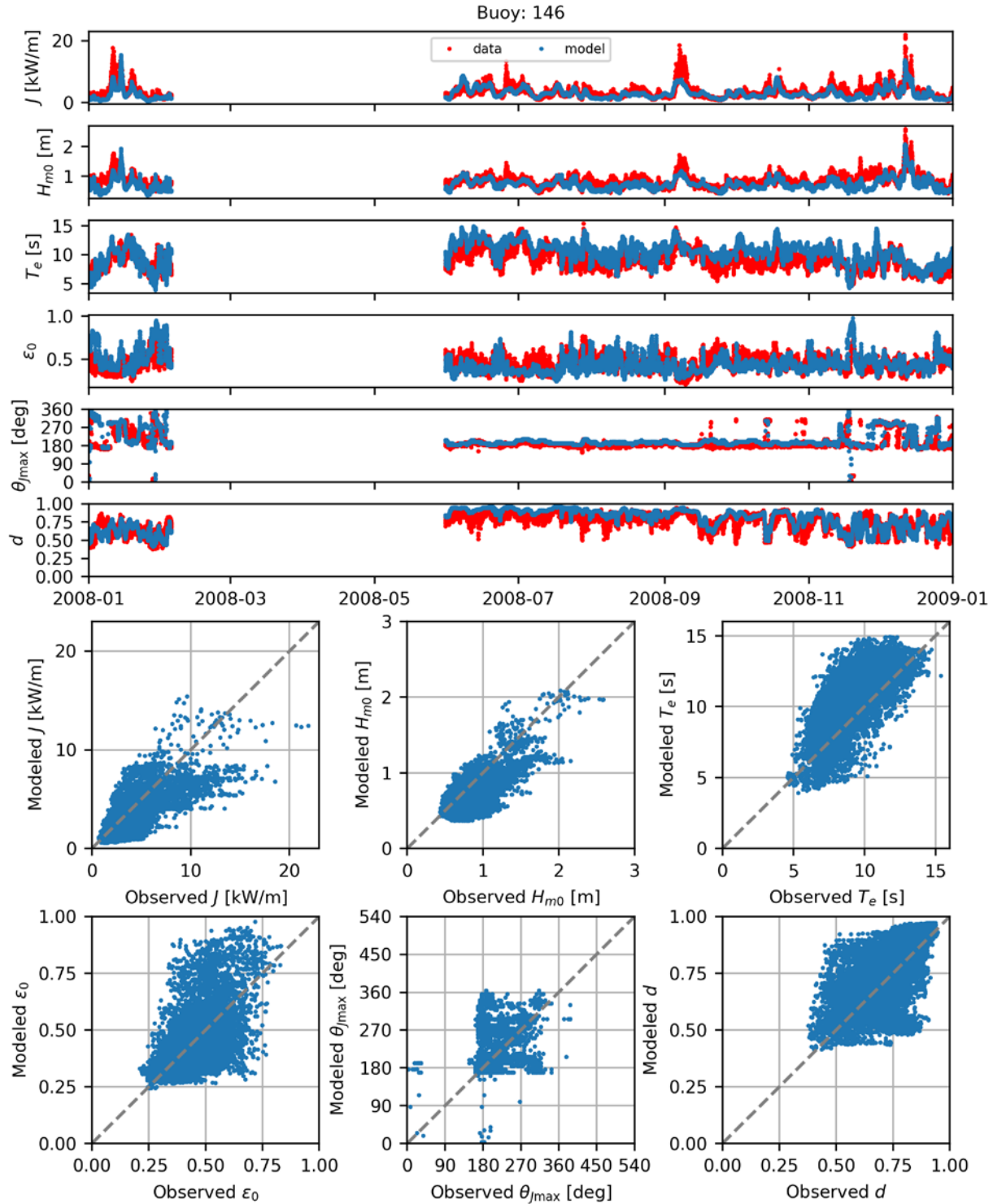


Figure B.50. Comparisons of time series (top) and scatter plots (bottom) the six model-simulated IEC parameters with observed data at CDIP Buoy 146 for 2008.

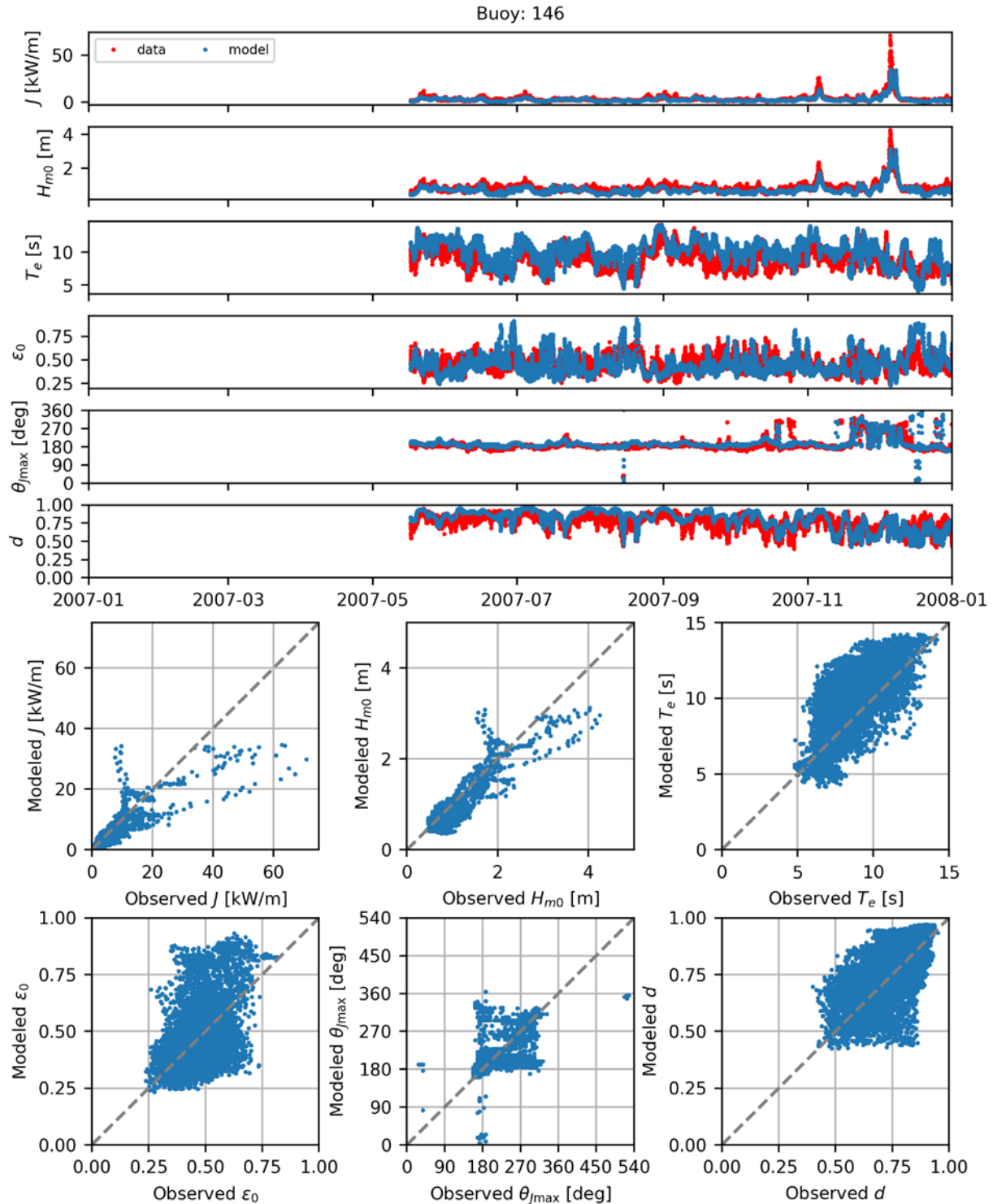


Figure B.51. Comparisons of time series (top) and scatter plots (bottom) the six model-simulated IEC parameters with observed data at CDIP Buoy 146 for 2007.

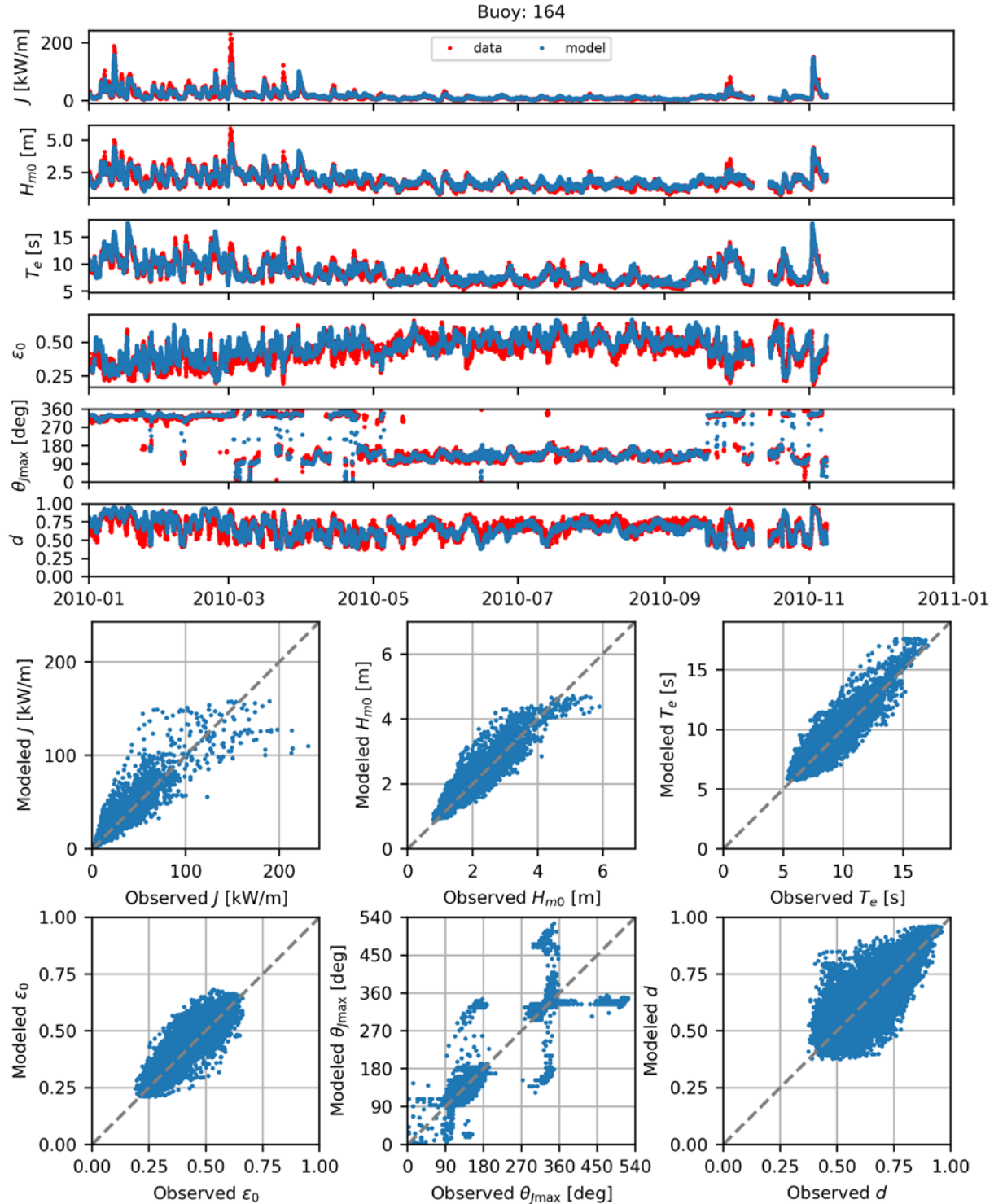


Figure B.52. Comparisons of time series (top) and scatter plots (bottom) the six model-simulated IEC parameters with observed data at CDIP Buoy 164 for 2010.

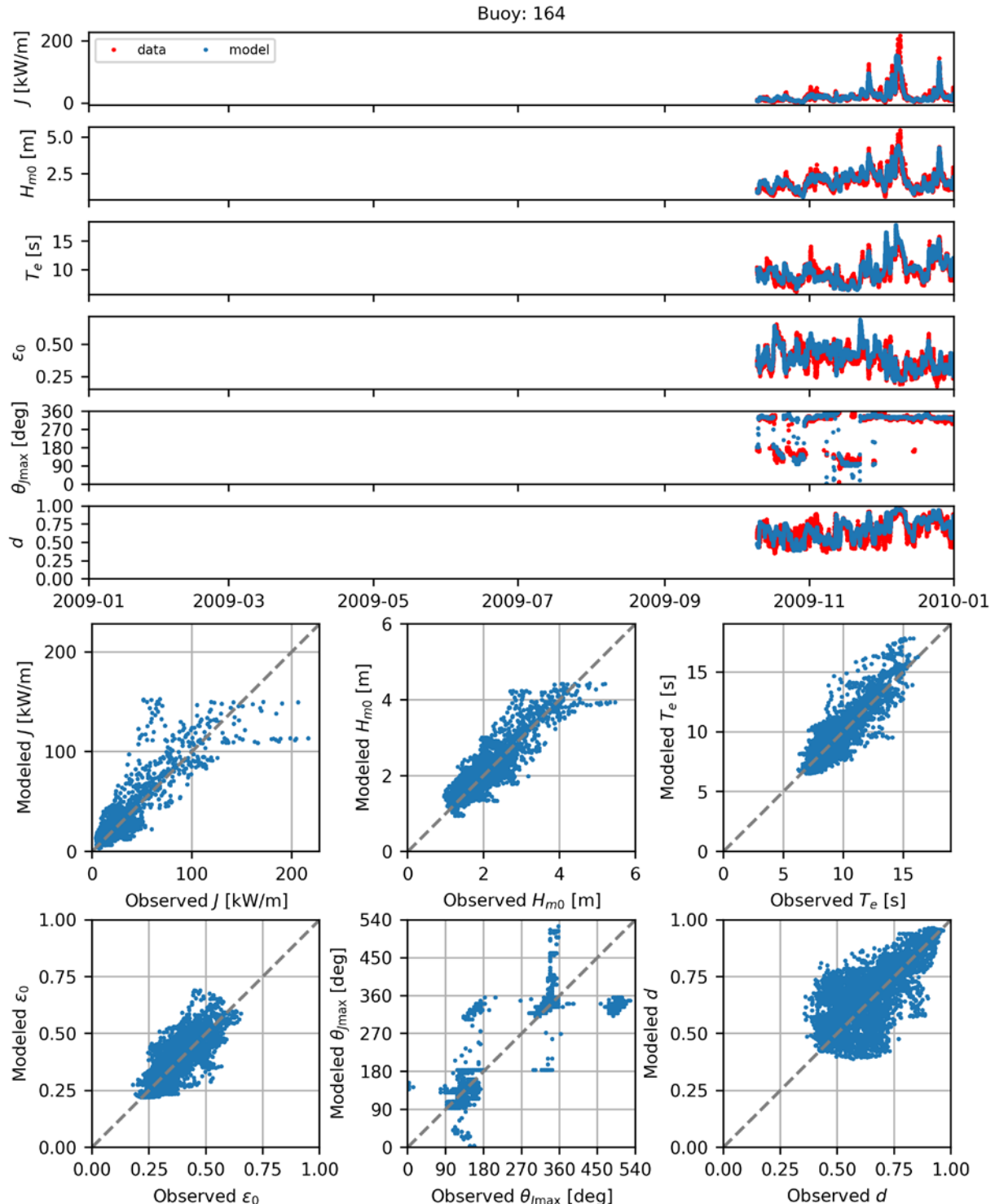


Figure B.53. Comparisons of time series (top) and scatter plots (bottom) the six model-simulated IEC parameters with observed data at CDIP Buoy 164 for 2009.

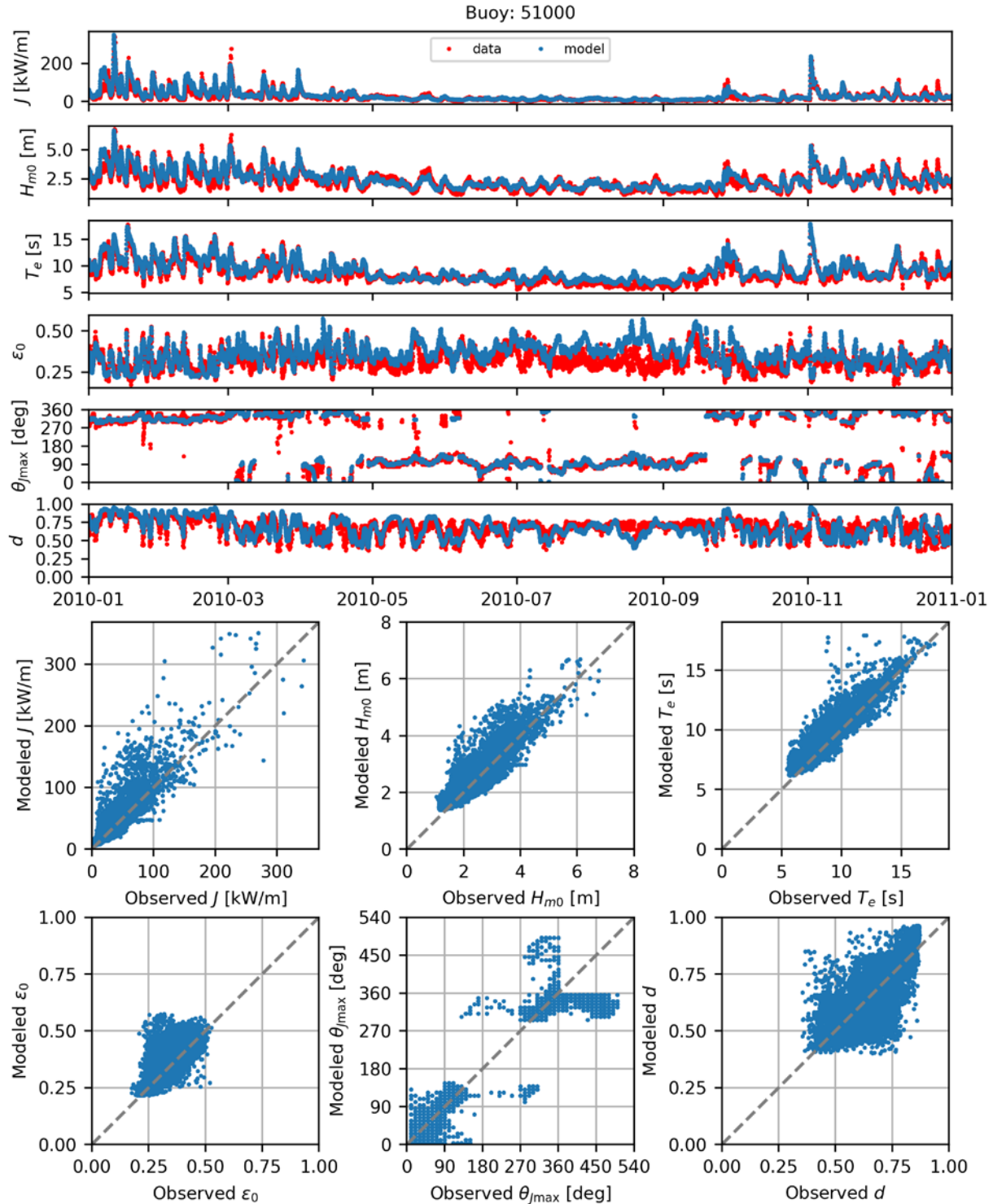


Figure B.54. Comparisons of time series (top) and scatter plots (bottom) the six model-simulated IEC parameters with observed data at NDBC Buoy 51000 for 2010.

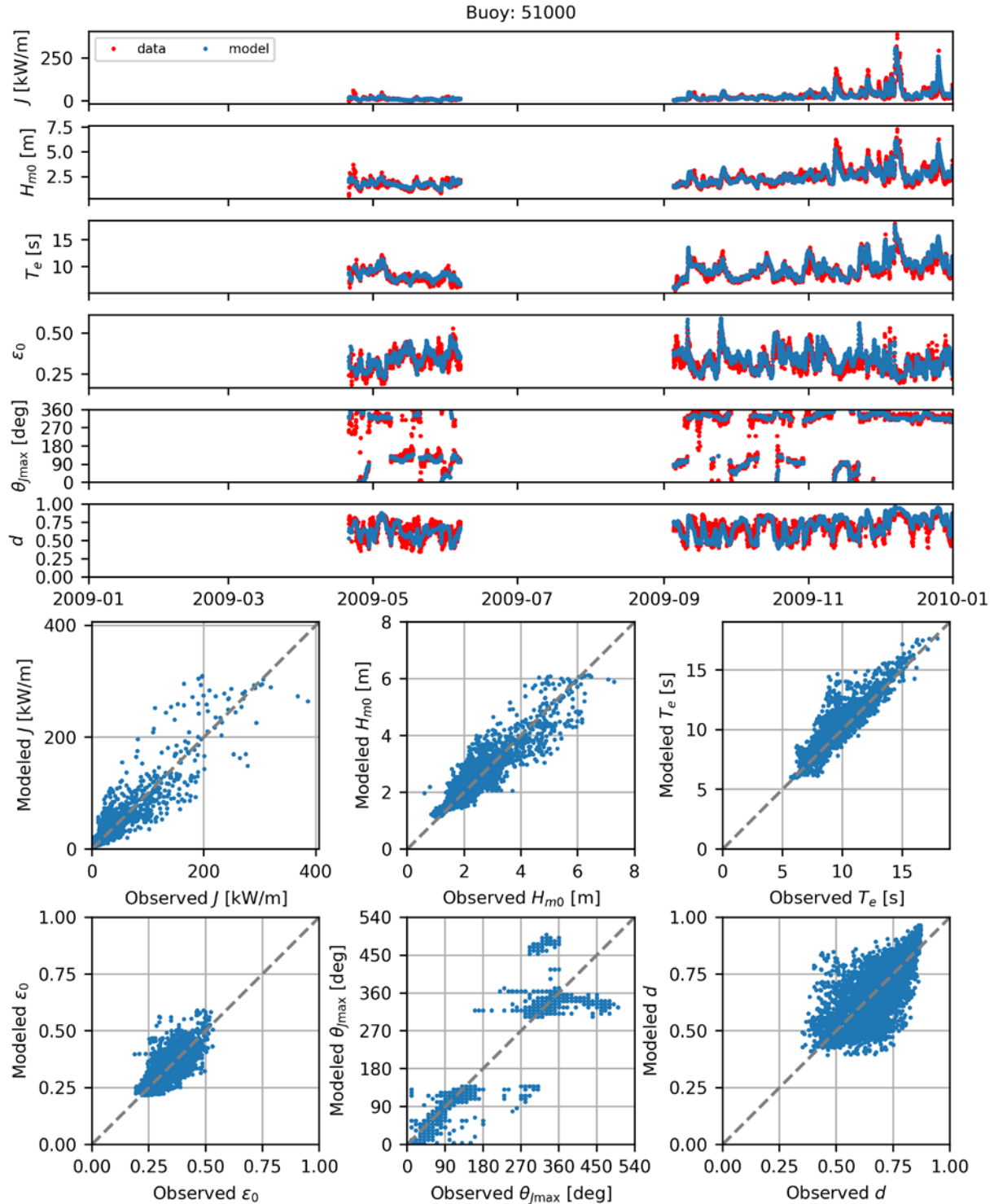


Figure B.55. Comparisons of time series (top) and scatter plots (bottom) the six model-simulated IEC parameters with observed data at NDBC Buoy 51000 for 2009.

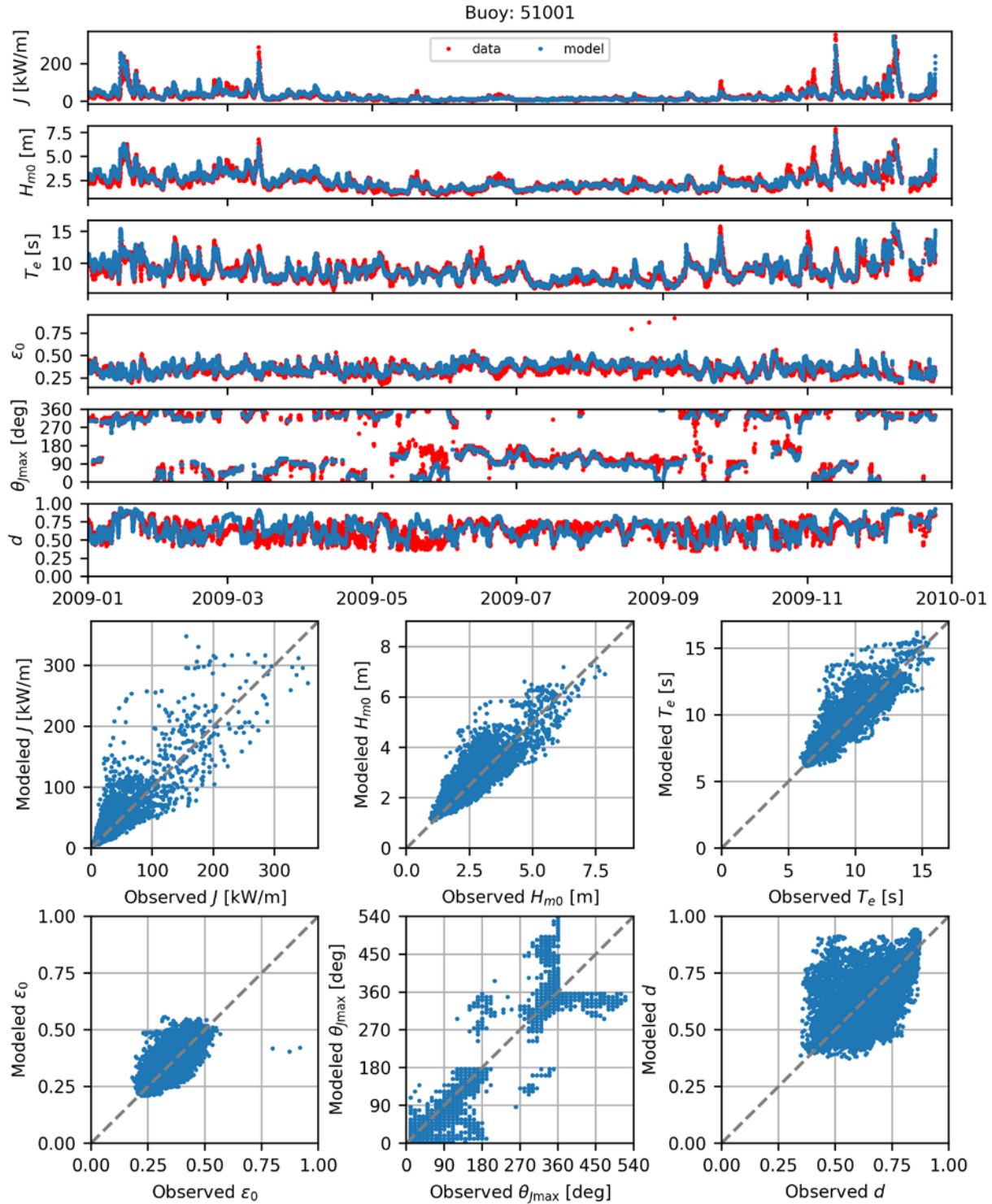


Figure B.56. Comparisons of time series (top) and scatter plots (bottom) the six model-simulated IEC parameters with observed data at NDBC Buoy 51001 for 2009.

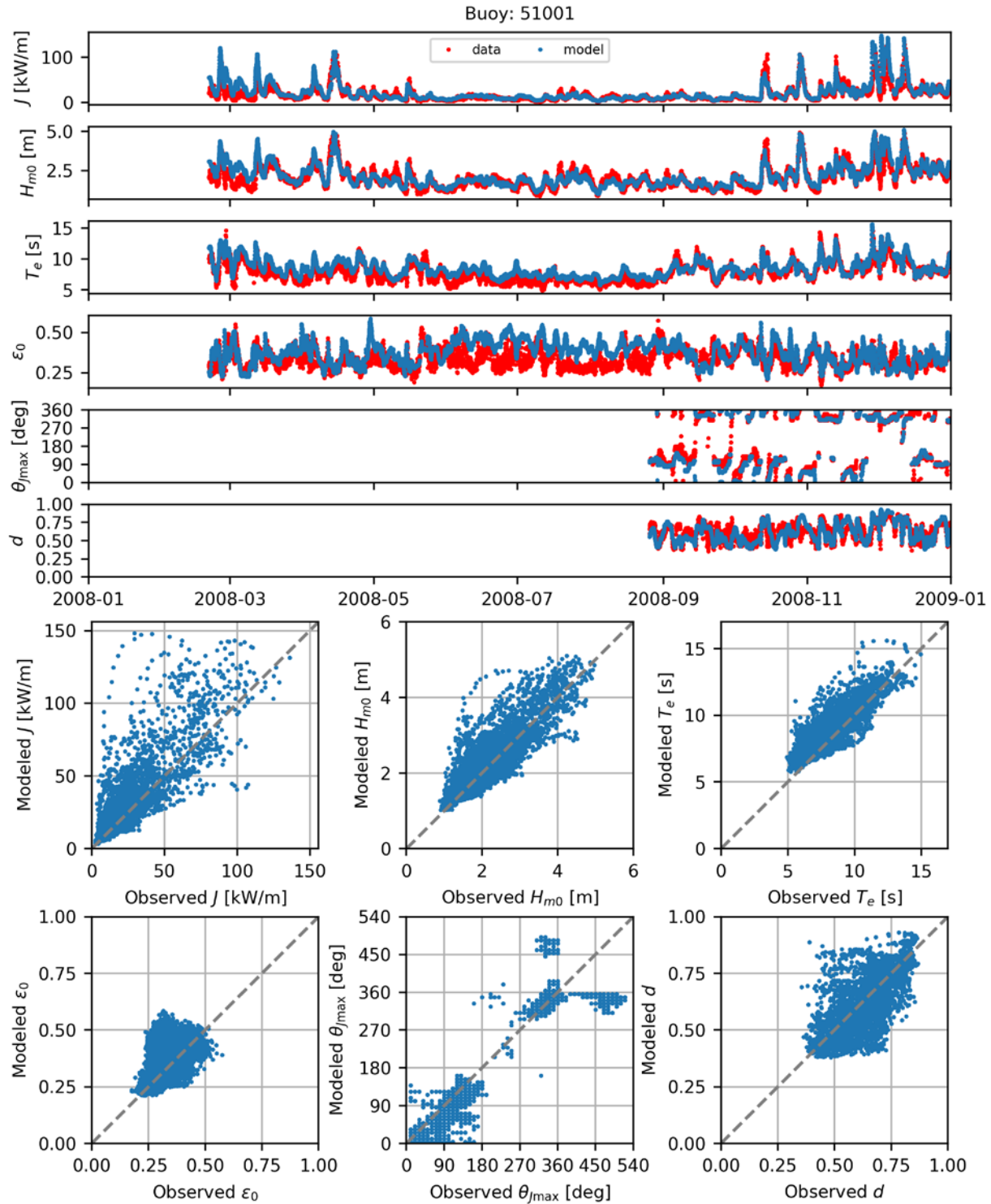


Figure B.57. Comparisons of time series (top) and scatter plots (bottom) the six model-simulated IEC parameters with observed data at NDBC Buoy 51001 for 2008.

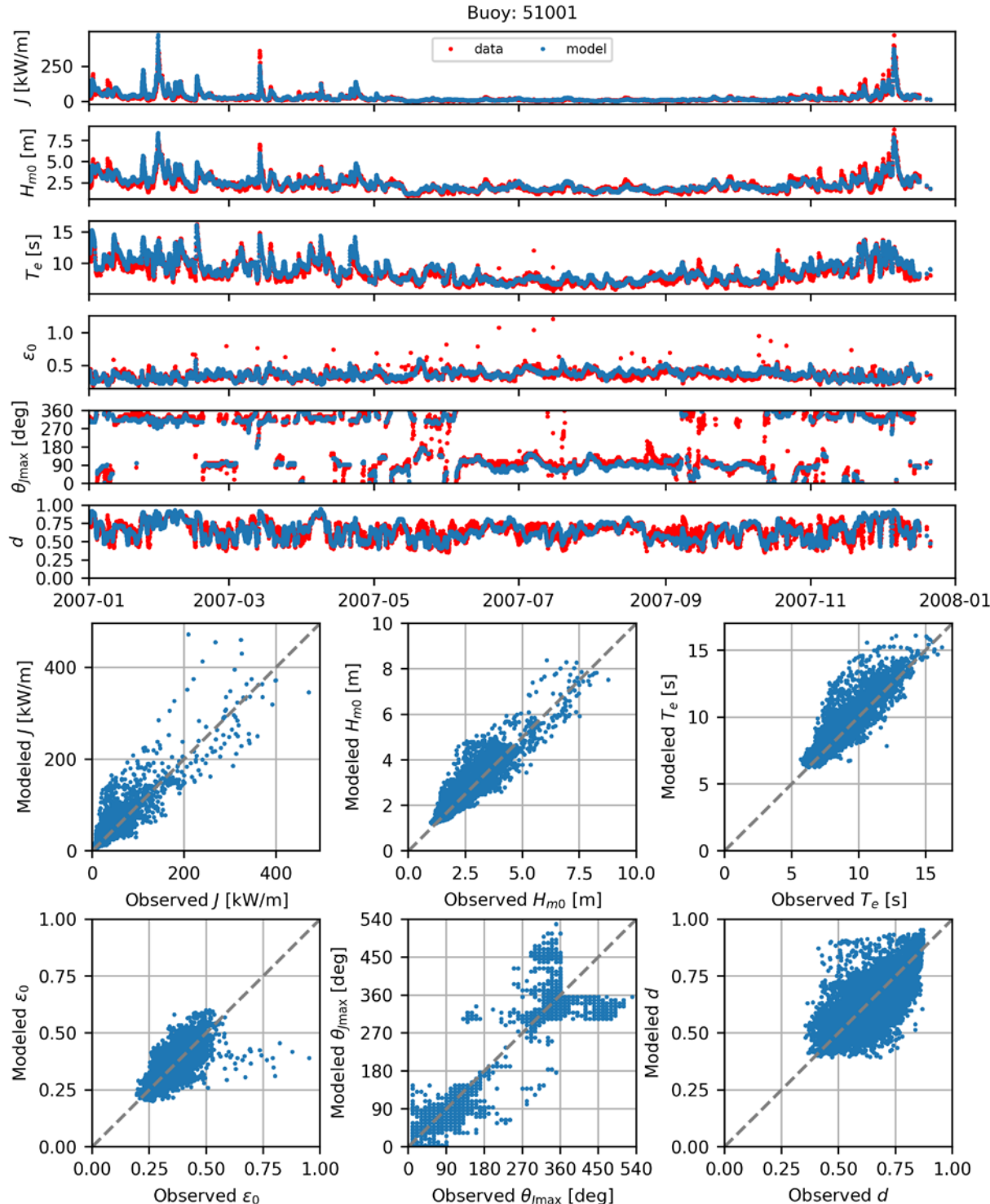


Figure B.58. Comparisons of time series (top) and scatter plots (bottom) the six model-simulated IEC parameters with observed data at NDBC Buoy 51001 for 2007.

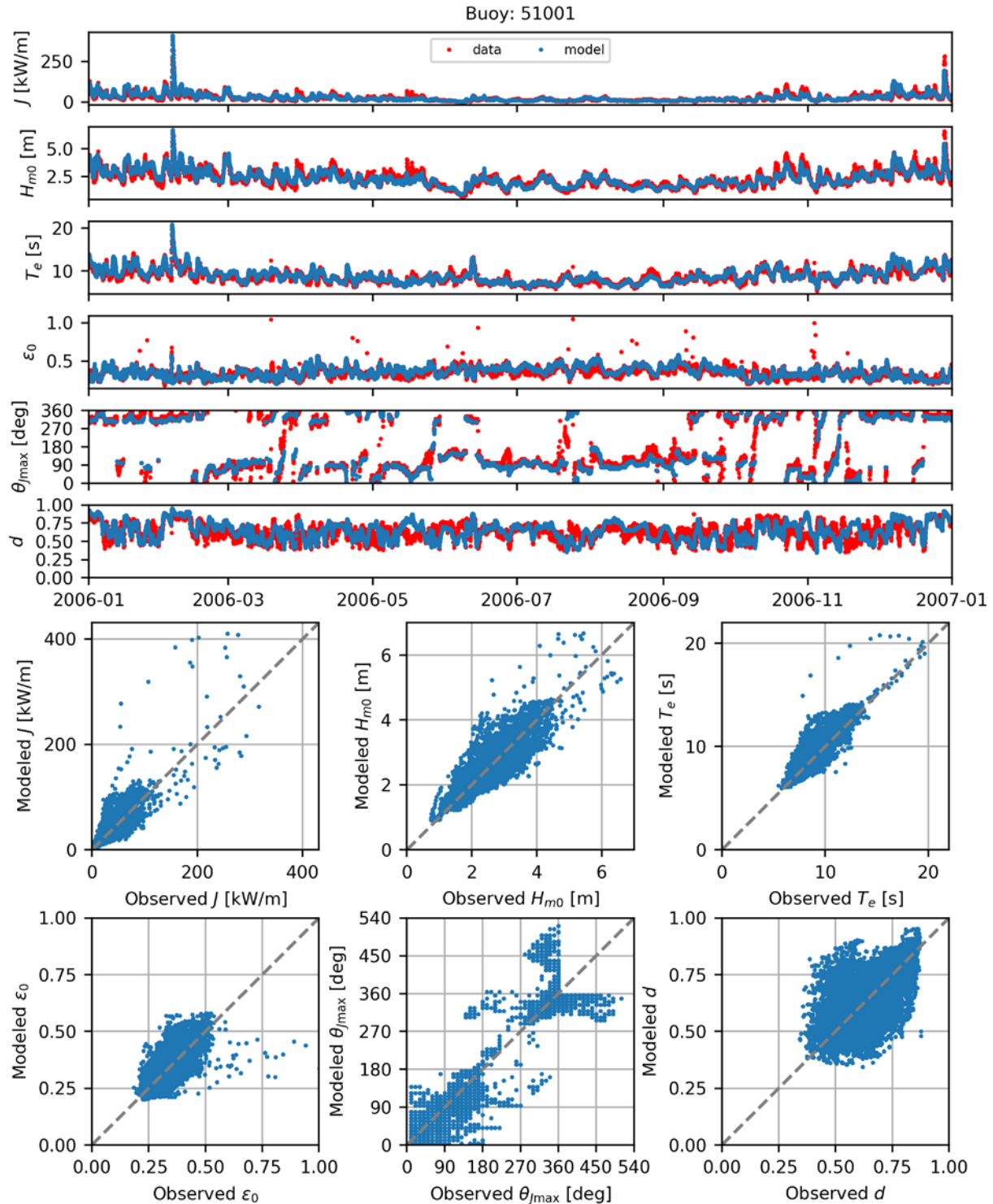


Figure B.59. Comparisons of time series (top) and scatter plots (bottom) the six model-simulated IEC parameters with observed data at NDBC Buoy 51001 for 2006.

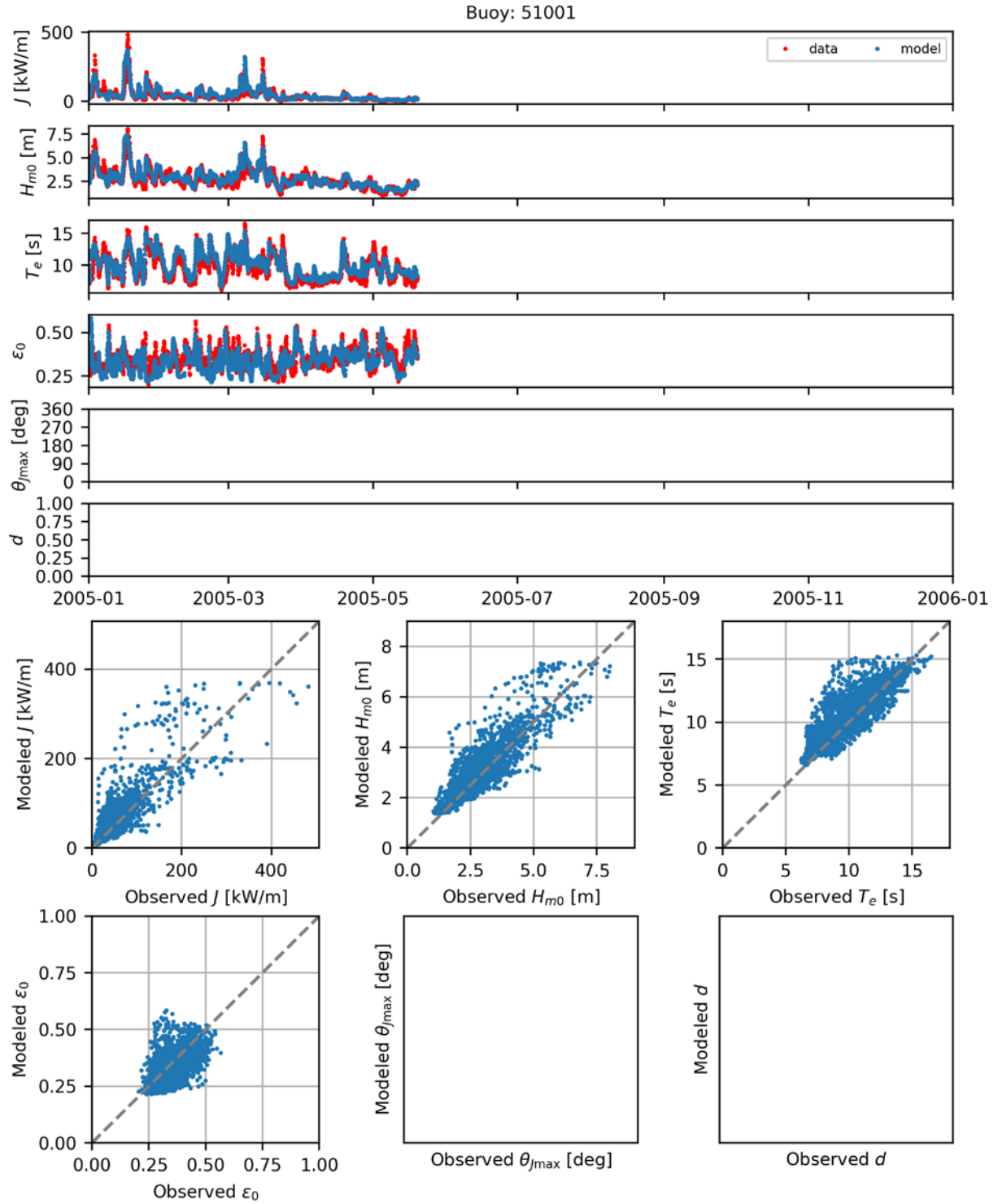


Figure B.60. Comparisons of time series (top) and scatter plots (bottom) the six model-simulated IEC parameters with observed data at NDBC Buoy 51001 for 2005.

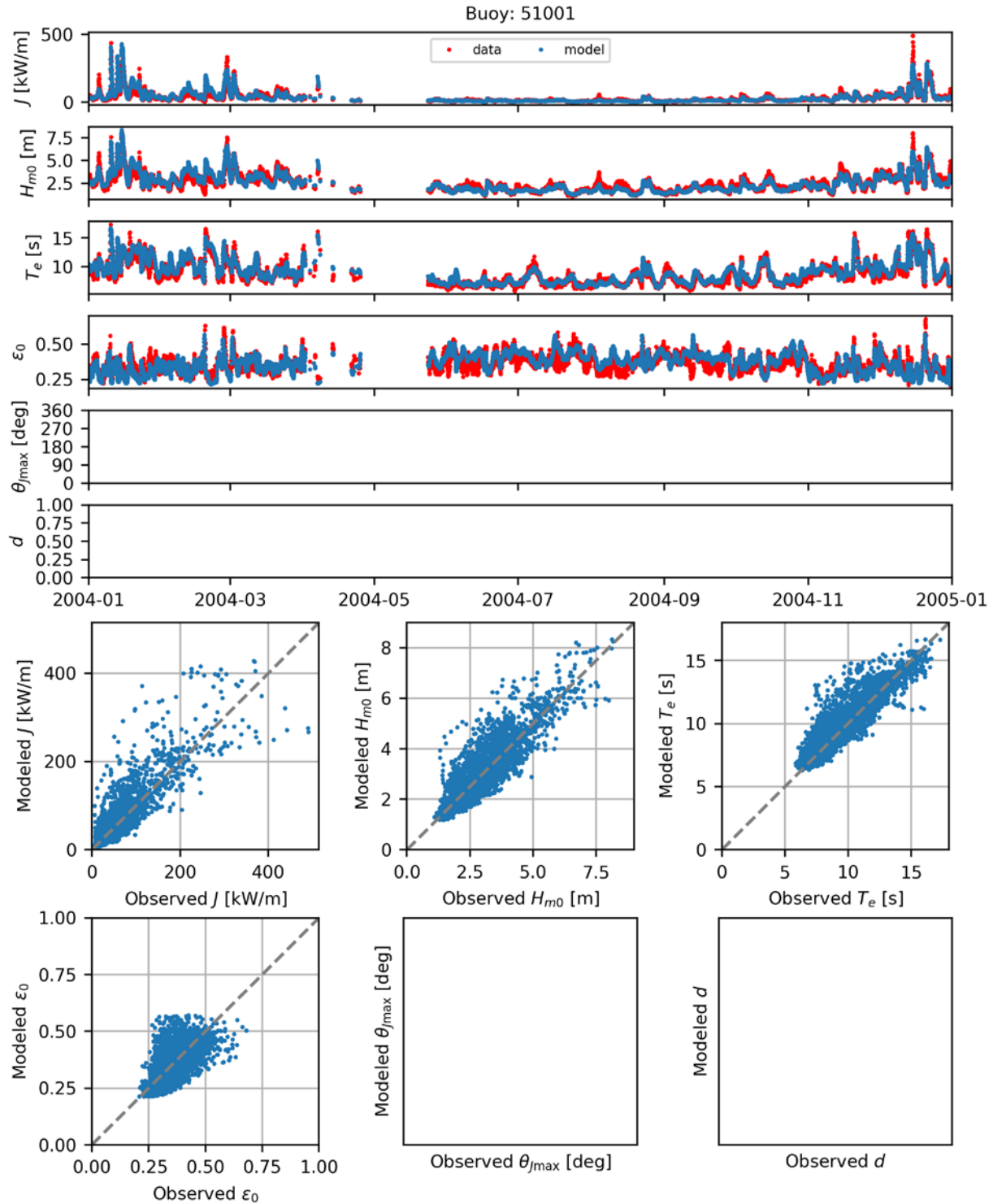


Figure B.61. Comparisons of time series (top) and scatter plots (bottom) the six model-simulated IEC parameters with observed data at NDBC Buoy 51001 for 2004.

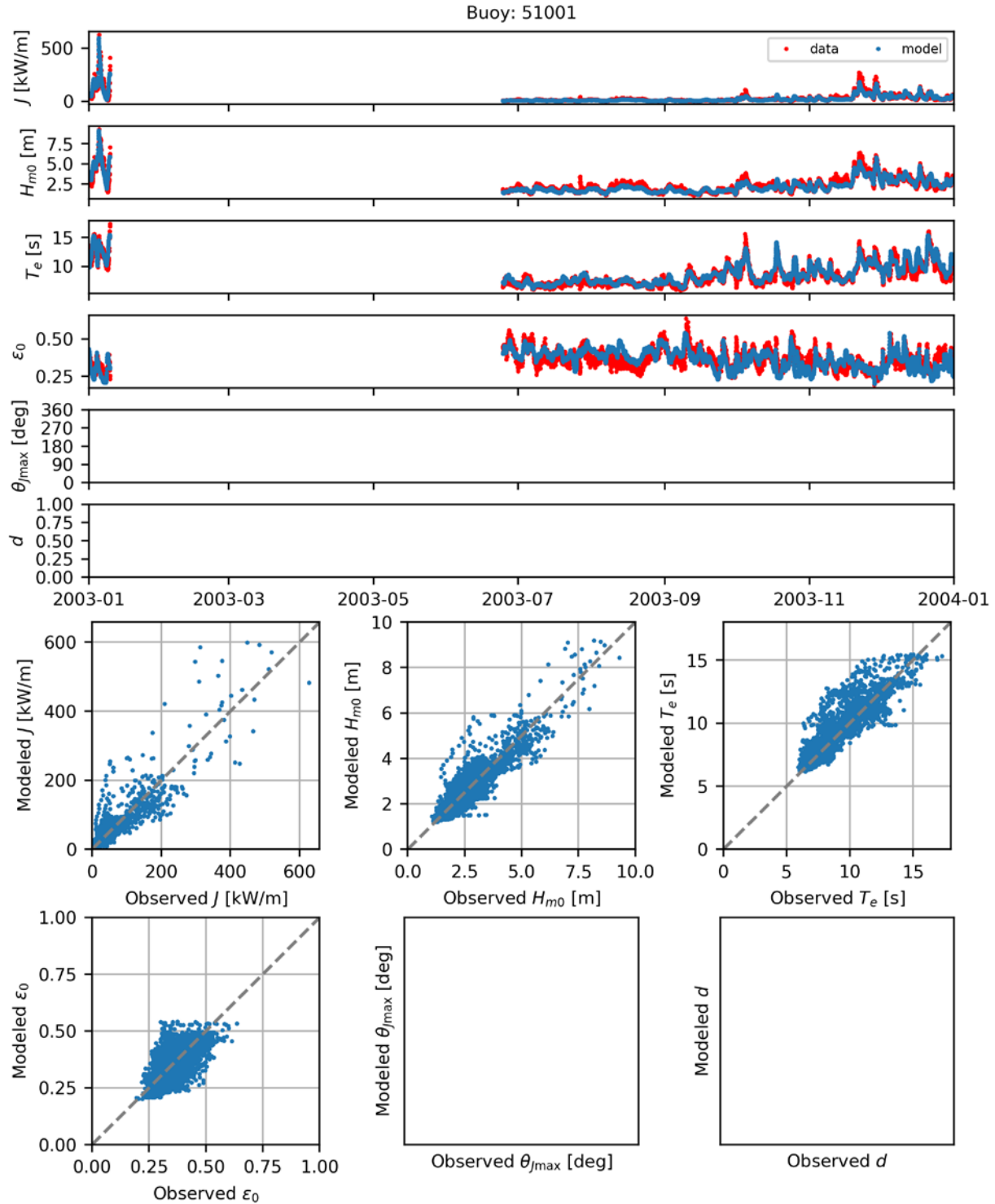


Figure B.62. Comparisons of time series (top) and scatter plots (bottom) the six model-simulated IEC parameters with observed data at NDBC Buoy 51001 for 2003.

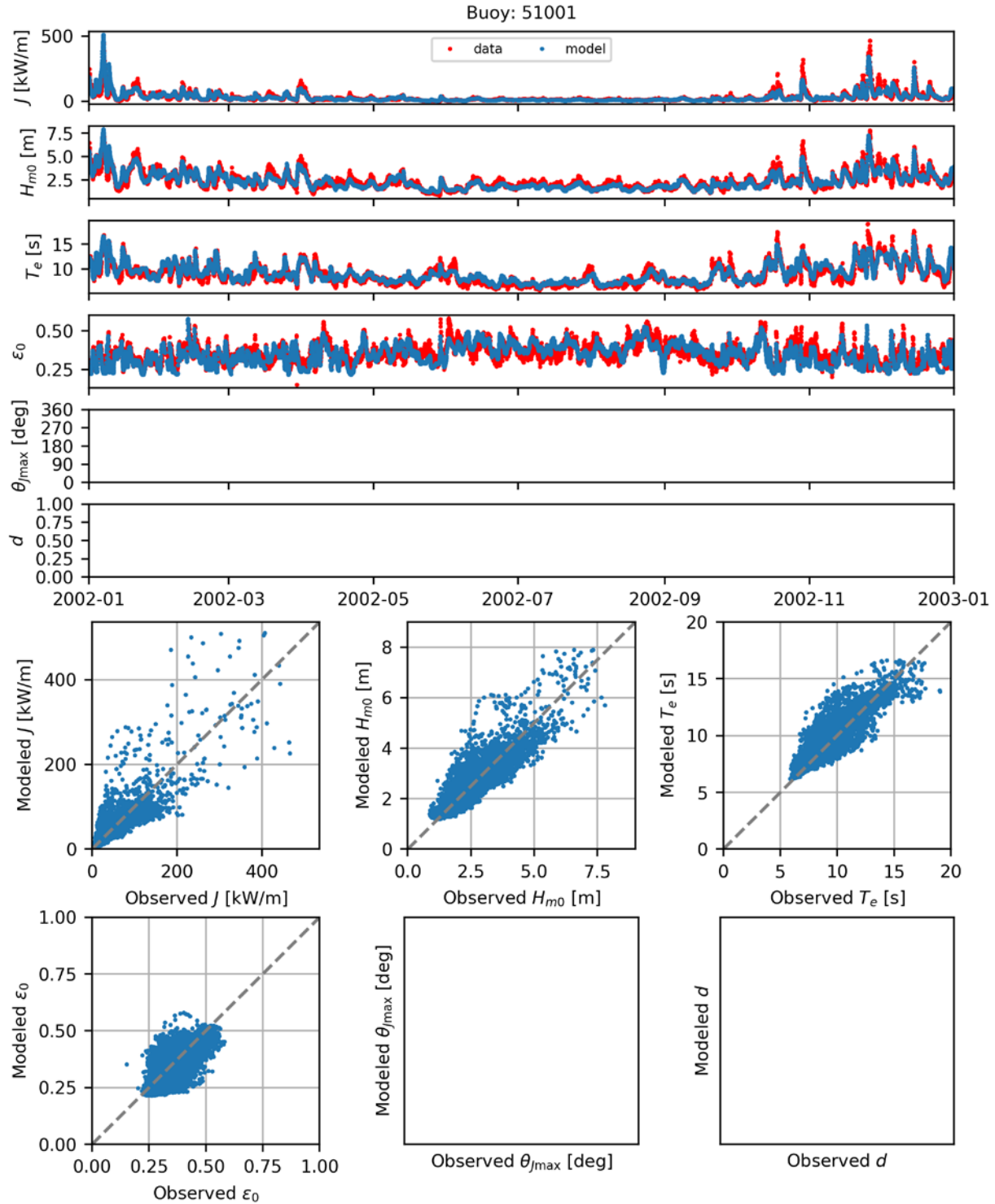


Figure B.63. Comparisons of time series (top) and scatter plots (bottom) the six model-simulated IEC parameters with observed data at NDBC Buoy 51001 for 2002.

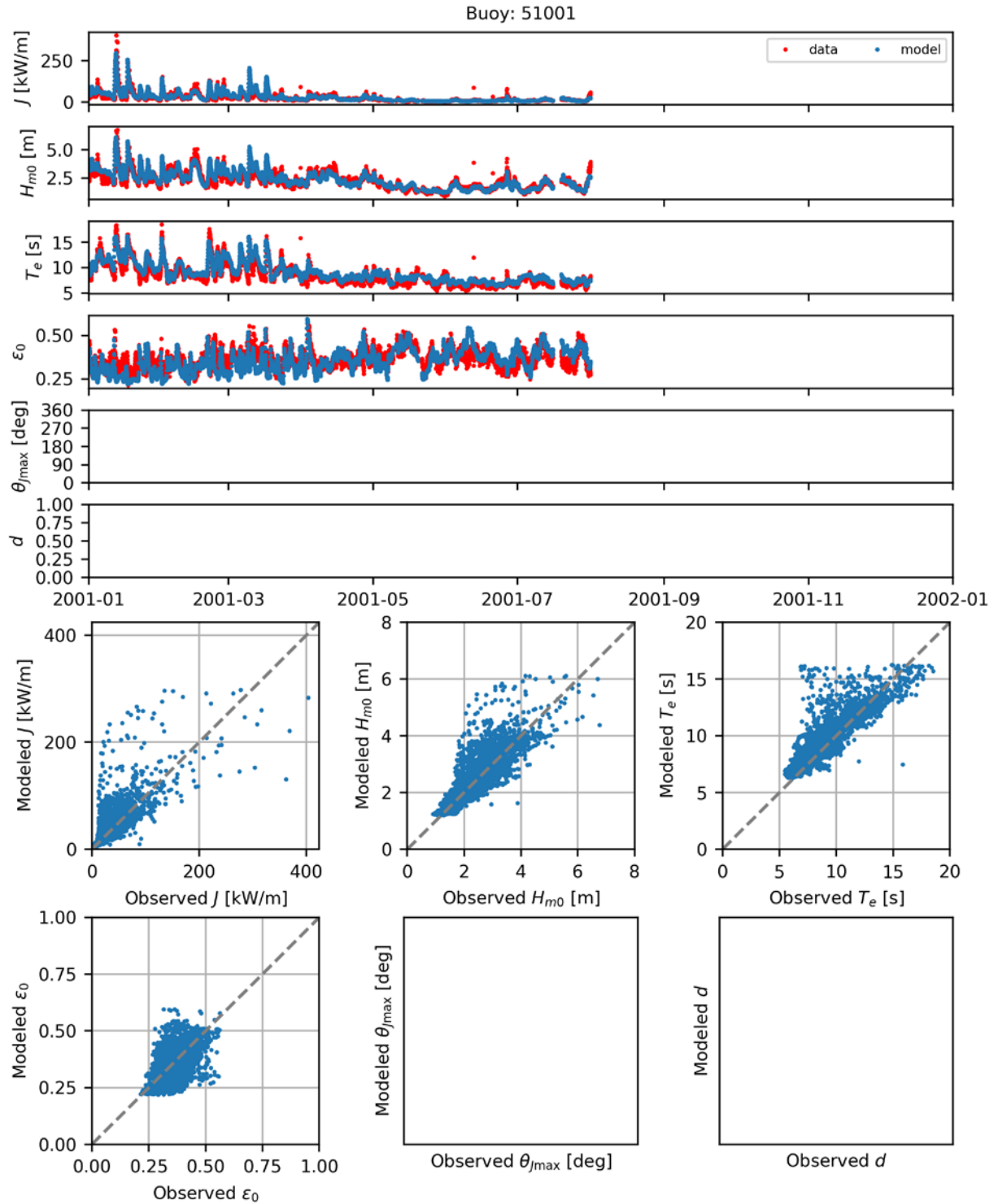


Figure B.64. Comparisons of time series (top) and scatter plots (bottom) the six model-simulated IEC parameters with observed data at NDBC Buoy 51001 for 2001.

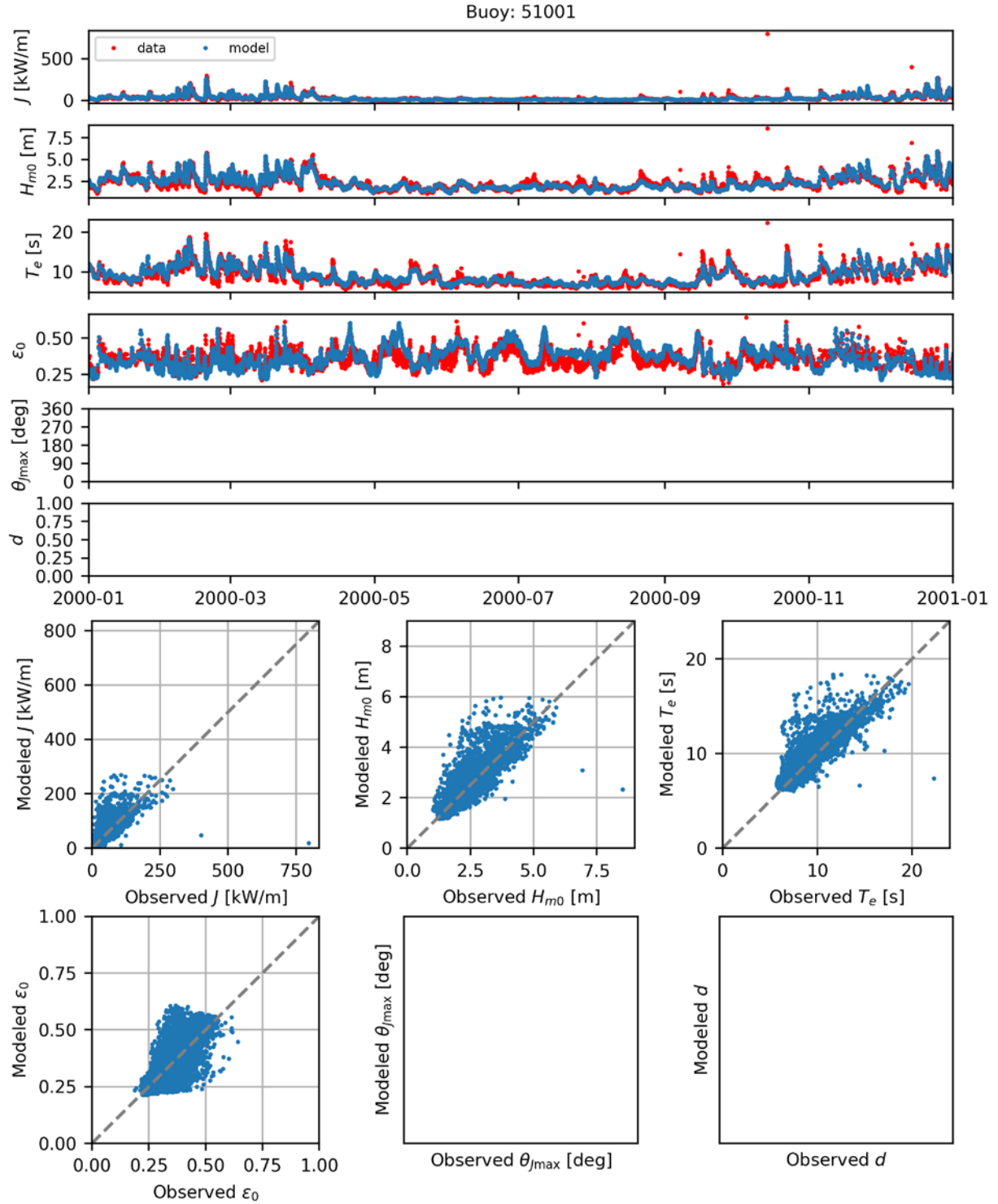


Figure B.65. Comparisons of time series (top) and scatter plots (bottom) the six model-simulated IEC parameters with observed data at NDBC Buoy 51001 for 2000.

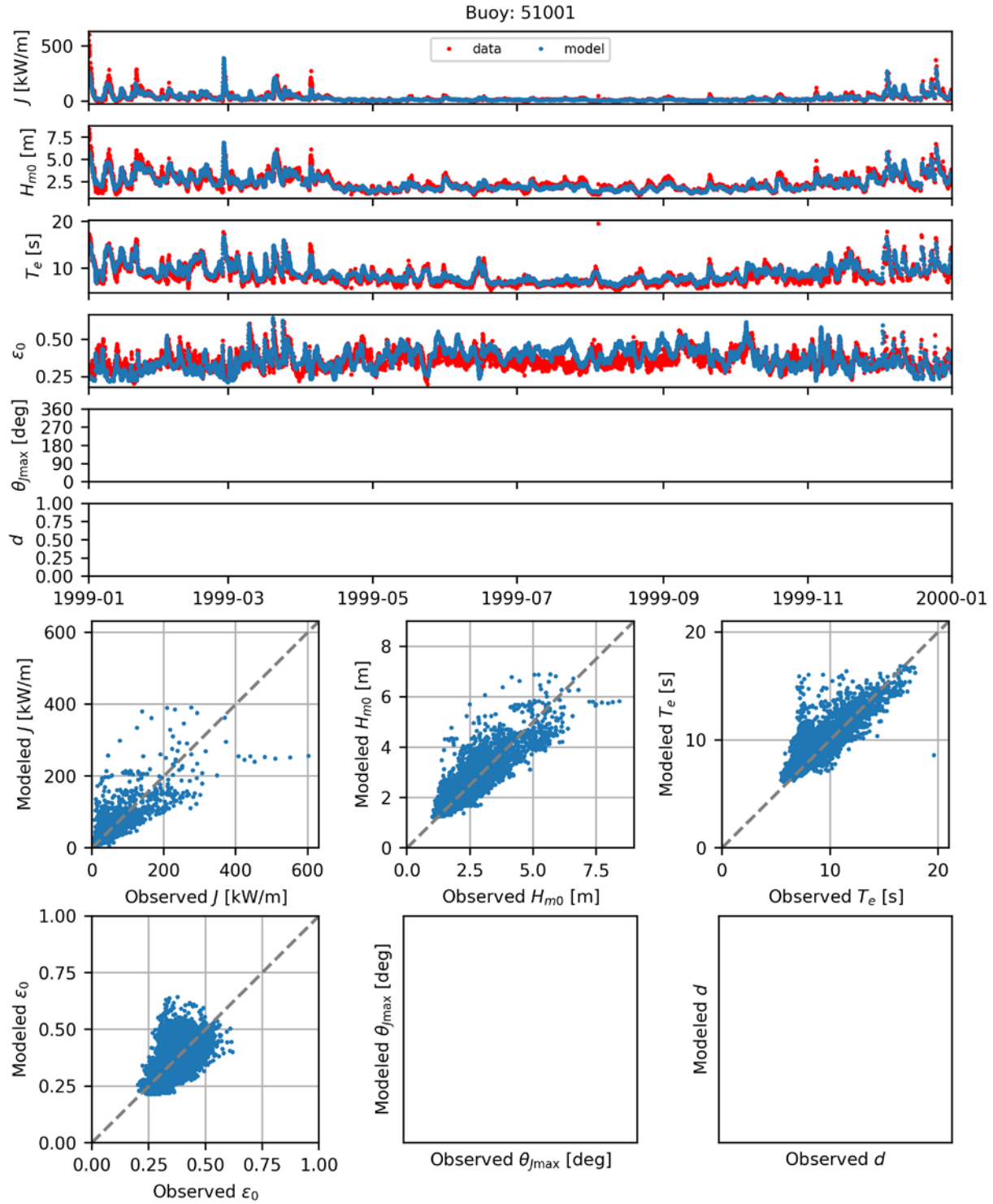


Figure B.66. Comparisons of time series (top) and scatter plots (bottom) the six model-simulated IEC parameters with observed data at NDBC Buoy 51001 for 1999.

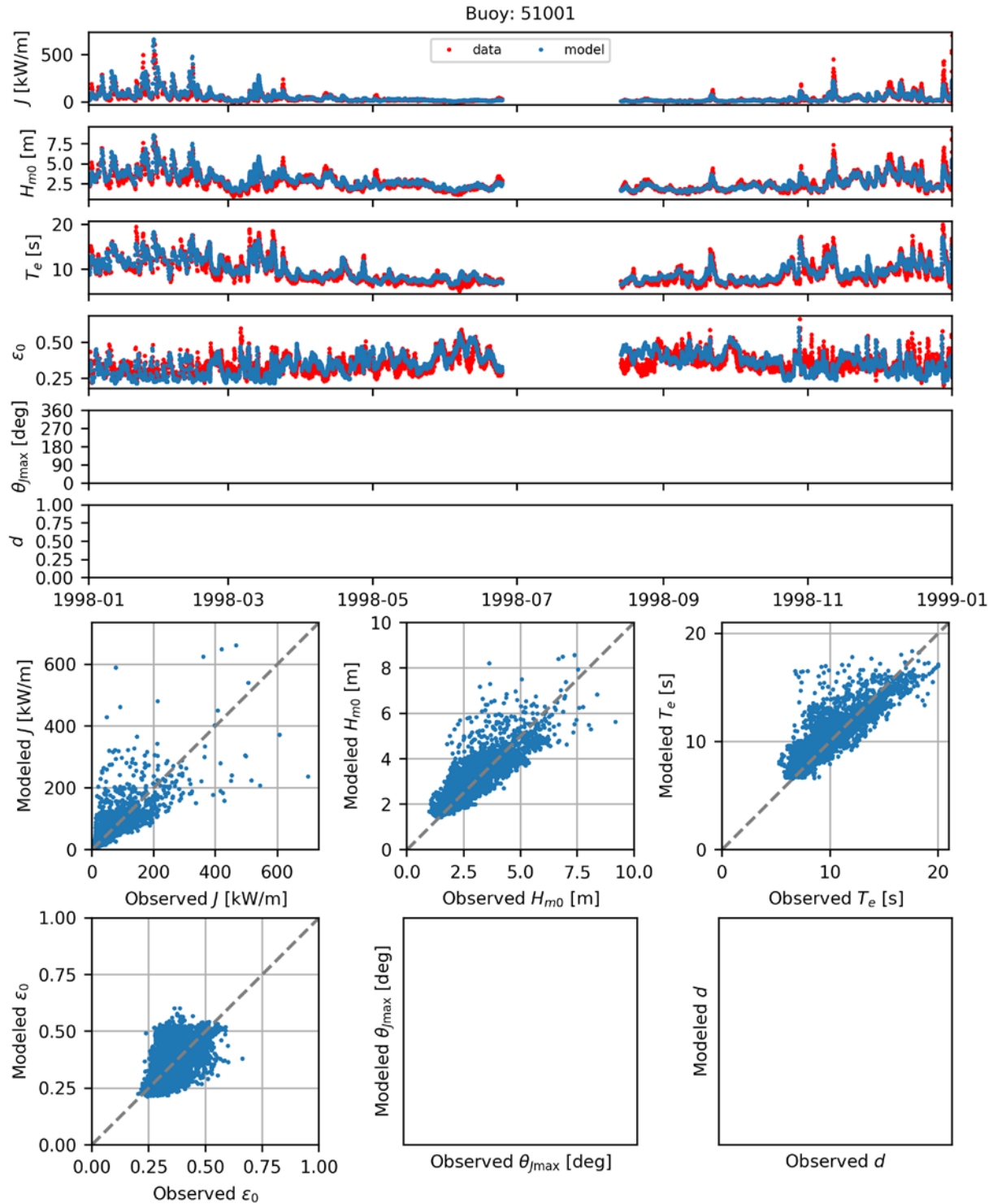


Figure B.67. Comparisons of time series (top) and scatter plots (bottom) the six model-simulated IEC parameters with observed data at NDBC Buoy 51001 for 1998.

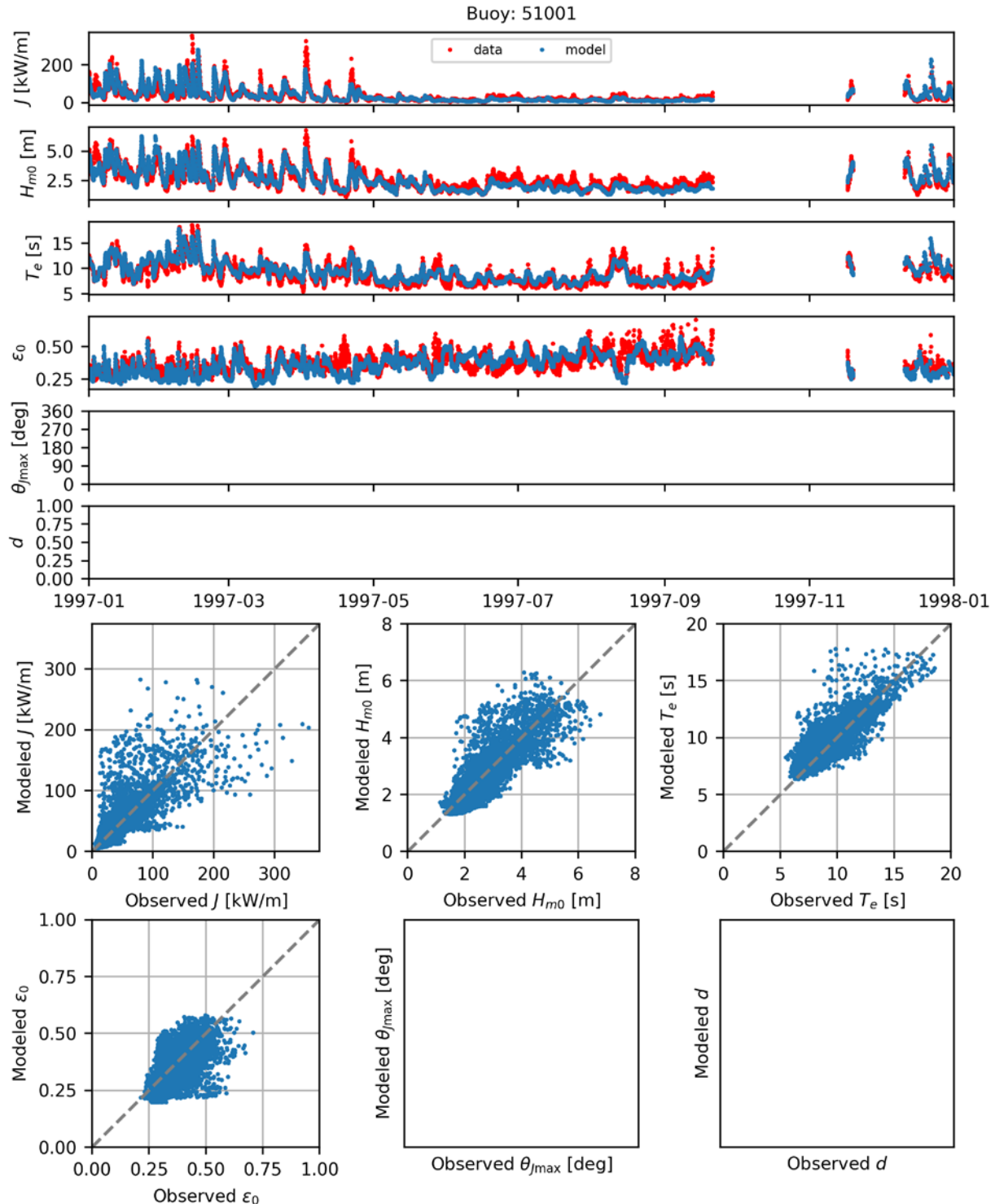


Figure B.68. Comparisons of time series (top) and scatter plots (bottom) the six model-simulated IEC parameters with observed data at NDBC Buoy 51001 for 1997.

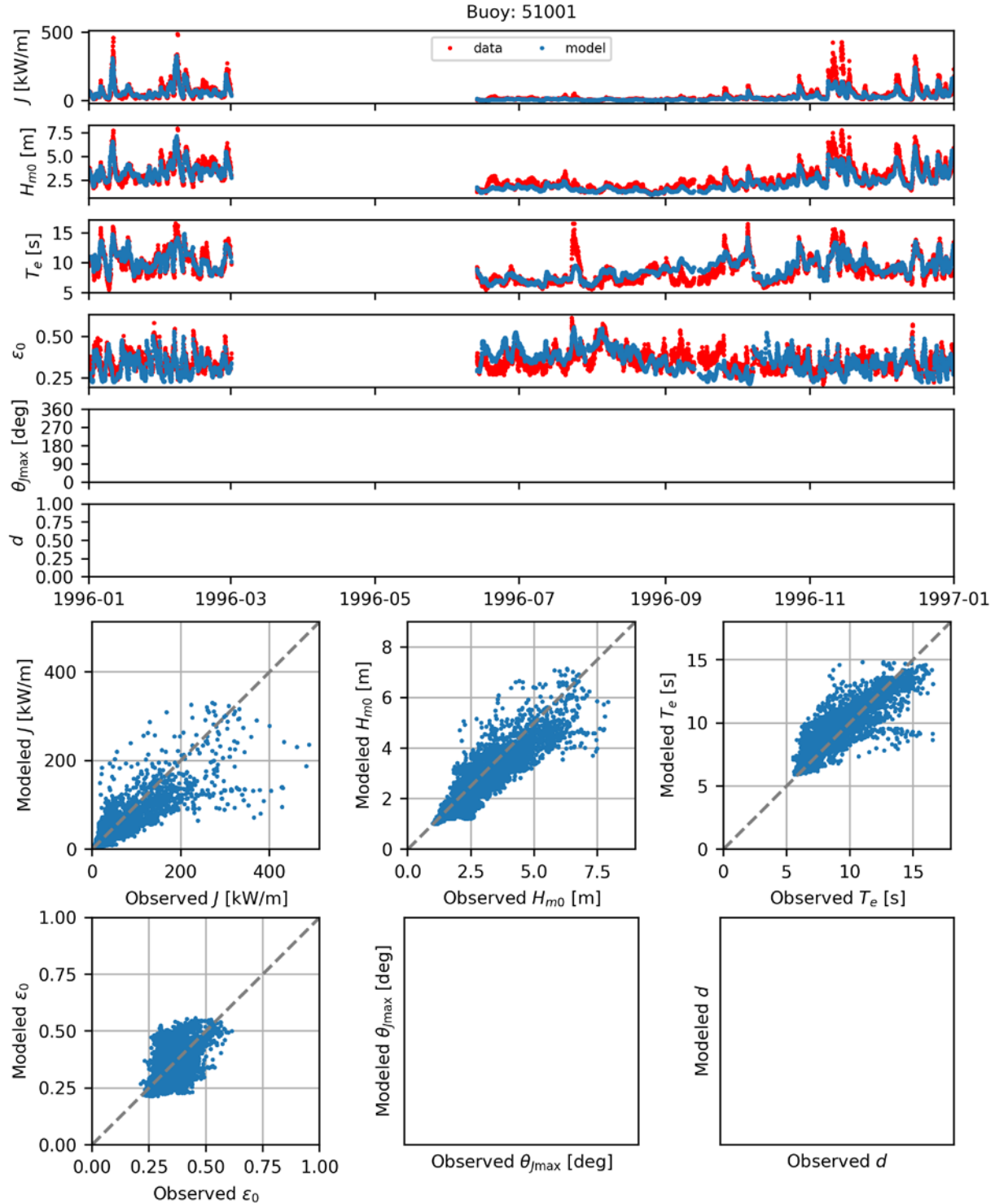


Figure B.69. Comparisons of time series (top) and scatter plots (bottom) the six model-simulated IEC parameters with observed data at NDBC Buoy 51001 for 1996.

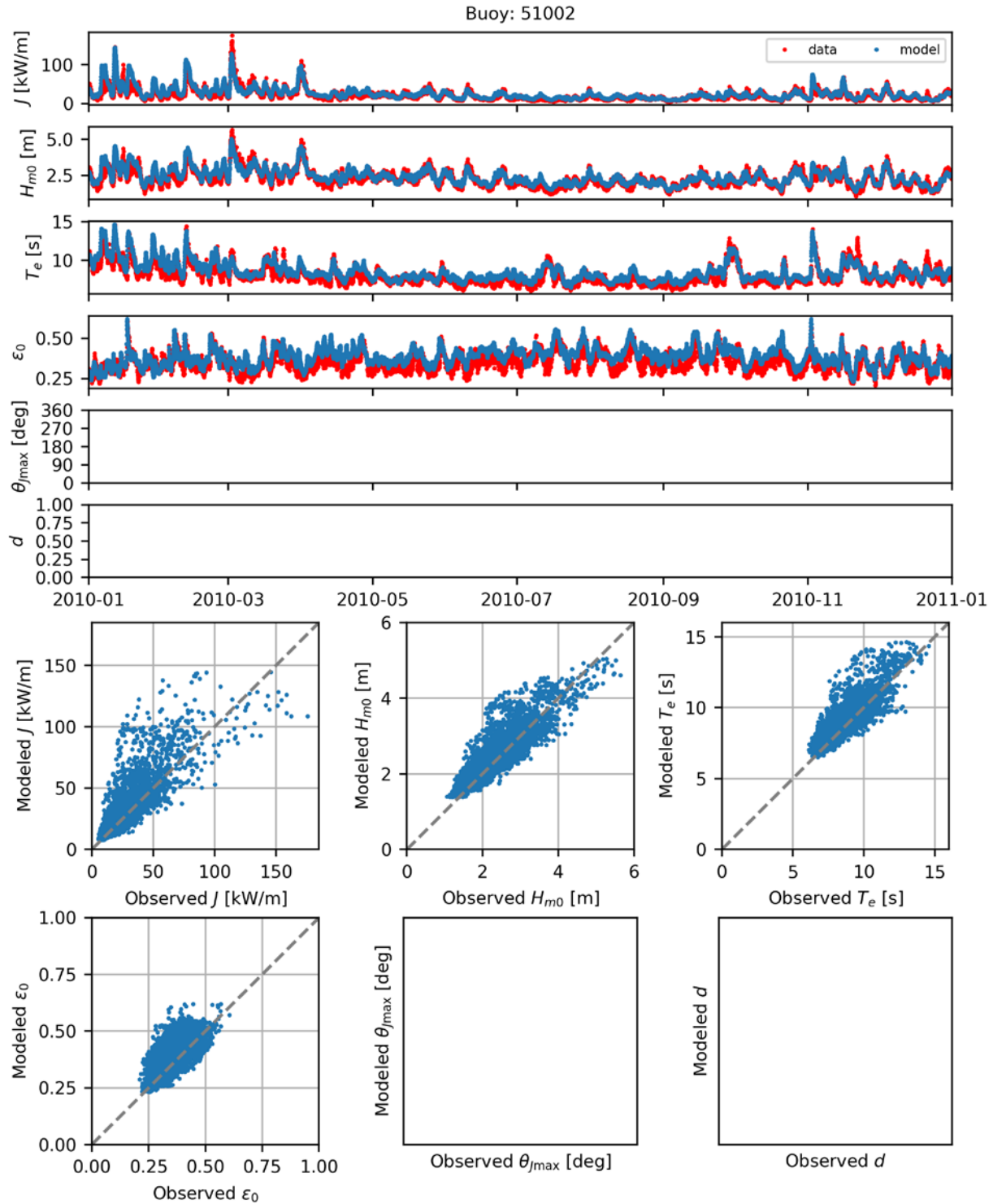


Figure B.70. Comparisons of time series (top) and scatter plots (bottom) the six model-simulated IEC parameters with observed data at NDBC Buoy 51002 for 2010.

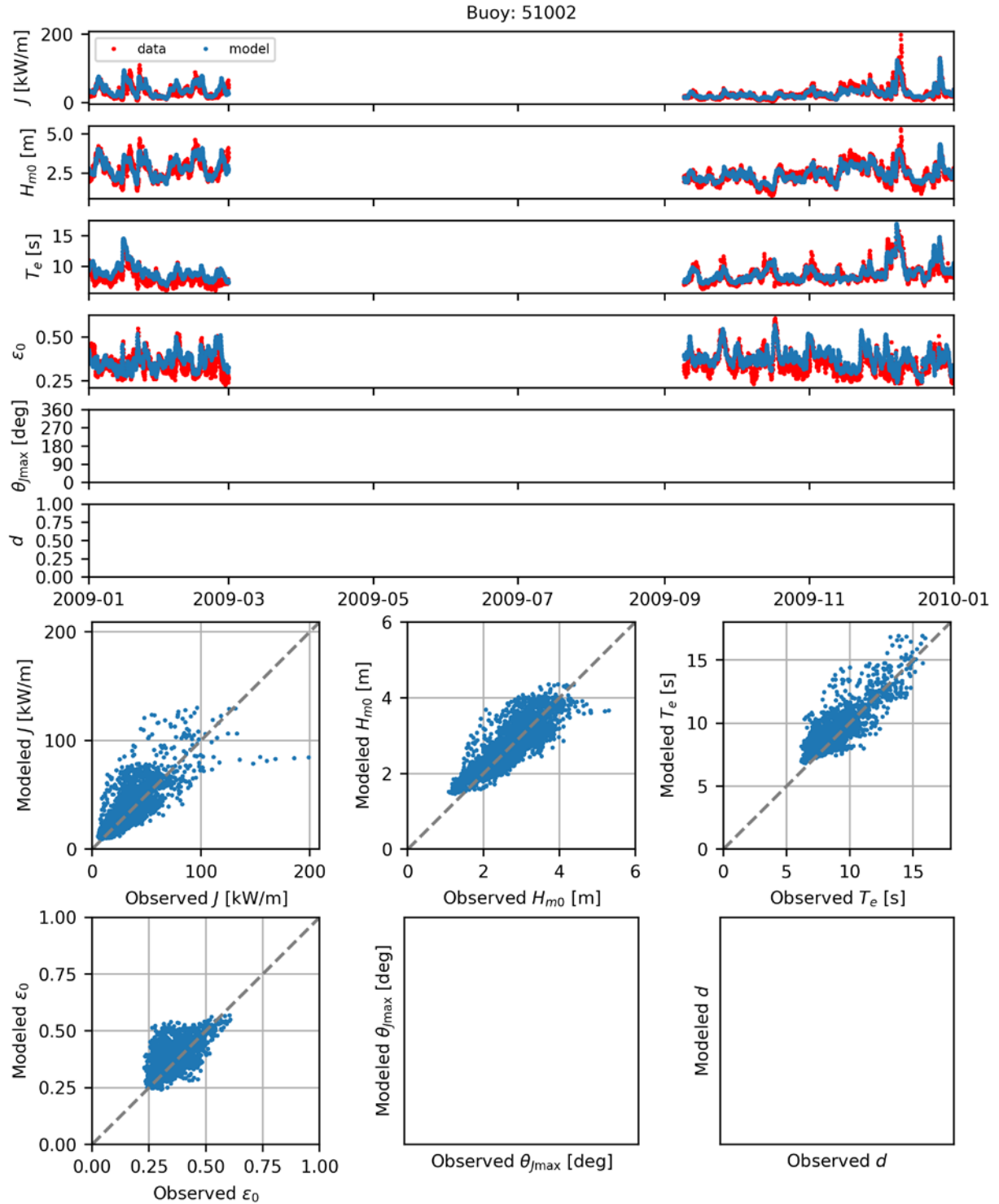


Figure B.71. Comparisons of time series (top) and scatter plots (bottom) the six model-simulated IEC parameters with observed data at NDBC Buoy 51002 for 2009.

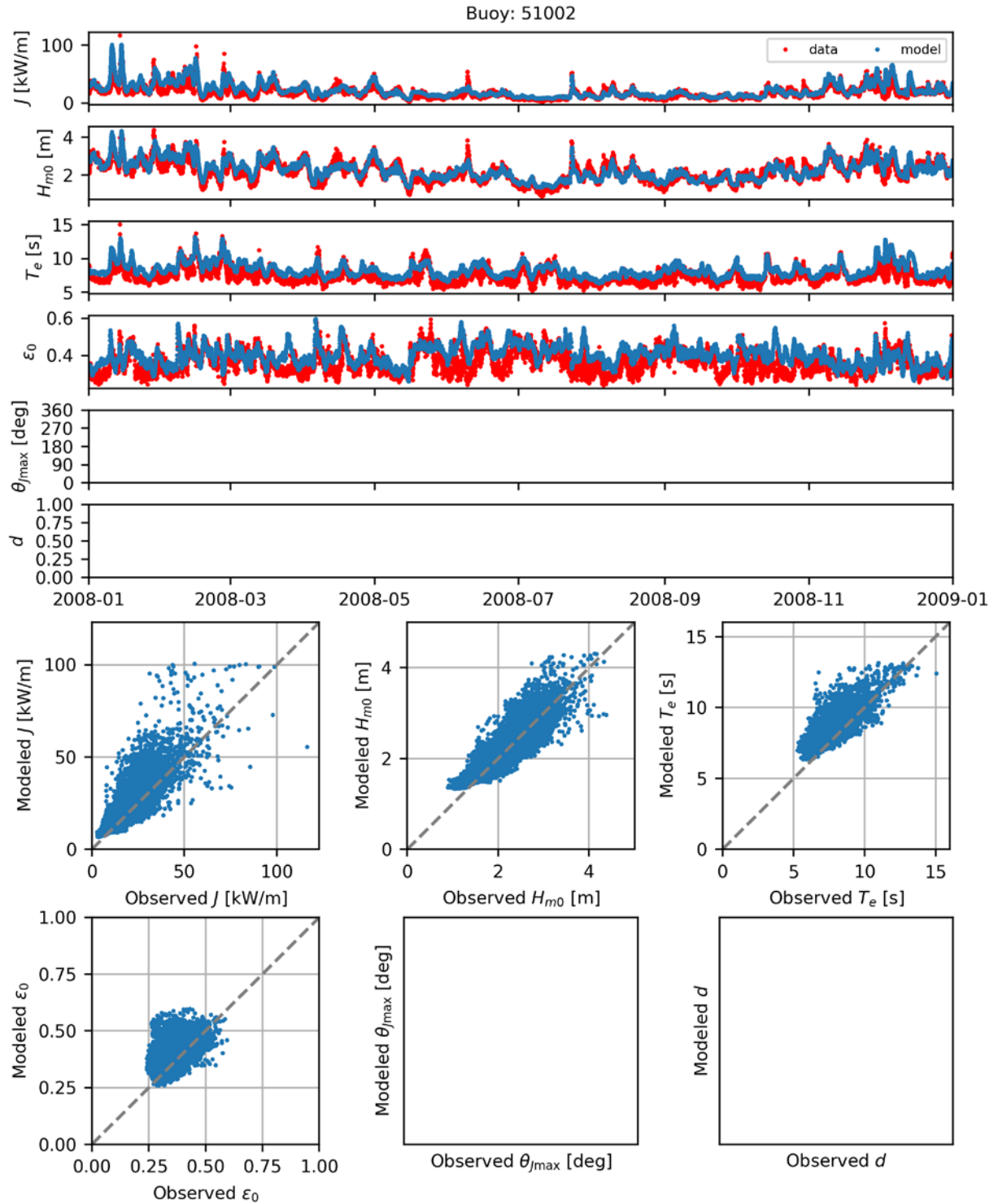


Figure B.72. Comparisons of time series (top) and scatter plots (bottom) the six model-simulated IEC parameters with observed data at NDBC Buoy 51002 for 2008.

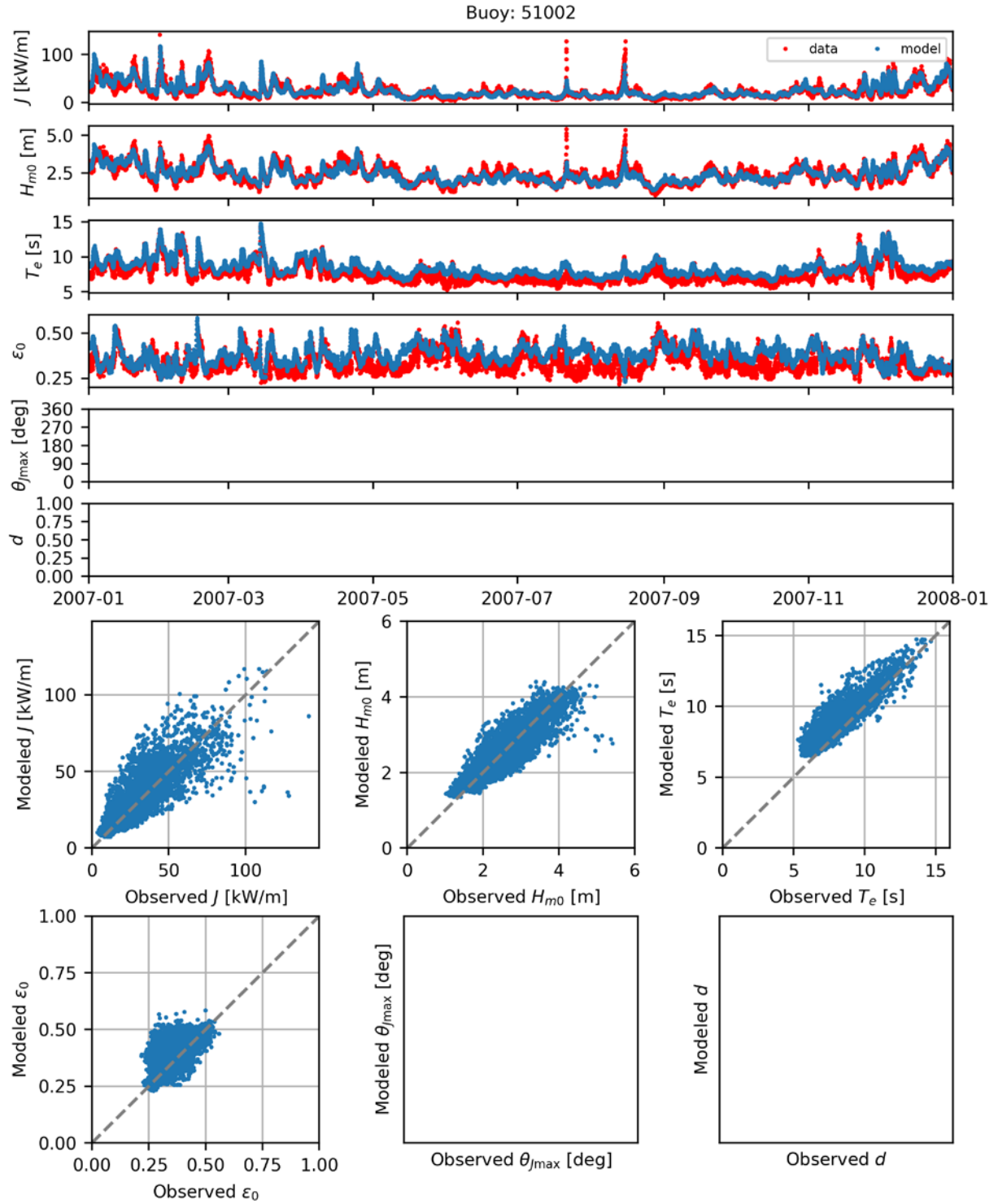


Figure B.73. Comparisons of time series (top) and scatter plots (bottom) the six model-simulated IEC parameters with observed data at NDBC Buoy 51002 for 2007.

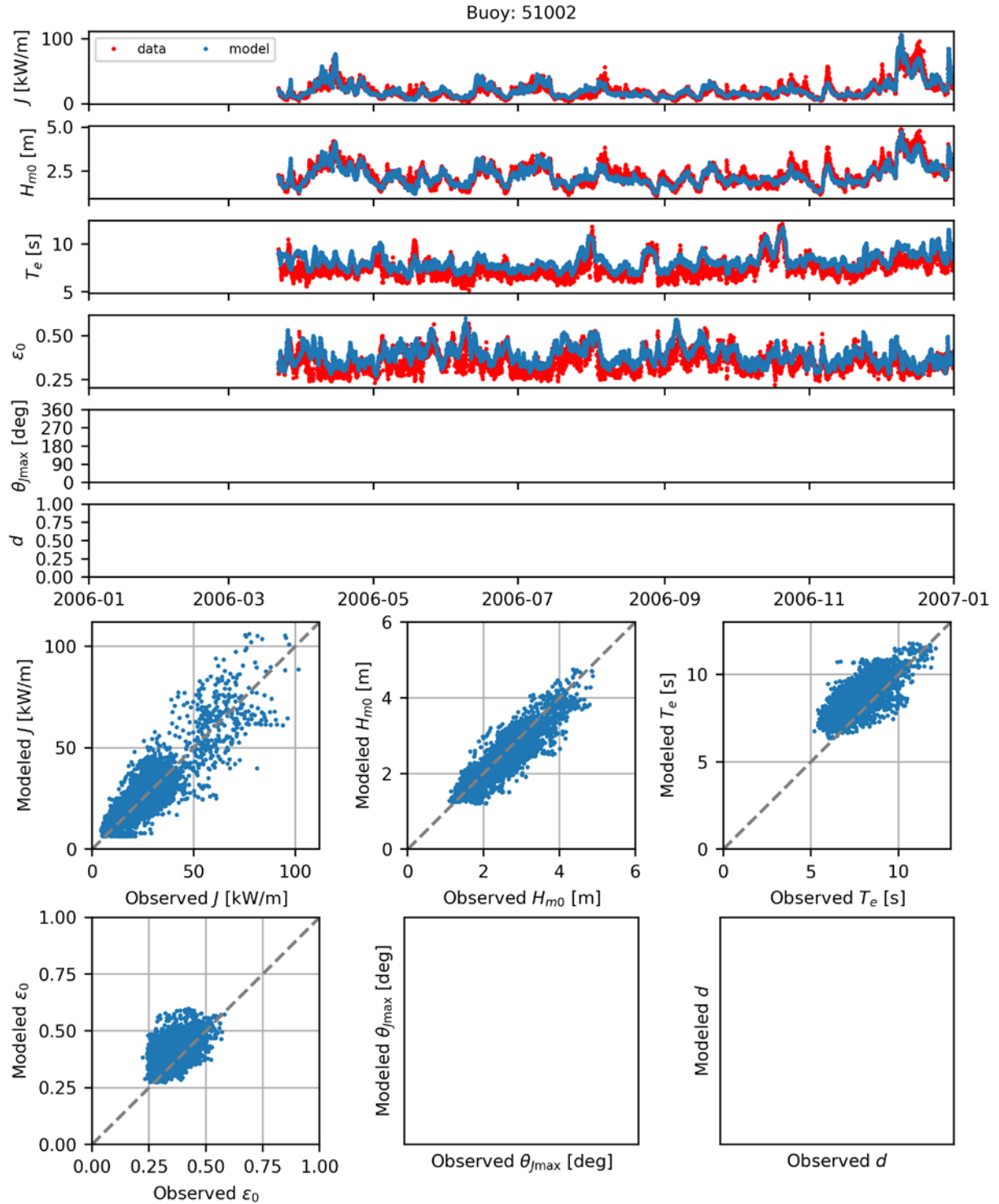


Figure B.74. Comparisons of time series (top) and scatter plots (bottom) the six model-simulated IEC parameters with observed data at NDBC Buoy 51002 for 2006.

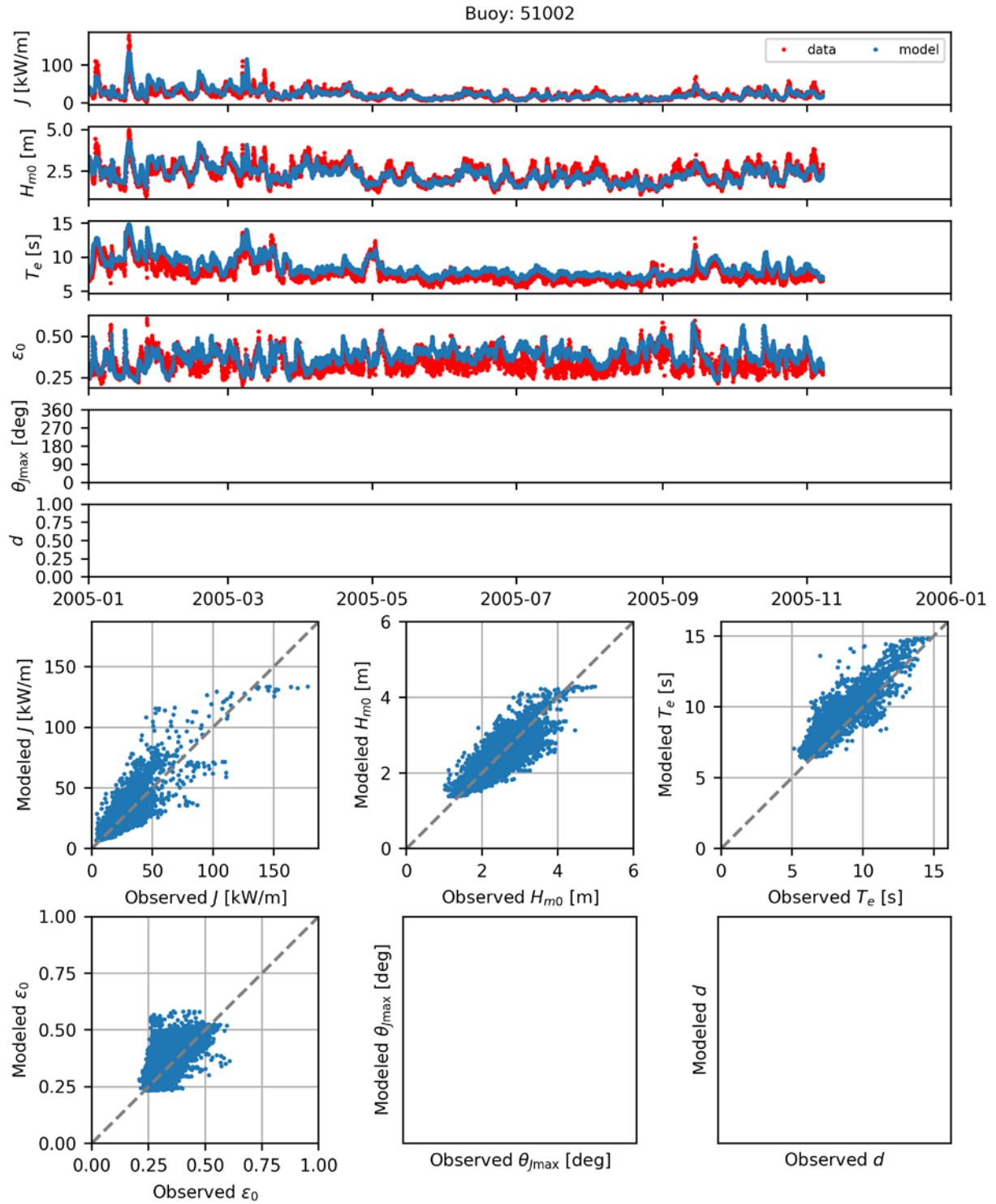


Figure B.75. Comparisons of time series (top) and scatter plots (bottom) the six model-simulated IEC parameters with observed data at NDBC Buoy 51002 for 2005.

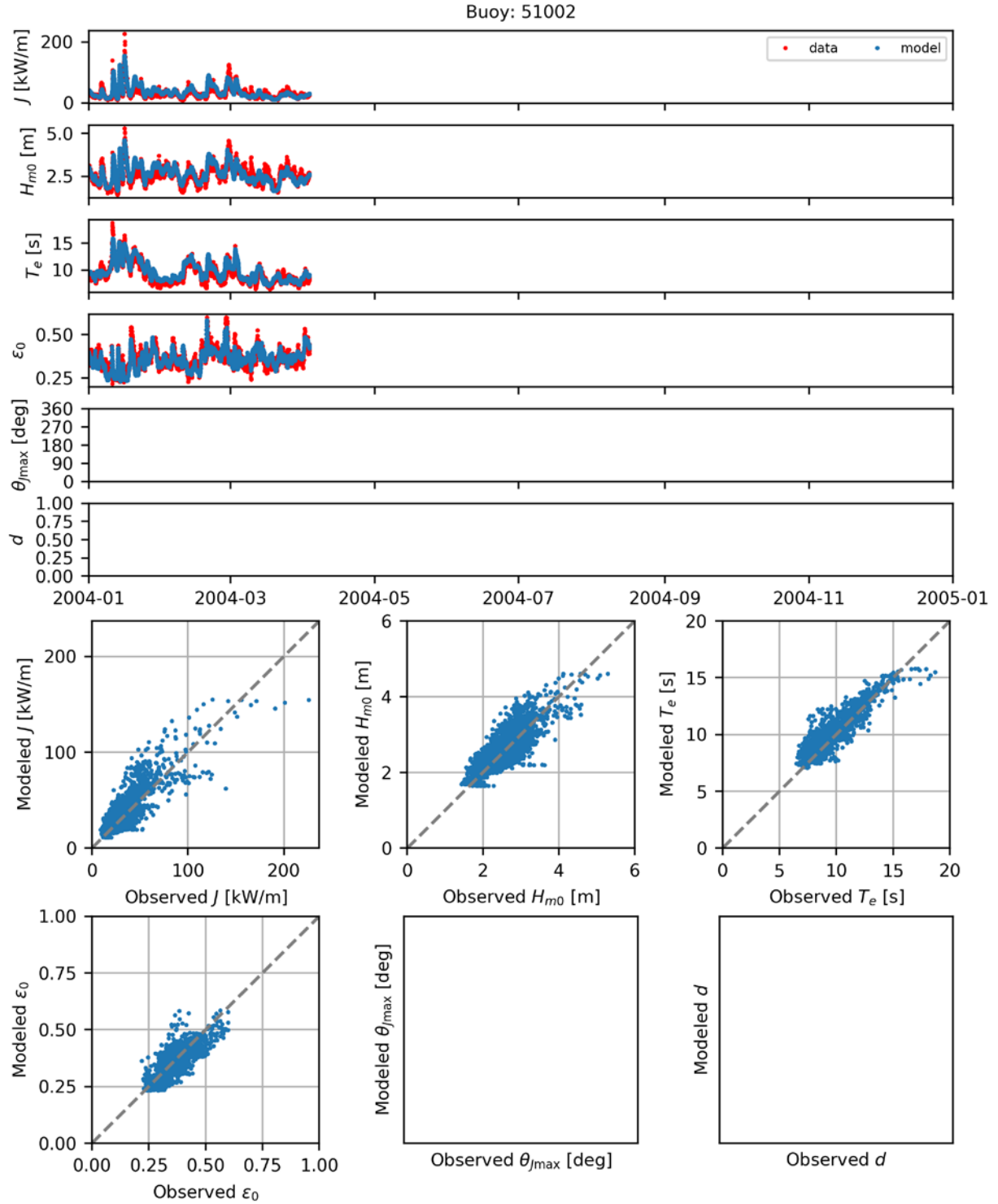


Figure B.76. Comparisons of time series (top) and scatter plots (bottom) the six model-simulated IEC parameters with observed data at NDBC Buoy 51002 for 2004.

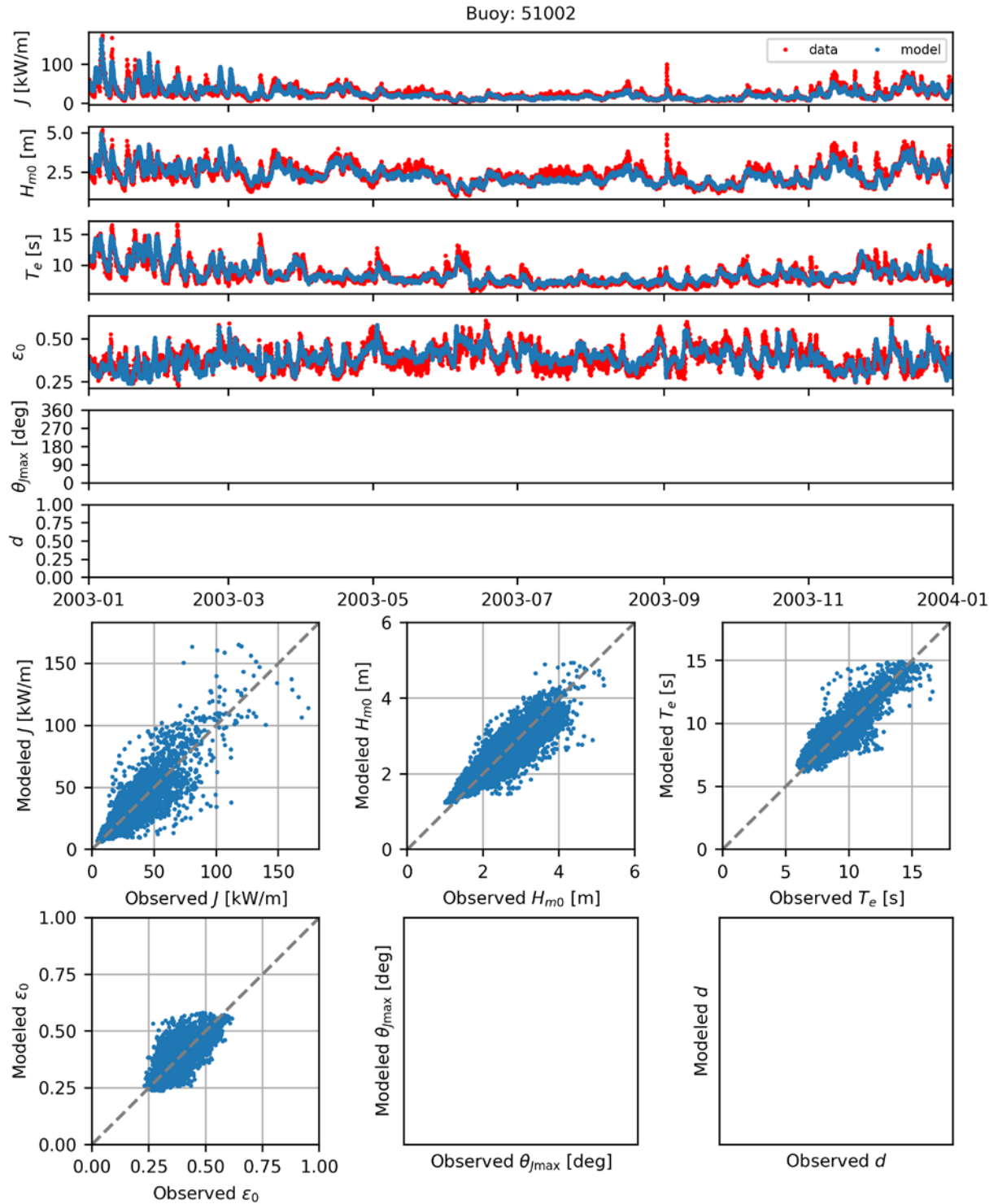


Figure B.77. Comparisons of time series (top) and scatter plots (bottom) the six model-simulated IEC parameters with observed data at NDBC Buoy 51002 for 2003.

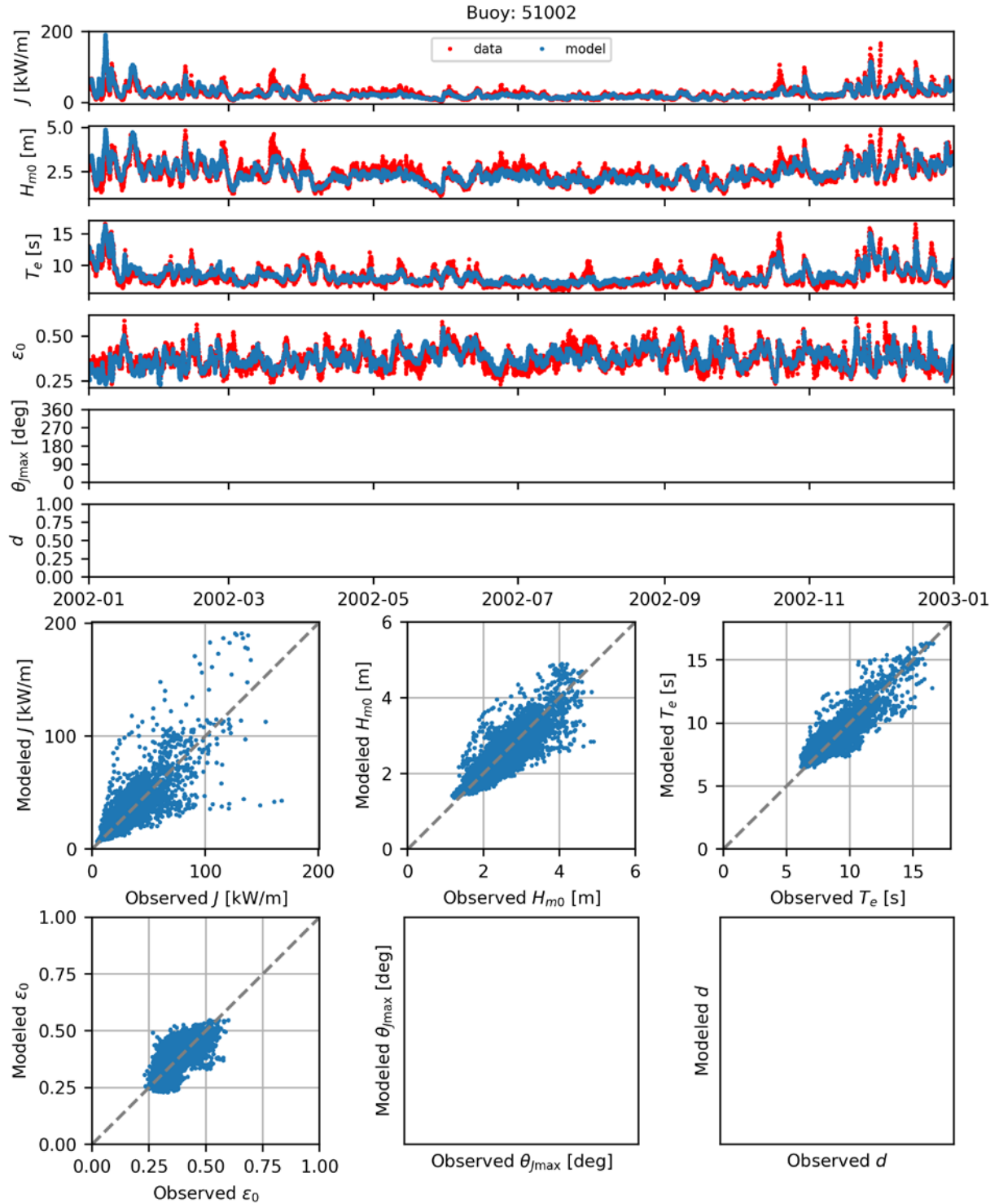


Figure B.78. Comparisons of time series (top) and scatter plots (bottom) the six model-simulated IEC parameters with observed data at NDBC Buoy 51002 for 2002.

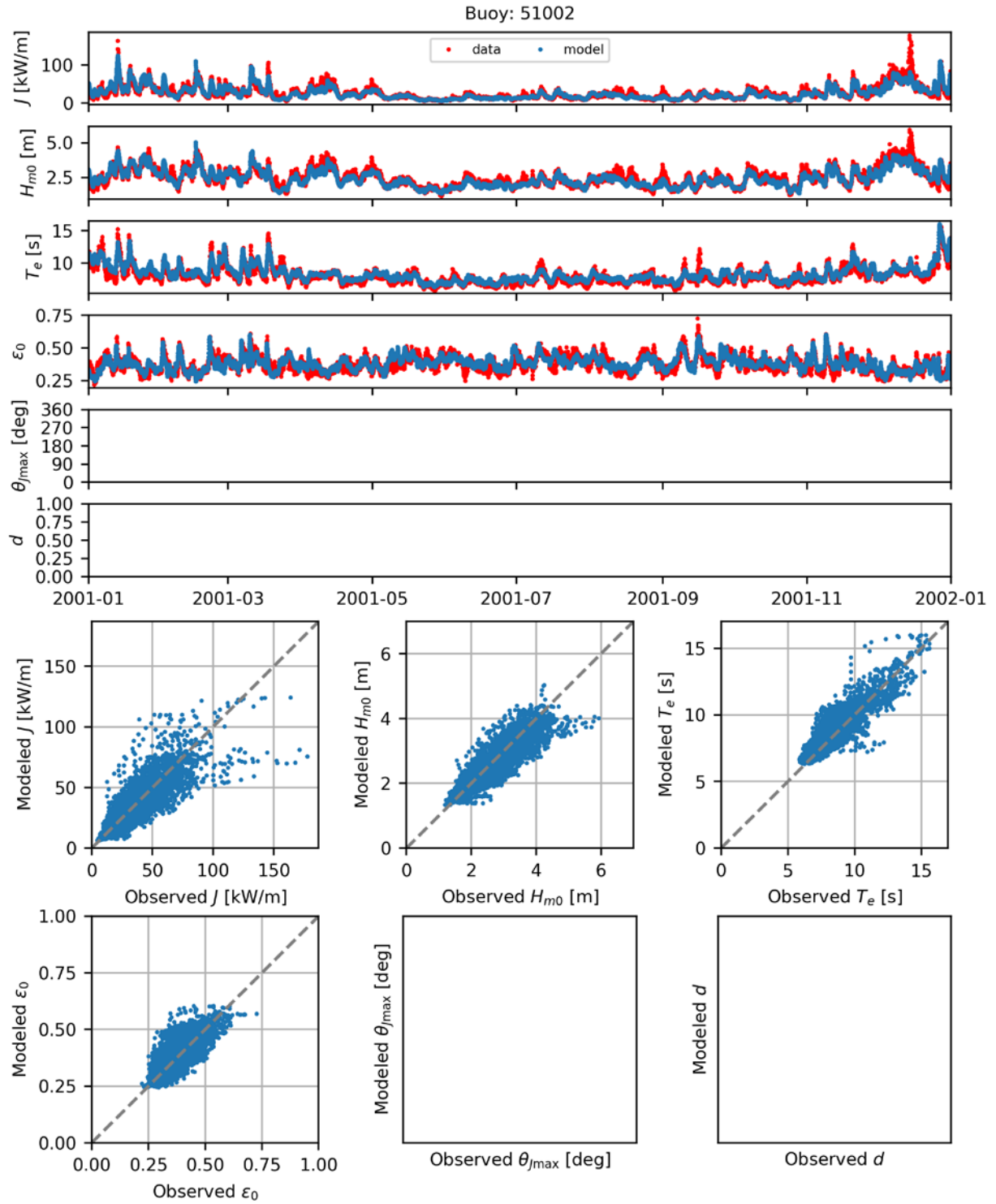


Figure B.79. Comparisons of time series (top) and scatter plots (bottom) the six model-simulated IEC parameters with observed data at NDBC Buoy 51002 for 2001.

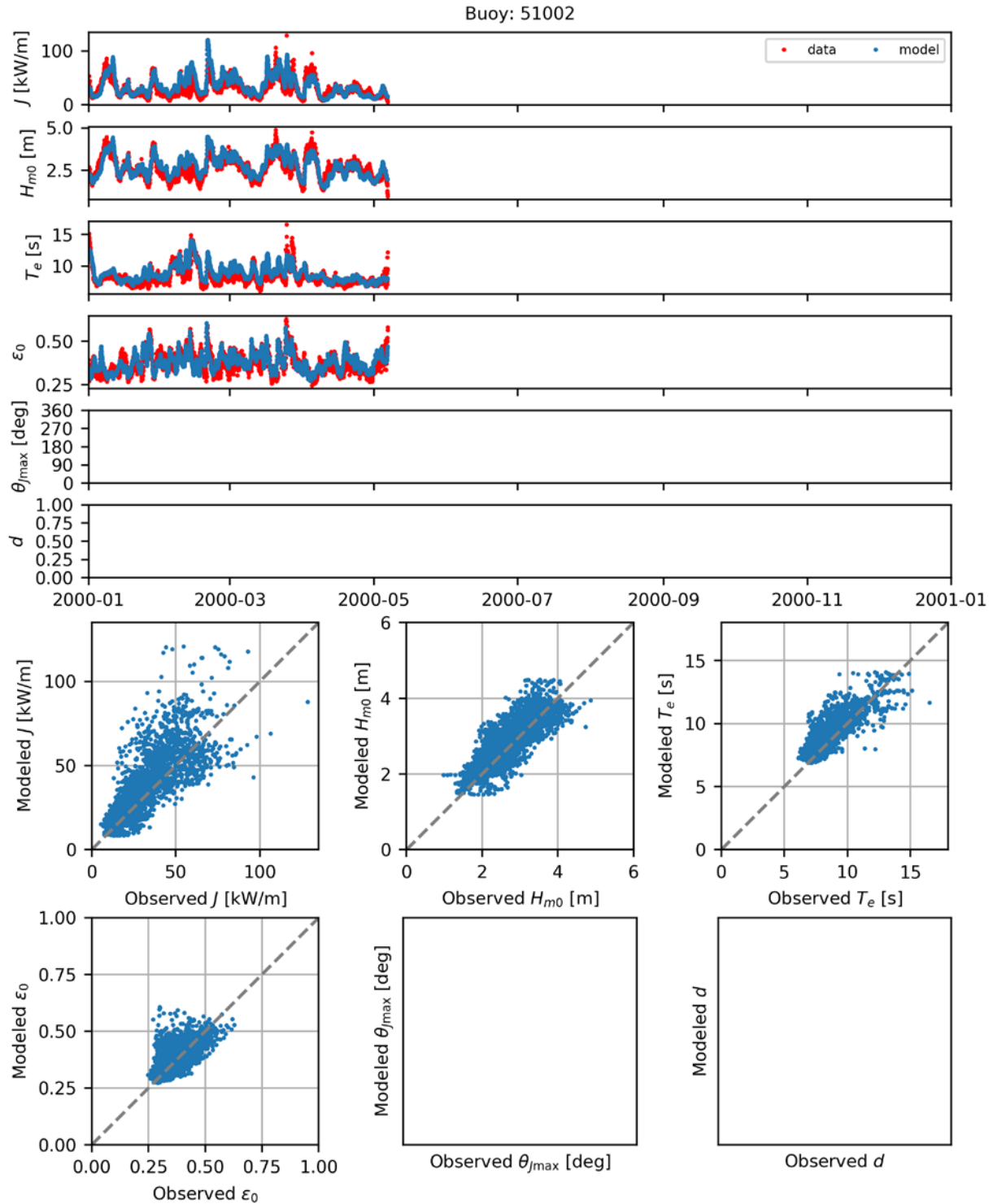


Figure B.80. Comparisons of time series (top) and scatter plots (bottom) the six model-simulated IEC parameters with observed data at NDBC Buoy 51002 for 2000.

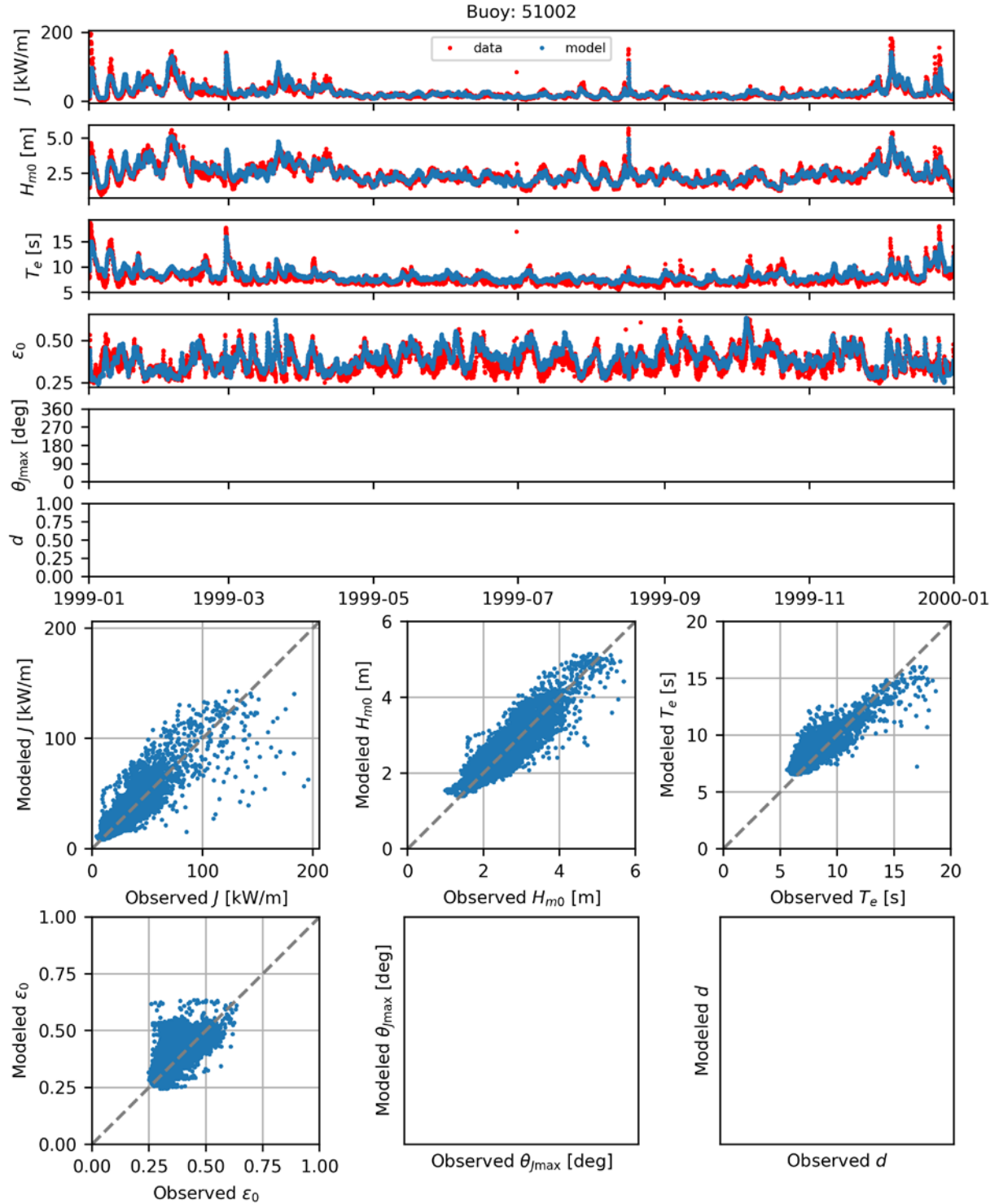


Figure B.81. Comparisons of time series (top) and scatter plots (bottom) the six model-simulated IEC parameters with observed data at NDBC Buoy 51002 for 1999.

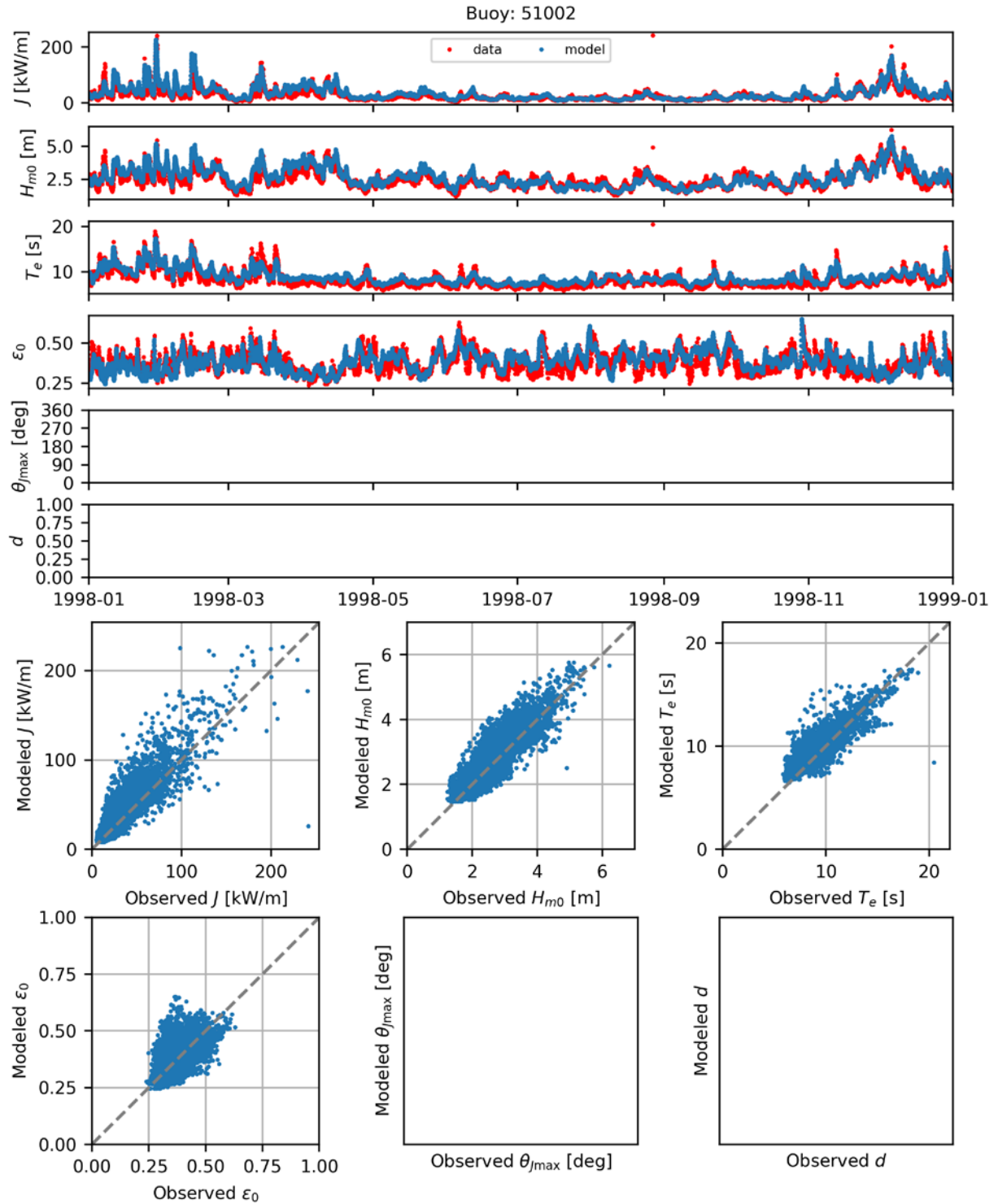


Figure B.82. Comparisons of time series (top) and scatter plots (bottom) the six model-simulated IEC parameters with observed data at NDBC Buoy 51002 for 1998.

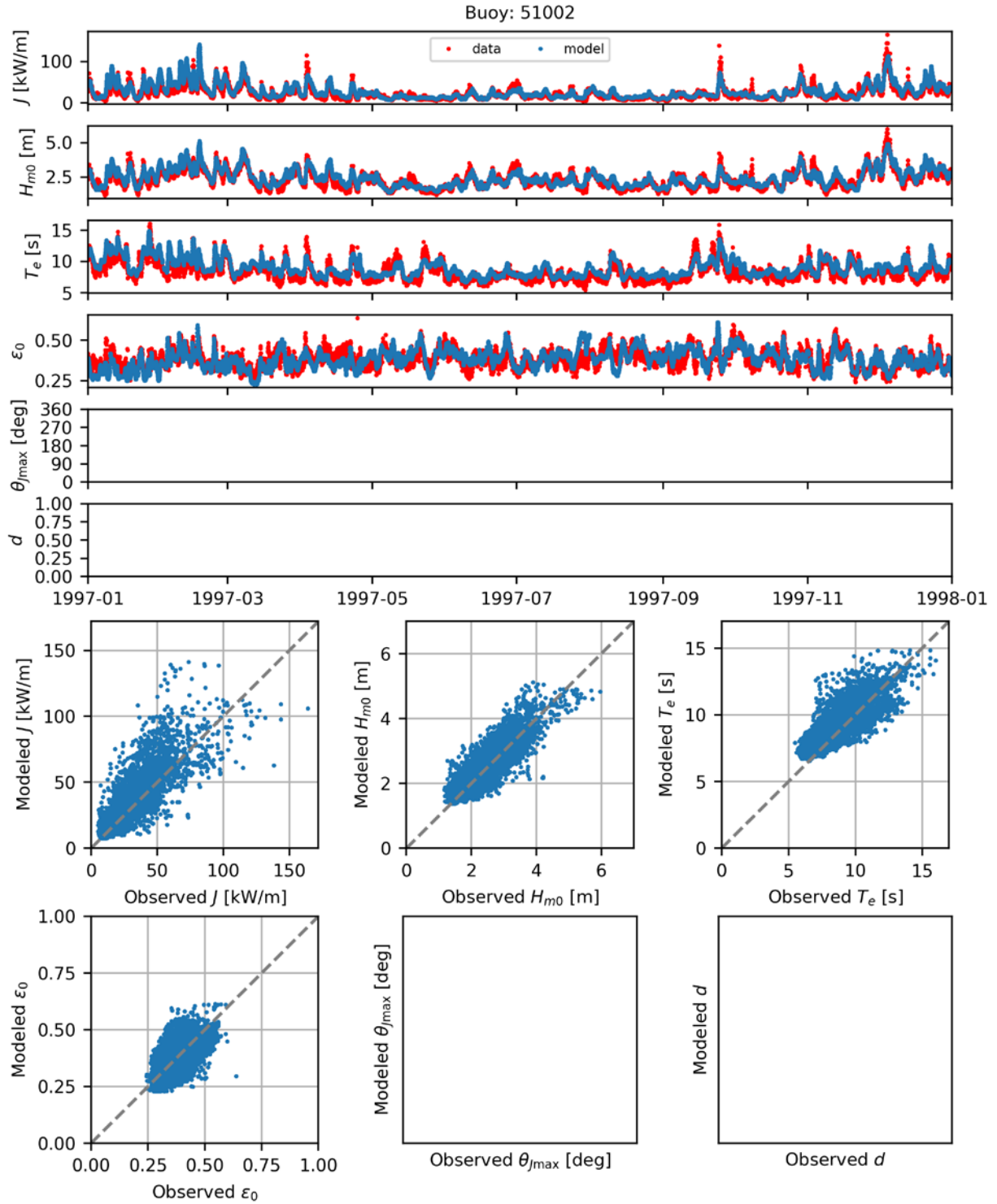


Figure B.83. Comparisons of time series (top) and scatter plots (bottom) the six model-simulated IEC parameters with observed data at NDBC Buoy 51002 for 1997.

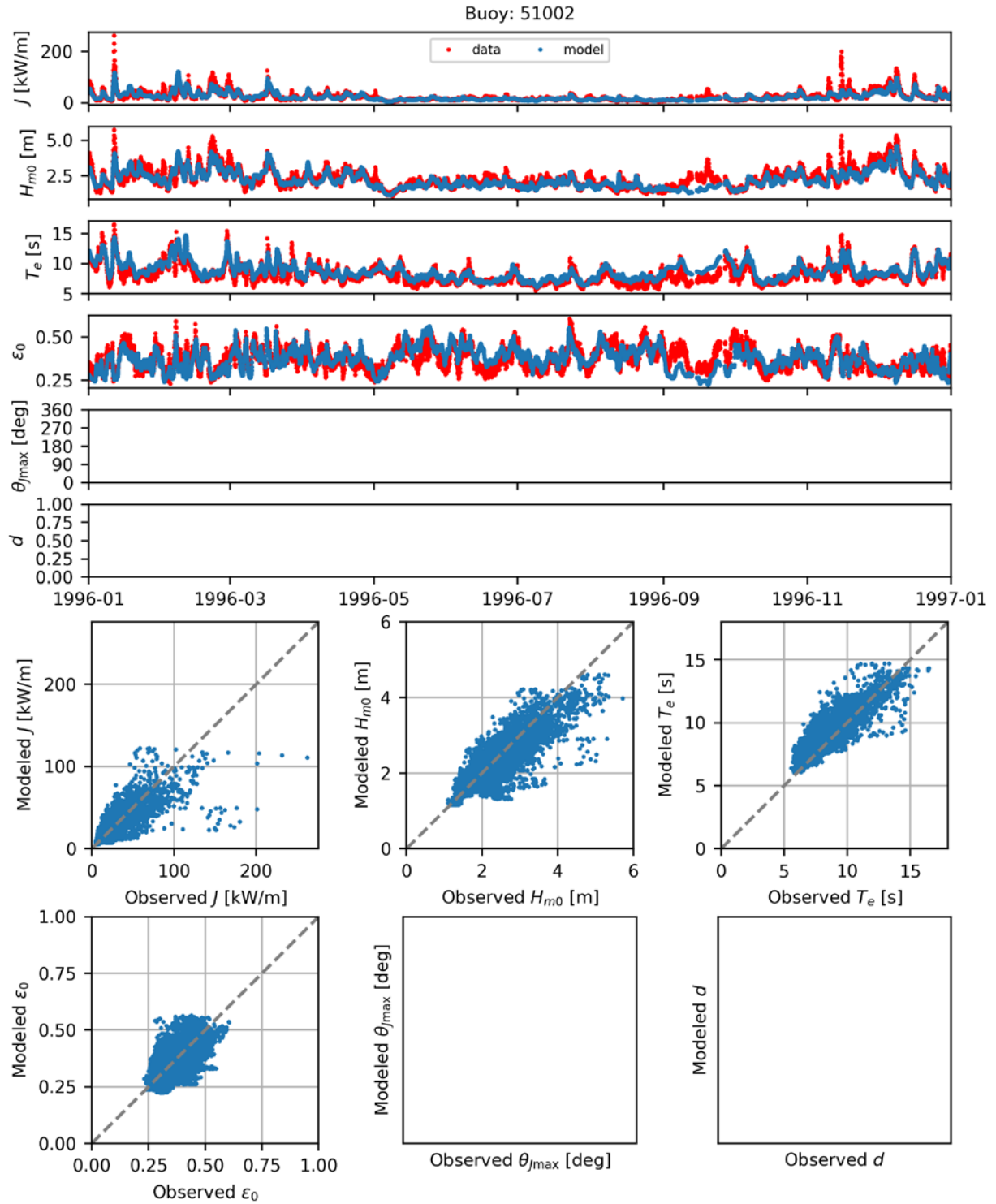


Figure B.84. Comparisons of time series (top) and scatter plots (bottom) the six model-simulated IEC parameters with observed data at NDBC Buoy 51002 for 1996.

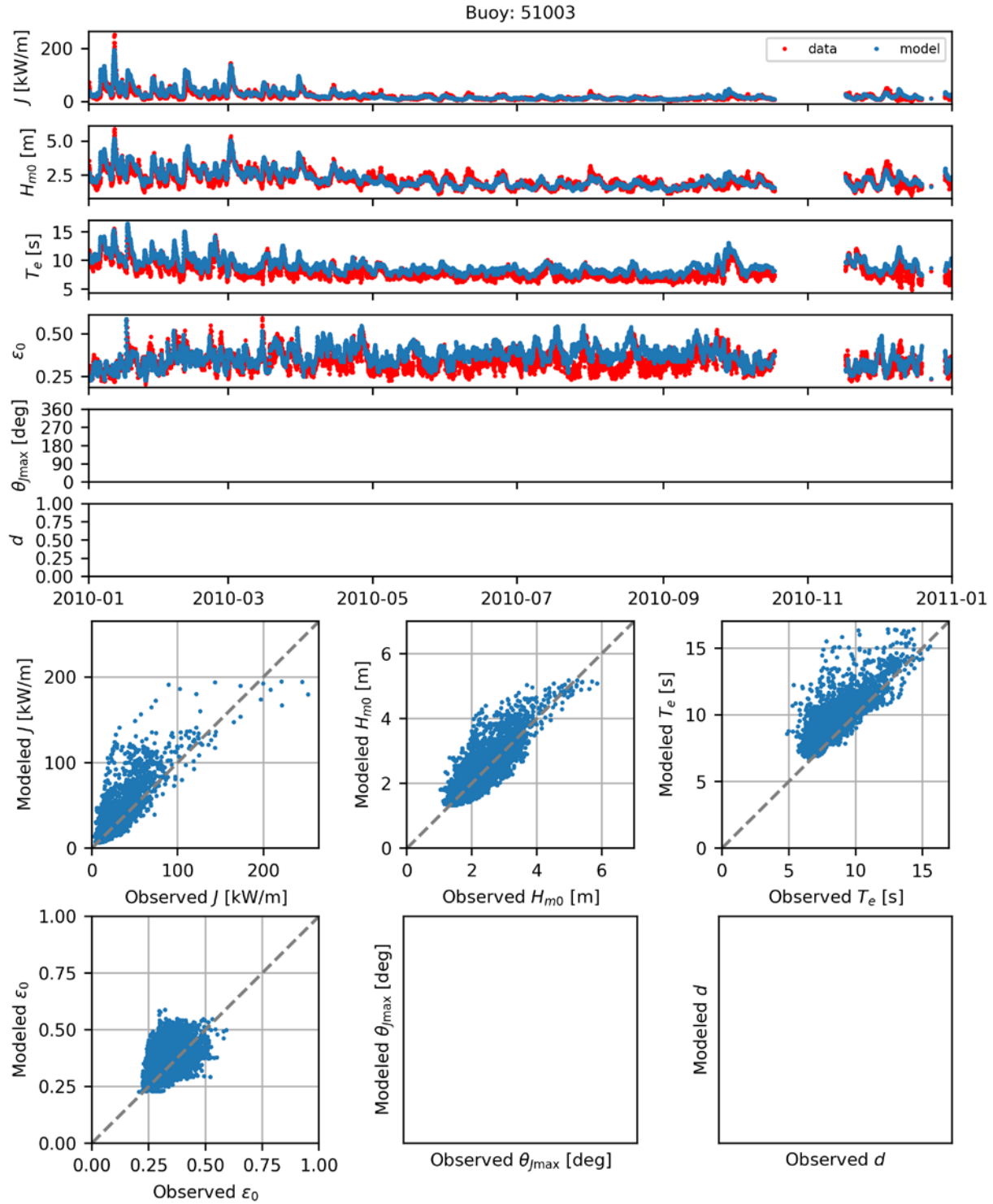


Figure B.85. Comparisons of time series (top) and scatter plots (bottom) the six model-simulated IEC parameters with observed data at NDBC Buoy 51003 for 2010.

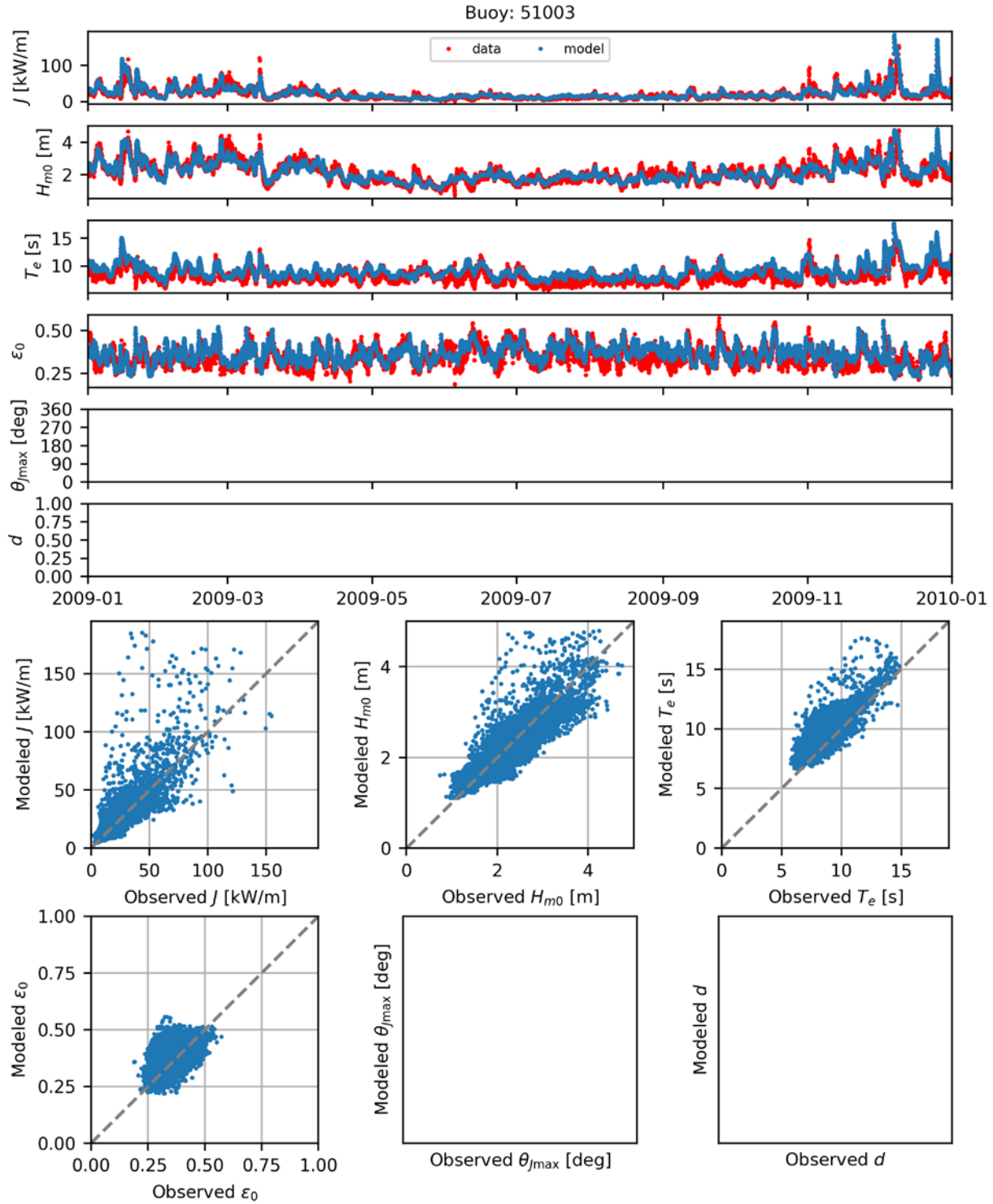


Figure B.86. Comparisons of time series (top) and scatter plots (bottom) the six model-simulated IEC parameters with observed data at NDBC Buoy 51003 for 2009.

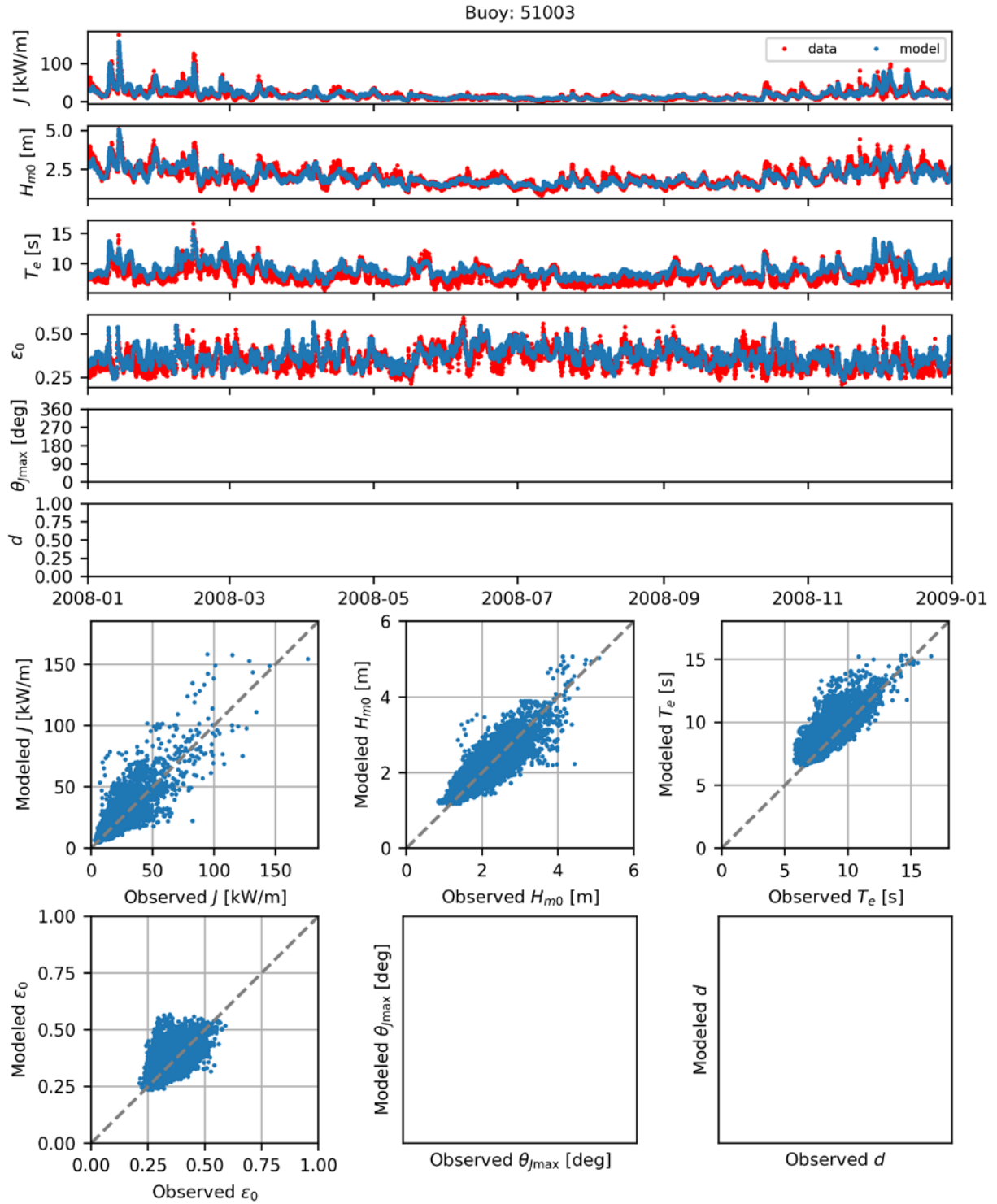


Figure B.87. Comparisons of time series (top) and scatter plots (bottom) the six model-simulated IEC parameters with observed data at NDBC Buoy 51003 for 2008.

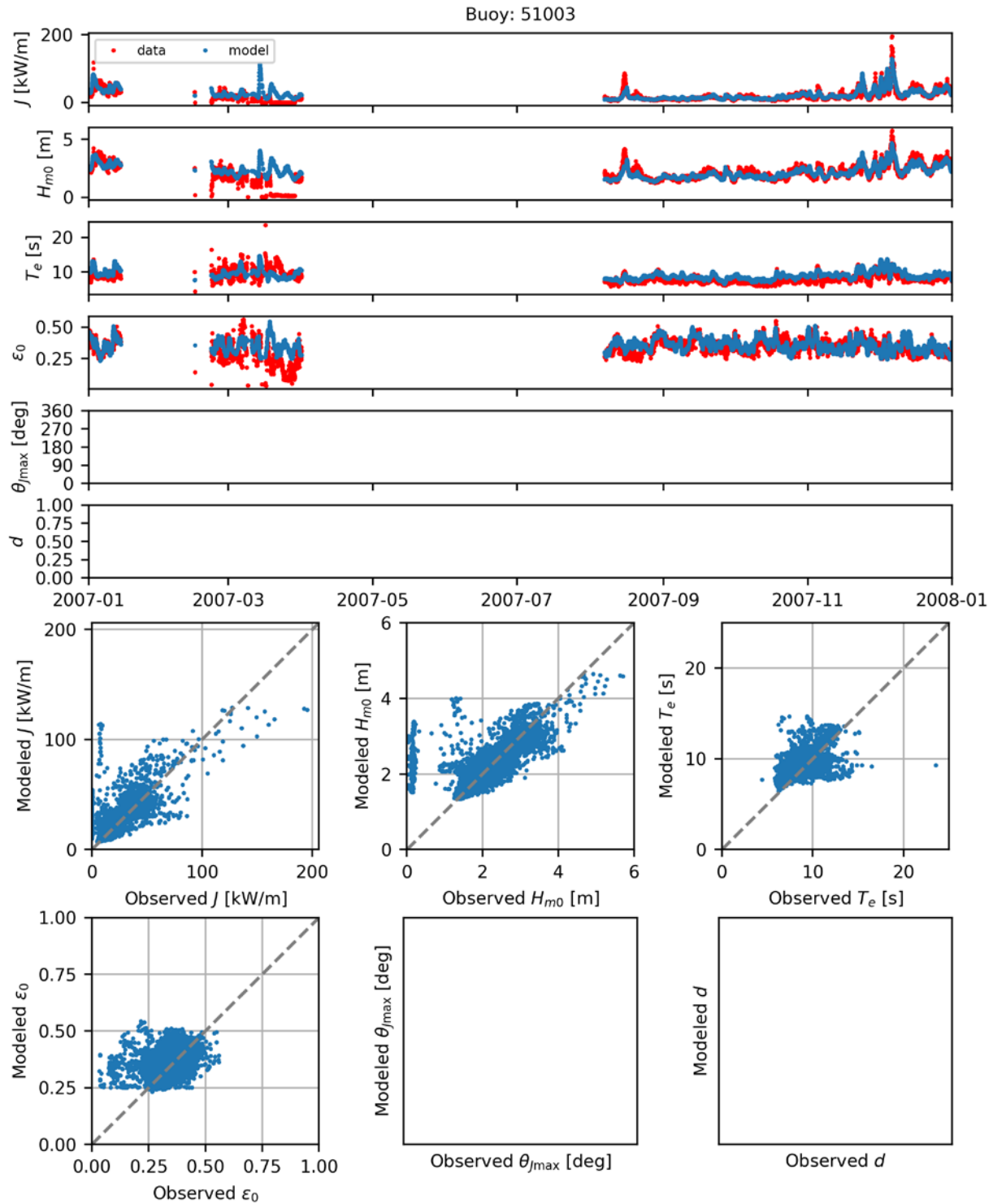


Figure B.88. Comparisons of time series (top) and scatter plots (bottom) the six model-simulated IEC parameters with observed data at NDBC Buoy 51003 for 2007.

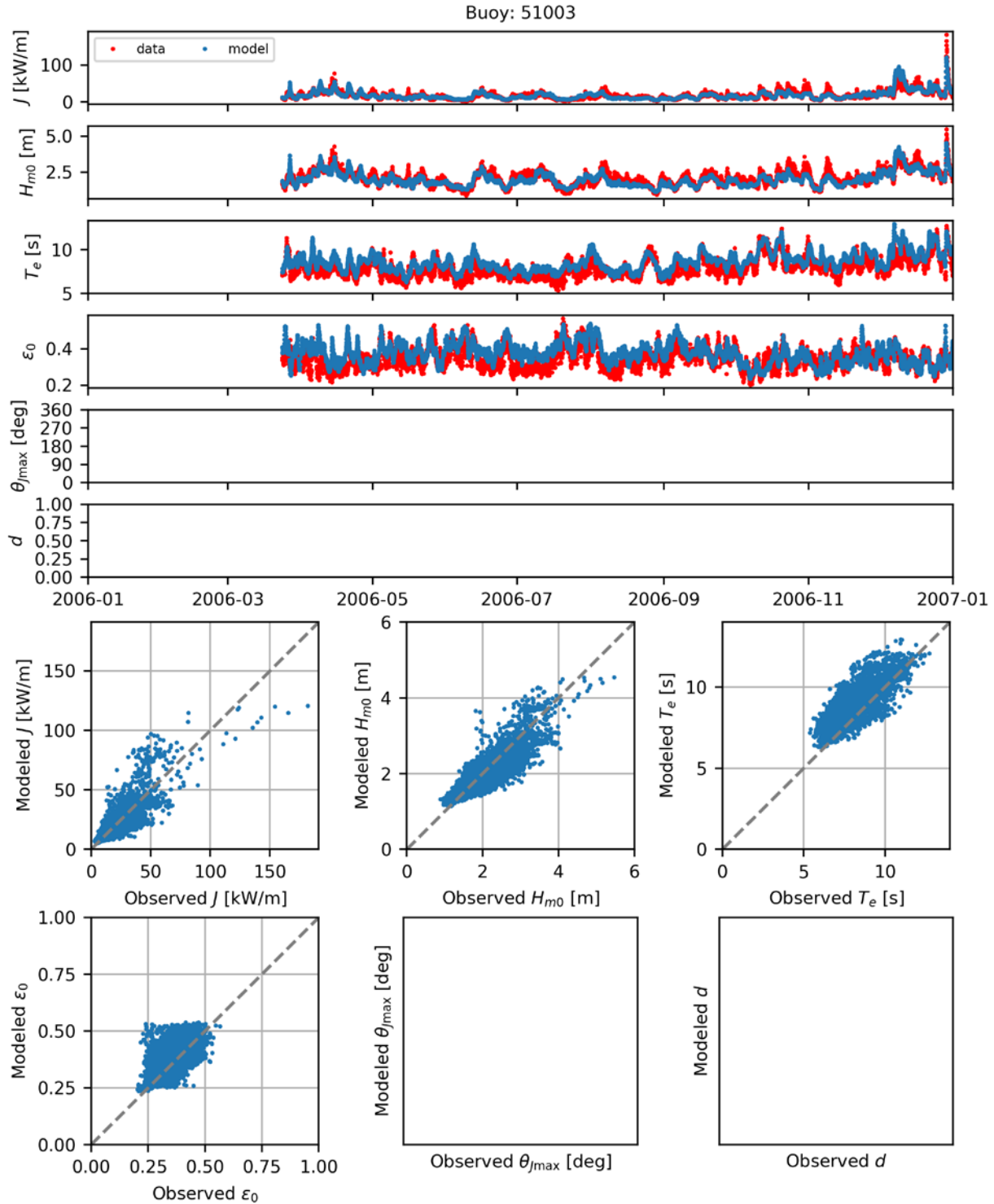


Figure B.89. Comparisons of time series (top) and scatter plots (bottom) the six model-simulated IEC parameters with observed data at NDBC Buoy 51003 for 2006.

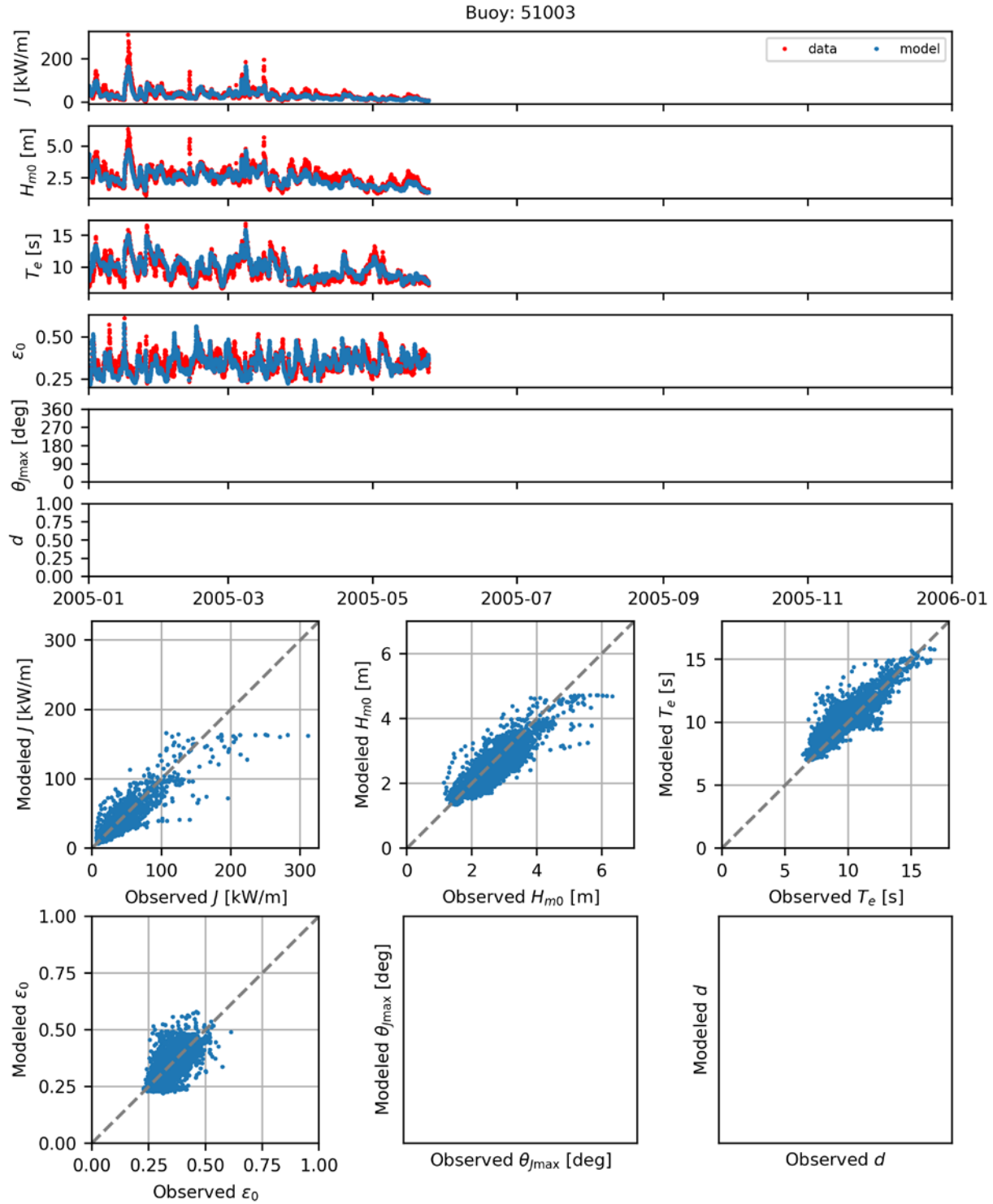


Figure B.90. Comparisons of time series (top) and scatter plots (bottom) the six model-simulated IEC parameters with observed data at NDBC Buoy 51003 for 2005.

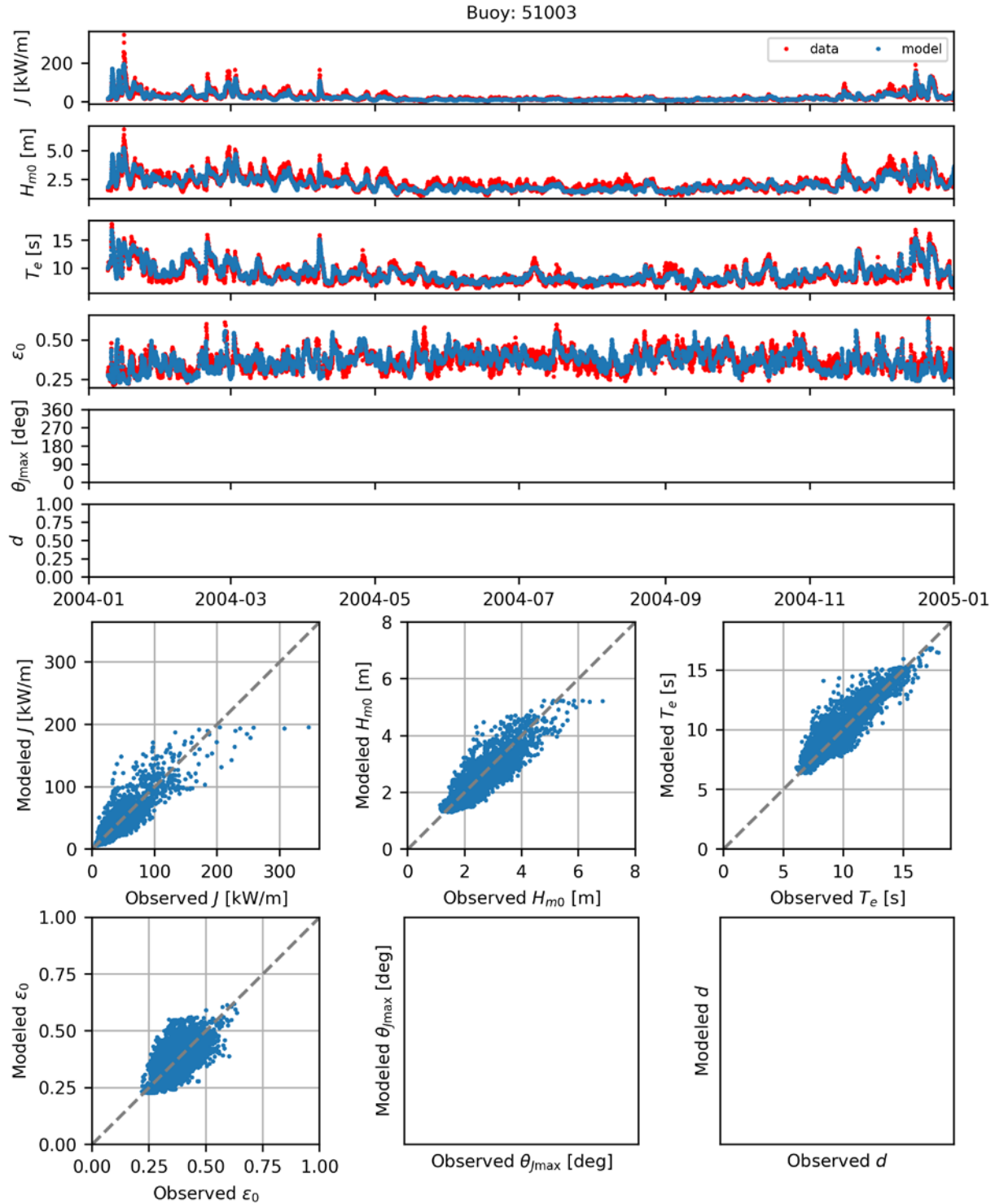


Figure B.91. Comparisons of time series (top) and scatter plots (bottom) the six model-simulated IEC parameters with observed data at NDBC Buoy 51003 for 2004.

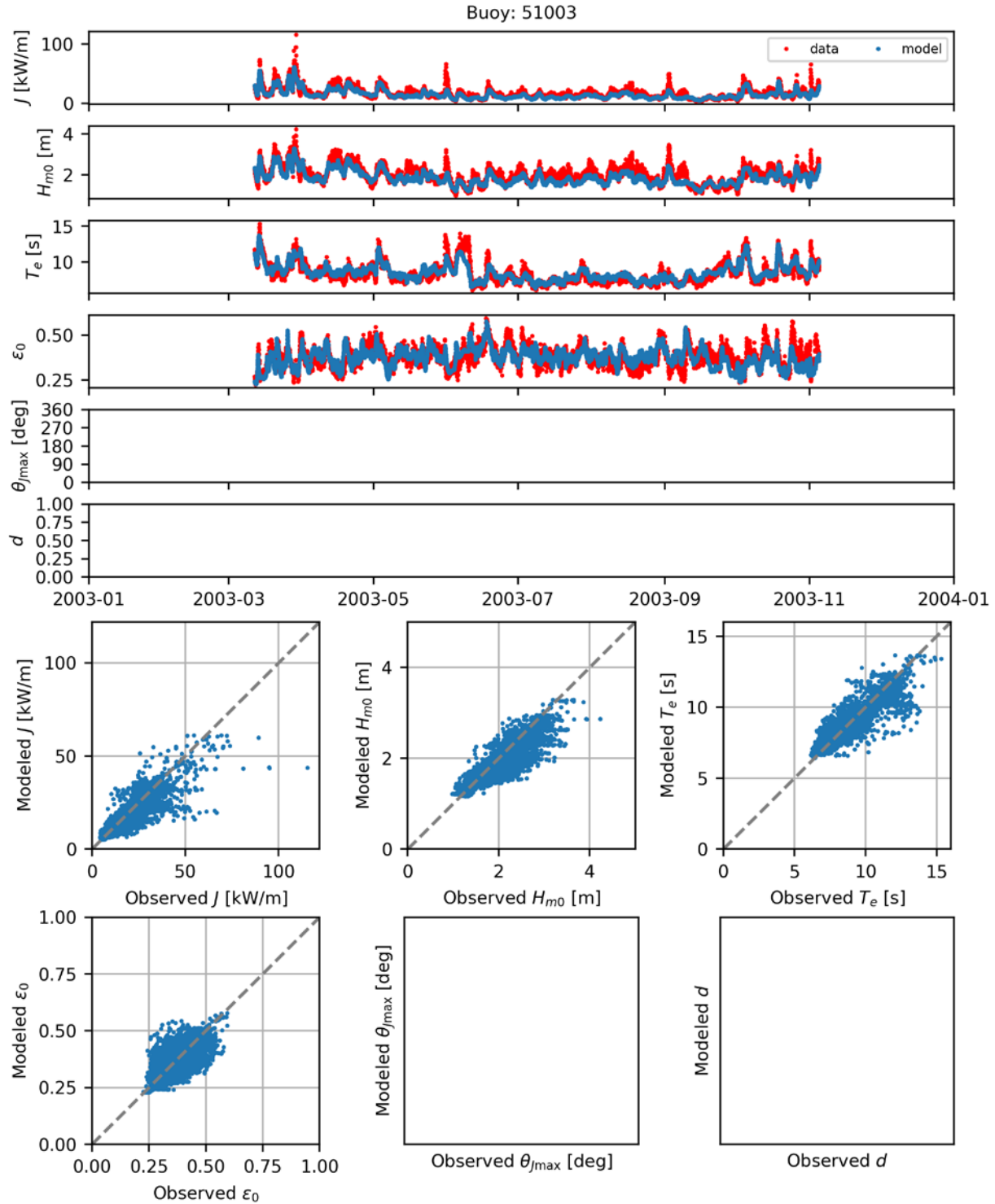


Figure B.92. Comparisons of time series (top) and scatter plots (bottom) the six model-simulated IEC parameters with observed data at NDBC Buoy 51003 for 2003.

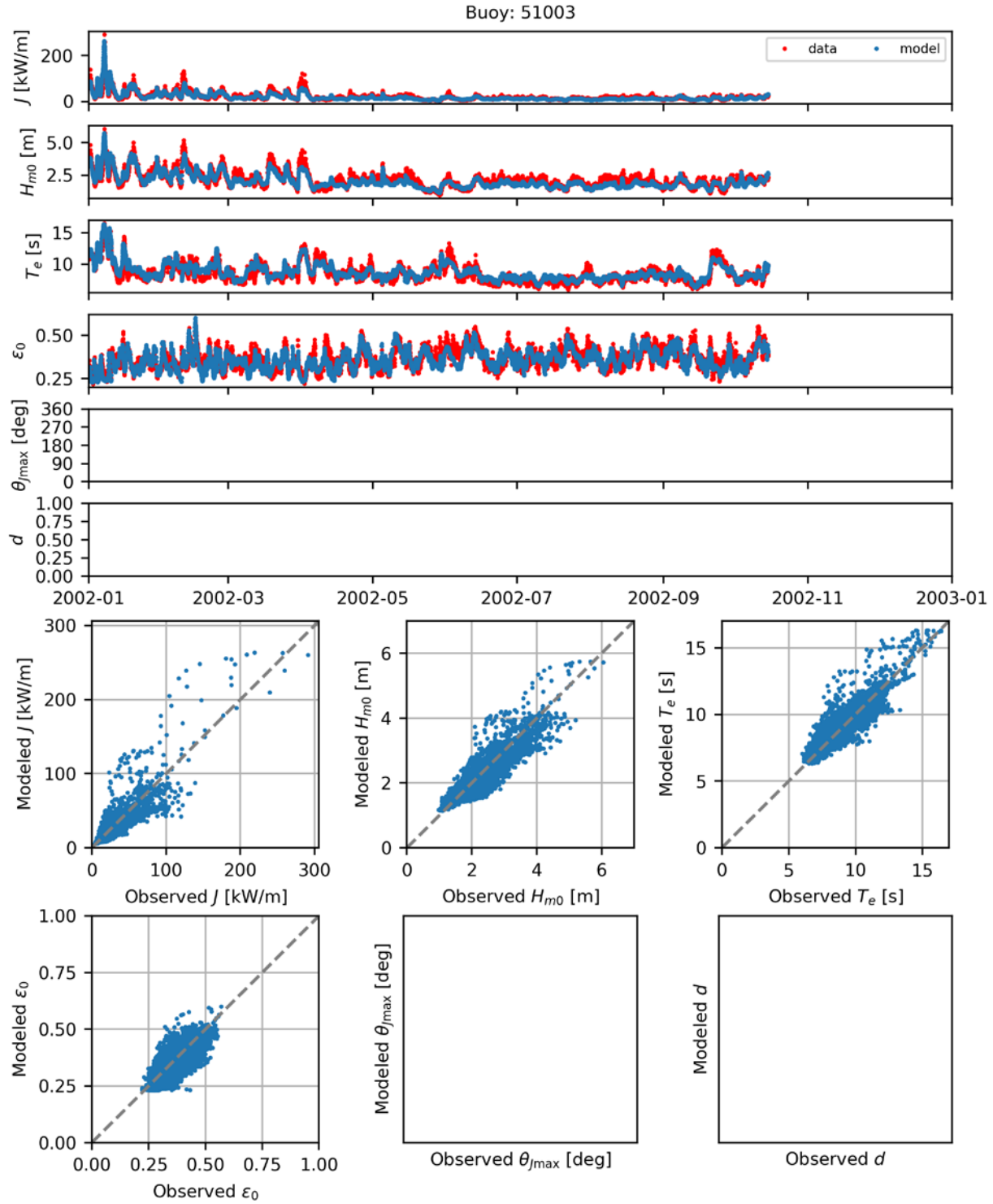


Figure B.93. Comparisons of time series (top) and scatter plots (bottom) the six model-simulated IEC parameters with observed data at NDBC Buoy 51003 for 2002.

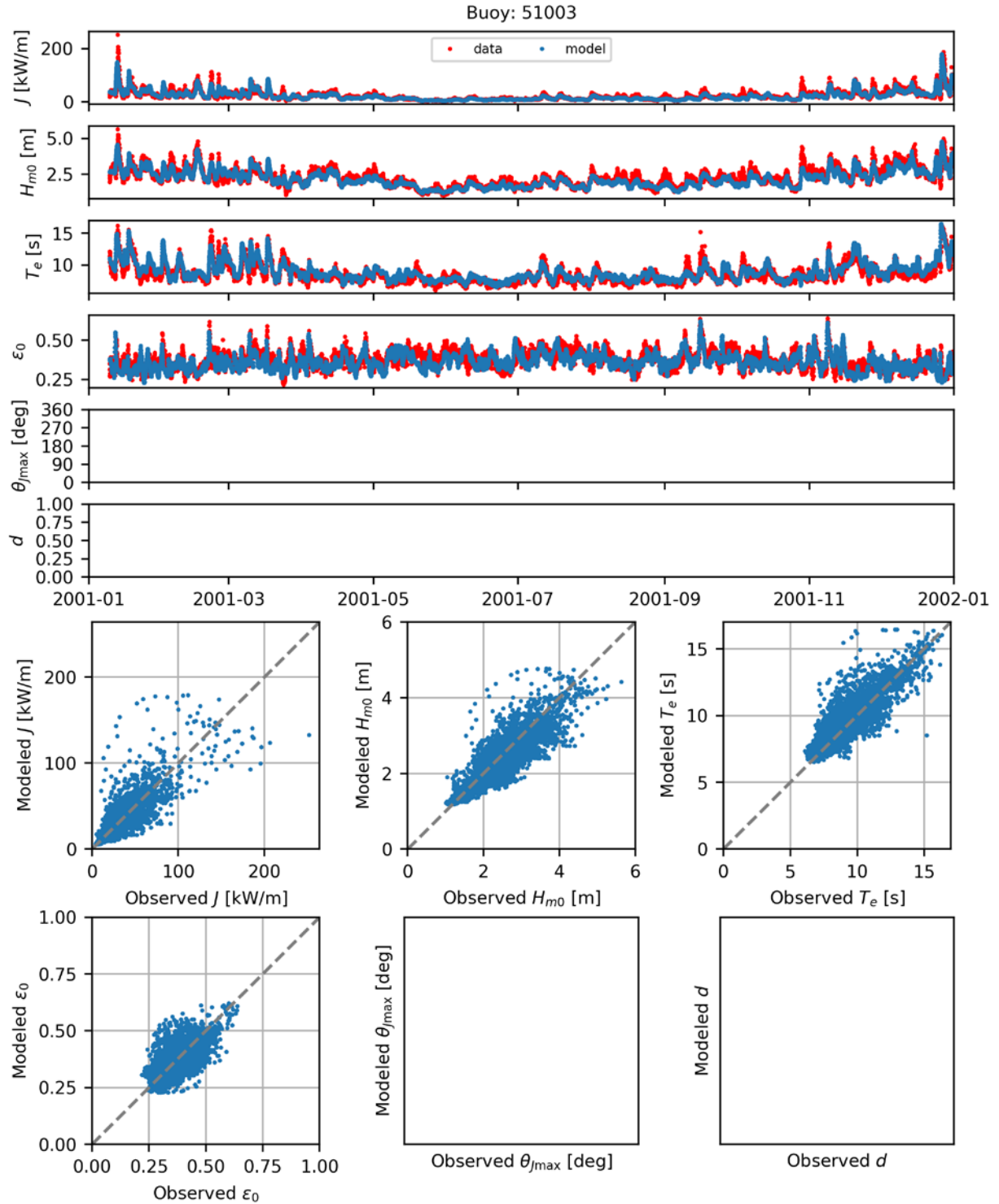


Figure B.94. Comparisons of time series (top) and scatter plots (bottom) the six model-simulated IEC parameters with observed data at NDBC Buoy 51003 for 2001.

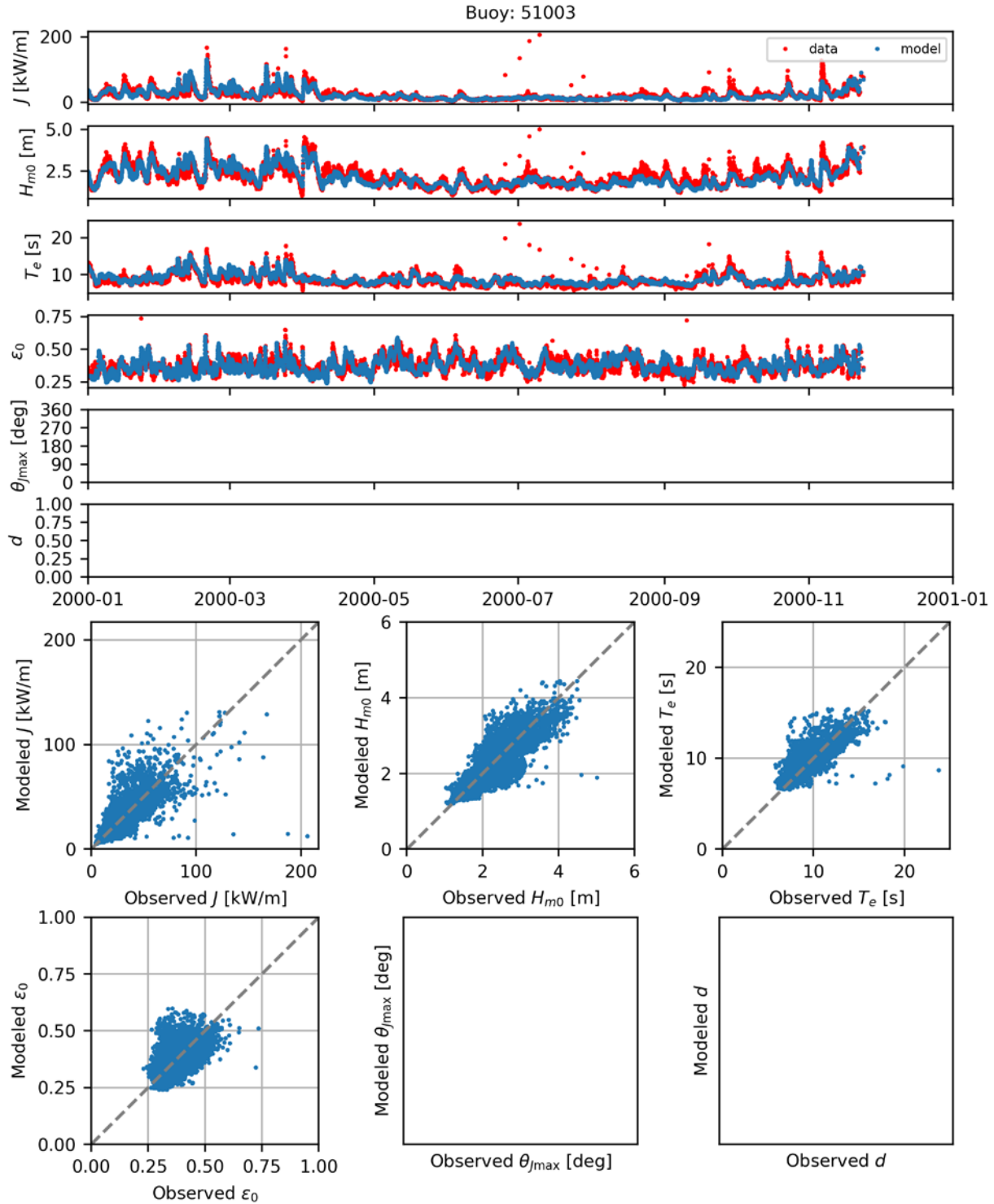


Figure B.95. Comparisons of time series (top) and scatter plots (bottom) the six model-simulated IEC parameters with observed data at NDBC Buoy 51003 for 2000.

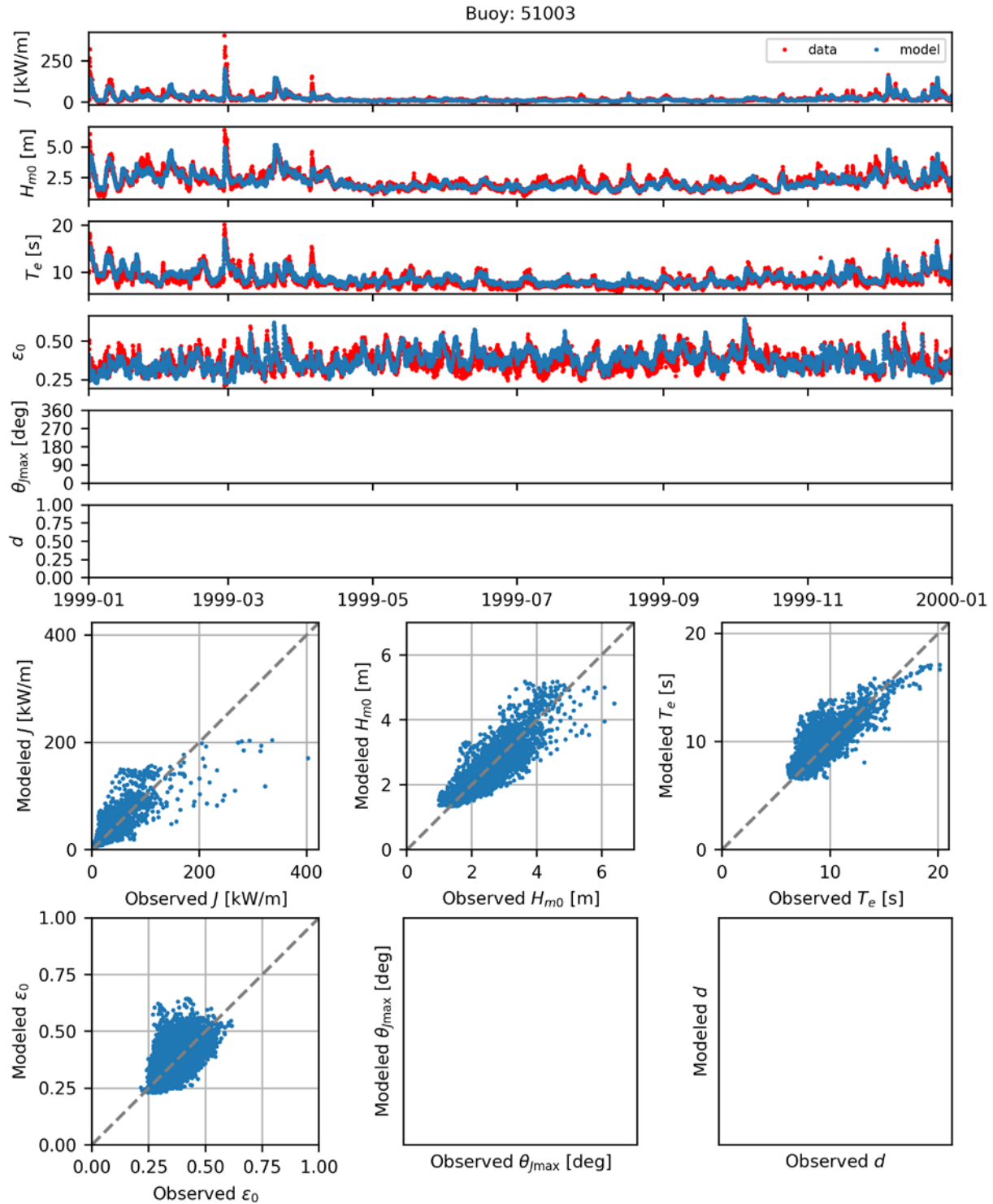


Figure B.96. Comparisons of time series (top) and scatter plots (bottom) the six model-simulated IEC parameters with observed data at NDBC Buoy 51003 for 1999.

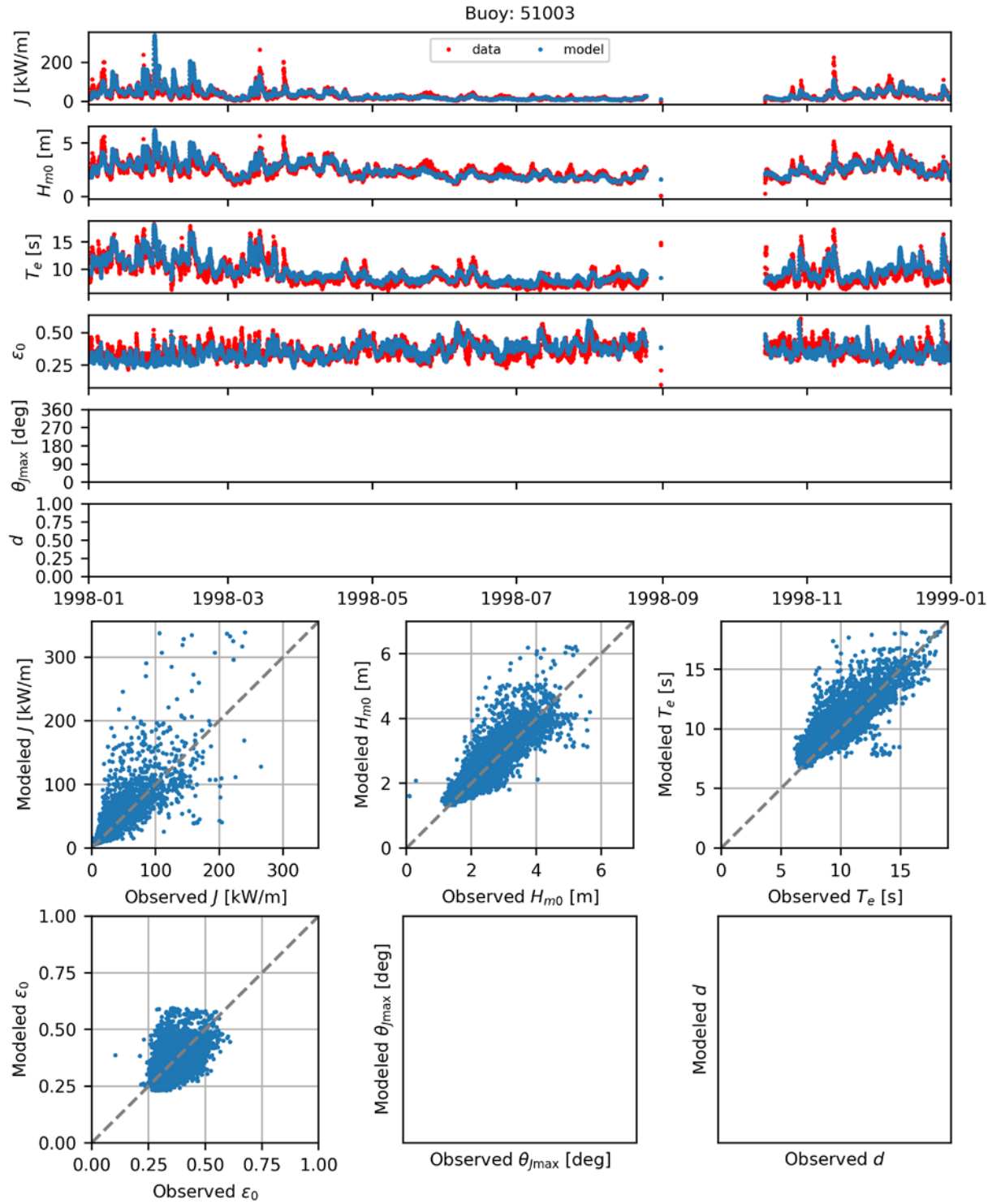


Figure B.97. Comparisons of time series (top) and scatter plots (bottom) the six model-simulated IEC parameters with observed data at NDBC Buoy 51003 for 1998.

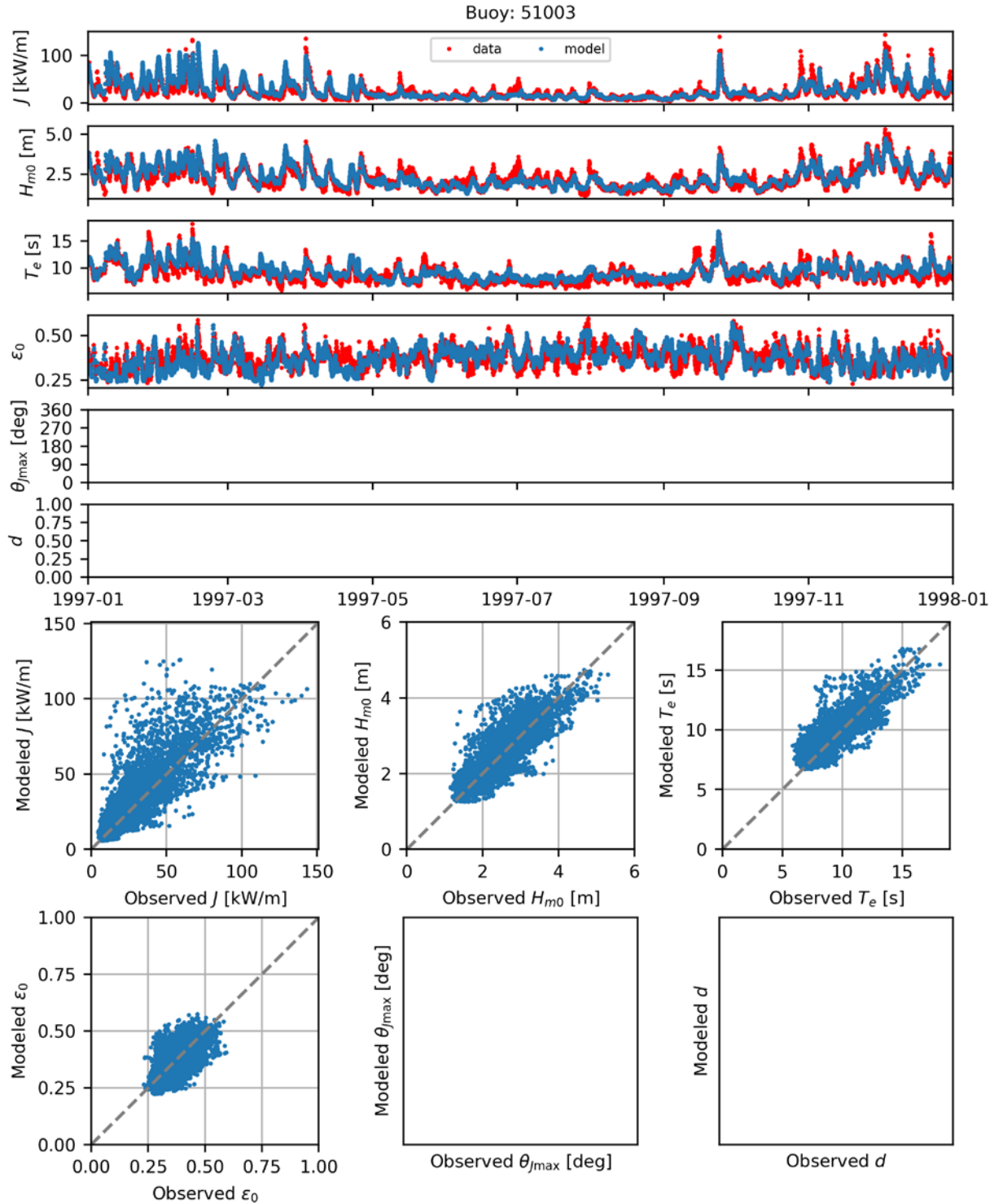


Figure B.98. Comparisons of time series (top) and scatter plots (bottom) the six model-simulated IEC parameters with observed data at NDBC Buoy 51003 for 1997.

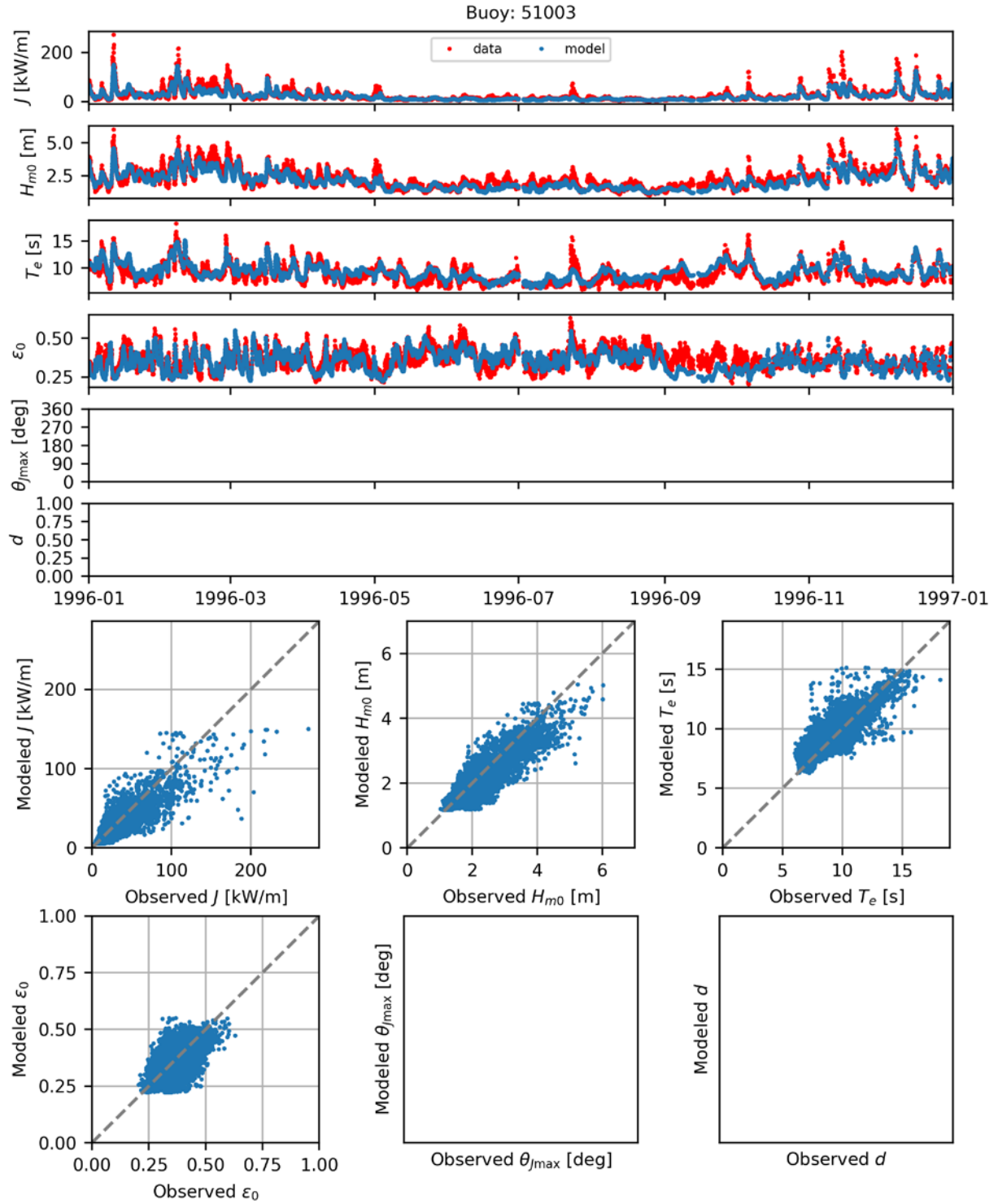


Figure B.99. Comparisons of time series (top) and scatter plots (bottom) the six model-simulated IEC parameters with observed data at NDBC Buoy 51003 for 1996.

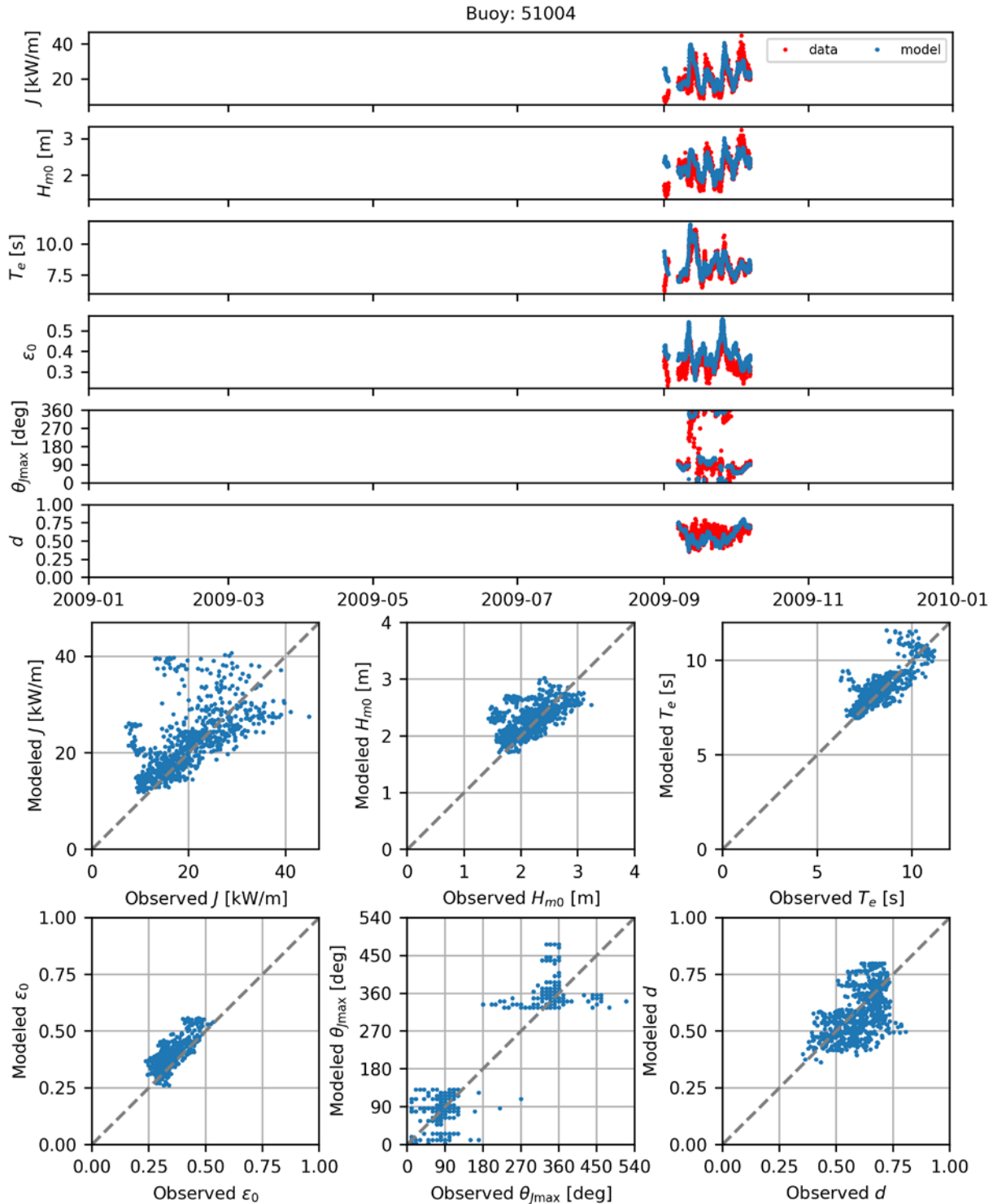


Figure B.100. Comparisons of time series (top) and scatter plots (bottom) the six model-simulated IEC parameters with observed data at NDBC Buoy 51004 for 2009.

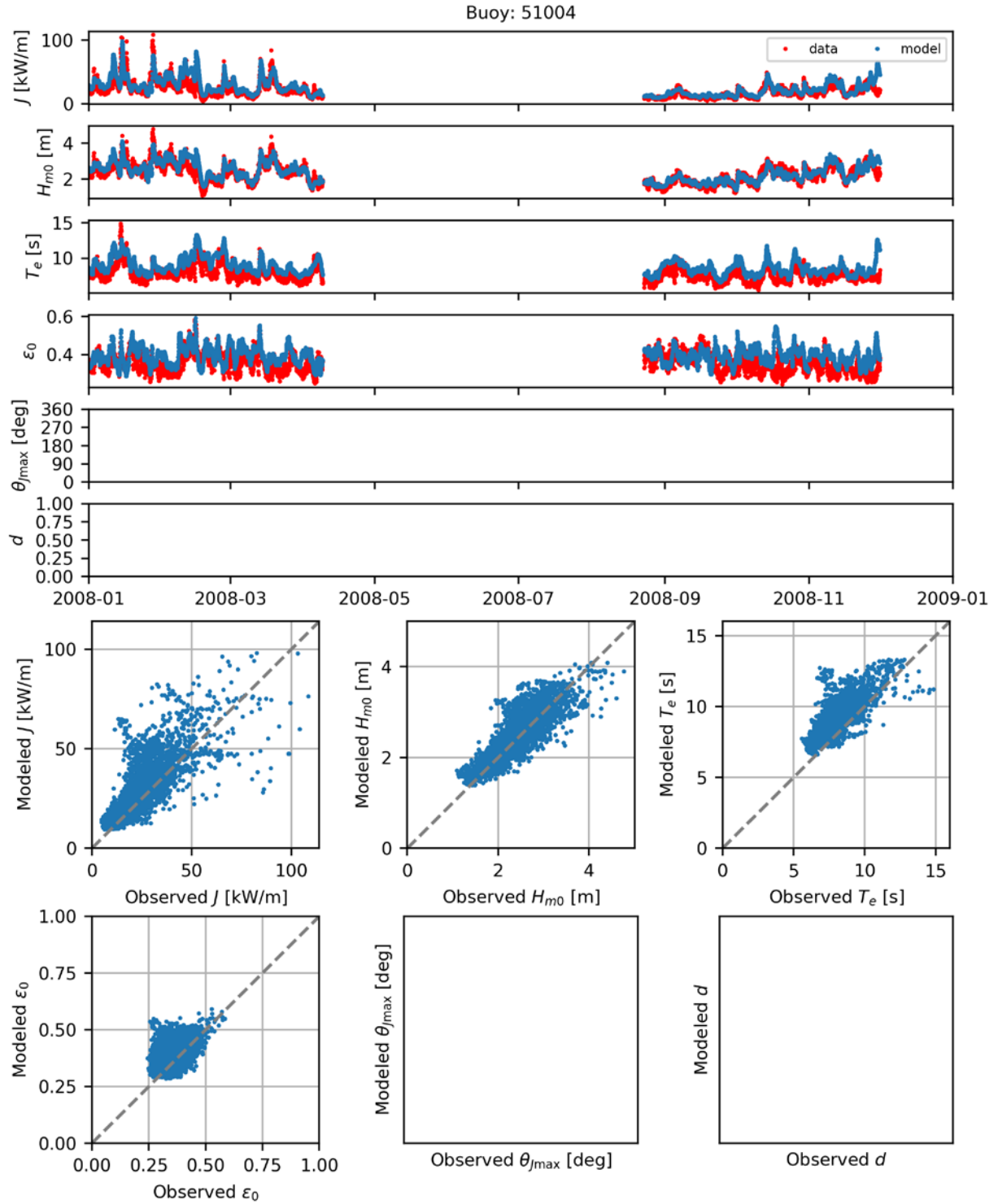


Figure B.101. Comparisons of time series (top) and scatter plots (bottom) the six model-simulated IEC parameters with observed data at NDBC Buoy 51004 for 2008.

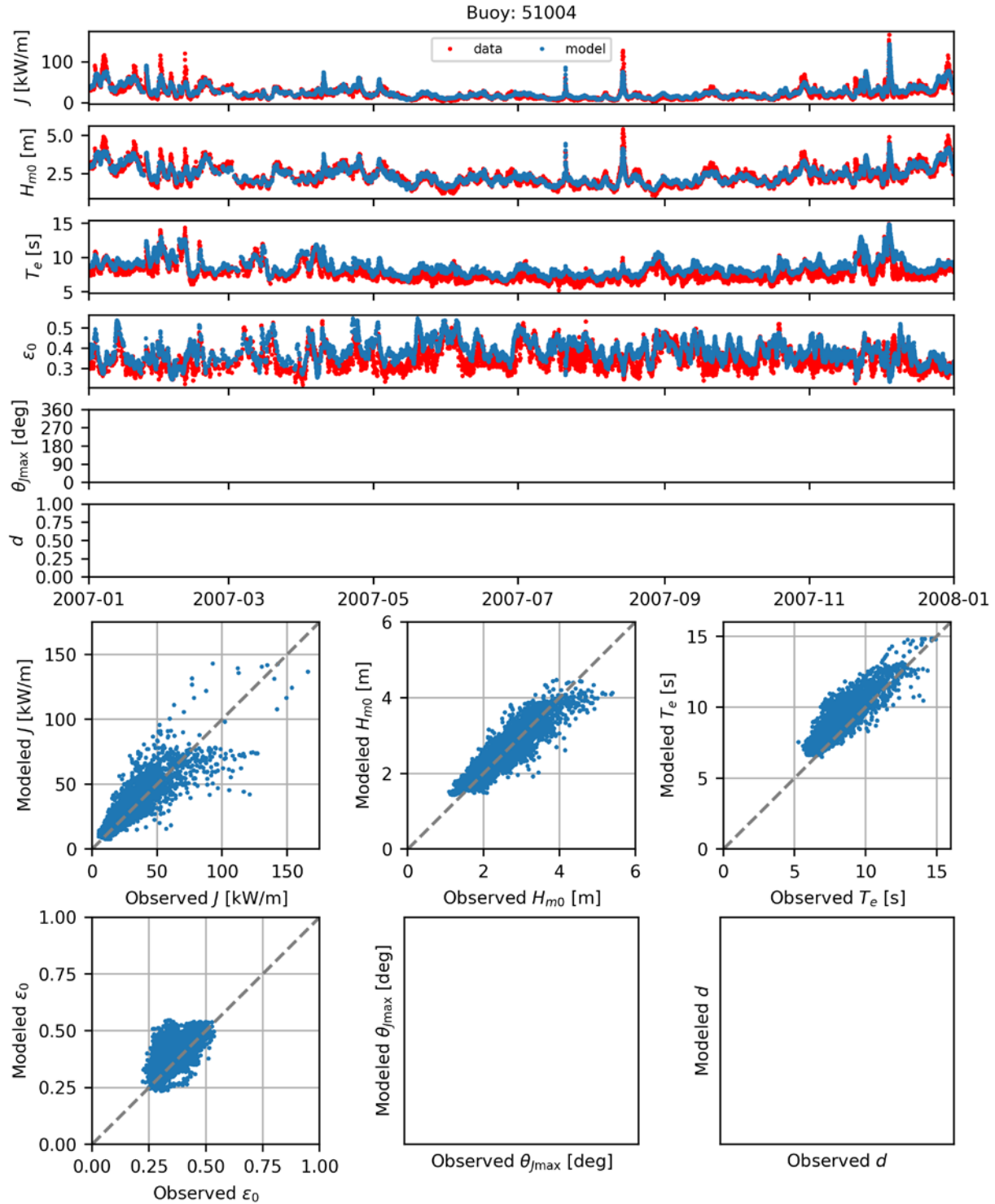


Figure B.102. Comparisons of time series (top) and scatter plots (bottom) the six model-simulated IEC parameters with observed data at NDBC Buoy 51004 for 2007.

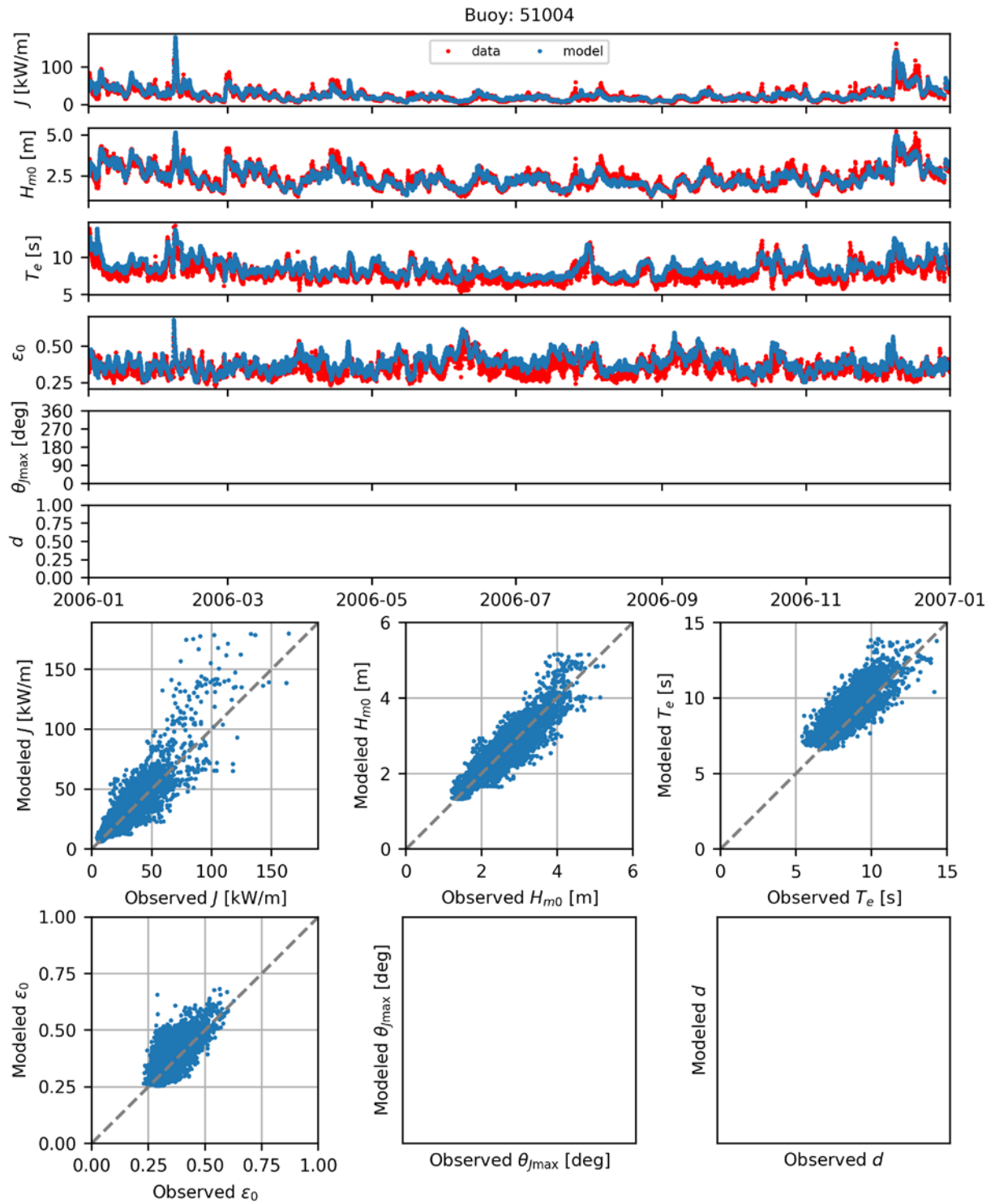


Figure B.103. Comparisons of time series (top) and scatter plots (bottom) the six model-simulated IEC parameters with observed data at NDBC Buoy 51004 for 2006.

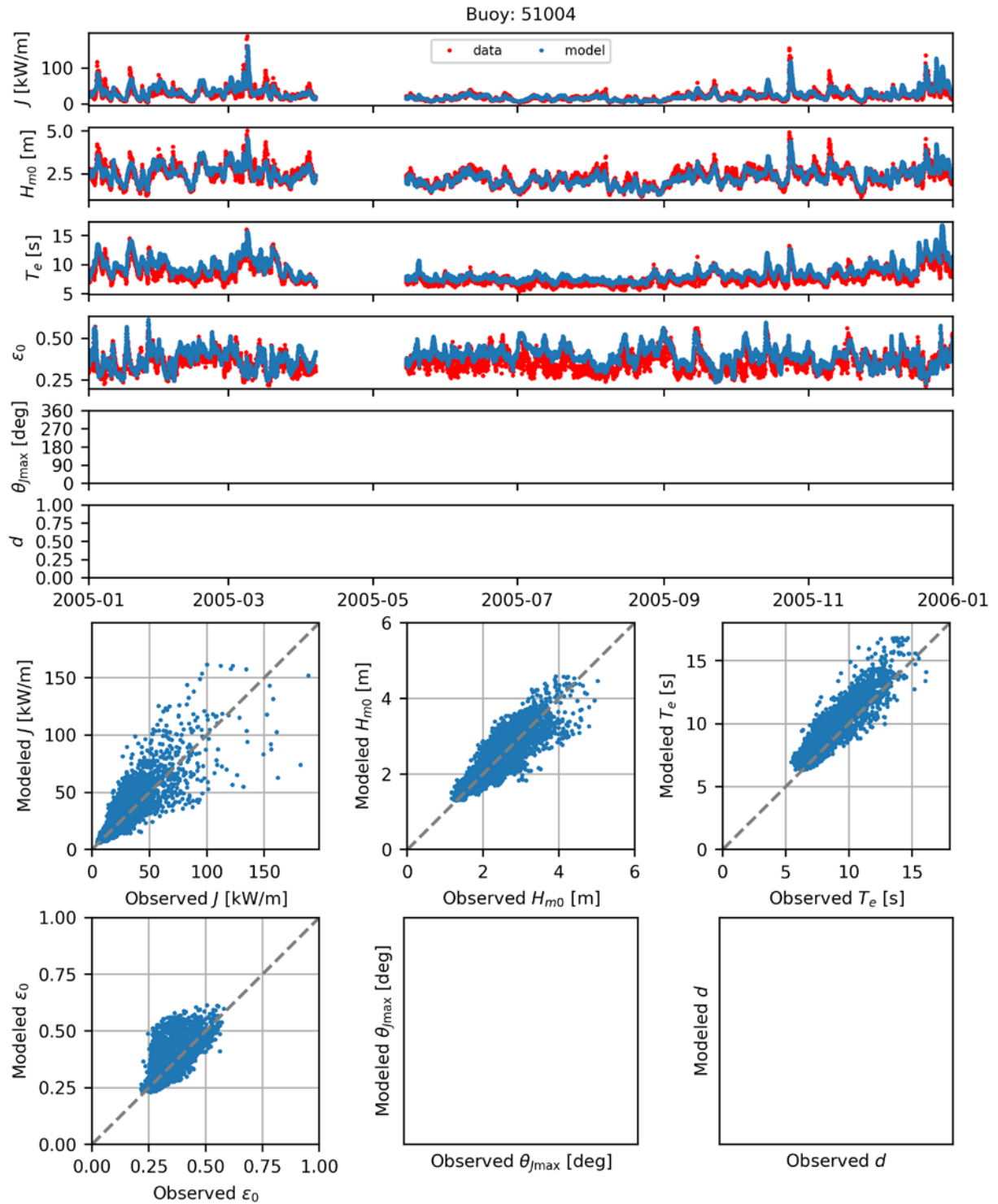


Figure B.104. Comparisons of time series (top) and scatter plots (bottom) the six model-simulated IEC parameters with observed data at NDBC Buoy 51004 for 2005.

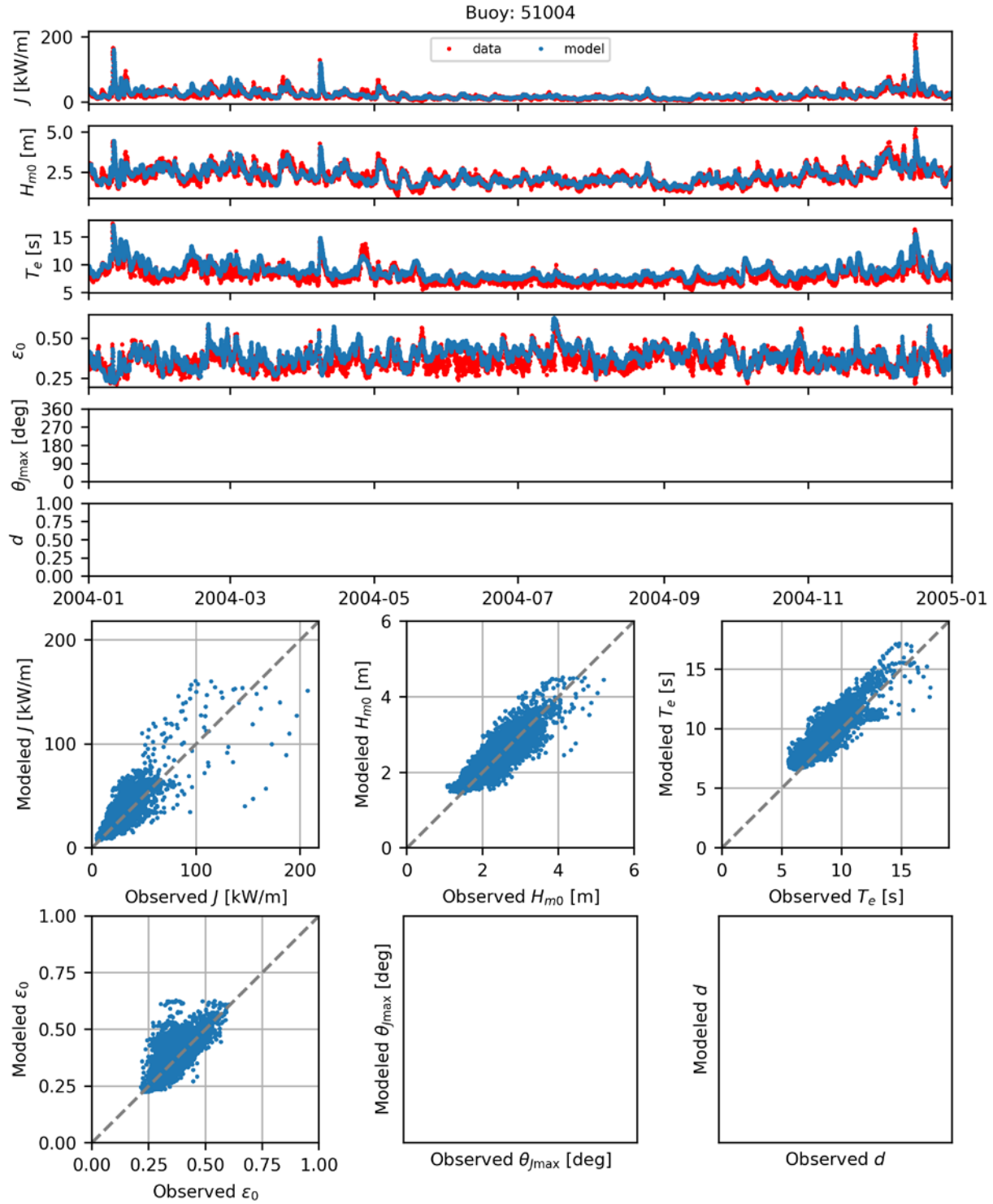


Figure B.105. Comparisons of time series (top) and scatter plots (bottom) the six model-simulated IEC parameters with observed data at NDBC Buoy 51004 for 2004.

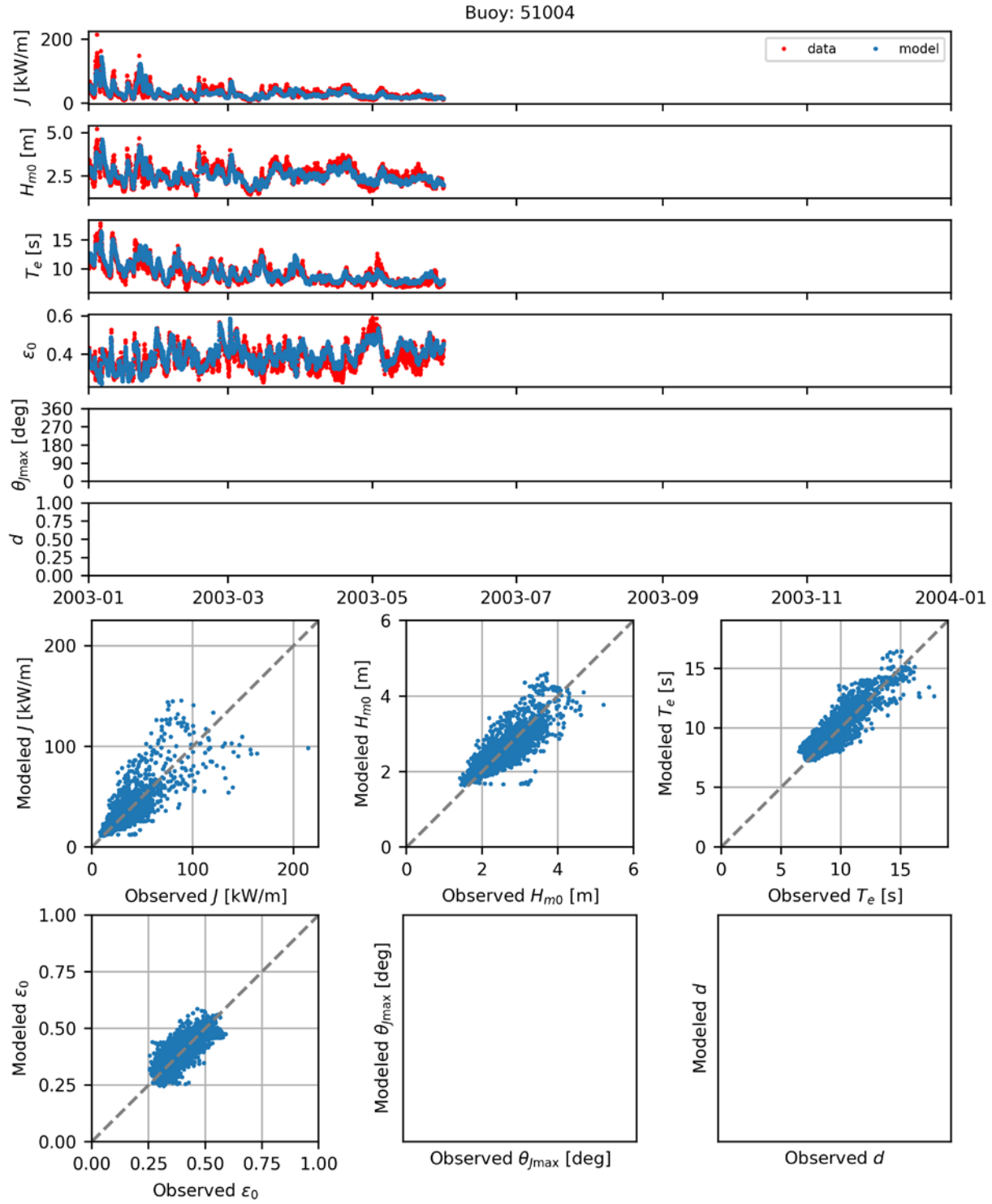


Figure B.106. Comparisons of time series (top) and scatter plots (bottom) the six model-simulated IEC parameters with observed data at NDBC Buoy 51004 for 2003.

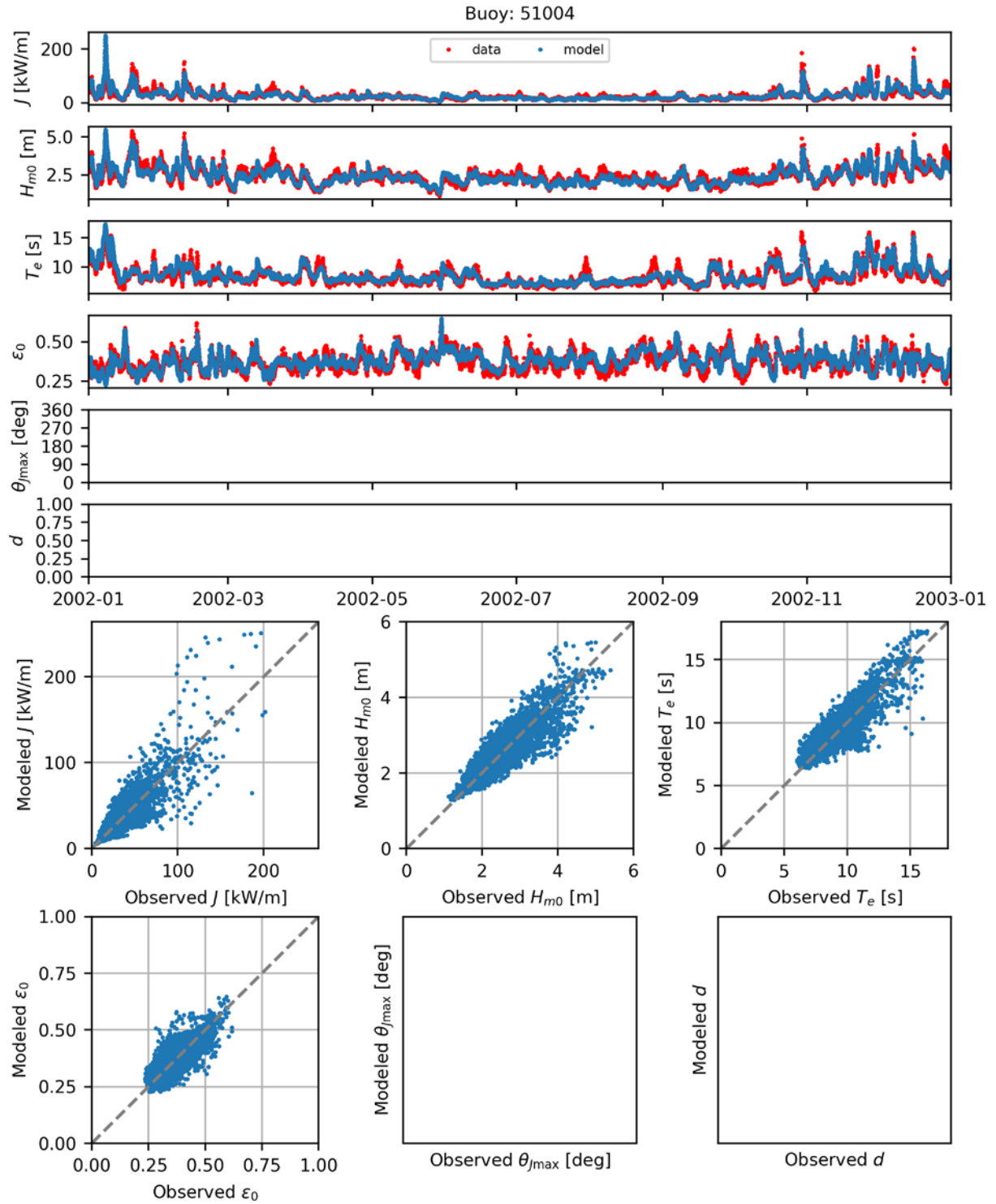


Figure B.107. Comparisons of time series (top) and scatter plots (bottom) the six model-simulated IEC parameters with observed data at NDBC Buoy 51004 for 2002.

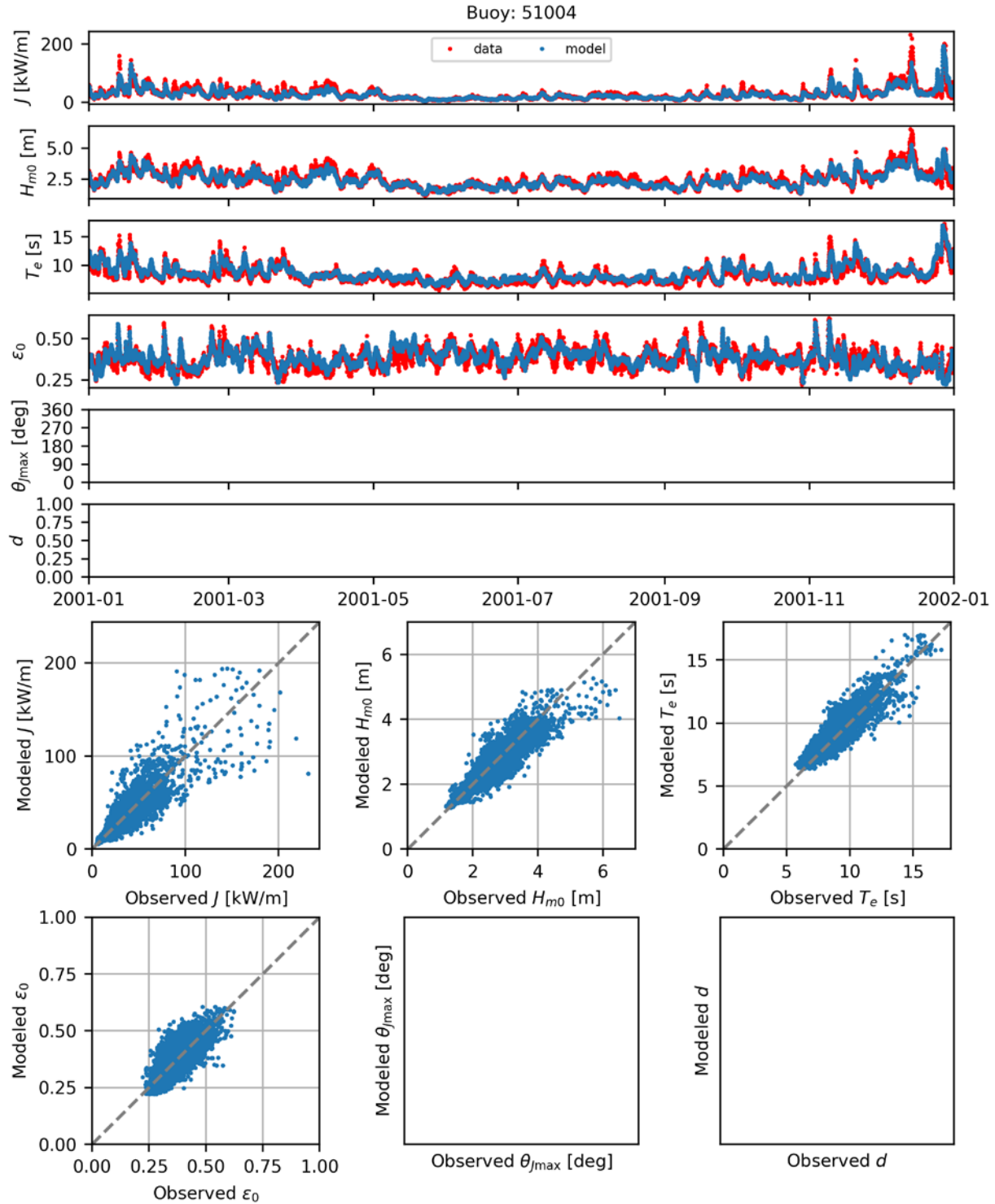


Figure B.108. Comparisons of time series (top) and scatter plots (bottom) the six model-simulated IEC parameters with observed data at NDBC Buoy 51004 for 2001.

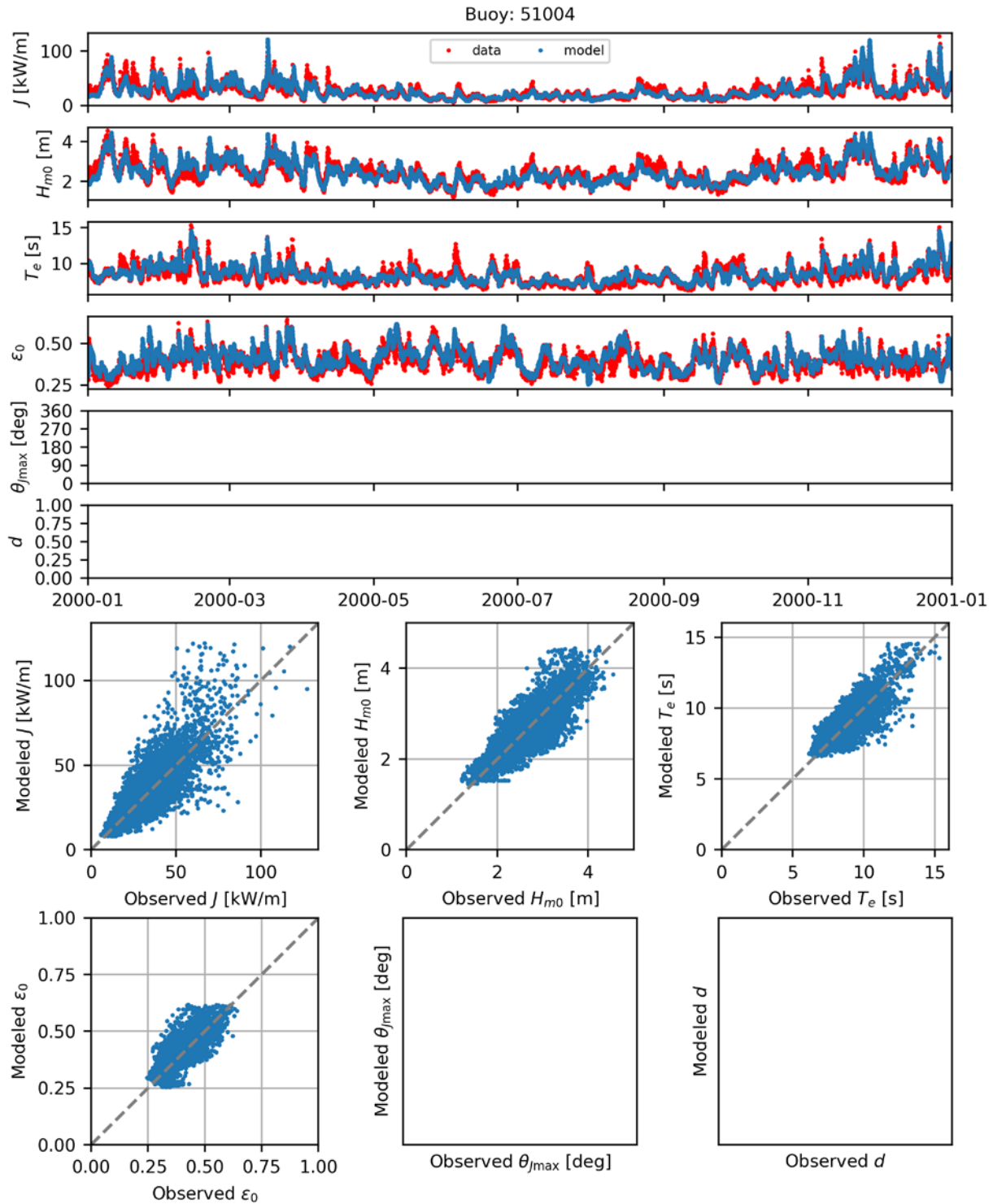


Figure B.109. Comparisons of time series (top) and scatter plots (bottom) the six model-simulated IEC parameters with observed data at NDBC Buoy 51004 for 2000.

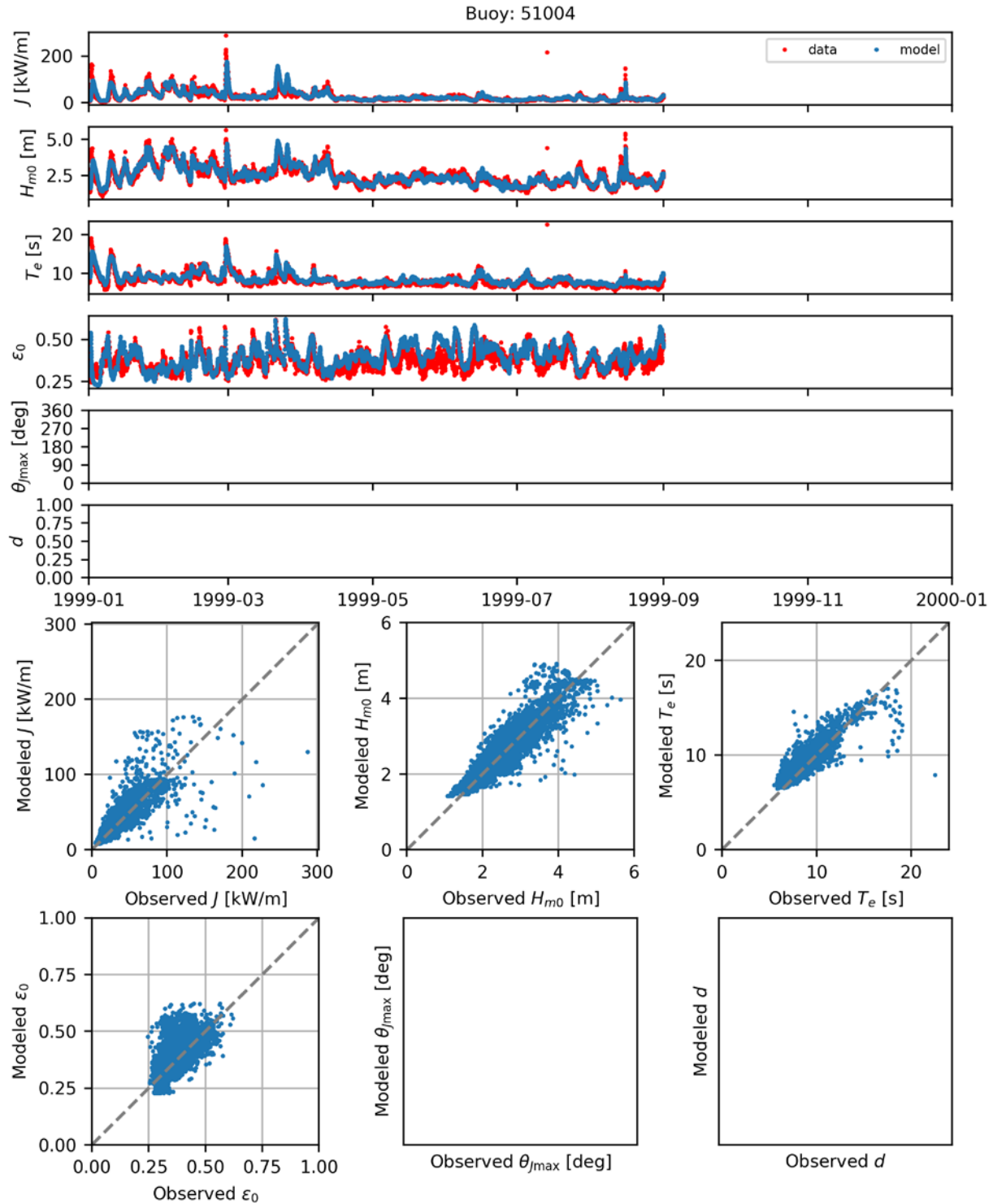


Figure B.110. Comparisons of time series (top) and scatter plots (bottom) the six model-simulated IEC parameters with observed data at NDBC Buoy 51004 for 1999.

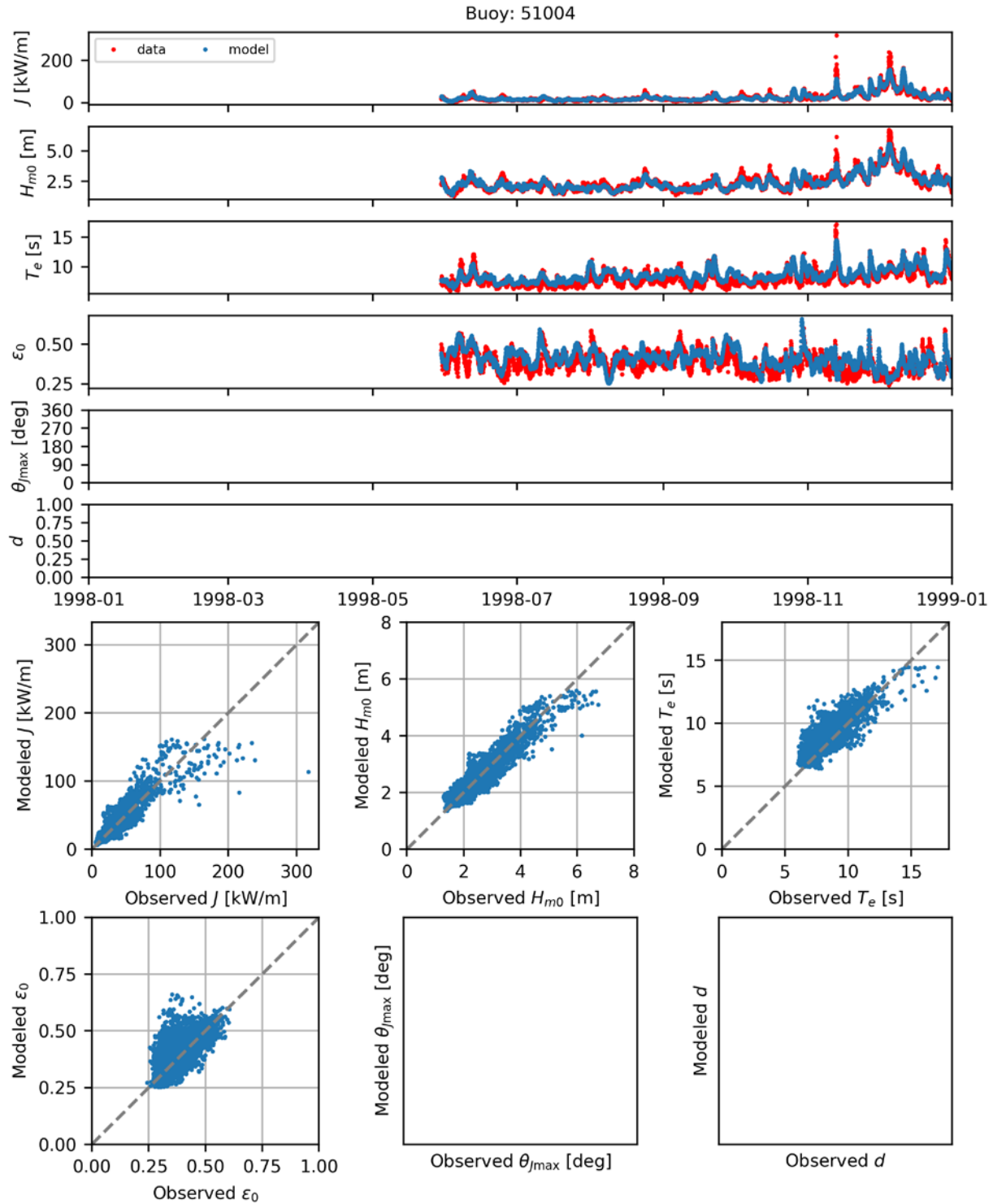


Figure B.111. Comparisons of time series (top) and scatter plots (bottom) the six model-simulated IEC parameters with observed data at NDBC Buoy 51004 for 1998.

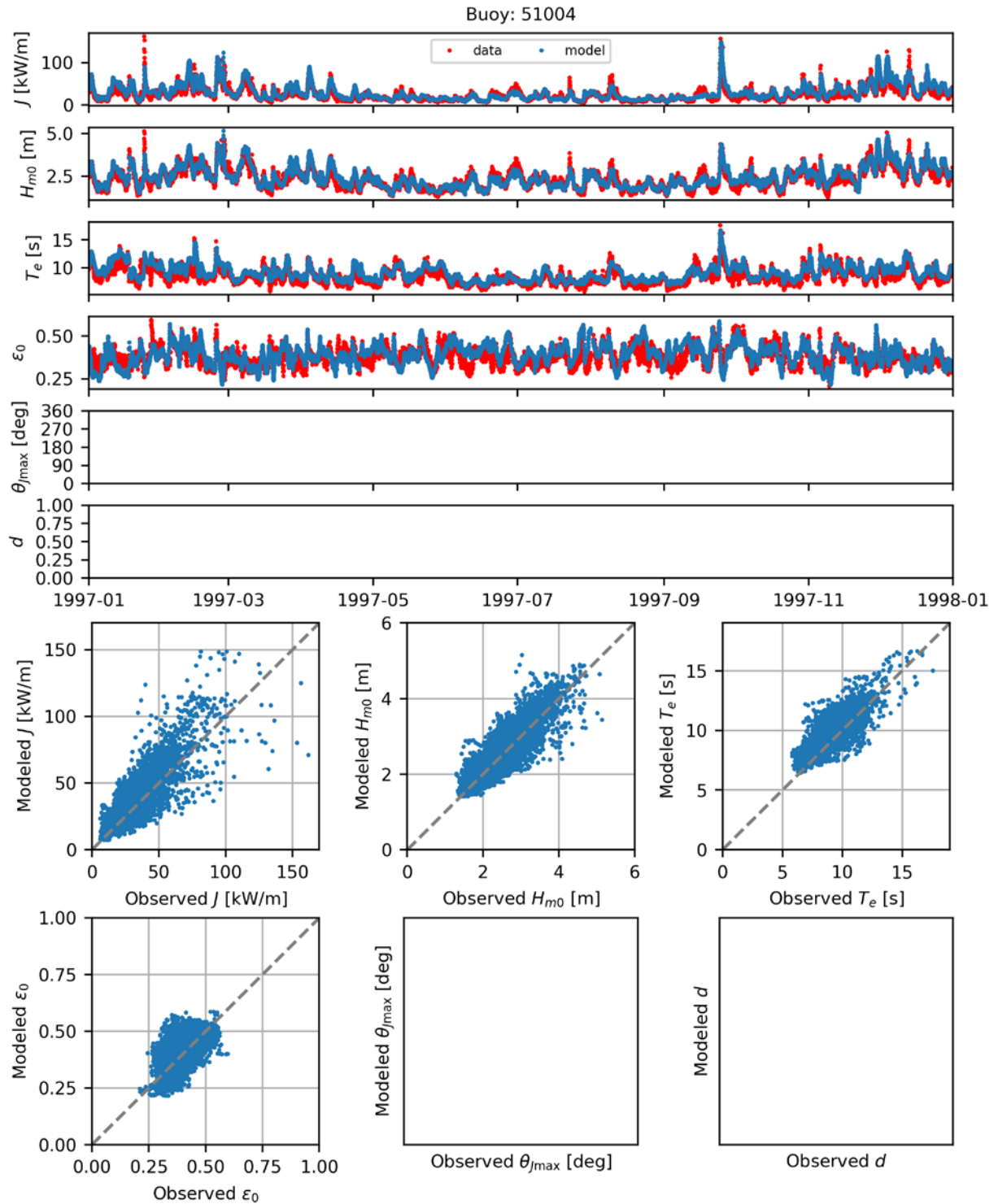


Figure B.112. Comparisons of time series (top) and scatter plots (bottom) the six model-simulated IEC parameters with observed data at NDBC Buoy 51004 for 1997.

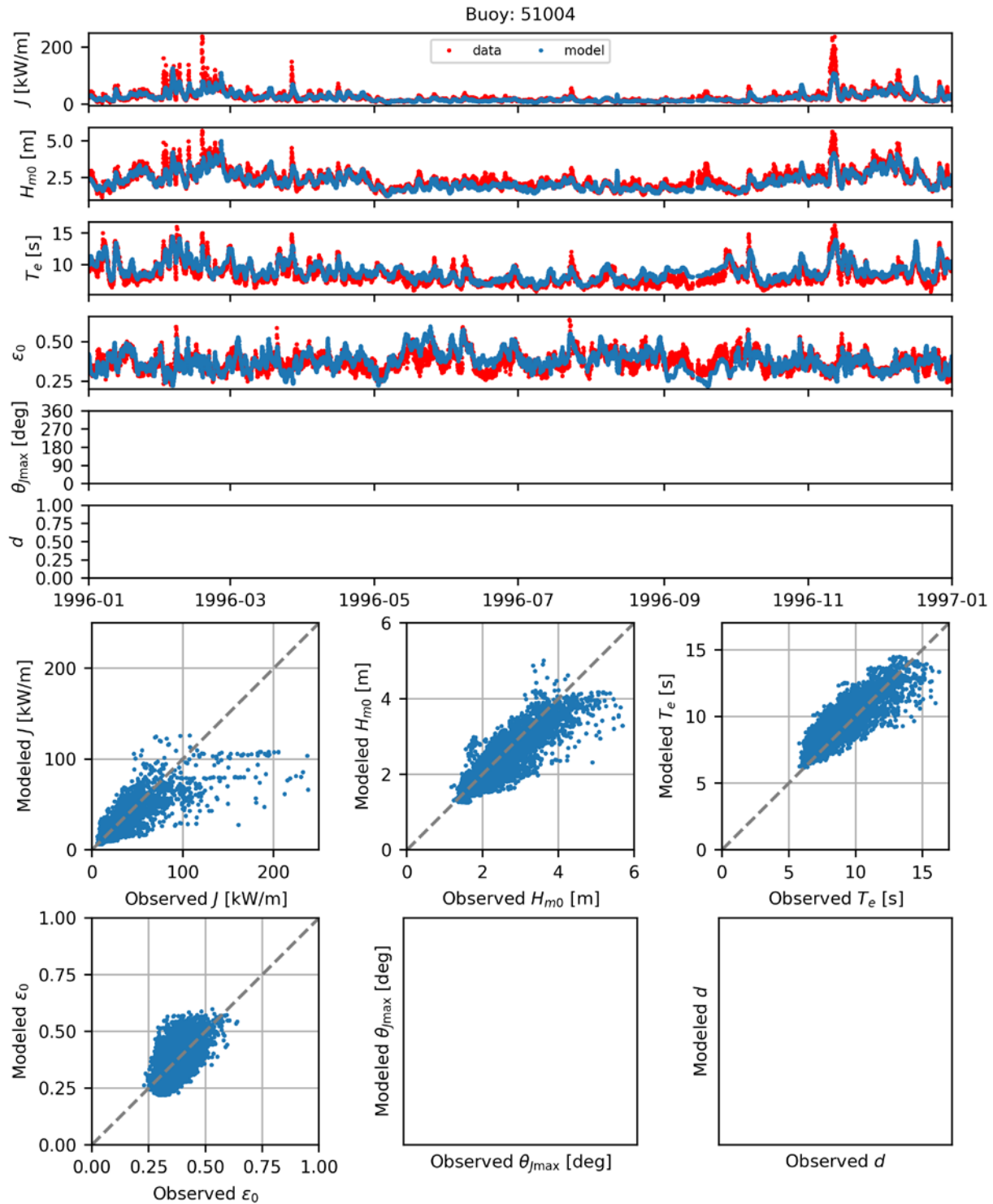


Figure B.113. Comparisons of time series (top) and scatter plots (bottom) the six model-simulated IEC parameters with observed data at NDBC Buoy 51004 for 1996.

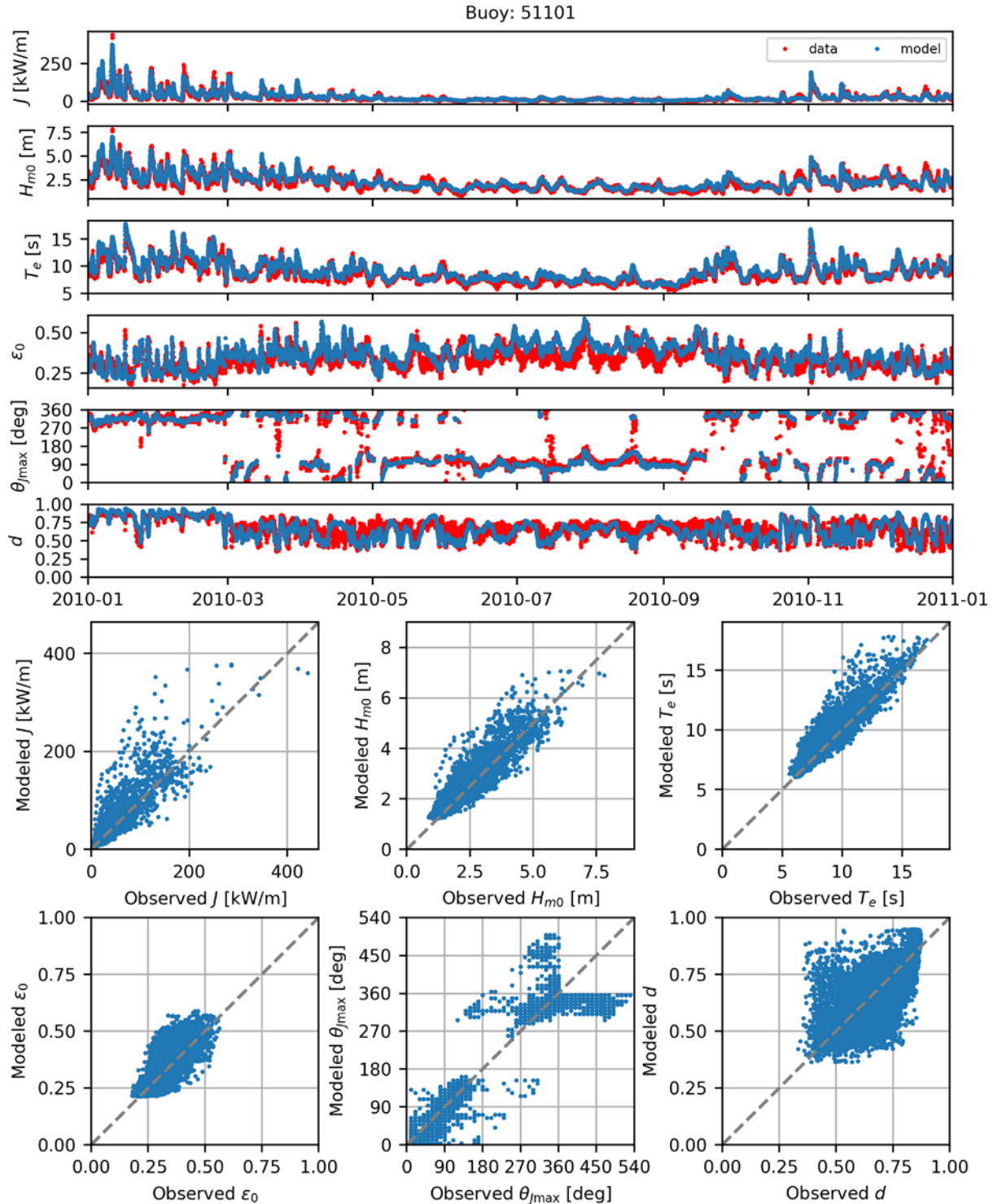


Figure B.114. Comparisons of time series (top) and scatter plots (bottom) the six model-simulated IEC parameters with observed data at NDBC Buoy 51101 for 2010.

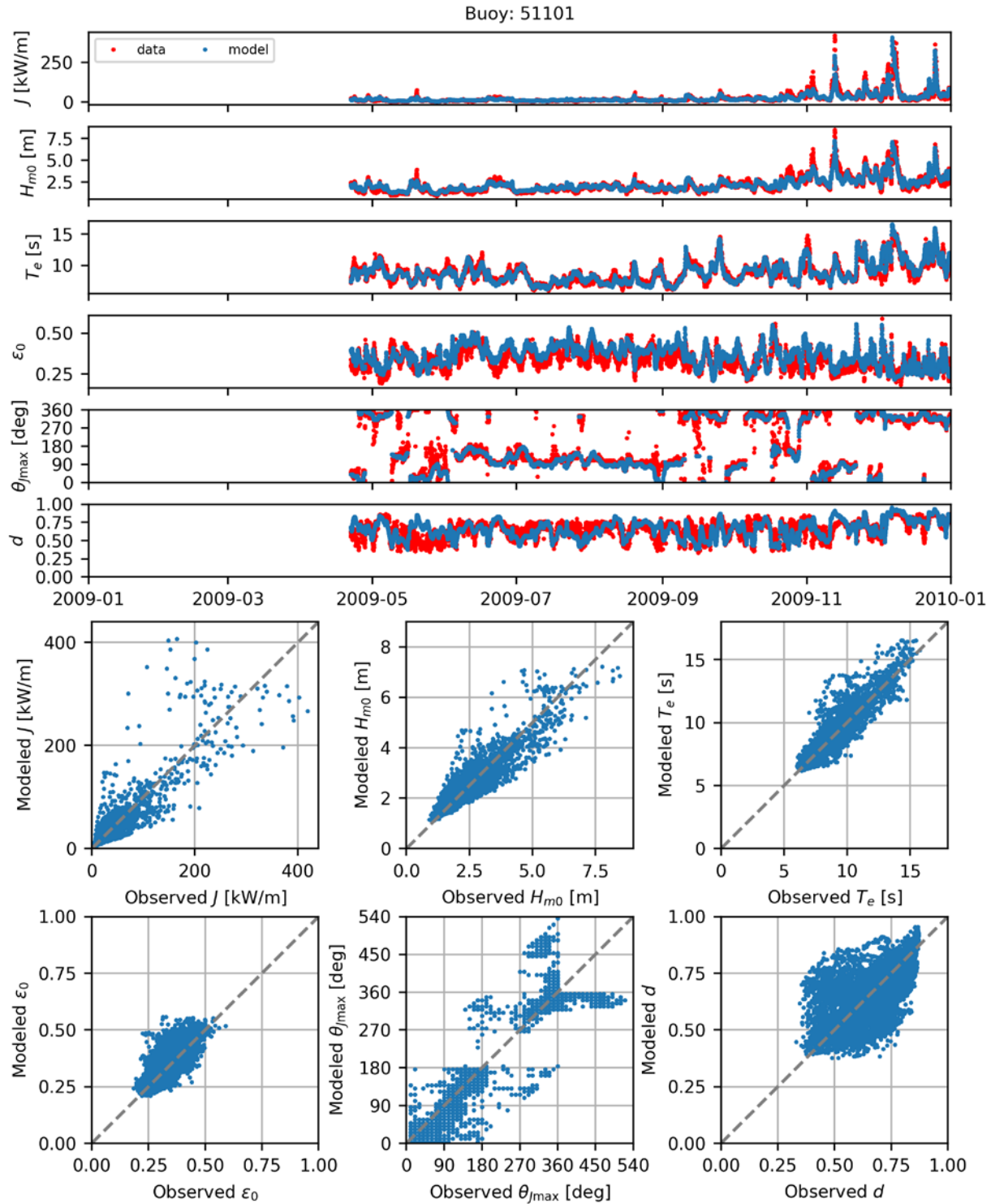


Figure B.115. Comparisons of time series (top) and scatter plots (bottom) the six model-simulated IEC parameters with observed data at NDBC Buoy 51101 for 2009.

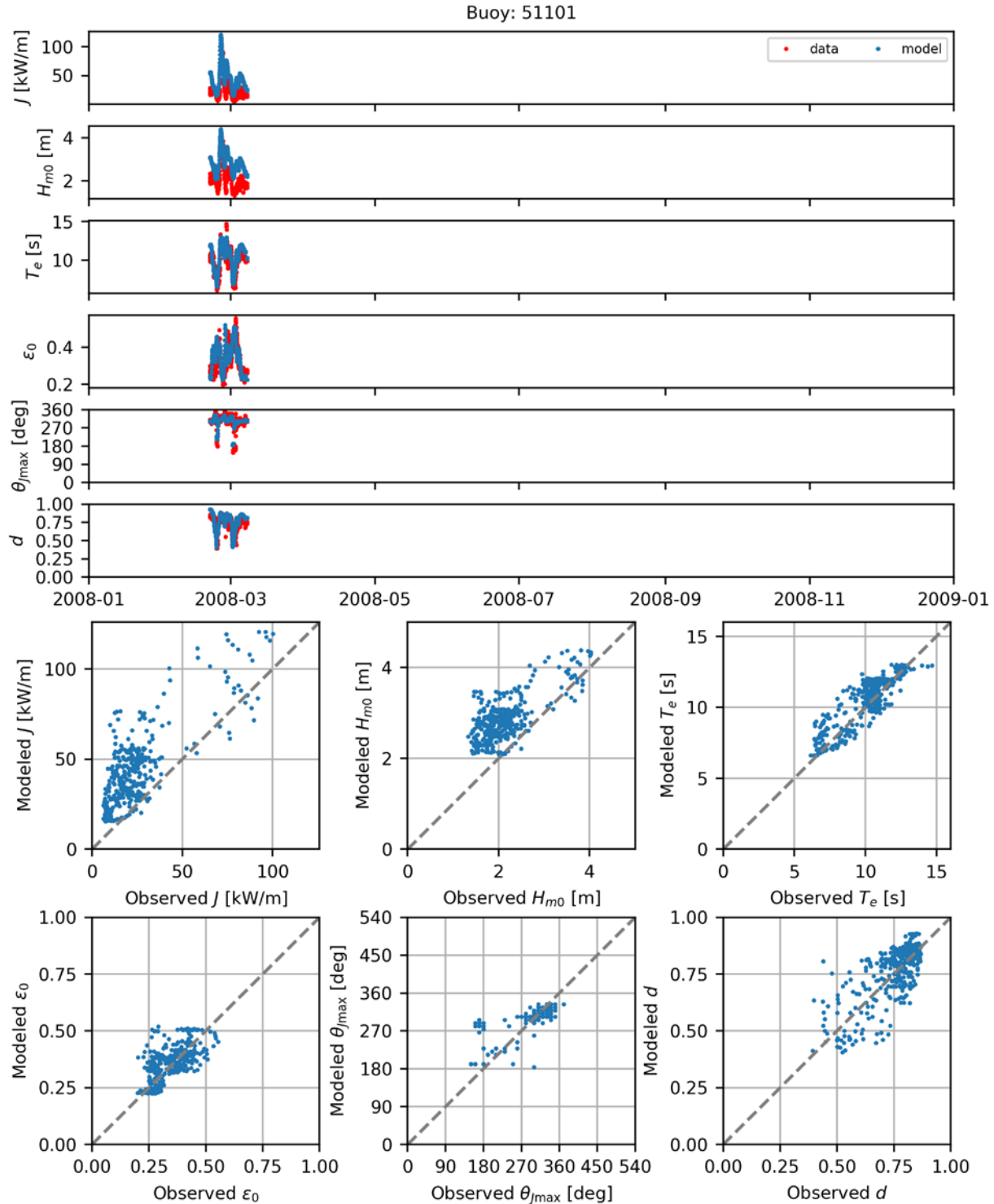


Figure B.116. Comparisons of time series (top) and scatter plots (bottom) the six model-simulated IEC parameters with observed data at NDBC Buoy 51101 for 2008.

Appendix C – Performance Metrics for Simulated IEC Resource Parameters

Table C.1 through Table C.53 are Coastal Data Information Program-related tables; Table C.54 through Table C.116 are National Data Buoy Center-related tables.

C.1 CDIP Tables

C.1.1 Station 034

Table C.1. Performance metrics for CDIP Station 034 for 1996.

Parameter	N	RMSE	PE (%)	SI	Bias	Bias (%)	R
J (kW/m)	2242	7	13.2	0.52	0	3.5	0.87
H_{m0} (m)	2242	0.30	4.8	0.17	0.04	2.6	0.80
T_e (s)	2242	0.9	-0.2	0.11	0	-0.5	0.77
ϵ_0 (-)	2242	0.07	13.7	0.20	0.05	13.3	0.76
θ_{Jmax} (deg)	-	-	-	-	-	-	-
d (-)	-	-	-	-	-	-	-

Table C.2. Performance metrics for CDIP Station 034 for 1995.

Parameter	N	RMSE	PE (%)	SI	Bias	Bias (%)	R
J (kW/m)	1517	6	24.4	0.46	2	16.8	0.85
H_{m0} (m)	1517	0.31	10.0	0.18	0.14	8.1	0.86
T_e (s)	1517	0.8	-1.7	0.09	-0.1	-1.5	0.87
ϵ_0 (-)	1517	0.07	16.2	0.21	0.05	15.7	0.68
θ_{Jmax} (deg)	-	-	-	-	-	-	-
d (-)	-	-	-	-	-	-	-

Table C.3. Performance metrics for CDIP Station 034 for 1994.

Parameter	N	RMSE	PE (%)	SI	Bias	Bias (%)	R
J (kW/m)	2076	8	35.7	0.52	4	27.2	0.89
H_{m0} (m)	2076	0.37	13.8	0.19	0.23	12.0	0.88
T_e (s)	2076	0.6	0.7	0.08	0.04	0.5	0.80
ϵ_0 (-)	2076	0.07	15.4	0.20	0.05	15.0	0.71
θ_{Jmax} (deg)	-	-	-	-	-	-	-
d (-)	-	-	-	-	-	-	-

Table C.4. Performance metrics for CDIP Station 034 for 1993.

Parameter	N	RMSE	PE (%)	SI	Bias	Bias (%)	R
J (kW/m)	2479	11	52.6	0.76	6	42.0	0.75
H_{m0} (m)	2479	0.46	18.6	0.25	0.30	16.7	0.80
T_e (s)	2479	0.7	2.1	0.09	0.2	2.0	0.81
ϵ_0 (-)	2479	0.09	21.4	0.26	0.08	21.4	0.81
θ_{Jmax} (deg)	-	-	-	-	-	-	-
d (-)	-	-	-	-	-	-	-

Table C.5. Performance metrics for CDIP Station 034 for 1992.

Parameter	N	RMSE	PE (%)	SI	Bias	Bias (%)	R
J (kW/m)	2080	8	38.0	0.58	4	30.4	0.84
H_{m0} (m)	2080	0.34	12.5	0.19	0.19	10.6	0.83
T_e (s)	2080	0.9	3.4	0.11	0.30	3.8	0.88
ϵ_0 (-)	2080	0.08	17.9	0.24	0.06	17.6	0.68
θ_{Jmax} (deg)	-	-	-	-	-	-	-
d (-)	-	-	-	-	-	-	-

Table C.6. Performance metrics for CDIP Station 034 for 1991.

Parameter	N	RMSE	PE (%)	SI	Bias	Bias (%)	R
J (kW/m)	1915	8	49.8	0.60	5	37.9	0.82
H_{m0} (m)	1915	0.39	17.8	0.22	0.27	15.4	0.83
T_e (s)	1915	0.8	2.7	0.10	0.21	2.7	0.85
ϵ_0 (-)	1915	0.08	19.2	0.23	0.07	18.9	0.76
θ_{Jmax} (deg)	-	-	-	-	-	-	-
d (-)	-	-	-	-	-	-	-

Table C.7. Performance metrics for CDIP Station 034 for 1990.

Parameter	N	RMSE	PE (%)	SI	Bias	Bias (%)	R
J (kW/m)	312	21	59.2	0.74	14	47.7	0.60
H_{m0} (m)	312	0.66	18.9	0.26	0.42	16.8	0.56
T_e (s)	312	0.9	5.7	0.10	0.48	5.6	0.84
ϵ_0 (-)	312	0.07	8.8	0.20	0.03	8.2	0.48
θ_{Jmax} (deg)	-	-	-	-	-	-	-
d (-)	-	-	-	-	-	-	-

Table C.8. Performance metrics for CDIP Station 034 for 1989.

Parameter	N	RMSE	PE (%)	SI	Bias	Bias (%)	R
J (kW/m)	2627	8	35.9	0.50	3	23.0	0.82
H_{m0} (m)	2627	0.34	11.0	0.18	0.16	8.7	0.84
T_e (s)	2627	0.8	4.3	0.10	0.33	4.2	0.84
ϵ_0 (-)	2627	0.10	21.4	0.28	0.07	20.6	0.62
θ_{Jmax} (deg)	-	-	-	-	-	-	-
d (-)	-	-	-	-	-	-	-

Table C.9. Performance metrics for CDIP Station 034 for 1988.

Parameter	N	RMSE	PE (%)	SI	Bias	Bias (%)	R
J (kW/m)	1388	8	31.5	0.54	3	19.2	0.80
H_{m0} (m)	1388	0.35	10.2	0.18	0.15	7.7	0.80
T_e (s)	1388	0.8	3.0	0.10	0.24	3.0	0.86
ϵ_0 (-)	1388	0.09	19.6	0.24	0.07	19.2	0.70
θ_{Jmax} (deg)	-	-	-	-	-	-	-
d (-)	-	-	-	-	-	-	-

Table C.10. Performance metrics for CDIP Station 034 for 1987.

Parameter	N	RMSE	PE (%)	SI	Bias	Bias (%)	R
J (kW/m)	1109	11	34.3	0.56	5	26.8	0.83
H_{m0} (m)	1109	0.38	8.8	0.18	0.15	7.2	0.84
T_e (s)	1109	1.0	7.1	0.12	0.60	7.1	0.84
ϵ_0 (-)	1109	0.08	17.6	0.24	0.06	17.3	0.73
θ_{Jmax} (deg)	-	-	-	-	-	-	-
d (-)	-	-	-	-	-	-	-

Table C.11. Performance metrics for CDIP Station 034 for 1986.

Parameter	N	RMSE	PE (%)	SI	Bias	Bias (%)	R
J (kW/m)	1144	10	39.3	0.58	5	28.8	0.78
H_{m0} (m)	1144	0.39	13.4	0.20	0.22	11.3	0.81
T_e (s)	1144	0.8	2.8	0.10	0.25	3.0	0.88
ϵ_0 (-)	1144	0.08	19.0	0.24	0.06	18.4	0.65
θ_{Jmax} (deg)	-	-	-	-	-	-	-
d (-)	-	-	-	-	-	-	-

Table C.12. Performance metrics for CDIP Station 034 for 1985.

Parameter	N	RMSE	PE (%)	SI	Bias	Bias (%)	R
J (kW/m)	504	18	33.1	0.76	5	22.2	0.84
H_{m0} (m)	504	0.45	8.8	0.22	0.12	5.9	0.89
T_e (s)	504	1.1	4.9	0.12	0.45	5.0	0.83
ϵ_0 (-)	504	0.08	16.3	0.24	0.05	16.2	0.76
θ_{Jmax} (deg)	-	-	-	-	-	-	-
d (-)	-	-	-	-	-	-	-

Table C.13. Performance metrics for CDIP Station 034 for 1984.

Parameter	N	RMSE	PE (%)	SI	Bias	Bias (%)	R
J (kW/m)	1387	9	38.1	0.59	4	27.2	0.82
H_{m0} (m)	1387	0.36	13.3	0.20	0.20	10.8	0.85
T_e (s)	1387	0.8	2.7	0.10	0.22	2.8	0.86
ϵ_0 (-)	1387	0.08	18.4	0.23	0.06	17.8	0.71
θ_{Jmax} (deg)	-	-	-	-	-	-	-
d (-)	-	-	-	-	-	-	-

Table C.14. Performance metrics for CDIP Station 034 for 1983.

Parameter	N	RMSE	PE (%)	SI	Bias	Bias (%)	R
J (kW/m)	1072	7	34.1	0.50	3	23.4	0.68
H_{m0} (m)	1072	0.35	11.4	0.19	0.17	9.2	0.76
T_e (s)	1072	0.8	2.8	0.10	0.21	2.7	0.80
ϵ_0 (-)	1072	0.09	22.5	0.26	0.08	22.0	0.71
θ_{Jmax} (deg)	-	-	-	-	-	-	-
d (-)	-	-	-	-	-	-	-

Table C.15. Performance metrics for CDIP Station 034 for 1982.

Parameter	N	RMSE	PE (%)	SI	Bias	Bias (%)	R
J (kW/m)	1210	8	26.8	0.46	3	16.8	0.77
H_{m0} (m)	1210	0.35	7.6	0.18	0.11	5.6	0.81
T_e (s)	1210	0.8	4.3	0.10	0.33	4.1	0.77
ϵ_0 (-)	1210	0.08	19.5	0.25	0.07	19.0	0.66
θ_{Jmax} (deg)	-	-	-	-	-	-	-
d (-)	-	-	-	-	-	-	-

Table C.16. Performance metrics for CDIP Station 034 for 1981.

Parameter	N	RMSE	PE (%)	SI	Bias	Bias (%)	R
J (kW/m)	529	12	43.0	0.65	4	21.5	0.79
H_{m0} (m)	529	0.42	13.8	0.21	0.19	9.6	0.87
T_e (s)	529	0.8	4.0	0.10	0.31	3.9	0.82
ϵ_0 (-)	529	0.09	20.4	0.25	0.07	20.0	0.75
θ_{Jmax} (deg)	-	-	-	-	-	-	-
d (-)	-	-	-	-	-	-	-

C.1.2 Station 039

Table C.17. Performance metrics for CDIP Station 039 for 1993.

Parameter	N	RMSE	PE (%)	SI	Bias	Bias (%)	R
J (kW/m)	835	5	42.9	0.65	3	35.2	0.73
H_{m0} (m)	835	0.29	17.5	0.23	0.20	15.8	0.73
T_e (s)	835	1.0	3.1	0.11	0.25	2.9	0.74
ϵ_0 (-)	835	0.10	24.3	0.28	0.09	23.4	0.61
θ_{Jmax} (deg)	-	-	-	-	-	-	-
d (-)	-	-	-	-	-	-	-

Table C.18. Performance metrics for CDIP Station 039 for 1991.

Parameter	N	RMSE	PE (%)	SI	Bias	Bias (%)	R
J (kW/m)	254	14	126.0	0.93	7	45.7	0.86
H_{m0} (m)	254	0.49	30.6	0.32	0.31	20.4	0.90
T_e (s)	254	2.1	25.2	0.26	1.91	23.4	0.89
ϵ_0 (-)	254	0.08	9.6	0.21	0.03	7.8	0.77
θ_{Jmax} (deg)	-	-	-	-	-	-	-
d (-)	-	-	-	-	-	-	-

Table C.19. Performance metrics for CDIP Station 039 for 1990.

Parameter	N	RMSE	PE (%)	SI	Bias	Bias (%)	R
J (kW/m)	889	17	46.9	0.78	1	5.8	0.74
H_{m0} (m)	889	0.55	9.6	0.28	0.04	2.1	0.77
T_e (s)	889	1.6	13.5	0.19	1.09	12.6	0.73
ϵ_0 (-)	889	0.10	22.3	0.31	0.07	20.3	0.48
θ_{Jmax} (deg)	-	-	-	-	-	-	-
d (-)	-	-	-	-	-	-	-

Table C.20. Performance metrics for CDIP Station 039 for 1989.

Parameter	N	RMSE	PE (%)	SI	Bias	Bias (%)	R
J (kW/m)	480	13	118.6	0.78	5	31.8	0.87
H_{m0} (m)	480	0.46	21.8	0.27	0.21	12.6	0.86
T_e (s)	480	1.6	16.2	0.19	1.2	14.8	0.86
ϵ_0 (-)	480	0.09	16.1	0.27	0.05	14.4	0.67
θ_{Jmax} (deg)	-	-	-	-	-	-	-
d (-)	-	-	-	-	-	-	-

Table C.21. Performance metrics for CDIP Station 039 for 1988.

Parameter	N	RMSE	PE (%)	SI	Bias	Bias (%)	R
J (kW/m)	167	38	150.0	1.27	23	77.4	0.71
H_{m0} (m)	167	0.88	38.8	0.41	0.66	30.6	0.74
T_e (s)	167	1.8	12.2	0.17	1.3	12.5	0.86
ϵ_0 (-)	167	0.06	10.6	0.21	0.03	10.5	0.75
θ_{Jmax} (deg)	-	-	-	-	-	-	-
d (-)	-	-	-	-	-	-	-

Table C.22. Performance metrics for CDIP Station 039 for 1987.

Parameter	N	RMSE	PE (%)	SI	Bias	Bias (%)	R
J (kW/m)	863	13	122.3	1.19	9	80.0	0.85
H_{m0} (m)	863	0.59	40.7	0.41	0.48	34.0	0.84
T_e (s)	863	1.3	10.1	0.14	0.69	9.7	0.82
ϵ_0 (-)	863	0.09	22.0	0.27	0.07	21.1	0.73
θ_{Jmax} (deg)	-	-	-	-	-	-	-
d (-)	-	-	-	-	-	-	-

Table C.23. Performance metrics for CDIP Station 039 for 1985.

Parameter	N	RMSE	PE (%)	SI	Bias	Bias (%)	R
J (kW/m)	413	17	52.5	0.84	5	23.6	0.91
H_{m0} (m)	413	0.49	16.0	0.28	0.19	10.9	0.88
T_e (s)	413	1.4	9.2	0.16	0.77	9.0	0.83
ϵ_0 (-)	413	0.07	6.9	0.19	0.02	4.6	0.79
θ_{Jmax} (deg)	-	-	-	-	-	-	-
d (-)	-	-	-	-	-	-	-

Table C.24. Performance metrics for CDIP Station 039 for 1984.

Parameter	N	RMSE	PE (%)	SI	Bias	Bias (%)	R
J (kW/m)	366	15	80.4	0.98	7	44.9	0.73
H_{m0} (m)	366	0.53	25.6	0.32	0.32	19.4	0.80
T_e (s)	366	1.4	10.8	0.15	0.95	10.6	0.81
ϵ_0 (-)	366	0.07	11.6	0.21	0.03	9.7	0.66
θ_{Jmax} (deg)	-	-	-	-	-	-	-
d (-)	-	-	-	-	-	-	-

Table C.25. Performance metrics for CDIP Station 039 for 1983.

Parameter	N	RMSE	PE (%)	SI	Bias	Bias (%)	R
J (kW/m)	772	24	130.4	1.22	14	69.0	0.92
H_{m0} (m)	772	0.62	36.3	0.37	0.48	28.4	0.92
T_e (s)	772	1.7	17.4	0.20	1.39	16.4	0.91
ϵ_0 (-)	772	0.13	28.4	0.40	0.09	28.6	0.68
θ_{Jmax} (deg)	-	-	-	-	-	-	-
d (-)	-	-	-	-	-	-	-

Table C.26. Performance metrics for CDIP Station 039 for 1982.

Parameter	N	RMSE	PE (%)	SI	Bias	Bias (%)	R
J (kW/m)	146	18	58.5	0.66	10	36.1	0.82
H_{m0} (m)	146	0.56	18.0	0.25	0.30	13.5	0.81
T_e (s)	146	1.4	10.2	0.14	0.96	10.0	0.81
ϵ_0 (-)	146	0.07	16.8	0.24	0.05	15.8	0.52
θ_{Jmax} (deg)	-	-	-	-	-	-	-
d (-)	-	-	-	-	-	-	-

C.1.3 Station 098

Table C.27. Performance metrics for CDIP Station 098 for 2010.

Parameter	N	RMSE	PE (%)	SI	Bias	Bias (%)	R
J (kW/m)	14144	6	17.4	0.41	-1.71	11.9	0.89
H_{m0} (m)	14144	0.25	6.5	0.13	0.10	5.3	0.90
T_e (s)	14144	0.53	1.5	0.07	-0.08	1.1	0.92
ϵ_0 (-)	14144	0.04	-4.2	0.12	-0.02	-4.6	0.76
θ_{Jmax} (deg)	14144	18.1	33.4	0.17	5.15	5.9	0.99
d (-)	14144	0.07	5.3	0.09	0.04	5.0	0.76

Table C.28. Performance metrics for CDIP Station 098 for 2009.

Parameter	N	RMSE	PE (%)	SI	Bias	Bias (%)	R
J (kW/m)	13790	6	9.2	0.39	0.29	1.9	0.88
H_{m0} (m)	13790	0.25	2.6	0.13	0.02	1.2	0.91
T_e (s)	13790	0.55	1.4	0.07	0.08	1.9	0.87
ϵ_0 (-)	13790	0.05	-6.9	0.14	-0.03	-7.5	0.77
θ_{Jmax} (deg)	13790	16.7	23.4	0.18	2.54	2.8	0.99
d (-)	13790	0.06	3.5	0.08	0.02	3.3	0.79

Table C.29. Performance metrics for CDIP Station 098 for 2008.

Parameter	N	RMSE	PE (%)	SI	Bias	Bias (%)	R
J (kW/m)	16430	5	12.7	0.39	0.22	1.7	0.87
H_{m0} (m)	16430	0.28	4.8	0.14	0.04	2.4	0.91
T_e (s)	16430	0.57	0.4	0.08	0.01	0.1	0.87
ϵ_0 (-)	16430	0.07	-8.4	0.17	-0.04	-9.6	0.63
θ_{Jmax} (deg)	16430	19.6	21.0	0.23	0.99	1.1	0.97
d (-)	16430	0.07	4.2	0.09	0.03	3.9	0.76

Table C.30. Performance metrics for CDIP Station 098 for 2007.

Parameter	N	RMSE	PE (%)	SI	Bias	Bias (%)	R
J (kW/m)	13853	7	11.3	0.41	0.39	2.4	0.87
H_{m0} (m)	13853	0.27	4.0	0.14	0.04	2.3	0.91
T_e (s)	13853	0.58	0.6	0.08	0.02	0.3	0.90
ϵ_0 (-)	13853	0.05	-5.0	0.13	-0.02	-5.5	0.72
θ_{Jmax} (deg)	13853	20.4	31.8	0.21	5.27	5.5	0.98
d (-)	13853	0.07	3.3	0.09	0.02	2.9	0.76

Table C.31. Performance metrics for CDIP Station 098 for 2006.

Parameter	N	RMSE	PE (%)	SI	Bias	Bias (%)	R
J (kW/m)	17095	6	4.6	0.36	-0.46	-2.8	0.85
H_{m0} (m)	17095	0.27	1.2	0.14	-0.01	-0.5	0.89
T_e (s)	17095	0.58	-0.1	0.08	-0.03	-0.4	0.87
ϵ_0 (-)	17095	0.06	-6.1	0.15	-0.03	-6.9	0.72
θ_{Jmax} (deg)	17095	17.5	19.8	0.23	1.07	1.42	0.97
d (-)	17095	0.06	3.7	0.09	0.03	3.4	0.75

Table C.32. Performance metrics for CDIP Station 098 for 2005.

Parameter	N	RMSE	PE (%)	SI	Bias	Bias (%)	R
J (kW/m)	17488	5	1.7	0.36	-1	-4.2	0.84
H_{m0} (m)	17488	0.25	-0.2	0.13	-0.03	-1.6	0.87
T_e (s)	17488	0.62	0	0.08	-0.02	-0.3	0.93
ϵ_0 (-)	17488	0.05	-4.5	0.14	-0.02	-5.0	0.71
θ_{Jmax} (deg)	17488	18.7	18.3	0.16	0.87	0.8	0.99
d (-)	17488	0.07	3.8	0.09	0.03	3.4	0.76

Table C.33. Performance metrics for CDIP Station 098 for 2004.

Parameter	N	RMSE	PE (%)	SI	Bias	Bias (%)	R
J (kW/m)	12634	5	-1.0	0.36	-1	-8.0	0.88
H_{m0} (m)	12634	0.25	-1.6	0.14	-0.06	-3.2	0.87
T_e (s)	12634	0.53	0.2	0.07	0.00	0.0	0.93
ϵ_0 (-)	12634	0.05	-4.5	0.13	-0.02	-5.3	0.67
θ_{Jmax} (deg)	12634	17.9	17.6	0.17	2.12	2.1	0.98
d (-)	12634	0.07	3.1	0.09	0.02	2.7	0.69

Table C.34. Performance metrics for CDIP Station 098 for 2003.

Parameter	N	RMSE	PE (%)	SI	Bias	Bias (%)	R
J (kW/m)	17243	9	-3.5	0.56	-2.00	-12.2	0.89
H_{m0} (m)	17243	0.28	-2.0	0.15	-0.07	-3.9	0.91
T_e (s)	17243	0.7	-1.4	0.09	0.14	-1.8	0.90
ϵ_0 (-)	17243	0.05	-4.0	0.14	-0.02	-4.8	0.66
θ_{Jmax} (deg)	17243	17.9	17.6	0.17	2.12	2.1	0.98
d (-)	17243	0.07	3.3	0.09	0.02	2.8	0.76

Table C.35. Performance metrics for CDIP Station 098 for 2002.

Parameter	N	RMSE	PE (%)	SI	Bias	Bias (%)	R
J (kW/m)	16879	8	0.40	0.48	-1	-7.8	0.88
H_{m0} (m)	16879	0.25	-0.01	0.13	-0.03	-1.8	0.91
T_e (s)	16879	0.64	-1.51	0.08	-0.1	-1.7	0.92
ϵ_0 (-)	16879	0.05	-3.60	0.13	-0.01	-4.2	0.69
θ_{Jmax} (deg)	16879	18.0	24.1	0.16	3.70	3.3	0.99
d (-)	16879	0.06	2.80	0.08	0.02	2.4	0.79

Table C.36. Performance metrics for CDIP Station 098 for 2001.

Parameter	N	RMSE	PE (%)	SI	Bias	Bias (%)	R
J (kW/m)	17444	7	8.9	0.39	0	1.4	0.89
H_{m0} (m)	17444	0.28	3.6	0.14	0.04	2.09	0.90
T_e (s)	17444	0.6	-0.5	0.07	-0.1	-0.8	0.93
ϵ_0 (-)	17444	0.05	-5.9	0.13	-0.02	-6.5	0.74
θ_{Jmax} (deg)	17444	16.9	35.2	0.19	6.40	7.3	0.98
d (-)	17444	0.06	2.9	0.08	0.02	2.7	0.77

Table C.37. Performance metrics for CDIP Station 098 for 2000.

Parameter	N	RMSE	PE (%)	SI	Bias	Bias (%)	R
J (kW/m)	6753	6	12.0	0.41	1	7.3	0.77
H_{m0} (m)	6753	0.28	4.5	0.15	0.06	3.3	0.83
T_e (s)	6753	0.5	0.4	0.07	0.0	0.1	0.89
ϵ_0 (-)	6753	0.05	-4.7	0.13	-0.02	-5.2	0.75
θ_{Jmax} (deg)	6753	17.2	30.8	0.21	3.5	4.3	0.98
d (-)	6753	0.06	2.3	0.08	0.01	1.9	0.77

C.1.4 Station 106

Table C.38. Performance metrics for CDIP Station 106 for 2010.

Parameter	N	RMSE	PE (%)	SI	Bias	Bias (%)	R
J (kW/m)	16375	13	42.8	0.87	5	29.8	0.90
H_{m0} (m)	16375	0.36	15.1	0.22	0.20	12.5	0.92
T_e (s)	16375	0.8	3.8	0.10	0.3	3.6	0.95
ϵ_0 (-)	16375	0.06	3.5	0.15	0.01	2.8	0.78
θ_{Jmax} (deg)	16375	17.1	1.9	0.09	-4.48	-2.4	0.99
d (-)	16375	0.07	1.3	0.08	0.01	0.96	0.62

Table C.39. Performance metrics for CDIP Station 106 for 2009.

Parameter	N	RMSE	PE (%)	SI	Bias	Bias (%)	R
J (kW/m)	17056	12	26.0	0.70	2	11.1	0.89
H_{m0} (m)	17056	0.33	8.3	0.20	0.09	5.4	0.92
T_e (s)	17056	0.9	3.8	0.10	0.3	3.4	0.93
ϵ_0 (-)	17056	0.06	-0.9	0.17	-0.01	-1.7	0.76
θ_{Jmax} (deg)	17056	20.5	6.5	0.10	-4.0	-2.0	0.99
d (-)	17056	0.07	3.4	0.09	0.09	3.0	0.70

Table C.40. Performance metrics for CDIP Station 106 for 2008.

Parameter	N	RMSE	PE (%)	SI	Bias	Bias (%)	R
J (kW/m)	14433	10	36.7	0.74	3	21.2	0.88
H_{m0} (m)	14433	0.32	13.4	0.21	0.15	9.7	0.90
T_e (s)	14433	0.8	2.1	0.10	0.2	2.4	0.95
ϵ_0 (-)	14433	0.06	1.1	0.16	0.00	0.5	0.76
θ_{Jmax} (deg)	14433	16.6	2.8	0.10	-3.99	-2.4	0.99
d (-)	14433	0.07	2.8	0.09	0.02	2.1	0.63

Table C.41. Performance metrics for CDIP Station 106 for 2007.

Parameter	N	RMSE	PE (%)	SI	Bias	Bias (%)	R
J (kW/m)	16449	9	33.8	0.63	3	19.0	0.91
H_{m0} (m)	16449	0.32	11.4	0.20	0.14	8.8	0.91
T_e (s)	16449	0.8	3.6	0.10	0.3	3.7	0.94
ϵ_0 (-)	16449	0.06	1.4	0.15	0.00	0.7	0.74
θ_{Jmax} (deg)	16449	18.0	-2.4	0.10	-6.0	-3.3	0.99
d (-)	16449	0.08	2.3	0.09	0.01	1.8	0.60

Table C.42. Performance metrics for CDIP Station 106 for 2006.

Parameter	N	RMSE	PE (%)	SI	Bias	Bias (%)	R
J (kW/m)	10533	8	32.0	0.77	2	18.5	0.88
H_{m0} (m)	10533	0.30	12.0	0.21	0.12	8.7	0.89
T_e (s)	10533	0.7	1.6	0.09	0.1	1.6	0.94
ϵ_0 (-)	10533	0.06	-2.3	0.16	-0.02	-3.8	0.77
θ_{Jmax} (deg)	10533	20.7	8.5	0.12	-1.2	-0.7	0.99
d (-)	10533	0.08	5.2	0.09	0.04	4.4	0.74

Table C.43. Performance metrics for CDIP Station 106 for 2005.

Parameter	N	RMSE	PE (%)	SI	Bias	Bias (%)	R
J (kW/m)	16247	10	32.0	0.63	3	19.7	0.92
H_{m0} (m)	16247	0.32	11.9	0.19	0.15	9.0	0.93
T_e (s)	16247	0.8	2.1	0.10	0.2	2.3	0.95
ϵ_0 (-)	16247	0.06	1.1	0.16	0.00	0.4	0.77
θ_{Jmax} (deg)	16247	16.4	-1.5	0.09	-3.6	-1.9	0.99
d (-)	16247	0.07	2.5	0.09	0.02	2.2	0.61

Table C.44. Performance metrics for CDIP Station 106 for 2004.

Parameter	N	RMSE	PE (%)	SI	Bias	Bias (%)	R
J (kW/m)	17081	11	30.7	0.66	4	22.5	0.92
H_{m0} (m)	17081	0.32	10.9	0.19	0.14	8.6	0.93
T_e (s)	17081	0.9	3.3	0.10	0.3	3.5	0.95
ϵ_0 (-)	17081	0.06	-2.1	0.15	-0.01	-2.3	0.81
θ_{Jmax} (deg)	17081	18.5	6.6	0.09	-4.0	-1.9	0.99
d (-)	17081	0.07	3.2	0.09	0.02	3.0	0.76

Table C.45. Performance metrics for CDIP Station 106 for 2003.

Parameter	N	RMSE	PE (%)	SI	Bias	Bias (%)	R
J (kW/m)	12244	15	34.3	0.64	4	17.4	0.91
H_{m0} (m)	12244	0.39	12.1	0.21	0.16	8.5	0.92
T_e (s)	12244	1.0	2.4	0.10	0.2	2.4	0.93
ϵ_0 (-)	12244	0.06	0.6	0.18	0.00	-0.2	0.73
θ_{Jmax} (deg)	12244	17.1	1.0	0.07	-6.1	-2.6	0.99
d (-)	12244	0.08	5.1	0.10	0.04	4.6	0.60

Table C.46. Performance metrics for CDIP Station 106 for 2002.

Parameter	N	RMSE	PE (%)	SI	Bias	Bias (%)	R
J (kW/m)	17092	14	25.1	0.82	3	17.5	0.90
H_{m0} (m)	17092	0.34	8.6	0.20	0.10	6.1	0.92
T_e (s)	17092	0.9	2.1	0.10	0.2	2.4	0.94
ϵ_0 (-)	17092	0.06	0.3	0.17	0.00	-0.3	0.76
θ_{Jmax} (deg)	17092	16.6	6.5	0.08	-3.6	-1.8	0.99
d (-)	17092	0.08	3.0	0.09	0.02	2.5	0.62

Table C.47. Performance metrics for CDIP Station 106 for 2001.

Parameter	N	RMSE	PE (%)	SI	Bias	Bias (%)	R
J (kW/m)	767	43	69.2	0.96	23	52.8	0.84
H_{m0} (m)	767	0.68	19.4	0.26	0.44	16.9	0.89
T_e (s)	767	1.6	10.4	0.16	1.1	10.1	0.82
ϵ_0 (-)	767	0.07	-2.6	0.18	-0.01	-2.1	0.73
θ_{Jmax} (deg)	767	19.5	7.6	0.06	-6.1	-2.0	0.98
d (-)	767	0.08	5.0	0.09	0.04	4.8	0.75

C.1.5 Station 146

Table C.48. Performance metrics for CDIP Station 146 for 2010.

Parameter	N	RMSE	PE (%)	SI	Bias	Bias (%)	R
J (kW/m)	15406	2	-8.6	0.43	-1	-14.8	0.82
H_{m0} (m)	15406	0.21	-13.4	0.23	-0.13	-14.6	0.76
T_e (s)	15406	2.3	19.5	0.25	1.6	17.9	0.54
ϵ_0 (-)	15406	0.10	-0.1	0.23	-0.01	-1.4	0.53
θ_{Jmax} (deg)	15406	28.5	6.3	0.14	11.1	5.4	0.81
d (-)	15406	0.11	7.0	0.14	0.05	6.2	0.70

Table C.49. Performance metrics for CDIP Station 146 for 2009.

Parameter	N	RMSE	PE (%)	SI	Bias	Bias (%)	R
J (kW/m)	13651	2	-2.4	0.46	0	-8.4	0.80
H_{m0} (m)	13651	0.18	-8.4	0.21	-0.08	9.6	0.76
T_e (s)	13651	1.7	12.8	0.18	1.1	11.7	0.66
ϵ_0 (-)	13651	0.09	-2.8	0.21	-0.02	-4.3	0.54
θ_{Jmax} (deg)	13651	26.7	2.8	0.13	3.5	1.7	0.70
d (-)	13651	0.11	8.4	0.14	0.06	7.6	0.72

Table C.50. Performance metrics for CDIP Station 146 for 2008.

Parameter	N	RMSE	PE (%)	SI	Bias	Bias (%)	R
J (kW/m)	12002	1	-10.3	0.44	-1	-15.2	0.75
H_{m0} (m)	12002	0.20	-12.6	0.23	-0.12	-14.0	0.70
T_e (s)	12002	1.9	14.4	0.20	1.2	13.4	0.71
ϵ_0 (-)	12002	0.11	-1.1	0.24	-0.01	-2.6	0.48
θ_{Jmax} (deg)	12002	38.9	10.0	0.20	14.3	7.3	0.52
d (-)	12002	0.11	6.2	0.14	0.04	5.3	0.71

Table C.51. Performance metrics for CDIP Station 146 for 2007.

Parameter	N	RMSE	PE (%)	SI	Bias	Bias (%)	R
J (kW/m)	10992	2	-15.5	0.60	-1.0	-19.8	0.85
H_{m0} (m)	10992	0.21	15.1	0.24	-0.14	-15.7	0.85
T_e (s)	10992	1.8	14.1	0.20	1.2	13.2	0.67
ϵ_0 (-)	10992	0.11	-0.1	0.25	-0.01	-1.2	0.45
θ_{Jmax} (deg)	10992	27.1	4.1	0.14	5.5	2.9	0.64
d (-)	10992	0.10	4.8	0.13	0.03	4.4	0.70

C.1.6 Station 164

Table C.52. Performance metrics for CDIP Station 164 for 2010.

Parameter	N	RMSE	PE (%)	SI	Bias	Bias (%)	R
J (kW/m)	14536	7	21.0	0.44	2	12.0	0.92
H_{m0} (m)	14536	0.27	8.2	0.15	0.12	6.7	0.92
T_e (s)	14536	0.8	1.8	0.09	0.1	1.5	0.93
ϵ_0 (-)	14536	0.06	5.6	0.13	0.02	4.6	0.83
θ_{Jmax} (deg)	14536	39.7	1.7	0.19	-1.9	-0.9	0.93
d (-)	14536	0.08	1.1	0.12	0.00	0.2	0.77

Table C.53. Performance metrics for CDIP Station 164 for 2009.

Parameter	N	RMSE	PE (%)	SI	Bias	Bias (%)	R
J (kW/m)	4000	11	15.9	0.50	2	8.3	0.89
H_{m0} (m)	4000	0.31	4.9	0.16	0.07	3.6	0.89
T_e (s)	4000	1.0	2.4	0.11	0.21	2.1	0.88
ϵ_0 (-)	4000	0.06	4.7	0.16	0.01	3.8	0.76
θ_{Jmax} (deg)	4000	53.8	5.8	0.18	-1.8	-0.6	0.84
d (-)	4000	0.11	6.1	0.17	0.03	4.1	0.71

C.2 NDBC Tables

C.2.1 Station 51000

Table C.54. Performance metrics for NDBC Station 51000 for 2010.

Parameter	N	RMSE	PE (%)	SI	Bias	Bias (%)	R
J (kW/m)	8019	17	29.9	0.62	6	21.5	0.89
H_{m0} (m)	8019	0.41	8.2	0.18	0.15	6.6	0.88
T_e (s)	8019	0.9	6.7	0.11	0.5	6.2	0.92
ϵ_0 (-)	8019	0.07	11.3	0.20	0.03	10.2	0.59
θ_{Jmax} (deg)	8019	37.3	1.4	0.17	-4.4	-2.0	0.96
d (-)	8019	0.09	0.1	0.14	0.00	-0.6	0.73

Table C.55. Performance metrics for NDBC Station 51000 for 2009.

Parameter	N	RMSE	PE (%)	SI	Bias	Bias (%)	R
J (kW/m)	3870	16	16.2	0.52	2	6.8	0.91
H_{m0} (m)	3870	0.37	3.8	0.16	0.04	1.8	0.90
T_e (s)	3870	0.8	4.4	0.09	0.38	4.2	0.91
ϵ_0 (-)	3870	0.05	3.7	0.14	0.01	3.0	0.73
θ_{Jmax} (deg)	3870	39.2	-0.1	0.16	-3.4	-1.4	0.95
d (-)	3870	0.10	1.6	0.14	0.00	0.6	0.71

C.2.2 Station 51001

Table C.56. Performance metrics for NDBC Station 51001 for 2009.

Parameter	N	RMSE	PE (%)	SI	Bias	Bias (%)	R
J (kW/m)	8344	18	22.4	0.61	4	13.7	0.87
H_{m0} (m)	8344	0.43	7.2	0.18	0.13	5.3	0.89
T_e (s)	8344	0.8	2.8	0.09	0.2	2.6	0.87
ϵ_0 (-)	8344	0.05	5.3	0.15	0.02	4.4	0.68
θ_{Jmax} (deg)	8344	43.6	-2.0	0.22	-4.4	-2.2	0.94
d (-)	8344	0.12	2.9	0.18	0.01	1.0	0.53

Table C.57. Performance metrics for NDBC Station 51001 for 2008.

Parameter	N	RMSE	PE (%)	SI	Bias	Bias (%)	R
J (kW/m)	7515	12	30.4	0.65	4	21.4	0.84
H_{m0} (m)	7515	0.39	6.7	0.19	0.10	4.9	0.85
T_e (s)	7515	1.0	9.7	0.13	0.7	8.6	0.86
ϵ_0 (-)	7515	0.08	12.9	0.23	0.04	11.3	0.44
θ_{Jmax} (deg)	7515	48.4	-6.6	0.23	-11.1	-5.3	0.94
d (-)	7515	0.11	-0.5	0.17	-0.01	-1.4	0.66

Table C.58. Performance metrics for NDBC Station 51001 for 2007.

Parameter	N	RMSE	PE (%)	SI	Bias	Bias (%)	R
J (kW/m)	8291	17	24.0	0.60	4	15.5	0.91
H_{m0} (m)	8291	0.40	6.9	0.17	0.12	5.3	0.91
T_e (s)	8291	0.8	5.2	0.10	0.4	5.0	0.91
ϵ_0 (-)	8291	0.05	3.4	0.15	0.01	2.6	0.69
θ_{Jmax} (deg)	8291	41.7	1.0	0.20	-5.5	-2.7	0.95
d (-)	8291	0.09	0.7	0.14	0.00	-0.2	0.71

Table C.59. Performance metrics for NDBC Station 51001 for 2006.

Parameter	N	RMSE	PE (%)	SI	Bias	Bias (%)	R
J (kW/m)	8682	14	10.6	0.50	2	5.7	0.86
H_{m0} (m)	8682	0.36	2.1	0.15	0.01	0.5	0.87
T_e (s)	8682	0.8	3.2	0.09	0.3	3.1	0.89
ϵ_0 (-)	8682	0.05	2.8	0.16	0.01	2.2	0.68
θ_{Jmax} (deg)	8682	40.2	-0.8	0.21	-4.4	-2.3	0.95
d (-)	8682	0.11	2.8	0.17	0.01	1.4	0.56

Table C.60. Performance metrics for NDBC Station 51001 for 2005.

Parameter	N	RMSE	PE (%)	SI	Bias	Bias (%)	R
J (kW/m)	3326	28	27.6	0.64	8	17.5	0.86
H_{m0} (m)	3326	0.53	7.1	0.19	0.14	5.2	0.87
T_e (s)	3326	1.2	6.4	0.12	0.53	5.5	0.86
ϵ_0 (-)	3326	0.06	-4.2	0.17	-0.02	-5.0	0.58
θ_{Jmax} (deg)	-	-	-	-	-	-	-
d (-)	-	-	-	-	-	-	-

Table C.61. Performance metrics for NDBC Station 51001 for 2004.

Parameter	N	RMSE	PE (%)	SI	Bias	Bias (%)	R
J (kW/m)	7549	21	7.0	0.61	2	7.0	0.89
H_{m0} (m)	7549	0.45	-0.7	0.18	-0.03	-1.0	0.89
T_e (s)	7549	0.8	4.2	0.10	0.3	3.8	0.92
ϵ_0 (-)	7549	0.06	1.5	0.15	0.00	0.9	0.65
θ_{Jmax} (deg)	-	-	-	-	-	-	-
d (-)	-	-	-	-	-	-	-

Table C.62. Performance metrics for NDBC Station 51001 for 2003.

Parameter	N	RMSE	PE (%)	SI	Bias	Bias (%)	R
J (kW/m)	4770	20	1.3	0.63	0	-1.3	0.91
H_{m0} (m)	4770	0.42	-3.2	0.17	-0.09	-3.9	0.91
T_e (s)	4770	0.9	3.8	0.10	0.3	3.3	0.91
ϵ_0 (-)	4770	0.05	0.7	0.15	0.00	-0.1	0.62
θ_{Jmax} (deg)	-	-	-	-	-	-	-
d (-)	-	-	-	-	-	-	-

Table C.63. Performance metrics for NDBC Station 51001 for 2002.

Parameter	N	RMSE	PE (%)	SI	Bias	Bias (%)	R
J (kW/m)	8592	21	7.3	0.63	0	0.7	0.87
H_{m0} (m)	8592	0.43	-0.3	0.18	-0.04	-1.7	0.89
T_e (s)	8592	0.9	4.1	0.11	0.3	3.3	0.89
ϵ_0 (-)	8592	0.05	-2.3	0.15	-0.01	-2.9	0.65
θ_{Jmax} (deg)	-	-	-	-	-	-	-
d (-)	-	-	-	-	-	-	-

Table C.64. Performance metrics for NDBC Station 51001 for 2001.

Parameter	N	RMSE	PE (%)	SI	Bias	Bias (%)	R
J (kW/m)	4878	21	21.7	0.74	4	15.1	0.80
H_{m0} (m)	4878	0.43	3.4	0.19	0.06	2.6	0.85
T_e (s)	4878	1.2	7.7	0.14	0.6	6.6	0.88
ϵ_0 (-)	4878	0.06	-2.3	0.16	-0.01	-2.9	0.56
θ_{Jmax} (deg)	-	-	-	-	-	-	-
d (-)	-	-	-	-	-	-	-

Table C.65. Performance metrics for NDBC Station 51001 for 2000.

Parameter	N	RMSE	PE (%)	SI	Bias	Bias (%)	R
J (kW/m)	7297	21	18.1	0.78	4	13.5	0.79
H_{m0} (m)	7297	0.43	3.5	0.19	0.06	2.6	0.85
T_e (s)	7297	1.1	4.9	0.13	0.3	3.9	0.89
ϵ_0 (-)	7297	0.06	2.7	0.18	0.01	2.1	0.60
θ_{Jmax} (deg)	-	-	-	-	-	-	-
d (-)	-	-	-	-	-	-	-

Table C.66. Performance metrics for NDBC Station 51001 for 1999.

Parameter	N	RMSE	PE (%)	SI	Bias	Bias (%)	R
J (kW/m)	8011	20	14.2	0.71	1	3.8	0.84
H_{m0} (m)	8011	0.42	0.9	0.18	-0.02	-0.7	0.88
T_e (s)	8011	1.1	7.2	0.13	0.5	6.2	0.88
ϵ_0 (-)	8011	0.07	3.6	0.18	0.01	2.7	0.48
θ_{Jmax} (deg)	-	-	-	-	-	-	-
d (-)	-	-	-	-	-	-	-

Table C.67. Performance metrics for NDBC Station 51001 for 1998.

Parameter	N	RMSE	PE (%)	SI	Bias	Bias (%)	R
J (kW/m)	6570	29	27.6	0.79	4	11.6	0.80
H_{m0} (m)	6570	0.50	6.8	0.19	0.11	4.4	0.86
T_e (s)	6570	1.2	6.4	0.13	0.4	5.1	0.89
ϵ_0 (-)	6570	0.06	1.8	0.18	0.00	0.9	0.55
θ_{Jmax} (deg)	-	-	-	-	-	-	-
d (-)	-	-	-	-	-	-	-

Table C.68. Performance metrics for NDBC Station 51001 for 1997.

Parameter	N	RMSE	PE (%)	SI	Bias	Bias (%)	R
J (kW/m)	6427	24	4.8	0.66	0	1.3	0.80
H_{m0} (m)	6427	0.52	-3.5	0.20	-0.10	-3.9	0.85
T_e (s)	6427	1.1	5.8	0.12	0.4	4.8	0.87
ϵ_0 (-)	6427	0.07	-3.7	0.18	-0.02	-4.4	0.62
θ_{Jmax} (deg)	-	-	-	-	-	-	-
d (-)	-	-	-	-	-	-	-

Table C.69. Performance metrics for NDBC Station 51001 for 1996.

Parameter	N	RMSE	PE (%)	SI	Bias	Bias (%)	R
J (kW/m)	5988	30	-8.8	0.66	-7	-16.2	0.86
H_{m0} (m)	5988	0.59	-9.0	0.21	-0.27	-9.6	0.89
T_e (s)	5988	1.1	5.1	0.13	0.3	3.6	0.85
ϵ_0 (-)	5988	0.06	-1.4	0.18	-0.01	-2.2	0.53
θ_{Jmax} (deg)	-	-	-	-	-	-	-
d (-)	-	-	-	-	-	-	-

C.2.3 Station 51002

Table C.70. Performance metrics for NDBC Station 51002 for 2010.

Parameter	N	RMSE	PE (%)	SI	Bias	Bias (%)	R
J (kW/m)	8739	10	23.6	0.45	4	18.0	0.84
H_{m0} (m)	8739	0.31	6.8	0.14	0.13	5.5	0.87
T_e (s)	8739	0.8	6.1	0.09	0.5	5.8	0.88
ϵ_0 (-)	8739	0.06	11.5	0.17	0.04	10.5	0.67
θ_{Jmax} (deg)	-	-	-	-	-	-	-
d (-)	-	-	-	-	-	-	-

Table C.71. Performance metrics for NDBC Station 51002 for 2009.

Parameter	N	RMSE	PE (%)	SI	Bias	Bias (%)	R
J (kW/m)	4150	11	18.3	0.39	3	11.1	0.81
H_{m0} (m)	4150	0.33	4.2	0.13	0.07	2.7	0.86
T_e (s)	4150	0.9	6.1	0.11	0.5	5.4	0.84
ϵ_0 (-)	4150	0.06	9.2	0.16	0.03	7.9	0.61
θ_{Jmax} (deg)	-	-	-	-	-	-	-
d (-)	-	-	-	-	-	-	-

Table C.72. Performance metrics for NDBC Station 51002 for 2008.

Parameter	N	RMSE	PE (%)	SI	Bias	Bias (%)	R
J (kW/m)	8774	8	25.9	0.43	4	20.3	0.82
H_{m0} (m)	8774	0.28	4.6	0.13	0.07	3.3	0.86
T_e (s)	8774	1.1	12.6	0.15	0.9	12.0	0.81
ϵ_0 (-)	8774	0.07	12.5	0.19	0.04	10.8	0.42
θ_{Jmax} (deg)	-	-	-	-	-	-	-
d (-)	-	-	-	-	-	-	-

Table C.73. Performance metrics for NDBC Station 51002 for 2007.

Parameter	N	RMSE	PE (%)	SI	Bias	Bias (%)	R
J (kW/m)	8682	9	15.0	0.35	2	8.0	0.85
H_{m0} (m)	8682	0.31	0.3	0.12	-0.03	-1.0	0.87
T_e (s)	8682	1.0	11.7	0.13	0.8	11.1	0.90
ϵ_0 (-)	8682	0.06	13.2	0.19	0.04	11.8	0.57
θ_{Jmax} (deg)	-	-	-	-	-	-	-
d (-)	-	-	-	-	-	-	-

Table C.74. Performance metrics for NDBC Station 51002 for 2006.

Parameter	N	RMSE	PE (%)	SI	Bias	Bias (%)	R
J (kW/m)	6788	6	10.2	0.31	1	4.2	0.88
H_{m0} (m)	6788	0.29	-1.4	0.11	-0.06	-2.7	0.89
T_e (s)	6788	1.0	11.2	0.13	0.8	10.6	0.79
ϵ_0 (-)	6788	0.06	12.7	0.18	0.04	11.3	0.64
θ_{Jmax} (deg)	-	-	-	-	-	-	-
d (-)	-	-	-	-	-	-	-

Table C.75. Performance metrics for NDBC Station 51002 for 2005.

Parameter	N	RMSE	PE (%)	SI	Bias	Bias (%)	R
J (kW/m)	7451	8	11.1	0.37	1	6.6	0.84
H_{m0} (m)	7451	0.31	-1.1	0.13	-0.06	-2.3	0.83
T_e (s)	7451	1.0	11.0	0.13	0.8	10.5	0.90
ϵ_0 (-)	7451	0.07	13.0	0.20	0.04	11.5	0.53
θ_{Jmax} (deg)	-	-	-	-	-	-	-
d (-)	-	-	-	-	-	-	-

Table C.76. Performance metrics for NDBC Station 51002 for 2004.

Parameter	N	RMSE	PE (%)	SI	Bias	Bias (%)	R
J (kW/m)	2240	12	13.8	0.36	4	10.9	0.85
H_{m0} (m)	2240	0.33	3.0	0.13	0.06	2.2	0.80
T_e (s)	2240	0.9	5.2	0.09	0.43	4.6	0.91
ϵ_0 (-)	2240	0.04	-1.2	0.12	-0.01	-1.8	0.74
θ_{Jmax} (deg)	-	-	-	-	-	-	-
d (-)	-	-	-	-	-	-	-

Table C.77. Performance metrics for NDBC Station 51002 for 2003.

Parameter	N	RMSE	PE (%)	SI	Bias	Bias (%)	R
J (kW/m)	8707	9	1.5	0.34	-1	-2.0	0.87
H_{m0} (m)	8707	0.32	-1.5	0.13	-0.07	-2.8	0.86
T_e (s)	8707	0.7	2.5	0.08	0.2	2.0	0.90
ϵ_0 (-)	8707	0.05	1.4	0.12	0.00	0.5	0.72
θ_{Jmax} (deg)	-	-	-	-	-	-	-
d (-)	-	-	-	-	-	-	-

Table C.78. Performance metrics for NDBC Station 51002 for 2002.

Parameter	N	RMSE	PE (%)	SI	Bias	Bias (%)	R
J (kW/m)	8567	10	3.4	0.37	0	0.0	0.83
H_{m0} (m)	8567	0.31	-0.9	0.13	-0.05	-1.9	0.84
T_e (s)	8567	0.7	3.2	0.09	0.2	2.6	0.89
ϵ_0 (-)	8567	0.04	1.7	0.11	0.00	0.9	0.71
θ_{Jmax} (deg)	-	-	-	-	-	-	-
d (-)	-	-	-	-	-	-	-

Table C.79. Performance metrics for NDBC Station 51002 for 2001.

Parameter	N	RMSE	PE (%)	SI	Bias	Bias (%)	R
J (kW/m)	8606	9	0.9	0.32	-1	-2.3	0.87
H_{m0} (m)	8606	0.31	-2.3	0.12	0.08	-3.2	0.89
T_e (s)	8606	0.6	3.9	0.08	0.3	3.6	0.90
ϵ_0 (-)	8606	0.04	1.9	0.11	0.00	1.1	0.72
θ_{Jmax} (deg)	-	-	-	-	-	-	-
d (-)	-	-	-	-	-	-	-

Table C.80. Performance metrics for NDBC Station 51002 for 2000.

Parameter	N	RMSE	PE (%)	SI	Bias	Bias (%)	R
J (kW/m)	2991	13	21.6	0.43	5	16.9	0.78
H_{m0} (m)	2991	0.39	5.2	0.15	0.10	3.9	0.82
T_e (s)	2991	0.9	6.9	0.11	0.5	6.4	0.83
ϵ_0 (-)	2991	0.05	3.7	0.14	0.01	2.6	0.60
θ_{Jmax} (deg)	-	-	-	-	-	-	-
d (-)	-	-	-	-	-	-	-

Table C.81. Performance metrics for NDBC Station 51002 for 1999.

Parameter	N	RMSE	PE (%)	SI	Bias	Bias (%)	R
J (kW/m)	8540	10	14.3	0.37	2	7.7	0.88
H_{m0} (m)	8540	0.29	2.4	0.12	0.03	1.3	0.90
T_e (s)	8540	0.9	6.8	0.11	0.5	5.9	0.88
ϵ_0 (-)	8540	0.05	6.3	0.15	0.02	5.3	0.68
θ_{Jmax} (deg)	-	-	-	-	-	-	-
d (-)	-	-	-	-	-	-	-

Table C.82. Performance metrics for NDBC Station 51002 for 1998.

Parameter	N	RMSE	PE (%)	SI	Bias	Bias (%)	R
J (kW/m)	8530	14	24.8	0.48	6	21.5	0.89
H_{m0} (m)	8530	0.38	6.0	0.15	0.14	5.4	0.88
T_e (s)	8530	1.0	8.6	0.12	0.6	7.6	0.89
ϵ_0 (-)	8530	0.06	2.7	0.15	0.01	1.7	0.58
θ_{Jmax} (deg)	-	-	-	-	-	-	-
d (-)	-	-	-	-	-	-	-

Table C.83. Performance metrics for NDBC Station 51002 for 1997.

Parameter	N	RMSE	PE (%)	SI	Bias	Bias (%)	R
J (kW/m)	8650	11	25.1	0.44	4	18.5	0.85
H_{m0} (m)	8650	0.33	6.2	0.14	0.11	4.8	0.87
T_e (s)	8650	1.0	8.3	0.12	0.6	7.4	0.83
ϵ_0 (-)	8650	0.05	0.2	0.14	0.00	-0.5	0.60
θ_{Jmax} (deg)	-	-	-	-	-	-	-
d (-)	-	-	-	-	-	-	-

Table C.84. Performance metrics for NDBC Station 51002 for 1996.

Parameter	N	RMSE	PE (%)	SI	Bias	Bias (%)	R
J (kW/m)	8598	11	2.7	0.45	-1	-4.7	0.81
H_{m0} (m)	8598	0.37	-3.4	0.16	-0.11	-4.8	0.84
T_e (s)	8598	1.0	7.4	0.12	0.5	6.6	0.86
ϵ_0 (-)	8598	0.06	0.4	0.15	0.00	-0.6	0.60
θ_{Jmax} (deg)	-	-	-	-	-	-	-
d (-)	-	-	-	-	-	-	-

C.2.4 Station 51003

Table C.85. Performance metrics for NDBC Station 51003 for 2010.

Parameter	N	RMSE	PE (%)	SI	Bias	Bias (%)	R
J (kW/m)	7779	12.3	27.7	0.60	5	23.0	0.85
H_{m0} (m)	7779	0.35	4.0	0.16	0.07	3.2	0.84
T_e (s)	7779	1.3	13.5	0.16	1.0	12.7	0.83
ϵ_0 (-)	7779	0.07	11.6	0.20	0.03	10.2	0.44
θ_{Jmax} (deg)	-	-	-	-	-	-	-
d (-)	-	-	-	-	-	-	-

Table C.86. Performance metrics for NDBC Station 51003 for 2009.

Parameter	N	RMSE	PE (%)	SI	Bias	Bias (%)	R
J (kW/m)	8756	11	17.5	0.52	2	10.9	0.82
H_{m0} (m)	8756	0.32	1.2	0.15	-0.01	-0.3	0.86
T_e (s)	8756	1.2	11.3	0.14	0.9	11.6	0.83
ϵ_0 (-)	8756	0.05	5.7	0.16	0.02	4.4	0.53
θ_{Jmax} (deg)	-	-	-	-	-	-	-
d (-)	-	-	-	-	-	-	-

Table C.87. Performance metrics for NDBC Station 51003 for 2008.

Parameter	N	RMSE	PE (%)	SI	Bias	Bias (%)	R
J (kW/m)	8770	8	13.7	0.42	2	8.2	0.85
H_{m0} (m)	8770	0.29	0.0	0.14	-0.03	-1.5	0.86
T_e (s)	8770	1.1	11.0	0.14	0.8	10.3	0.83
ϵ_0 (-)	8770	0.06	5.3	0.16	0.01	3.9	0.53
θ_{Jmax} (deg)	-	-	-	-	-	-	-
d (-)	-	-	-	-	-	-	-

Table C.88. Performance metrics for NDBC Station 51003 for 2007.

Parameter	N	RMSE	PE (%)	SI	Bias	Bias (%)	R
J (kW/m)	4387	11	26.0	0.50	2	9.7	0.79
H_{m0} (m)	4387	0.39	2.5	0.18	-0.01	-0.4	0.79
T_e (s)	4387	1.4	12.6	0.17	0.9	11.3	0.69
ϵ_0 (-)	4387	0.06	6.4	0.18	0.01	4.2	0.39
θ_{Jmax} (deg)	-	-	-	-	-	-	-
d (-)	-	-	-	-	-	-	-

Table C.89. Performance metrics for NDBC Station 51003 for 2006.

Parameter	N	RMSE	PE (%)	SI	Bias	Bias (%)	R
J (kW/m)	6744	7	5.2	0.38	0	-0.7	0.83
H_{m0} (m)	6744	0.31	-3.4	0.15	-0.10	-4.8	0.84
T_e (s)	6744	1.0	9.8	0.12	0.7	9.3	0.81
ϵ_0 (-)	6744	0.06	9.8	0.18	0.03	8.4	0.54
θ_{Jmax} (deg)	-	-	-	-	-	-	-
d (-)	-	-	-	-	-	-	-

Table C.90. Performance metrics for NDBC Station 51003 for 2005.

Parameter	N	RMSE	PE (%)	SI	Bias	Bias (%)	R
J (kW/m)	3437	13	0.1	0.37	-2	-5.0	0.88
H_{m0} (m)	3437	0.37	-3.7	0.14	-0.13	-5.0	0.87
T_e (s)	3437	0.9	5.2	0.10	0.4	4.6	0.89
ϵ_0 (-)	3437	0.05	-1.8	0.15	-0.01	-2.5	0.61
θ_{Jmax} (deg)	-	-	-	-	-	-	-
d (-)	-	-	-	-	-	-	-

Table C.91. Performance metrics for NDBC Station 51003 for 2004.

Parameter	N	RMSE	PE (%)	SI	Bias	Bias (%)	R
J (kW/m)	8369	10	-1.2	0.40	-1	-3.8	0.90
H_{m0} (m)	8369	0.33	-3.6	0.14	-0.10	-4.6	0.88
T_e (s)	8369	0.8	4.0	0.09	0.31	3.5	0.91
ϵ_0 (-)	8369	0.05	0.7	0.14	0.00	-0.2	0.64
θ_{Jmax} (deg)	-	-	-	-	-	-	-
d (-)	-	-	-	-	-	-	-

Table C.92. Performance metrics for NDBC Station 51003 for 2003.

Parameter	N	RMSE	PE (%)	SI	Bias	Bias (%)	R
J (kW/m)	5682	6	-9.5	0.32	-2	-13.5	0.84
H_{m0} (m)	5682	0.28	-6.5	0.14	0.16	-7.8	0.83
T_e (s)	5682	0.7	2.0	0.08	0.1	1.3	0.86
ϵ_0 (-)	5682	0.05	-0.2	0.14	-0.01	-1.4	0.59
θ_{Jmax} (deg)	-	-	-	-	-	-	-
d (-)	-	-	-	-	-	-	-

Table C.93. Performance metrics for NDBC Station 51003 for 2002.

Parameter	N	RMSE	PE (%)	SI	Bias	Bias (%)	R
J (kW/m)	6716	10	-4.5	0.43	-2	-7.1	0.88
H_{m0} (m)	6716	0.32	-4.7	0.15	-0.13	-5.8	0.88
T_e (s)	6716	0.7	3.0	0.08	0.2	2.5	0.88
ϵ_0 (-)	6716	0.05	-1.9	0.12	-0.01	-2.5	0.69
θ_{Jmax} (deg)	-	-	-	-	-	-	-
d (-)	-	-	-	-	-	-	-

Table C.94. Performance metrics for NDBC Station 51003 for 2001.

Parameter	N	RMSE	PE (%)	SI	Bias	Bias (%)	R
J (kW/m)	8399	10	-1.6	0.40	-1	-4.1	0.86
H_{m0} (m)	8399	0.32	-4.0	0.14	-0.11	-4.8	0.88
T_e (s)	8399	0.8	4.4	0.10	0.3	3.9	0.86
ϵ_0 (-)	8399	0.05	-2.4	0.14	-0.01	-3.3	0.60
θ_{Jmax} (deg)	-	-	-	-	-	-	-
d (-)	-	-	-	-	-	-	-

Table C.95. Performance metrics for NDBC Station 51003 for 2000.

Parameter	N	RMSE	PE (%)	SI	Bias	Bias (%)	R
J (kW/m)	7690	10	4.4	0.44	0	0.5	0.81
H_{m0} (m)	7690	0.31	-1.8	0.14	-0.06	-2.6	0.86
T_e (s)	7690	1.0	5.4	0.12	0.4	4.5	0.81
ϵ_0 (-)	7690	0.05	0.1	0.15	0.00	-0.8	0.54
θ_{Jmax} (deg)	-	-	-	-	-	-	-
d (-)	-	-	-	-	-	-	-

Table C.96. Performance metrics for NDBC Station 51003 for 1999.

Parameter	N	RMSE	PE (%)	SI	Bias	Bias (%)	R
J (kW/m)	8601	12	9.3	0.51	1	2.8	0.85
H_{m0} (m)	8601	0.32	-0.2	0.14	-0.03	-1.5	0.88
T_e (s)	8601	1.0	6.6	0.12	0.5	5.9	0.85
ϵ_0 (-)	8601	0.06	2.6	0.16	0.01	1.4	0.53
θ_{Jmax} (deg)	-	-	-	-	-	-	-
d (-)	-	-	-	-	-	-	-

Table C.97. Performance metrics for NDBC Station 51003 for 1998.

Parameter	N	RMSE	PE (%)	SI	Bias	Bias (%)	R
J (kW/m)	7402	18	15.5	0.59	3	11.1	0.82
H_{m0} (m)	7402	0.38	2.1	0.16	0.03	1.2	0.86
T_e (s)	7402	1.1	7.2	0.13	0.6	6.2	0.88
ϵ_0 (-)	7402	0.06	-0.6	0.16	-0.01	-1.6	0.49
θ_{Jmax} (deg)	-	-	-	-	-	-	-
d (-)	-	-	-	-	-	-	-

Table C.98. Performance metrics for NDBC Station 51003 for 1997.

Parameter	N	RMSE	PE (%)	SI	Bias	Bias (%)	R
J (kW/m)	8538	11	15.9	0.44	3	10.9	0.86
H_{m0} (m)	8538	0.34	2.7	0.15	0.04	1.6	0.87
T_e (s)	8538	1.0	6.7	0.12	0.5	5.8	0.84
ϵ_0 (-)	8538	0.05	-1.1	0.14	-0.01	-1.8	0.58
θ_{Jmax} (deg)	-	-	-	-	-	-	-
d (-)	-	-	-	-	-	-	-

Table C.99. Performance metrics for NDBC Station 51003 for 1996.

Parameter	N	RMSE	PE (%)	SI	Bias	Bias (%)	R
J (kW/m)	7592	12	-3.7	0.48	-3	-11.4	0.87
H_{m0} (m)	7592	0.39	-6.3	0.18	-0.17	-7.7	0.87
T_e (s)	7592	1.1	6.3	0.12	0.5	5.2	0.83
ϵ_0 (-)	7592	0.06	-3.6	0.16	-0.02	-4.6	0.58
θ_{Jmax} (deg)	-	-	-	-	-	-	-
d (-)	-	-	-	-	-	-	-

C.2.5 Station 51004

Table C.100. Performance metrics for NDBC Station 51004 for 2009.

Parameter	N	RMSE	PE (%)	SI	Bias	Bias (%)	R
J (kW/m)	773	7	20.5	0.34	2	11.6	0.59
H_{m0} (m)	773	0.31	6.8	0.14	0.11	4.9	0.61
T_e (s)	773	0.6	2.5	0.07	0.2	2.2	0.81
ϵ_0 (-)	773	0.06	14.7	0.18	0.05	13.9	0.75
θ_{Jmax} (deg)	730	41.8	16.6	0.28	4.8	3.3	0.94
d (-)	730	0.09	-2.2	0.16	-0.02	-3.1	0.52

Table C.101. Performance metrics for NDBC Station 51004 for 2008.

Parameter	N	RMSE	PE (%)	SI	Bias	Bias (%)	R
J (kW/m)	4766	9	24.5	0.42	4	19.2	0.80
H_{m0} (m)	4766	0.28	3.7	0.12	0.07	2.8	0.87
T_e (s)	4766	1.2	13.3	0.16	1.0	12.8	0.78
ϵ_0 (-)	4766	0.07	12.5	0.19	0.04	11.1	0.39
θ_{Jmax} (deg)	-	-	-	-	-	-	-
d (-)	-	-	-	-	-	-	-

Table C.102. Performance metrics for NDBC Station 51004 for 2007.

Parameter	N	RMSE	PE (%)	SI	Bias	Bias (%)	R
J (kW/m)	6841	8	18.5	0.34	3	11.3	0.88
H_{m0} (m)	6841	0.25	2.4	0.11	0.03	1.1	0.91
T_e (s)	6841	1.0	11.3	0.13	0.8	10.8	0.88
ϵ_0 (-)	6841	0.06	11.3	0.17	0.04	10.3	0.63
θ_{Jmax} (deg)	-	-	-	-	-	-	-
d (-)	-	-	-	-	-	-	-

Table C.103. Performance metrics for NDBC Station 51004 for 2006.

Parameter	N	RMSE	PE (%)	SI	Bias	Bias (%)	R
J (kW/m)	8319	8	10.4	0.34	2	7.2	0.89
H_{m0} (m)	8319	0.26	-0.3	0.11	-0.02	-1.0	0.90
T_e (s)	8319	1.0	9.2	0.12	0.7	8.8	0.84
ϵ_0 (-)	8319	0.06	9.5	0.16	0.03	8.6	0.69
θ_{Jmax} (deg)	-	-	-	-	-	-	-
d (-)	-	-	-	-	-	-	-

Table C.104. Performance metrics for NDBC Station 51004 for 2005.

Parameter	N	RMSE	PE (%)	SI	Bias	Bias (%)	R
J (kW/m)	7832	9	12.9	0.39	2	9.9	0.84
H_{m0} (m)	7832	0.28	0.5	0.12	-0.01	-0.2	0.85
T_e (s)	7832	1.0	9.7	0.12	0.8	9.3	0.92
ϵ_0 (-)	7832	0.06	10.2	0.17	0.03	9.3	0.63
θ_{Jmax} (deg)	-	-	-	-	-	-	-
d (-)	-	-	-	-	-	-	-

Table C.105. Performance metrics for NDBC Station 51004 for 2004.

Parameter	N	RMSE	PE (%)	SI	Bias	Bias (%)	R
J (kW/m)	8744	8	18.5	0.38	3	13.9	0.86
H_{m0} (m)	8744	0.25	2.8	0.11	0.04	1.8	0.88
T_e (s)	8744	1.0	10.5	0.13	0.80	9.9	0.89
ϵ_0 (-)	8744	0.05	7.8	0.15	0.03	6.9	0.66
θ_{Jmax} (deg)	-	-	-	-	-	-	-
d (-)	-	-	-	-	-	-	-

Table C.106. Performance metrics for NDBC Station 51004 for 2003.

Parameter	N	RMSE	PE (%)	SI	Bias	Bias (%)	R
J (kW/m)	3539	11	4.4	0.35	0	0.2	0.80
H_{m0} (m)	3539	0.30	-0.3	0.12	-0.04	-1.4	0.81
T_e (s)	3539	0.8	3.0	0.08	0.2	2.5	0.90
ϵ_0 (-)	3539	0.04	3.6	0.11	0.01	2.9	0.76
θ_{Jmax} (deg)	-	-	-	-	-	-	-
d (-)	-	-	-	-	-	-	-

Table C.107. Performance metrics for NDBC Station 51004 for 2002.

Parameter	N	RMSE	PE (%)	SI	Bias	Bias (%)	R
J (kW/m)	8545	10	4.4	0.37	0.6	2.0	0.87
H_{m0} (m)	8545	0.28	0.0	0.13	-0.02	-0.7	0.87
T_e (s)	8545	0.7	2.7	0.09	0.2	2.3	0.90
ϵ_0 (-)	8545	0.04	2.7	0.11	0.01	1.5	0.76
θ_{Jmax} (deg)	-	-	-	-	-	-	-
d (-)	-	-	-	-	-	-	-

Table C.108. Performance metrics for NDBC Station 51004 for 2001.

Parameter	N	RMSE	PE (%)	SI	Bias	Bias (%)	R
J (kW/m)	8606	10	1.9	0.34	0	-1.5	0.88
H_{m0} (m)	8606	0.28	-1.8	0.11	-0.07	-2.7	0.91
T_e (s)	8606	0.7	4.3	0.08	0.3	4.0	0.91
ϵ_0 (-)	8606	0.04	2.1	0.11	0.01	1.4	0.74
θ_{Jmax} (deg)	-	-	-	-	-	-	-
d (-)	-	-	-	-	-	-	-

Table C.109. Performance metrics for NDBC Station 51004 for 2000.

Parameter	N	RMSE	PE (%)	SI	Bias	Bias (%)	R
J (kW/m)	8499	9	5.0	0.32	1	3.2	0.85
H_{m0} (m)	8499	0.29	0.4	0.12	-0.04	-0.2	0.86
T_e (s)	8499	0.7	2.3	0.09	0.2	1.9	0.83
ϵ_0 (-)	8499	0.04	4.5	0.11	0.02	3.9	0.80
θ_{Jmax} (deg)	-	-	-	-	-	-	-
d (-)	-	-	-	-	-	-	-

Table C.110. Performance metrics for NDBC Station 51004 for 1999.

Parameter	N	RMSE	PE (%)	SI	Bias	Bias (%)	R
J (kW/m)	5655	13	11.9	0.45	2	6.5	0.84
H_{m0} (m)	5655	0.30	1.4	0.12	0.01	0.5	0.90
T_e (s)	5655	0.9	6.7	0.11	0.5	5.9	0.88
ϵ_0 (-)	5655	0.06	8.0	0.17	0.03	7.3	0.63
θ_{Jmax} (deg)	-	-	-	-	-	-	-
d (-)	-	-	-	-	-	-	-

Table C.111. Performance metrics for NDBC Station 51004 for 1998.

Parameter	N	RMSE	PE (%)	SI	Bias	Bias (%)	R
J (kW/m)	5068	10	10.7	0.37	1	5.5	0.91
H_{m0} (m)	5068	0.27	0.5	0.11	-0.01	-0.4	0.93
T_e (s)	5068	0.9	7.9	0.11	0.6	7.3	0.85
ϵ_0 (-)	5068	0.06	7.2	0.15	0.02	6.1	0.60
θ_{Jmax} (deg)	-	-	-	-	-	-	-
d (-)	-	-	-	-	-	-	-

Table C.112. Performance metrics for NDBC Station 51004 for 1997.

Parameter	N	RMSE	PE (%)	SI	Bias	Bias (%)	R
J (kW/m)	8599	10	20.0	0.40	4	16.1	0.86
H_{m0} (m)	8599	0.31	4.2	0.13	0.08	3.5	0.87
T_e (s)	8599	1.0	8.2	0.12	0.6	7.6	0.84
ϵ_0 (-)	8599	0.06	3.7	0.15	0.01	3.0	0.58
θ_{Jmax} (deg)	-	-	-	-	-	-	-
d (-)	-	-	-	-	-	-	-

Table C.113. Performance metrics for NDBC Station 51004 for 1996.

Parameter	N	RMSE	PE (%)	SI	Bias	Bias (%)	R
J (kW/m)	8611	12	-0.4	0.46	-2	-7.0	0.84
H_{m0} (m)	8611	0.34	-4.6	0.14	-0.13	-5.5	0.87
T_e (s)	8611	1.0	7.3	0.12	0.5	6.4	0.86
ϵ_0 (-)	8611	0.05	1.9	0.15	0.00	1.2	0.59
θ_{Jmax} (deg)	-	-	-	-	-	-	-
d (-)	-	-	-	-	-	-	-

C.2.6 Station 51101

Table C.114. Performance metrics for NDBC Station 51101 for 2010.

Parameter	N	RMSE	PE (%)	SI	Bias	Bias (%)	R
J (kW/m)	8735	17	26.6	0.63	5	18.4	0.89
H_{m0} (m)	8735	0.39	7.6	0.17	0.13	5.8	0.91
T_e (s)	8735	0.9	5.6	0.10	0.5	5.4	0.92
ϵ_0 (-)	8735	0.05	6.8	0.16	0.02	6.4	0.72
θ_{Jmax} (deg)	8735	38.6	-3.0	0.19	-6.6	-3.2	0.96
d (-)	8735	0.10	-0.5	0.15	-0.01	-1.7	0.67

Table C.115. Performance metrics for NDBC Station 51101 for 2009.

Parameter	N	RMSE	PE (%)	SI	Bias	Bias (%)	R
J (kW/m)	6087	17	15.8	0.65	1	4.8	0.89
H_{m0} (m)	6087	0.37	5.4	0.17	0.06	2.8	0.91
T_e (s)	6087	0.7	1.1	0.08	0.1	1.0	0.91
ϵ_0 (-)	6087	0.05	8.0	0.16	0.02	7.2	0.73
θ_{Jmax} (deg)	6087	41.5	-1.9	0.21	-4.1	-2.1	0.95
d (-)	6087	0.11	2.0	0.17	0.00	0.2	0.60

Table C.116. Performance metrics for NDBC Station 51101 for 2008.

Parameter	N	RMSE	PE (%)	SI	Bias	Bias (%)	R
J (kW/m)	366	24	114.3	0.96	20	79.4	0.79
H_{m0} (m)	366	0.8	39.2	0.40	0.73	34.8	0.72
T_e (s)	366	1.0	5.1	0.10	0.4	4.4	0.86
ϵ_0 (-)	366	0.06	5.6	0.19	0.01	4.0	0.70
θ_{Jmax} (deg)	366	29.5	3.2	0.10	3.9	1.3	0.78
d (-)	366	0.09	3.0	0.12	0.02	2.5	0.73

Pacific Northwest National Laboratory

902 Battelle Boulevard
P.O. Box 999
Richland, WA 99354
1-888-375-PNNL (7665)

www.pnnl.gov